TESIS DE LA UNIVERSIDAD DE ZARAGOZA

2020 146

José Alejandro Roche Areta

Visible and NIR responsive nanocarriers from amphiphilic diblock copolymers

Departamento
Química Orgánica

Director/es
Piñol Lacambra, Milagros
Tejedor Bielsa, Rosa María

ISSN 2254-7606

Prensas de la Universidad
Universidad Zaragoza

ISSN 2254-7606

Universidad Zaragoza
1542

Tesis Doctoral

VISIBLE AND NIR RESPONSIVE NANOCARRIERS FROM AMPHIPHILIC DIBLOCK COPOLYMERS

Autor

José Alejandro Roche Areta

Director/es

Piñol Lacambra, Milagros
Tejedor Bielsa, Rosa María

UNIVERSIDAD DE ZARAGOZA

Química Orgánica

2020

TESIS DOCTORAL

Visible and NIR responsive nanocarriers from amphiphilic diblock copolymers

José Alejandro Roche Areta

Departamento de Química Orgánica

Facultad de Ciencias – ICMA

Universidad de Zaragoza – CSIC

Zaragoza, Febrero 2020

TESIS DOCTORAL

Visible and NIR responsive nanocarriers from amphiphilic diblock copolymers

Memoria presentada en la Universidad de Zaragoza para optar al Grado de Doctor

José Alejandro Roche Areta

Departamento de Química Orgánica

Facultad de Ciencias – ICMA

Universidad de Zaragoza – CSIC

Zaragoza, Febrero 2020

La Dra. MILAGROS PIÑOL LACAMBRA, Profesora Titular del Departamento de Química Orgánica en la Facultad de Ciencias de la Universidad de Zaragoza y perteneciente al Instituto de Ciencia de Materiales de Aragón de la Universidad de Zaragoza – CSIC.

y la Dra. ROSA MARÍA TEJEDOR BIELSA, Profesora del Centro Universitario de la Defensa – AGM y perteneciente al Instituto de Ciencia de Materiales de Aragón de la Universidad de Zaragoza – CSIC.

HACEN CONSTAR:

que el trabajo original titulado "Visible and NIR responsive nanocarriers from amphiphilic diblock copolymers", ha sido realizado bajo nuestra supervisión por D. JOSÉ ALEJANDRO ROCHE ARETA en el Departamento de Química Orgánica de la Facultad de Ciencias y el Instituto de Ciencia de Materiales de Aragón de la Universidad de Zaragoza – CSIC y reúne las condiciones para su presentación como tesis doctoral.

Zaragoza, Febrero de 2020

Fdo: Dra. Milagros Piñol Lacambra Fdo. Dra. Rosa María Tejedor Bielsa

Resumen

La habilidad de los copolímeros dibloque anfífilos al ser dispersados en agua de autoensamblarse en micelas y vesículas, capaces de encapsular moléculas pequeñas en su interior, hace que estos materiales sean muy interesantes para su posible aplicación como nanotransportadores de fármacos. La administración de un fármaco mediante esta vía permite reducir sus efectos secundarios, evitar su degradación hasta que alcanza el objetivo deseado y, en el caso de trabajar con fármacos no solubles en medio fisiológico, aumentar su solubilidad. Introduciendo una unidad sensible a estímulos en la estructura del copolímero dibloque anfífilo es posible inducir cambios morfológicos en los autoensamblados al aplicar el estímulo adecuado y, así, producir la liberación de las moléculas encapsuladas en su interior. De todos los estímulos disponibles, la luz es especialmente interesante ya que se puede aplicar con un excelente control espaciotemporal.

Durante los últimos años, el Grupo de Cristales Líquidos y Polímeros ha trabajado con copolímeros bloque anfífilos de arquitecturas novedosas, dendrítico-lineal y miktoarm, con unidades azobenceno. La presencia de estas unidades fotosensibles ha permitido obtener autoensamblados en agua (micelas y vesículas) con respuesta a la luz UV, cuyo potencial como sistemas para la encapsulación y liberación de pequeñas moléculas se ha demostrado usando sondas fluorescentes sensibles a la polaridad del medio. Estos polímeros con las unidades azobenceno unidas covalentemente se obtienen a través de estrategias sintéticas con una versatilidad reducida, ya que cuando se desea cambiar la unidad sensible a la luz es necesario abordar la síntesis desde las etapas iniciales. Más recientemente, se han sintetizado polimetacrilatos de 2,6-diacilaminopiridina, un análogo de la adenina, cuya funcionalización con unidades azobenceno portadoras de grupos timina es posible mediante reconocimiento por enlace de hidrógeno. Esta estrategia de funcionalización supramolecular de un polímero preformado es sintéticamente más versátil y ha permitido obtener autoensamblados con respuesta a la luz UV, cuya principal limitación es la escasa biodegradabilidad de los polimetacrilatos.

En cualquier caso, tanto los ejemplos citados como la mayoría de los ejemplos disponibles en la bibliografía hacen uso de luz UV como estímulo, la cual es dañina para los tejidos humanos y además presenta poca capacidad penetrante. La

aplicación de unidades sensibles a la luz en regiones de menor energía como el visible o el infrarrojo cercano (NIR) es de particular interés, al poseer mayor capacidad penetrante en tejidos humanos y ser menos dañinas sobre ellos.

El objetivo sobre el que se ha desarrollado esta tesis doctoral ha sido la preparación de nanotransportadores capaces de liberar su carga al ser estimulados con luz NIR o luz visible. Con esta finalidad, se planteó la síntesis de copolímeros dibloque anfífilos biodegradables con unidades sensibles a la luz NIR o visible, incorporadas como sustituyentes laterales del bloque hidrófobo. Las propiedades y la reproducibilidad de autoensamblado de este tipo de copolímeros está considerablemente condicionada por el grado de control estructural que se tiene sobre el polímero. Por ello, se proyectó la utilización de estrategias de síntesis reproducibles y versátiles que combinarán el uso técnicas de polimerización controlada, con las que se puede ejercer un buen control estructural sobre el polímero, con la funcionalización posterior del polímero para introducir diferentes unidades fotosensibles con menor esfuerzo sintético. Como polímero biodegradable se seleccionó un policarbonato alifático y, de las diferentes posibilidades para incorporar funcionalidad al polímero, se contemplaron tanto estrategias de modificación supramolecular como covalente. Para los copolímeros preparados siguiendo estos criterios, se planteó la generación de autoemsablados en agua y la evaluación de su respuesta a la luz, capacidad de encapsulación y liberación fotoestimulada de pequeñas moléculas, y potencial como nanotransportadores de fármacos.

Los objetivos específicos planteados en cada capítulo de esta tesis doctoral son:

- **Capítulo 2:** Preparación de copolímeros dibloque anfífilos funcionalizados con éster de cumarina sensible al NIR en un proceso de absorción a dos fotones y estudio de sus autoensamblados en agua. El anclaje de la unidad sensible a la luz ha sido abordado mediante enlace supramolecular y el comportamiento de este polímero se ha comparado con un modelo covalente.
- **Capítulo 3:** Preparación de copolímeros dibloque anfífilos funcionalizados con unidades de azobenceno sensibles a luz visible. Se han generado

autoensamblados en agua, se ha evaluado su respuesta a la luz visible y se ha comparado con sistemas equivalentes portadores de azobencenos estimulables con luz UV. Asimismo, se ha analizado el efecto de la longitud del bloque hidrófilo en la morfología de los autoensamblados obtenidos en las dos series de polímeros.

- **Capítulo 4:** Preparación de vesículas a partir de copolímeros dibloque anfífilos azobenceno seleccionados en el capítulo anterior. Se ha evaluado la posibilidad de modular la respuesta a la luz incorporando cadenas alifáticas en el bloque hidrófobo en distintas proporciones.
- **Capítulo 5:** Estudios *in vitro* de una selección de los materiales preparados. Se ha evaluado la citotoxicidad de los ensamblados, su capacidad para encapsular Paclitaxel y la actividad de estos autoensamblados cargados con fármaco.

Acronym list

2PA	Two-photon absorption
AIBN	2,2′-Azobis(2-methylpropionitrile)
APC	Aliphatic poly(carbonate)
BC	Block copolymer
bis-MPA	2,2-Bis(hydroxymethyl)propionic acid
CAC	Critical aggregation concentration
CuAAC	Cu(I)-catalysed alkyne-azide cycloaddition
Đ	Dispersity
DAP	2,6-Diacylaminopyridine
DBU	1,8-Diazabicyclo(5.4.0)undec-7-ene
DEACM	7-(Diethylamino)-4-(hydroxymethyl)coumarin
DEGMA	Di(ethylene glycol) methyl ether methacrylate
DL	Drug loading
DLS	Dynamic light scattering
DMF	*N,N*-Dimethylformamide
DMPA	2,2-Dimethoxy-2-phenyl acetophenone
DMSO	Dimethyl sulfoxide
DSC	Differential scanning calorimetry
DTC	Dimethyltrimethylene carbonate
EE	Encapsulation efficiency
EPR	Enhanced permeability and retention
ΔH_m	Enthalpy associated to a melt transition
IC50	Half maximal inhibitory concentration
LDBC	Linear-dendritic block copolymer
MAC	5-Methyl-5-allyloxycarbonyl-1,3-dioxan-2-one

mCTA	Macrochain transfer agent
MPC	5-Methyl-5-propargyloxycarbonyl-1,3-dioxan-2-one
OEGMA	Oligo(ethylene glycol) methyl ether methacrylate
PCL	Poly(caprolactone)
PEG	Poly(ethylene glycol)
PEG-OH	Poly(ethylene glycol) methyl ether
PMDETA	*N,N,N′,N″,N‴*-Pentamethyldiethylenetriamine
PMMA	Poly(methyl methacrylate)
PNIPAM	Poly(*N*-isopropylacrylamide)
ROP	Ring opening polymerisation
SAXS	Small-angle X-ray scattering
SEC	Size exclusion chromatography
T_g	Glass transition temperature
T_m	Melting temperature
T_{M-I}	Mesophase to isotropic liquid transition temperature
TBD	1,5,7-Triazabicyclo[4.4.0]dec-5-ene
TEM	Transmission electron microscopy
TGA	Thermogravimetric analysis
THF	Tetrahydrofuran
TMC	Trimethylene carbonate
TU	1-(3,5-Bis(trifluoromethyl)-phenyl)-3-cyclohexylthiourea
UCNPs	Upconverting nanoparticles

Contents

CHAPTER 1

INTRODUCTION

1.1 Nanocarriers from amphiphilic block copolymers

A block copolymer (BC) is a copolymer where the constituent macromolecules are derived from two or more different monomers grouped in discrete polymeric blocks that are then constitutionally different and covalently bonded.[1,2,3,4] BCs can be configured into many different topologies on the basis of the arrangement of the blocks and the linear or branched sequencing of the monomers. Accessible architectures include linear BCs, with the blocks connected end to end, and miktoarm star like BCs, when several blocks are connected at a single junction. Besides, with the development of highly branched topologies, a pool of novel BCs architectures are available incorporating hyperbranched or dendritic blocks.[5,6] The simplest BC structure, and the one studied in this work, comprises two linear blocks, A and B (Figure 1.1). If the physical or chemical properties of the blocks are significantly different, these so-called linear BCs, are able to segregate and self-assemble into nanostructures, either in bulk or in solution.

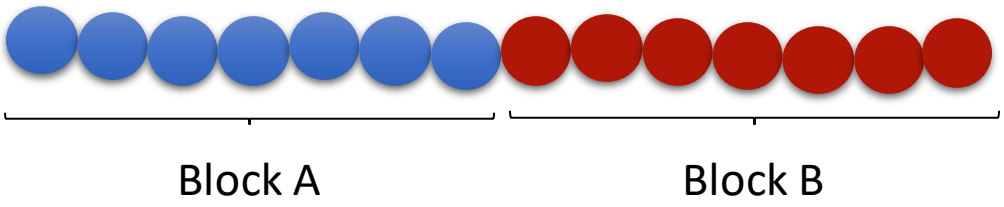

Figure 1.1: Schematic representation of a linear AB diblock copolymer.

In bulk, the phase separation induced by the incompatibility along with the chemical bond constraints between the blocks leads to well-defined nanostructures with periodic morphologies and controllable length scales. The microphase separation of an AB diblock copolymer depends on the total degree of polymerisation ($N = N_A+N_B$), the volume fractions of the A and B blocks (f_A and f_B, with $f_A + f_B = 1$) and the Flory-Huggins parameter (χ_{AB}), indicative of the degree of incompatibility between A and B blocks. Based on these parameters, the morphology of a linear diblock copolymer in bulk can be predicted according to Self-Consistent Mean Field theory, proposed by Matsen and Bates.[7,8,9,10]

In solution, a diblock copolymer can undergo phase separation in selective solvents where one of the blocks is soluble while the other is not. The soluble block is organized around the non-soluble block, lowering the interfacial area between the insoluble block and the solvent, so the interactions balance between the solvent and the blocks induces the formation of well-defined structures.[11] The properties of the BCs such as molecular weight, chemical functionality or volume fraction of the blocks can be tailored during the synthesis of the copolymer and, thus, their self-assembly capabilities.

Amphiphilic diblock copolymers, which are comprised by a hydrophilic and a hydrophobic segment, have recently deserved particular interest because of their self-assembly capacity when dispersed in water and the remarkable potential of the resulting self-assemblies as drug nanocarriers. In aqueous solutions, amphiphilic BCs organize themselves to minimize the energetically unfavourable interactions of the hydrophobic blocks with water. During self-assembly, the water insoluble segments interact forming hydrophobic domains that are stabilized by the hydrophilic segments aligned at the interface and extending into the aqueous media. The self-assembly process is accompanied by an entropy loss, as the order of the system increases, but circumvents thermodynamically unfavourable hydrophobic-water interactions and lowers the total free energy of the system.[12]

Depending on the concentration, the molar mass and the volume ratio between the hydrophilic and hydrophobic blocks, amphiphilic diblock copolymers can self-assemble into different morphologies. The dimensionless 'packing parameter', p, firstly described for small amphiphiles in water but applicable to diblock copolymers, is defined in Figure 1.2 and usually commands the most likely self-assembled structure.[13] The volume of the hydrophobic chains is represented by v, while a_0 is the optimal area of the hydrophobic block in the hydrophilic-hydrophobic interphase and d is the length of the hydrophobic tail. In general terms, spherical micelles are formed for $p \leq \frac{1}{3}$, cylindrical micelles are formed for $\frac{1}{3} < p \leq \frac{1}{2}$ and bilayer structures such as vesicles for $\frac{1}{2} < p \leq 1$.[11,3,14] Spherical and cylindrical micelles are comprised by an inner core formed by the hydrophobic block, surrounded by a corona formed from the hydrophilic block. In

vesicles, the hydrophilic blocks assemble forming two coronas that face an inner cavity and the aqueous medium with the hydrophobic chains separating them. It has been predicted and experimentally confirmed that on increasing the hydrophobic-to-hydrophobic mass ratio the formation of vesicles becomes favoured (Figure 1.2).[10,11]

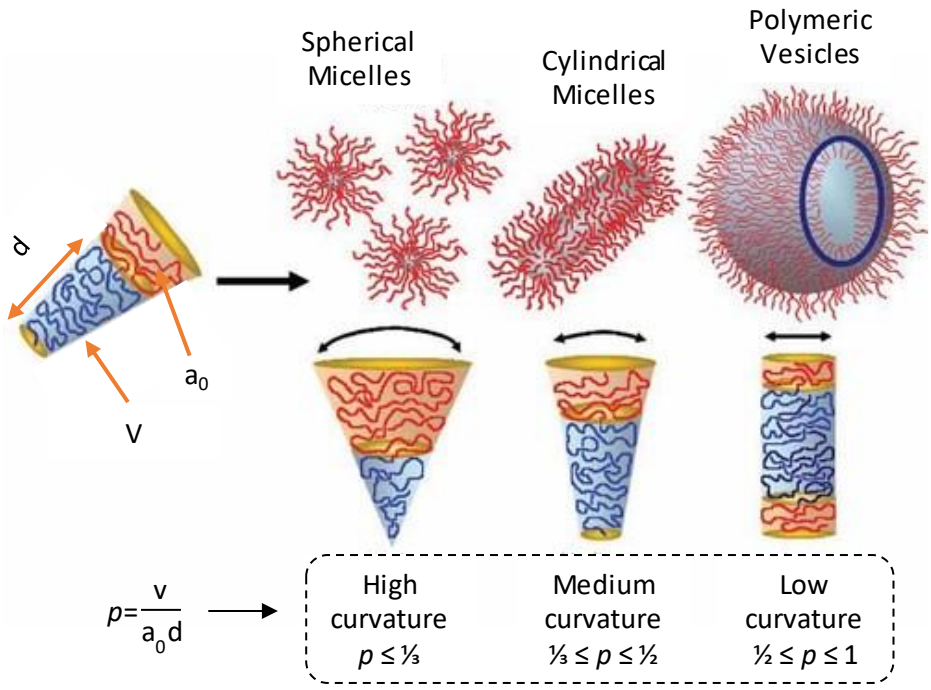

Figure 1.2: Self-assembled structures formed by amphiphilic block copolymers according to the packing parameter, p, which is determined by v, the volume of the hydrophobic chains, a_0, the optimal area of the hydrophobic block in the hydrophilic–hydrophobic interphase and d, the length of the hydrophobic tail.[15]

Spherical micelles and vesicles are especially attractive as they grant the possibility of encapsulating small molecules. The inner core of spherical micelles can be used for the solubilisation of small hydrophobic molecules. Alternatively, vesicles can be used to encapsulate both hydrophilic molecules into their hollow cavity and hydrophobic molecules into the bilayer. Therefore, the possibility of loading these self-assemblies with small molecules makes them very interesting systems as nanocarriers for drug delivery. The encapsulation of drugs provides several advantages such as the solubilisation of poorly soluble drugs in physiological media, the reduction of secondary effects, the protection of the drug until it reaches the desired target and the possibility of regulating the drug release in time at specific sites.[12,16,17]

Micelles diameters typically range from 10 to 100 nm, whereas vesicles are larger in size with diameters up to 5 μm.[18,19] Polymeric self-assemblies with diameters below 200 nm are specially interesting, as they may selectively accumulate into tumour tissues by the enhanced permeability and retention (EPR) effect (Figure 1.3).[20] In order to grow quickly, tumour tissues possess larger and more porous vascularization than healthy tissues. Low molar mass drugs can leak in healthy tissues what leads to undesirable effects. However, due to their larger sizes, drug loaded polymeric self-assemblies cannot pass to healthy tissues but the higher permeability of the tumour tissues facilitates the uptake of these relatively large particles. This enhanced permeability associated to an impaired lymphatic drainage, which increases the retention, causes the accumulation of the polymeric particles in solid tumours.

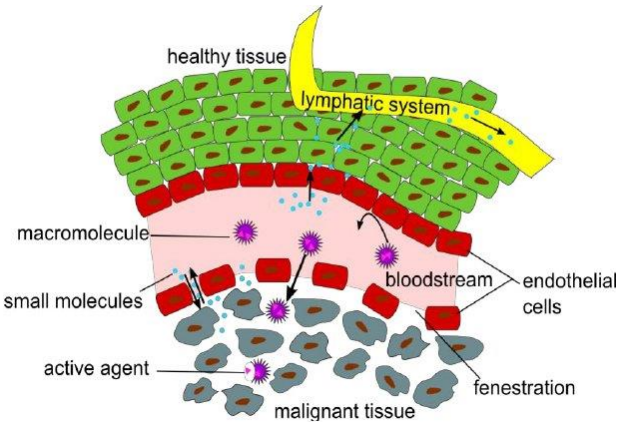

Figure 1.3: Representation of enhanced permeability and retention (EPR) effect.[21]

The stability of the self-assemblies against dissociation under highly diluted conditions is a critical parameter since this is what occurs if micelles or vesicles are incorporated into bloodstream. The thermodynamic stability of the self-assemblies is characterised by the critical aggregation concentration (CAC) considered as the minimum concentration of the polymer required for stable self-assemblies to form. Above CAC, polymers spontaneously form stable self-assemblies but below CAC disassembly occurs. Classical low molar weight surfactants possess CAC values between 10^{-3} and 10^{-4} M whereas those for amphiphilic BCs are from 10^{-6} to 10^{-7} M, indicating that self-assemblies formed from amphiphilic BCs are thermodynamically more stable.[22] Even at concentrations below CAC, the dissociation of the

self-assemblies is kinetically slower for amphiphilic BCs self-assemblies than for those from low molar weight surfactants.[23] CAC of the self-assemblies can be determined by diverse methods, including surface tension measurements or the use of polarity sensitive molecular fluorescent probes.

Surface tension of amphiphiles solutions decreases linearly with the amphiphile concentration. However, at a concentration equal or above CAC, surface tension becomes constant or evolves with a lower slope.[24] Plot of surface tension *versus* polymer concentration in logarithmic scale results in a curve break, with an onset point at a concentration equal to CAC (Figure 1.4).

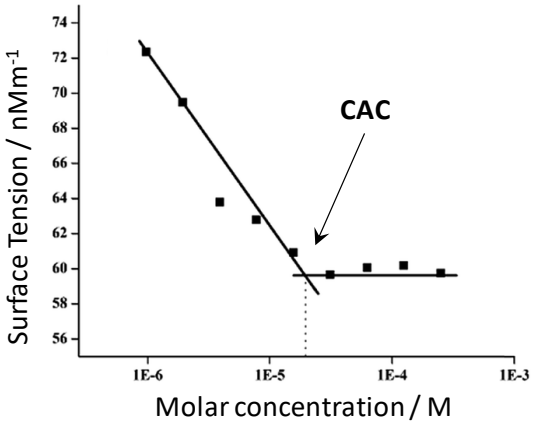

Figure 1.4: Determination of CAC by the surface tension method.[24]

CAC can also be determined by fluorescence experiments using fluorescent molecules whose emission properties change upon self-assembly. Pyrene is a hydrophobic fluorescent molecule and one of the most popular for this purpose because its emission, in particular the vibronic structure of its emission spectrum, depends on the polarity of the environment. Pyrene first energy emission peak, I_1 at 373 nm, is sensitive to the environment polarity, being more intense in polar environments. Whereas, its third energy emission peak, I_3 at 383 nm, is much less sensitive to polarity.[25,26] Above CAC, when assembly occurs, pyrene migrates from the aqueous media to the hydrophobic domains of the self-assemblies and, in this less polar environment, I_3/I_1 increases. By representing the I_3/I_1 emission ratio values *versus* the BC concentration in logarithmic scale, CAC can be estimated from the intersection between the two extrapolated lines (Figure 1.5). Nile Red is another good fluorescent probe whose emission at 620 nm (λ_{exc} = 550 nm) is strongly

quenched in aqueous solution but increases substantially when is localized in the hydrophobic environments provided by the micelles core or the vesicles bilayer. Plotting the emission intensity of Nile Red against the BC concentration a discontinuity occurs with a sharp increase of the emission at the CAC, above which self-assembly occurs.

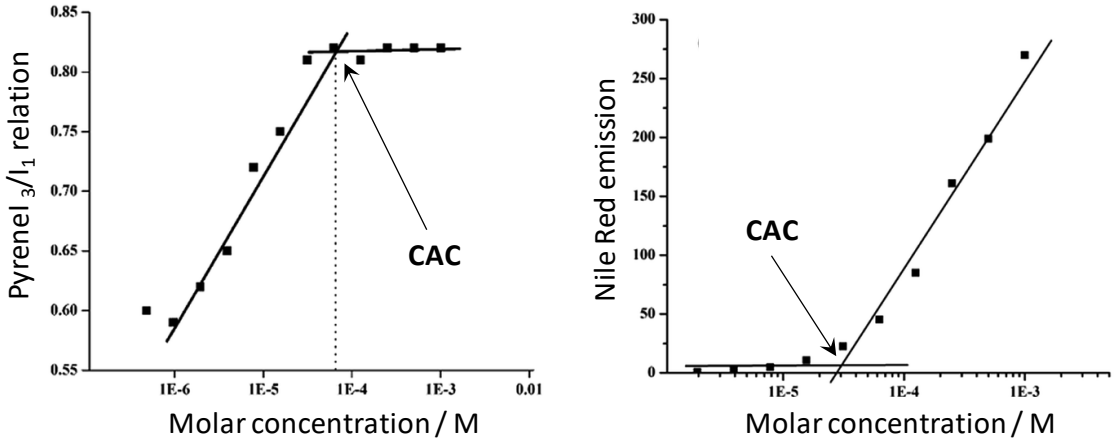

Figure 1.5: Determination of CAC by fluorescence using Pyrene (left) and Nile Red (right).[24]

The preparation of polymeric self-assemblies from amphiphilic BCs can be addressed in several ways. One of the simplest methods is nanoprecipitation that relies on the diffusion into an aqueous medium of a solution of the BC in a miscible organic solvent.[27] Mixing leads to the nanoprecipitation of the polymer forming self-assembled structures. The organic solvent is frequently removed by dialysis. The principal drawback of this method is that the use of a surfactant may be necessary to obtain stable nanoparticles. Also reasonably simple is the co-solvent method, which is one of the most popular methodologies.[28] In this case, water is gradually added over a solution of BC in a water miscible organic solvent until self-assembly occurs. THF, DMF or DMSO are commonly used solvents. The organic solvent is also removed by dialysis against water. Recently, microfluidic technology has been used for the preparation of polymeric nanoparticles in a straight way, with high control over the process, good reproducibility and large scale production applicability.[29] Self-assembly occurs when the BC copolymer solution and the precipitant solvent are pumped at controlled flows and instantly mixed inside the channels of a microreactor. In contrast to traditional methods, heterogeneous multiphase liquids and suspensions can be used.

1.2 Stimuli-responsive polymeric nanocarriers

Stimuli-responsive polymers are those that, upon small external changes in the environmental conditions, undergo abrupt and relatively large physical or chemical changes.[30] The use of stimuli-responsive polymers has been reported for different purposes such as data storage, on-demand drug delivery, tissue generation/repair, biosensing, smart coatings, or artificial muscles.[31] Particularly interesting is the application of the stimulus-responsiveness to amphiphilic BCs based nanocarriers for drug delivery purposes.

Polymeric self-assemblies can be design to respond to different stimuli, allowing for the on-demand release of any encapsulated cargoes. The stimuli can be internal, from the physiological microenvironment, such as pH, redox or enzyme activity. Also, there are some readily available and relatively easily-controlled external stimuli such light, ultrasounds, magnetic fields or mechanical forces.[32,33] Temperature, which can be either an internal or external stimulus, is probably the most used stimuli to induce modifications in polymeric nanocarriers.

For example, Yang, Discher and co-workers reported the synthesis of thermo-responsive BCs comprised by poly(ethylene glycol) (PEG) and poly(*N*-isopropylacrylamide) (PNIPAM).[34] The polymers, which were amphiphilic at body temperature (37 °C), self-assembled into vesicles. With a decrease of the temperature below 32 °C, PNIPAM suffered a phase transition from a shrunken dehydrated state to swollen hydrated one, which altered the hydrophilic-hydrophobic balance and causes the destabilization of the vesicular structures. The thermo-responsive vesicles were used to encapsulate a hydrophobic fluorescent dye, PKH26, and a hydrophilic drug, doxorubicin, which were released upon a decrease of temperature.

pH-responsive polymers are particularly interesting for drug delivery systems because the difference in pH between solid tumours (6.5 to 7.0) and normal tissues (7.1 to 7.4) can induce selective release of encapsulated drugs in tumour sites.[35,36] Polymers with ionizable functional groups (*e.g.* amine groups) can respond to pH, as they may accept or donate protons upon changes in the pH of their surrounding

media, leading to changes in the solubility of the polymers. For instance, Kataoka *et al.* reported the synthesis of an amphiphilic diblock copolymer comprised by hydrophilic PEG and hydrophobic poly(β-benzyl-L-aspartate), that was able to self-assemble into spherical micelles in which doxorubicin was loaded.[37] Lowering the pH from 7.4 to 5.0 induced the release of doxorubicin, and studies on mouse C26 tumours showed a highly improved cytotoxicity of encapsulated doxorubicin in comparison to free doxorubicin.

Polymeric nanocarriers with redox-sensitive groups, such as disulphide bonds, have been devised to trigger the release of encapsulated drugs in response to intracellular redox potential.[38] Zhang *et al.* reported an amphiphilic diblock copolymer comprised by hydrophilic PEG and hydrophobic poly(caprolactone) (PCL), that was able to form spherical micelles into which an hydrophobic drug, docetaxel, was anchored *via* a disulphide bond.[39] *In vitro* studies showed the release of docetaxel upon the application of dithiothreitol, a reducing agent.

1.2.1 Light-responsive polymeric nanocarriers

Light is an especially interesting triggering agent because it is an efficient and clean stimulus that can be applied in a non-invasive way with excellent spatiotemporal control.[40] Several parameters such as light intensity, wavelength, pulse duration and exposure time can be easily tuned.[41,42] Light presents additional advantages compared to other stimuli such as temperature or pH, which usually offer poor control because they depend on physiological parameters that can vary between individuals, and even between different parts of the same individual.[43]

Light-responsive units can be classified in two categories depending on whether the changes or reorganizations induced by light are non-reversible or reversible. Upon application of adequate wavelength light, units such as *o*-nitrobenzoyl, coumarinyl or perylenylmethyl esters suffer irreversible cleavage of photolabile bonds. Units with reversible photoresponse include azobenzenes that undergo *trans*-to-*cis* photoisomerisation, spiropyrans that experience a reversible photoinduced ring opening/closure or coumarins that give photocycloadditions (Figure 1.6).

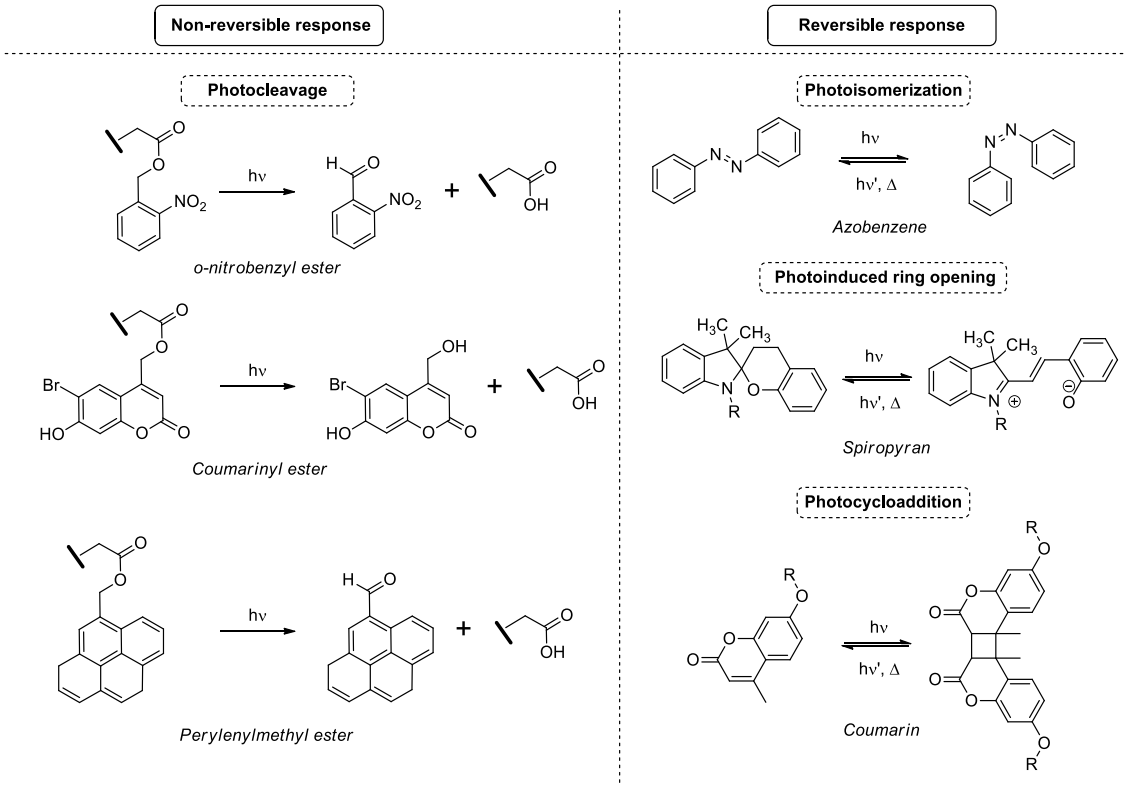

Figure 1.6: Light-responsive units and structural changes upon the application of light of adequate wavelength.

For the most common light-responsive units reported up to date, light-response is triggered upon application of UV light. However, when potential biological applications are devised, the use of UV light is not adequately because it has a low penetration power and produces photodamage of biological tissues.[44] Moving from UV- to visible- or near infrared- (NIR) responsive units is advisable as light of these wavelengths is less harmful. Besides, visible and NIR light have higher penetration power into biological tissues in comparison to UV light, from 1.0 mm at λ = 408 nm, to 6.3 nm at λ = 633 nm or 8.0 mm at λ = 705 nm.[45]

Organic units with response in the NIR region of the electromagnetic spectrum generally follow a two-photon absorption (2PA) process. 2PA processes were originally predicted by Maria Goeppert-Mayer in 1930s, although experimental verification had to wait to the development of laser technology late in 1960s when two-photon excited fluorescence was measured in an europium doped crystal by Kaiser and Garrett.[46] A 2PA process consists on the absorption of two photons of the same or different energy to excite a molecule from its ground state to a higher energy state, the excited state. The energy difference between the ground and the

excited states is equal to the sum of the energy of the two photons involved in the process. Usually, a 2PA process occurs at the double wavelength of the analogous one-photon absorption process. Two-photon responsive units have to meet two criteria: (1) an extended π-conjugated system with strong electron donor and electron acceptor groups at the extreme of the chromophores and, (2) a good two-photon cross-section. Whereas one-photon absorption processes depend linearly on the light intensity, 2PA processes increases with the square of the light intensity. Thus, most of applications that make use of 2PA require intense laser beams, in particular focused pulse lasers, able to generate very high instantaneous photon density because the inherent efficiency of 2PA processes is quite low.[47] Main drawbacks of 2PA processes are that irradiation is applied spot by spot hindering the use in large areas and, besides, their *in vivo* application is limited to superficial treatments as biological tissues defocus the laser.

When considering the incorporation of light-responsive units in amphiphilic BCs several approaches are possible. Units can be located at the juncture between the blocks, in the main chain or pending from one of the blocks (Figure 1.7). When a photocleavable unit is introduced in the juncture between the blocks as a linker, light stimulation breaks-up the covalent union of the blocks, separating them and destabilizing the self-assembled structure.[48] When a photocleavable unit is introduced in the main chain as part of the constitutive unit of one of the blocks, upon light-irradiation, the block is degraded into small molecules and, so, the self-assembled structure disrupted.

Introducing the light-responsive unit as a pendant substituent on one of the blocks, usually the hydrophobic one, is synthetically the easiest strategy and the most used in literature. Light might induce either shifting the hydrophilic/hydrophobic balance or reversible cross-linking. When looking for a shift in the hydrophilic/hydrophobic balance, photocleavable or photoisomerisable units are used. On the other hand, if the desired response is a reversible cross-linking, oftenly for increasing the stability of the self-assembled structures, units that undergo photocycloadditions are used. Inserting the light-responsive unit in the side chain offers the possibility of combining different light-responsive units or even units

sensitive to different stimuli to afford multi-wavelength light-responsive or multi-stimuli-responsive nanocarriers, respectively.

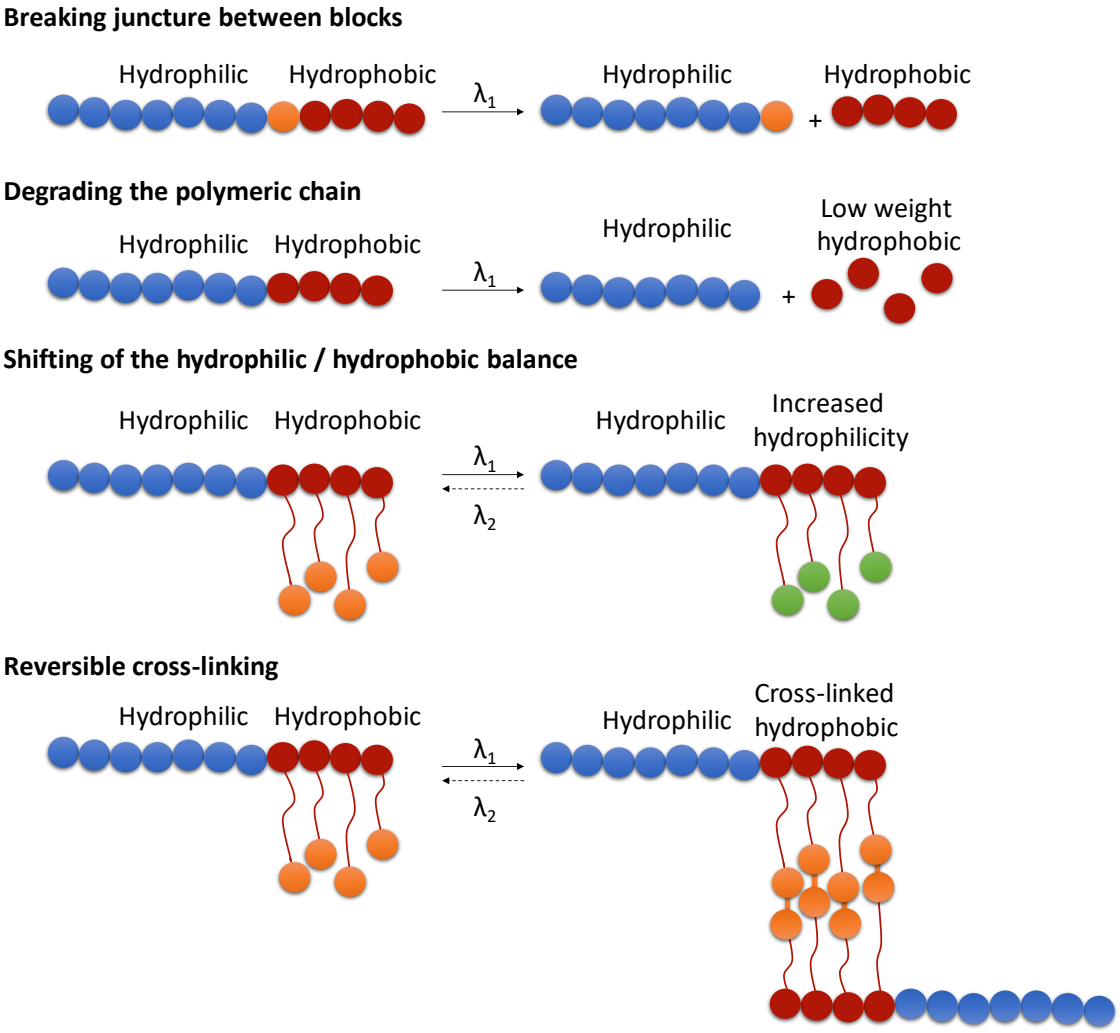

Figure 1.7: Photoinduced structural changes in amphiphilic BCs upon light application.

In this thesis we have focused our attention in photocleveable coumarinyl esters and photoisomerizable azobenzene as light-responsive units. The induced light-response of amphiphilic BCs carrying these units is associated to a shift in the hydrophilic/hydrophobic balance.

1.2.1.1 Coumarin units

Coumarins, also known as benzo-α-pyrones, are formed by the fusion of a pyrone ring with a benzene ring (Figure 1.8) and, along with benzo-γ-pyrones or chromones, form the class of heterocyclic compounds known as benzopyrones. Coumarins are fluorescent molecules with high fluorescence quantum yields in the blue region whose absorption/emission properties can be tailored by incorporating substituents at different positions. Several applications have been found for coumarin and its derivatives, from medical applications as anticoagulants, cosmetic additives, agrochemical industries or food additives to optical applications such as OLEDs,[49] chemical sensors,[50] light-harvesting materials,[51] or fluorescent probes in Biomedicine.[52]

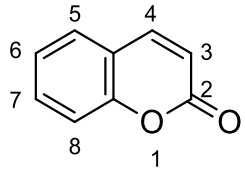

Figure 1.8: Chemical structure and numbering of coumarin.

One on the most recognized photoreactions of coumarins is [2+2] cycloaddition under UV irradiation, which can be reversed using UV light of higher energy. This photoreaction has been widely used in Materials Chemistry as a cross-linking alternative to methacrylate or epoxy cross-linking that require chemical reagents or produce unwanted by-products.[53]

In 1984, Givens and Matuszewski demonstrated the use of the (coumarin-4-yl)methyl group with a methoxy group in C7 as photoremovable protecting group. They synthesised a coumarinyl diethylphosphate derivative, which under 360 nm light and in the presence of nucleophiles as methanol, piperidine or cysteine rendered the free phosphoric acid diethyl ester and the nucleophile covalently bonded to the coumarin (Figure 1.9).[54] Since then, the photolabile properties of (coumarin-4-yl)methyl have been exploited to protect functional groups such as phosphates, amines, carboxylates, diols and carbonyls.[55,56]

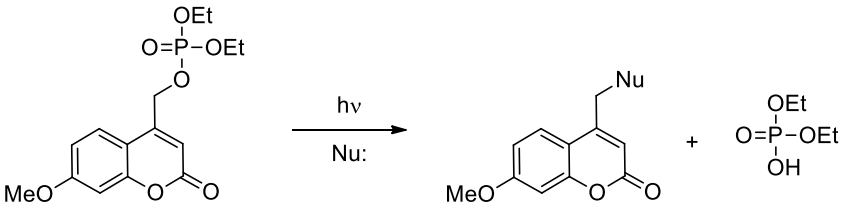

Figure 1.9: Chemical structure and photocleavage of a 7-methoxy(coumarin-4-yl)methyl unit.

This first generation of C7 hydroxy and methoxy substituted (coumarin-4-yl)methyl radicals presents two main drawbacks: poor solubility and low quantum yields for all protected groups except phosphates.[57] Introduction of bromine atoms in C6 lowers the pKa of the 7-hydroxy group by two units, easing the hydrolysis process and enhancing the solubility in water. Besides, the absorption maximum is displaced to 380 nm. The main weakness of bromo-substituted coumarins is that some of them tend to hydrolyse even in the dark. Thionation of the carbonyl displaces the absorption to the blue region, 470-500 nm with very low residual absorption in the UV region, which is very interesting for orthogonal activations with UV sensitive groups.[58,59]

Introduction of amino groups at C7 improves considerably the properties of the (coumarin-4-yl)methyl moieties by displacing their absorption maximum to 400 nm, which allows an efficient photorelease avoiding biologically harmful UV wavelengths. Particularly interesting is the coumarin radical with a diethylamino electro donor group at C7, (7-diethylaminocoumarin-4-yl)methyl (DEACM). DEACM has a strong absorption centred at 390 nm (ε = 2000 cm^{-1} M^{-1}) and extended up to 470 nm with a photolysis quantum yield of ≈ 0.3, the highest ever reported for analogous coumarins.[57] Besides, DEACM shows excellent water solubility.

Some (coumarin-4-yl)methyl moieties, including DEACM, present an extended π-conjugated system, with strong electron donor and electron acceptor groups and good 2PA cross-section values.[60,61]

1.2.1.2 Amphiphilic coumarin nanocarriers

There are few examples of coumarin amphiphilic BCs in the literature. Until today, most of examples use the reversible [2+2] cycloaddition of coumarin to improve the

stability of polymeric micelles by cross-linking either of the core (core cross-linking) or the shell (shell cross-linking).

Zhao and co-workers were the first to use [2+2] photocycloaddition of coumarin units in amphiphilic BCs.[53] The hydrophilic block was PEG, while the hydrophobic block was an statistical copolymer of coumarin methacrylate and methyl methacrylate (Figure 1.10). They found that upon [2+2] photocycloaddition of the coumarin units located in the hydrophobic core under 310 nm, the stability of the micellar system increased, while the de-crosslinking under 260 nm induced the release of encapsulated hydrophobic Nile Red.

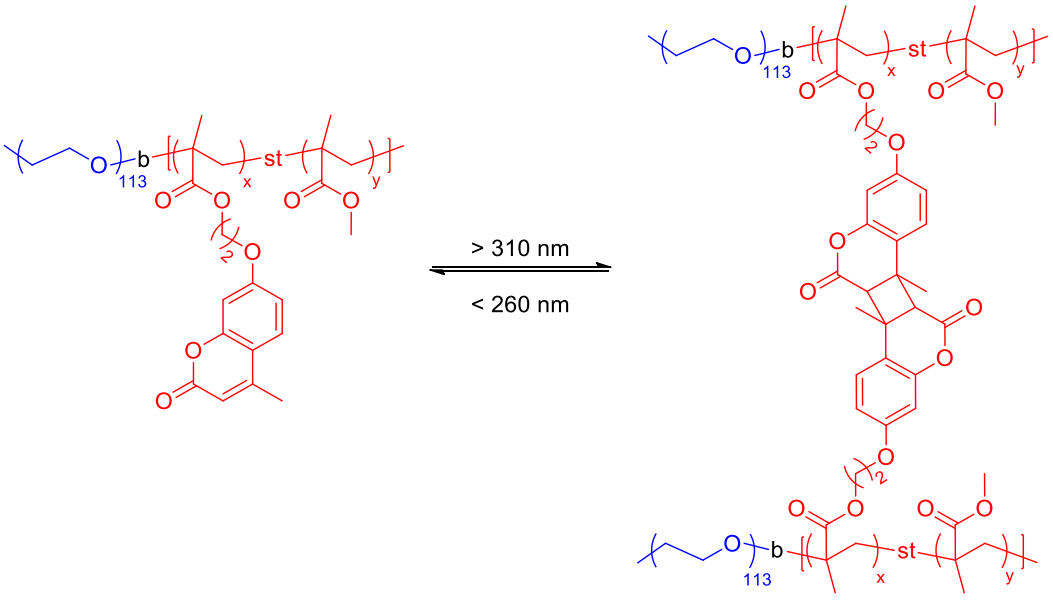

Figure 1.10: Structure of a coumarin functionalised amphiphilic diblock copolymer and reversible [2+2] cycloaddition upon light irradiation.[53]

Jin *et al.* reported the synthesis of an amphiphilic BC with coumarin units in the side chain of a poly(methacrylate) hydrophobic block.[62] The BC was used to covalently immobilise the hydrophilic 5-fluorouracil chemotherapeutic agent *via* a [2+2] cycloaddition between the coumarin and the uracil under 350 nm light. After drug conjugation, the copolymer was able to self-assemble into spherical micelles when dispersed in water and the micelle-drug conjugate system was able to release free 5-fluorouracil upon irradiating with 254 nm light. To prevent the favoured coumarin self-dimerisation instead of the 5-fluorouracil attachment, the number of

the photoresponsive coumarin groups was kept relatively low by copolymerising with butyl methacrylate.

Photolabile properties of (coumarin-4-yl)methyl esters have also been exploited to conjugate drugs to polymeric segments. Under light of adequate wavelength, the photolysis of coumarin units takes place, releasing the covalently bonded drug. Chen *et al.* have recently reported an amphiphilic molecule formed by linking the hydrophobic anticancer drug methotrexate to hydrophilic PEG *via* a 7-amino-(coumarin-4-yl)methyl moiety.[63] The amphiphilic molecule self-assembled into spherical micelles. UV light irradiation induced the photolysis of the coumarin ester unit, the destabilization of the micellar structure and the concomitant release of methotrexate. *In vitro* studies demonstrated an excellent anticancer activity of the drug conjugate. Following a similar strategy, Karthik *et al.* prepared photoresponsive polymeric nanocarriers consisting on a PCL segment conjugated to chlorambucil *via* a 7-hydroxy(coumarin-4-yl)methyl photolabile unit (Figure 1.11).[64] These nanocarriers were also able to encapsulate doxorubicin. Under 365 nm light irradiation, the photoscission of the coumarin unit led to the release of conjugated chlorambucil and encapsulated doxorubicin.

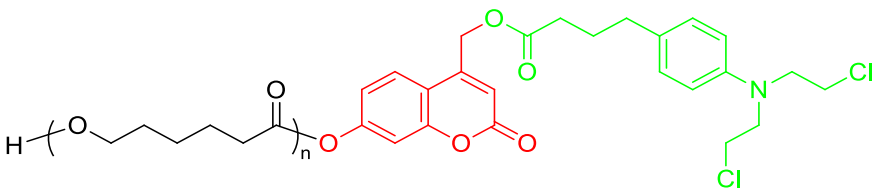

Figure 1.11: Structure of the caprolactone-chlorambucil conjugate *via* a 7-hydroxy(coumarin-4-yl)methyl ester photolabile unit. Chlorambucil appears in green and the coumarin unit in red.[64]

Nanocomposites of hollow mesoporous silica nanoparticles coated with BCs containing photocleavable coumarin units have been reported.[65] Upon NIR light irradiation, the cleavage of coumarin units from the BC led to the destabilization of the polymeric layer, inducing the release of doxorubicin loaded inside the porous of silica nanoparticles.

Up to date, few examples of amphiphilic BCs with photocleavable coumarin units are reported in literature. The use of photocleavable (coumarin-4-yl)methyl esters

in amphiphilic BCs leads to a large variation in the local polarity due to the transformation of an ester group into a carboxylic acid. Zhao and co-workers reported the first example of a diblock copolymer comprised by PEG and a poly(methacrylate) functionalised with DEACM moieties, able to self-assemble into spherical micelles (Figure 1.12).[66] Upon UV or NIR irradiation, the micelles were severely degraded, which induced the release of loaded Nile Red. Aiming to enhance the biocompatibility and biodegradability of the hydrophobic block, the coumarin methacrylate block was changed by poly(L-glutamic acid) partially esterified with 6-bromo-7-hydroxycoumarin-4-yl-methanol (Figure 1.12).[67] The UV- and NIR-responsiveness of the diblock copolymer was not altered, and the encapsulation and release of an anticancer drug, Paclitaxel, and an antibacterial drug, Rifampicin, was proved.

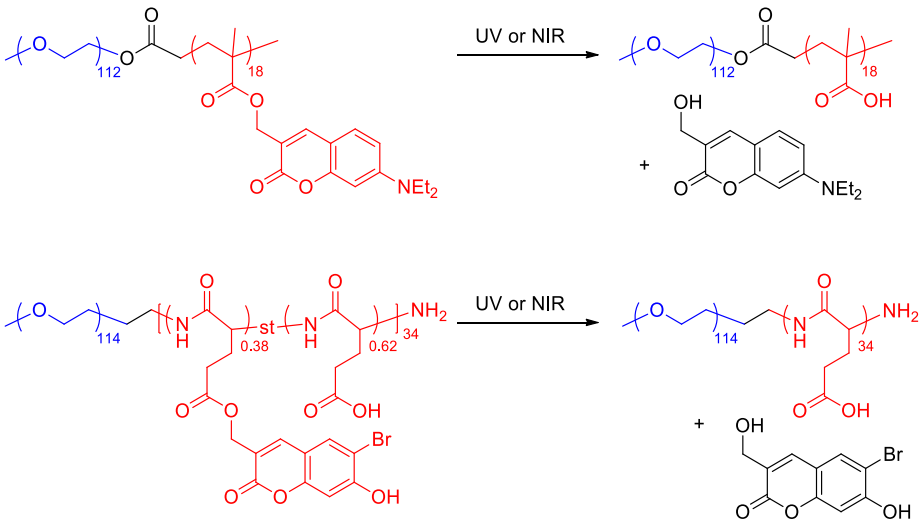

Figure 1.12: UV and NIR sensitive amphiphilic diblock copolymers with coumarinyl methyl esters reported by Zhao and co-workers and their photocleavage reaction.[68]

A novel reduction and light-responsive amphiphilic BC with DEACM and disulphide bonds was reported by Sun *et al.* (Figure 1.13).[69] The BC, which was able to self-assemble into vesicles, was used for encapsulation of small and large drugs, doxorubicin and TR-dextran respectively. This was the first reported polymeric vesicular system for which the release of small encapsulated molecules was possible while retaining the large ones. Thus, 365 nm light irradiation induced the cleavage of coumarin ester units and release of small molecules, while reduction with glutathione led to the release of the large molecules.

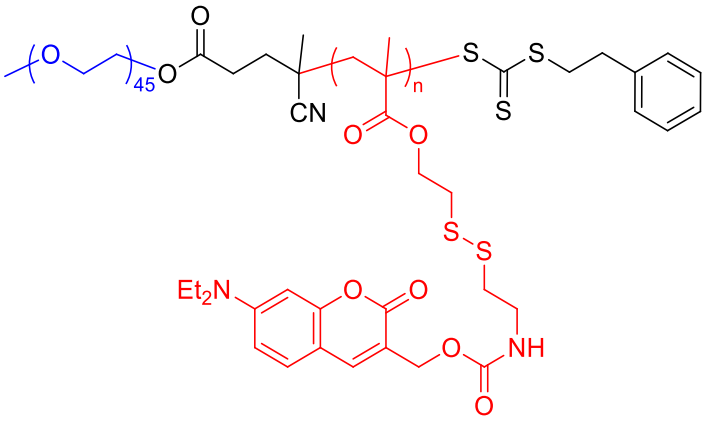

Figure 1.13: Redox and UV sensitive amphiphilic diblock copolymer with disulphide bonds and coumarinyl methyl esters reported by Sun and co-workers.[69]

Last, a series of dual-stimuli responsive random copolymers formed by thermo-responsive poly(triethylene glycol methyl ether methacrylate) and poly(6-bromo-4-hydroxymethyl-7-coumarinyl methacrylate) have been recently reported.[70] The cloud point temperatures could be finely adjusted depending on the proportion of each monomer, but moreover, it was also possible to tune the cloud point temperatures upon UV and NIR irradiation. However, encapsulation and stimulated release of small molecules was not studied.

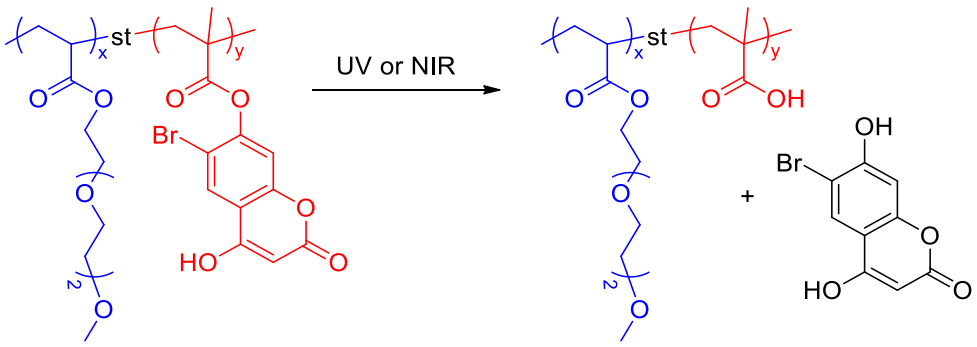

Figure 1.14: Structure of the amphiphilic diblock copolymer with 4-hydroxymethyl-7-coumarinyl units reported by Benoit *et al.* [70]

1.2.1.3 Azobenzene units

Amongst all light-responsive units used in polymer chemistry, the most widely studied are azobenzene derivatives, due to their high chemical and thermal stability.[71] Azobenzene molecule exists in a thermodynamically stable *trans* form with a strong π-π* absorption band centred in the UV region, and a weak n-π* absorption band in the visible region. Under illumination with UV light, azobenzene

undergoes a reversible *trans*-to-*cis* isomerisation that induces changes in the shape, from the lineal and coplanar *trans* to the bend and twisted *cis*. These structural changes increase the polarity the azobenzene from zero to 3.0 D (Figure 1.15).[72] The isomerisation is accompanied by a decrease in the intensity of the π-π* band and an increase in the intensity of the n-π* band. The metastable *cis* state will thermally relax back to the *trans* isomer or photochemically under visible light. Several applications of azobenzene containing polymers can be found in literature such as materials for optical storage,[73] photomechanical actuators,[74,75] or light-responsive nanocarriers.[76]

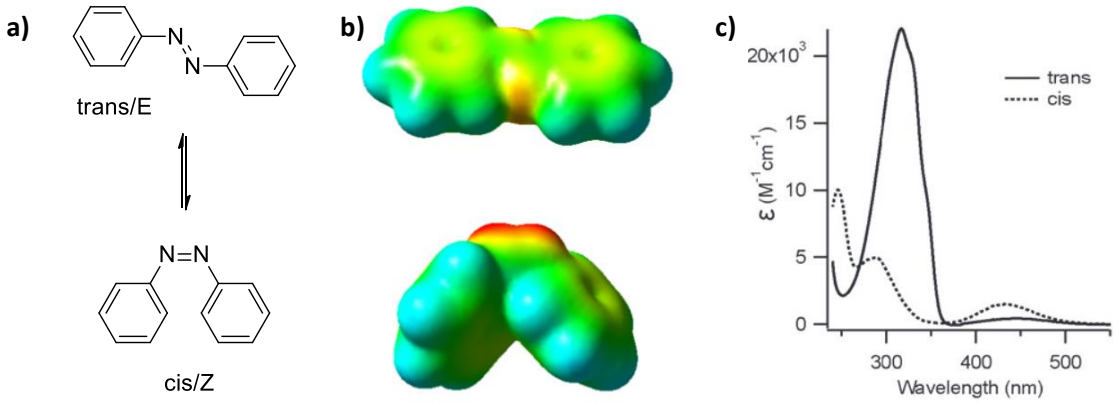

Figure 1.15: Structure of *trans* and *cis* azobenzene (a), ESP surface of *trans* and *cis* azobenzene coloured by electrostatic potential (red negative to blue positive) (b) and its absorption spectra (c).[77]

Azobenzene polymeric nanocarriers exploits the shift in the hydrophilic/hydrophobic balance induced by the change in polarity associated to *trans*-to-*cis* isomerisation because contributes to disruption of the self-assemblies morphologies. In this context, reaching high *cis* content states by light irradiation is advisable. For classical azobenzenes, the fastest way to get *cis* rich states is irradiating at the wavelength corresponding to the maximum π-π* absorption band. Because most of azobenzenes reported in literature present their π-π* absorption band in the UV region, getting *cis* rich photostationary states with either visible or NIR light is essential for the majority of biological uses.

The photochemical properties of azobenzenes can be tuned by changing the substituents located in the aromatic rings.[78] Reaching *cis* rich states using lower energy radiation than UV radiation can be achieved with diverse strategies, such as

displacing π-π* absorption band from UV to visible region or separating the n-π* absorption bands of *trans* and *cis* isomers, so *cis* rich states can be reached by irradiating in the n-π* band.

Aprahamian *et al.* in 2012 reported a BF_2 bridged azobenzene, with the *trans* and *cis* π-π* absorption bands displaced to the visible region.[79] The electronic structure is modified by coordination of BF_2 with the nitrogen lone-pair of the azo group and the extension of the π-conjugation, which lead to a new absorption band centred at 530 nm. Under irradiation at 570 nm, the *cis* form become dominant, with its absorption displaced to 480 nm (Figure 1.16). It is noteworthy that both the *trans*-to-*cis* and *cis*-to-*trans* isomerisations can be induced with visible light. Nevertheless, this kind of azobenzenes have a major drawback as in aqueous media the BF_2 bridge is converted to hydrazones.[80]

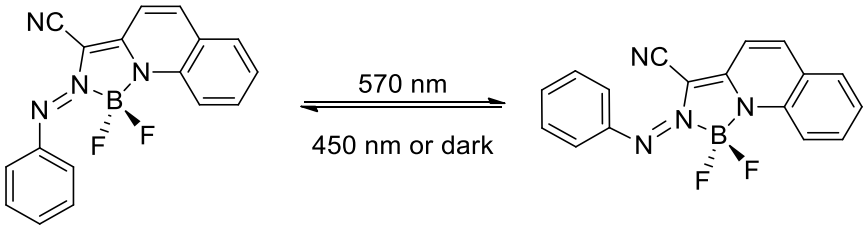

Figure 1.16: Structure of a BF_2 bridged azobenzene and its isomerisation.[79]

In 2009, Siewersten *et al.* reported the outstanding photochemical properties of C2 bridged azobenzenes or diazocines whose *cis* isomer is thermodynamically more stable than the *trans* one.[81] Because their *cis* and *trans* n-π* absorption bands are separated by 100 nm, the *cis*-to-*trans* and *trans*-to-*cis* isomerisations can be induced at a wavelength equal to n-π* absorption bands in an unusual complete way. Similar bridged azobenzenes with amino groups in the 3 and 3' positions have been reported whose *cis*-to-*trans* isomerisation is induced by irradiation with blue light, while the *trans* isomer can be converted completely back to the *cis* isomer with red light due to the good absorption coefficient of the *trans* isomer at this wavelength (Figure 1.17).[82] Nitrogen bridged diazocines also have been recently reported for which switching back to the *cis* isomer is accomplished with NIR light (up to 740 nm).[83] The fact that the *cis* isomer is more stable than the *trans* one has been used to

develop potassium channel blockers/openers whose activity is controlled by light irradiation.[84]

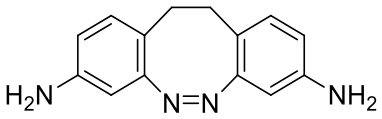

Figure 1.17: Structure of 3,3'-diamino-ethylene-bridged azobenzene.[82]

Azobenzenes with electron donor and electron acceptor groups at 4 and 4' positions, known as pseudo-stillbenes or push-pull azobenzenes, present a strongly asymmetric electron distribution within the conjugated system that leads to a displacement of the π-π* band to the visible region, which usually overlaps with the n-π* band (Figure 1.18).[85] Thus, *trans*-to-*cis* and *cis*-to-*trans* isomerisations can be induced with light of the same wavelength, being difficult to obtain a *cis* rich state. Push-pull azobenzenes with relaxation times as fast as 40 ns have been recently reported.[86]

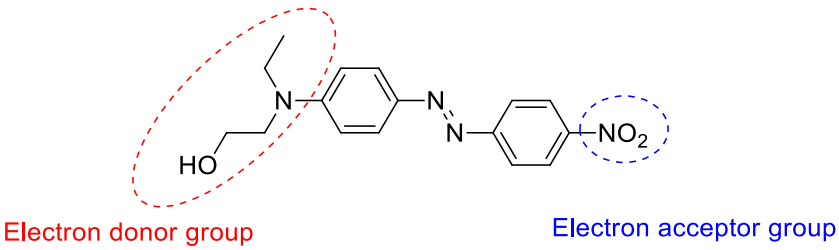

Figure 1.18: Structure of the push-pull azobenzene Disperse Red 1.

Wooley *et al.* described for first time the synthesis of tetra-*ortho*-substituted azobenzenes (Figure 1.19). By substituting the four *ortho*-positions of the azobenzene unit with halogen atoms, thioethers or methoxy groups, the aromatic rings in the *trans* isomer cannot be accommodated in the same plane, acquiring a twisted (non-planar) conformation.[87,88] This twisted conformation of the *trans* isomer blue-shifts the π -π* absorption band and red-shifts the n-π* absorption band. The red-shifting of the n-π* band is not observed for the *cis* isomer, as it is less affected by the repulsions between the *ortho*-substituents. Consequently, the n-π* absorption bands of the *trans* and *cis* isomers are separated enough to allow the independent *trans*-to-*cis* and *cis*-to-*trans* isomerisations upon irradiating in n-π* absorption band. Furthermore, because the red-shifted n-π* absorption band

of the *trans* isomer extends beyond 600 nm, the *trans*-to-*cis* isomerisation under red light was detected even if the absorption coefficient beyond 600 nm is almost negligible.[89]

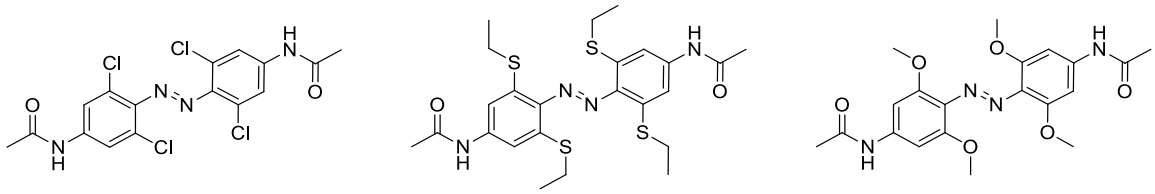

Figure 1.19: Tetra-*ortho*-substituted azobenzenes synthesised by Wooley's group.[87,88]

Push-pull azobenzenes with a strong asymmetric electron distribution are good candidates for 2PA processes and several studies have proved the sensitivity of some push-pull azobenzenes under 2PA. Mendonça *et al.* reported the induction of birefringence in poly(methyl methacrylate) (PMMA) films doped with Disperse Red 13 caused by the isomerisation of the dye under two-photon excitation at 775 nm.[90] Similar studies were performed by Ishitobi *et al.* in poly(methyl methacrylate) films doped with Disperse Red 1.[91,92]

Gorostiza *et al.* synthesised push-pull azobenzenes with covalently bonded naphthalene and pyrene antennas as sensitizers (Figure 1.20).[93] Under two-photon excitation at 730 nm, the antennas emitted in a spectral region overlapped with the absorption of azobenzene moieties, inducing its isomerisation *via* a radiative energy transfer process. Moreover, Isacoff *et al.* measured the 2PA cross-section spectra and proved the direct photoisomerisation of those push-pull azobenzenes irradiating at 840 nm no need to draw on the antenna effect (Figure 1.20).[94]

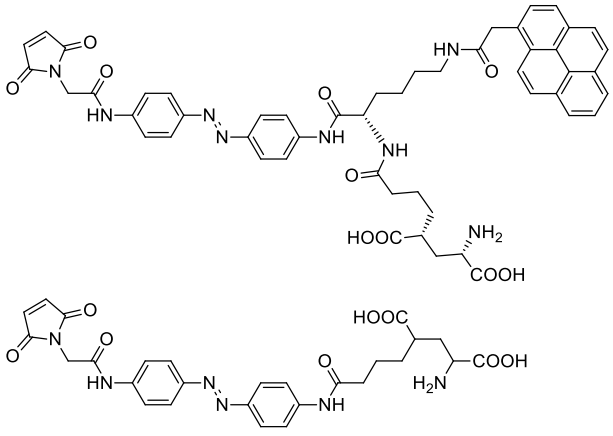

Figure 1.20: 2PA sensitive azobenzenes with[93] (top) and without[94] (bottom) antenna effect.

Last, the use of upconverting nanoparticles (UCNPs) is an attractive strategy to induce the indirect *trans*-to-*cis* isomerisation with UV light stimulation. UCNPs have the capacity of absorbing two photons of low energy and convert them into one single photon of higher energy.[95] Commonly, the upconversion is a 2PA process of NIR radiation with the subsequent emission of one single photon of UV-visible light that can be used to stimulate the isomerisation of an azobenzene. The use UCNPs benefits from advantages of NIR radiation such as light penetration in tissues compared to UV stimulation and, moreover, the emitted UV light produces minimum photodamage because the emission takes place in a nanometric scale.[96]

1.2.1.4 Amphiphilic azobenzene nanocarriers

Kano *et al.* described in 1980 the first light-responsive nanocarrier based on a low molar mass azobenzene.[97] The system, which consisted on a mixture of dipalmitoylphosphatidylcholine and an amphiphilic azobenzene compound, was able to self-assemble into vesicles when dispersed in water (Figure 1.21). The effective release of bromothymol, a blue dye, from the interior of vesicle upon light irradiation at 366 nm was assessed.

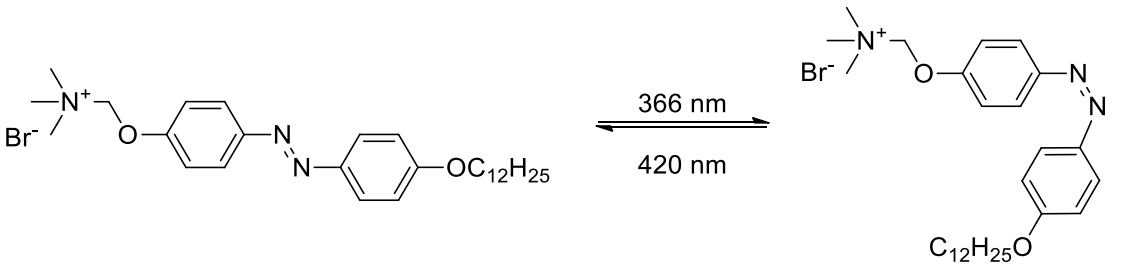

Figure 1.21: Isomerisation of the amphiphilic azobenzene molecule used by Kano *et al.*[97]

Zhao and co-workers, reported the first light-responsive nanocarrier from an azobenzene containing amphiphilic BC. The system consisted on a diblock copolymer formed by hydrophilic poly(methacrylic acid) and a hydrophobic poly(methacrylate) with mesogenic 4-methoxyazobenzene moieties anchored into the side chain (Figure 1.22).[76] Micelles and vesicles were formed by the co-solvent method with dioxane and water. Upon UV light irradiation a liquid crystal-to-isotropic liquid transition was induced by the *trans*-to-*cis* isomerisation on the

liquid crystalline azobenzene block, causing changes in the morphology of the self-assemblies. The encapsulation and the light-triggered release properties of the self-assemblies were not tested (Figure 1.22).

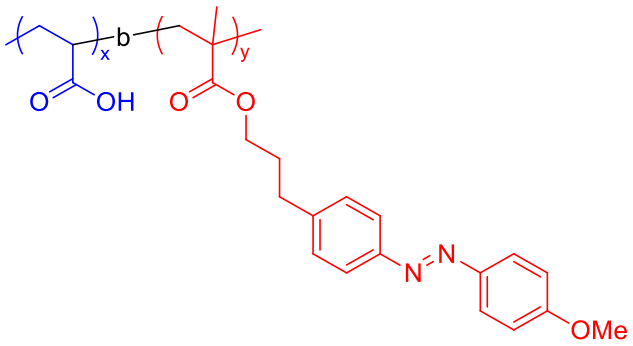

Figure 1.22: Structure of the azobenzene functionalised amphiphilic BC reported by Zhao *et al.*[76]

Amphiphilic BCs with azobenzene moieties have been reported by the Liquid Crystals and Polymers Group (University of Zaragoza), which include diverse polymeric architectures. Del Barrio *et al.* described a series of linear-dendritic block copolymers (LDBC) comprised by PEG of 2000 g mol^{-1} average molar mass as hydrophilic block, and different generations of 2,2-bis(hydroxymethyl)propionic acid (bis-MPA) dendrons (from the 1st to 4th generation) with cyanoazobenzene units anchored into the periphery as hydrophobic block (Figure 1.23).[98] A dendron generation-dependent morphology of the self-assemblies was observed from nanofibers, sheet-like aggregates, tubular micelles and sheet-like aggregates, to vesicles for the 1st, 2nd, 3rd and 4th generation, respectively. Disruption of the vesicles morphology was observed by Cryo-TEM upon UV light illumination.

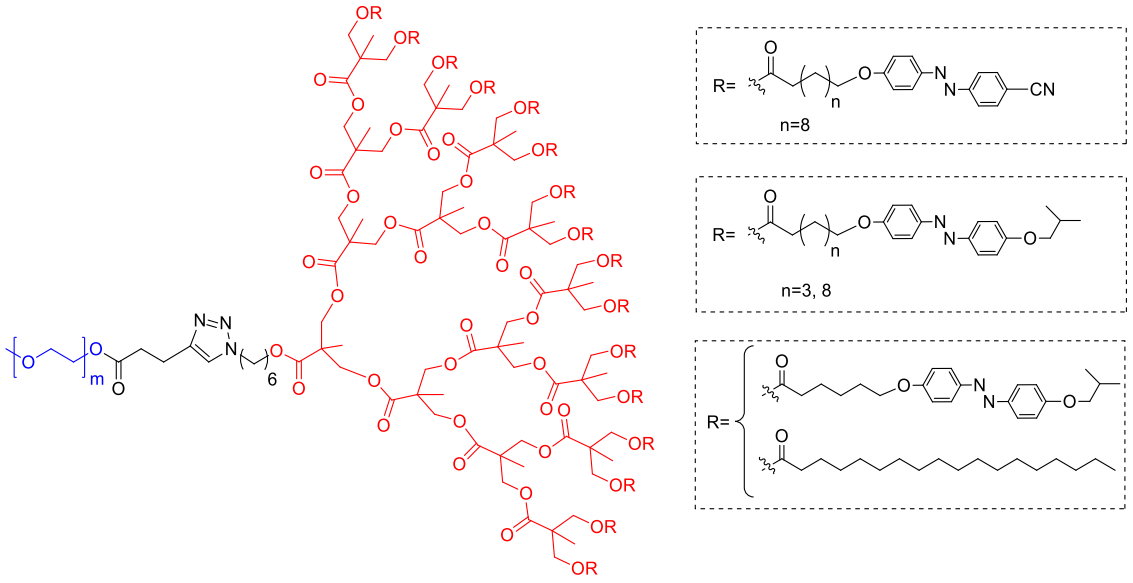

Figure 1.23: Structure of the azobenzene functionalised LDBC synthesised in the Liquid Crystals and Polymers Group (University of Zaragoza).

Afterwards, Blasco *et al.* reported the synthesis of a LDBC consisting of PEG with an average mass of 2000 g mol^{-1} and the 4th generation bis-MPA dendron with isobutyloxyazobenzene moieties into the periphery (Figure 1.23).[99] Changing the azobenzene substituent from cyano to isobutyloxy had no influence on the self-assembly behaviour, but it was found that the disruption of the self-assemblies morphology took place under UV light of significantly lower intensity. Besides, the encapsulation and light-induced release of hydrophobic Nile Red and hydrophilic Rhodamine B was demonstrated. Aimed by the results, authors also demonstrated that the light induced release profile was modulated by dilution of azobenzene moieties in the periphery with C18 hydrocarbon chains (Figure 1.23). When using the 4th generation dendron with a 50/50 molar ratio of isobutyloxyazobenzene/C18 light triggered release was much faster.[100]

Later on, García-Juan *et al.* reported dual-stimuli self-assemblies by replacing the PEG block by a thermoresponsive random copolymer of di(ethylene glycol) methyl ether methacrylate (DEGMA) and oligo(ethylene glycol) methyl ether methacrylate (OEGMA).[101] This LDBC was able to self-assemble into vesicles and encapsulate hydrophobic Nile Red or hydrophilic Rhodamine B. Release of the payloads was induced by both light and temperature.

A series of miktoarm polymers of A_3B type were reported by Blasco *et al.* , formed by a hydrophobic arm with an isobutyloxyazobenzene poly(methacrylate) and three hydrophilic arms of either PEG or thermoresponsive poly(*N,N*-diethylacrylamide) (Figure 1.24).[102,103] The polymers were found to self-assemble into vesicles or micelles, being demonstrated the encapsulation and UV-triggered release of fluorescent probes

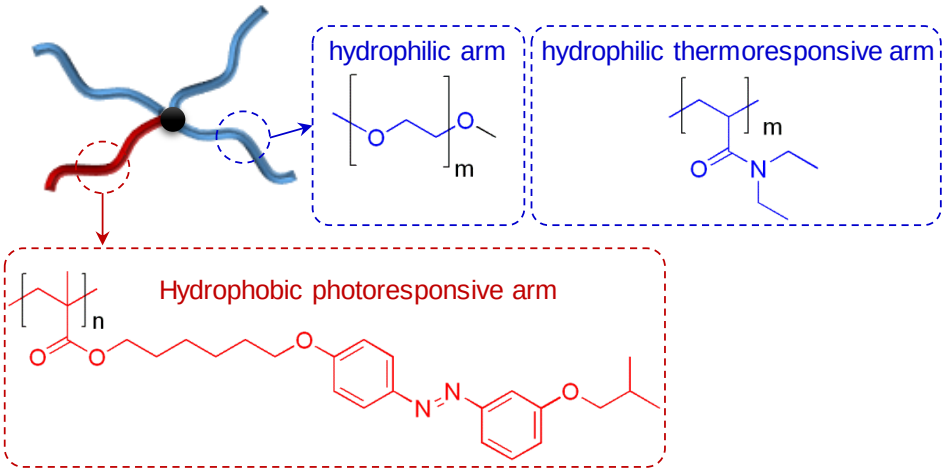

Figure 1.24: Structure of the azobenzene functionalised miktoarm polymers synthesised in the Liquid Crystals and Polymers Group (University of Zaragoza).

Concellón *et al.* recently reported the synthesis of linear diblock copolymers comprised by hydrophilic PEG and an hydrophobic polymethacrylate block with 2,6-diacylaminopyridine (DAP) pendant groups.[104,105] The azobenzene units were introduced by complexation of DAP and complementary thymines or carboxylic acids unit *via* hydrogen bonding (Figure 1.25). Depending on the length of the PEG chain, both micelles and vesicles were obtained in water. Low intensity UV illumination of the self-assemblies resulted in morphological changes, confirmed by TEM, DLS and SAXS, that ultimately led to the release of encapsulated molecules.

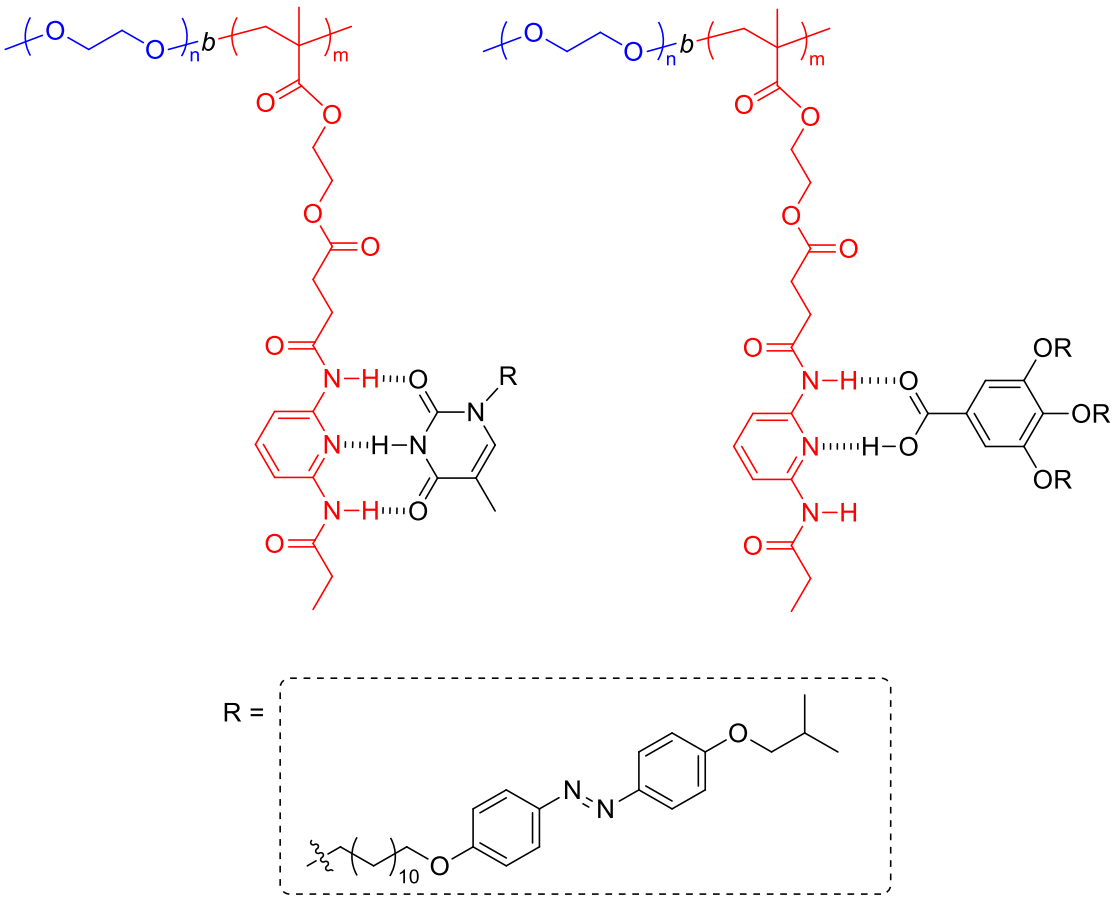

Figure 1.25: Structure of the azobenzene functionalised by H-bond supramolecular polymers synthesised in the Liquid Crystals and Polymers Group (University of Zaragoza).[105]

Recently, Xia *et al.* have reported a light and pH dual-sensitive amphiphilic diblock copolymer consisting on hydrophilic PEG and a hydrophobic aliphatic polycarbonate block functionalised both with ethylendiethylamine and an azobenzene moiety (Figure 1.26).[106] The polymer was able to form spherical micelles into which the encapsulation of doxorubicin was proved. Under UV light or pH stimuli, the release of encapsulated doxorubicin took place. Besides, the materials proved to be non-cytotoxic against HepG2 and SMCC-7721 cells.

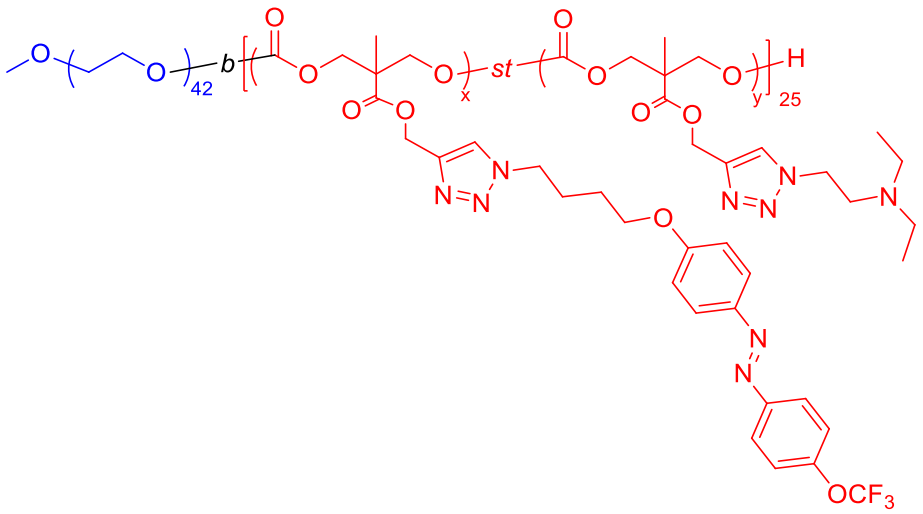

Figure 1.26: Structure of the azobenzene functionalised amphiphilic BCs reported by Xia *et al.* [106]

All the aforementioned examples require of UV light to stimulate the release and present the already referred limitations when biological applications are considered. Dong *et al.* prepared a visible-responsive BC by introduction of a push-pull azobenzene in the BC structure (Figure 1.27).[107] The *trans*-to-*cis* isomerisation in solution by irradiating in the π -π* band at 450 nm was proved. The BC self-assembled into vesicles when dispersed in water and morphological changes were observed by TEM and DLS upon illumination with 450 nm light. However, the encapsulation/light-stimulated release properties were not evaluated.

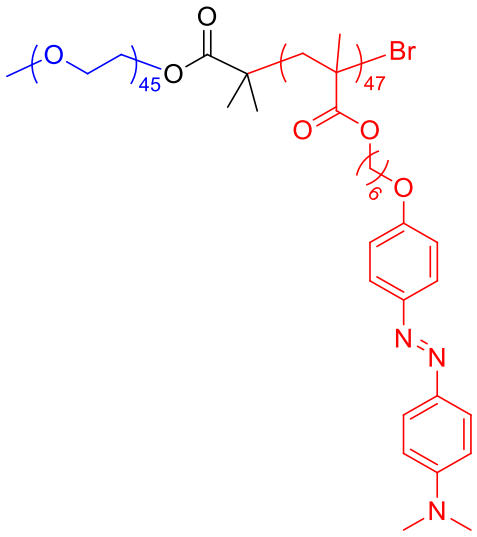

Figure 1.27: Structure of the push-pull azobenzene amphiphilic BC reported by Dong *et al.* [107]

Wang *et al.* reported a random copolymer of poly(acrylic acid) and tetra-*ortho*-methoxy substituted azobenzene poly(methacrylate) (Figure 1.28).[108]

The copolymer was able to self-assemble into spherical micelles in water. Though the isomerisation of azobenzene under green light was demonstrated in solution, the slight morphological changes appreciated in the self-assemblies upon green light irradiation did not trigger the release of encapsulated Nile Red.

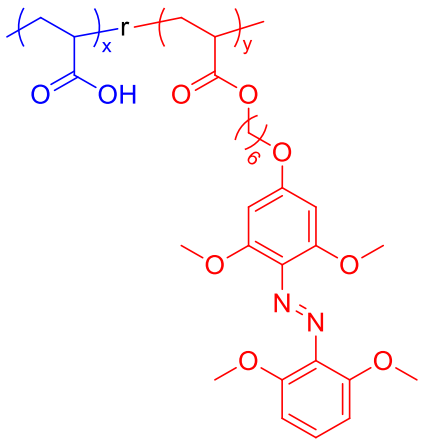

Figure 1.28: Structure of the tetra-*ortho*-methoxyazobenzene amphiphilic random copolymer reported by Wang *et al.*[108]

Recently, Zheng and co-workers have reported a visible light-, pH-, and cyclodextrin-responsive azobenzene polymeric nanocarrier formed by poly(2-dimethylaminoethyl methacrylate) functionalised with a tetra-*ortho*-methoxy substituted azobenzene (Figure 1.29).[109] The random amphiphilic copolymer self-assembled into micelles, in which Nile Red was encapsulated. Upon irradiation with green light, small variations in the morphology of the micelles were induced and Nile Red release was triggered to a minor extent. Nonetheless, pH and cyclodextrin were able to trigger appreciable changes in the morphology of the micelles and so, release the encapsulated Nile Red.

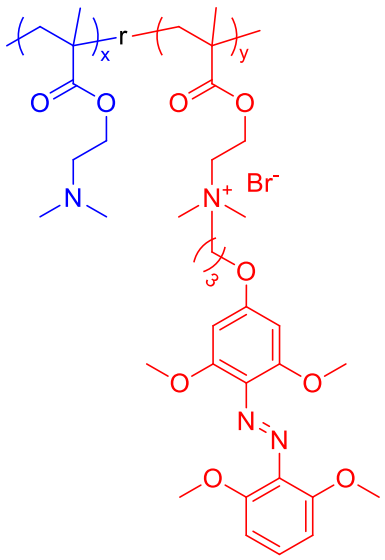

Figure 1.29: Structure of the tetra-*ortho*-methoxyazobenzene amphiphilic random copolymer reported by Zheng *et al.* [109]

As a last example of amphiphilic BCs with visible-responsive azobenzenes, Qian *et al.* have published very recently a block copolymer comprised by PNIPAM as hydrophilic block and a poly(methacrylate) functionalised with a tetra-*ortho*-methoxyazobenzene as hydrophobic block (Figure 1.30).[110] The self-assembly into micelles when dispersed in water was tested, and moreover, it was possible to tune the size of the self-assemblies under visible light irradiation. However, the encapsulation and the light-stimulated release of small molecules was not evaluated.

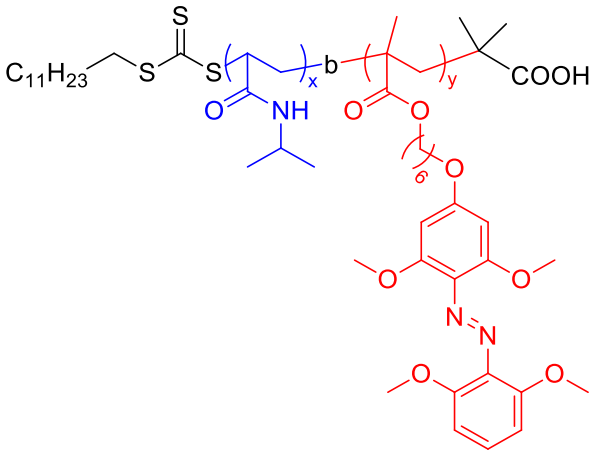

Figure 1.30: Structure of the tetra-*ortho*-methoxyazobenzene amphiphilic BC reported by Qian *et al.* [110]

As azobenzene presents low 2PA sensitivity, and 2PA processes require high power density to trigger the photoreaction, up to date there are no examples of light-responsive nanocarriers based on direct 2PA excitation of azobenzene units.[111] However, indirect NIR excitation of an amphiphilic diblock copolymer with azobenzene units *via* UCNPs has been reported. A colloidal nanocluster of $NaYF_4$:Gd/Yb/Tm UCNPs and an amphiphilic diblock copolymer comprised by hydrophilic OEGMA and an hydrophobic azobenzene poly(methacrylate) was reported by Yan *et al.* (Figure 1.31).[112] Under NIR excitation, the *trans*-to-*cis* isomerisation of azobenzene units took place induced by the emitted UV light from UCNPs. Doxorubicin was loaded into the colloidal nanocluster and release under NIR irradiation.

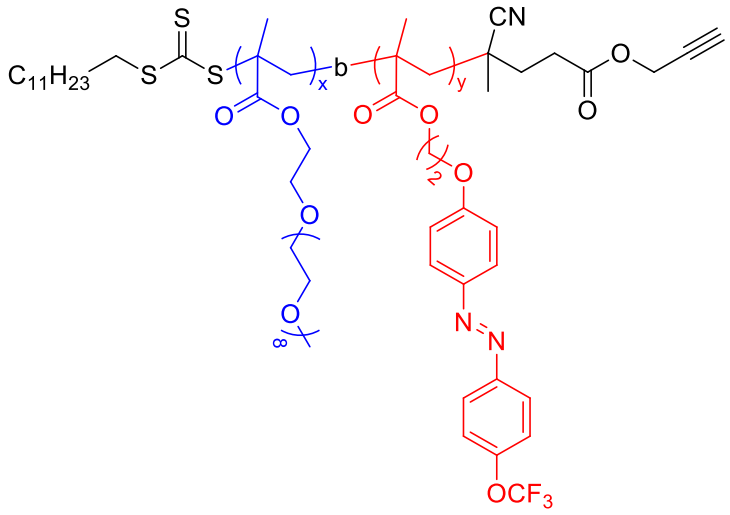

Figure 1.31: Structure of the amphiphilic BC assembled onto $NaYF_4$:Gd/Yb/Tm UCNPs reported by Yan *et al.*[112]

1.3 Synthesis of functional block copolymers

Advances in the polymer chemistry field over the last decades have enabled the synthesis of well-defined polymeric structures with controlled composition, chain-ends and length, molecular weight distribution and diverse topologies. Controlling the design and properties of the amphiphilic BCs, such as polymerisation degree and dispersity (*Đ*) of each block, plays a key role in controlling the interaction between the different polymeric segments with each other and within the solvent, and so, it has a drastic influence over the self-assemblies properties as morphology, size or dispersity.[10,113] As the final properties of the polymeric nanocarriers are intimately linked with the synthesis of the BC, finding polymerisation techniques with good control over the polymerisation process is crucial.

The discovery of living polymerisations in the 1950's and the later development of controlled polymerisation techniques, combined with click chemistry reactions for the post-polymerisation modification of the polymeric backbone, have eased the synthesis of precision and functionalised amphiphilic diblock copolymers, including those with response to stimulus as light. Post-polymerisation modifications can be introduced by supramolecular chemistry as well, being a much more versatile strategy and synthetically easier than covalent post-functionalisation.

1.3.1 Synthesis of amphiphilic diblock copolymers

The synthesis of a diblock copolymer can be addressed by three methods: sequential monomer addition, coupling blocks previously synthesised or polymerisation of a monomer using a macroinitiator (Figure 1.32).

When using the sequential monomer addition approach, a monomer is first polymerised by an adequate technique and then, once it is completely consumed, the polymerisation is reactivated by adding the second monomer. The main disadvantage of this strategy is that both monomers need to be polymerised by the same mechanism.

The coupling of preformed blocks methodology requires that the terminal groups of each block have complementary reactivity. The main advantage of this approximation is that both blocks can be separately polymerised by using different techniques and, consequently, isolated and characterised prior to be conjugated.

Last, using a macronitiator for the polymerisation of a monomer is rather straightforward and closely related to the first described approach. In this case, the first monomer is polymerised rendering a polymer that it is used as a macroinitiator for the polymerisation of the second monomer. The macroinitiator is isolated, purified, and even its chemical reactivity can be tuned prior to use. Thus, when using this strategy, the monomers do not have to be polymerised by the same polymerisation mechanism.

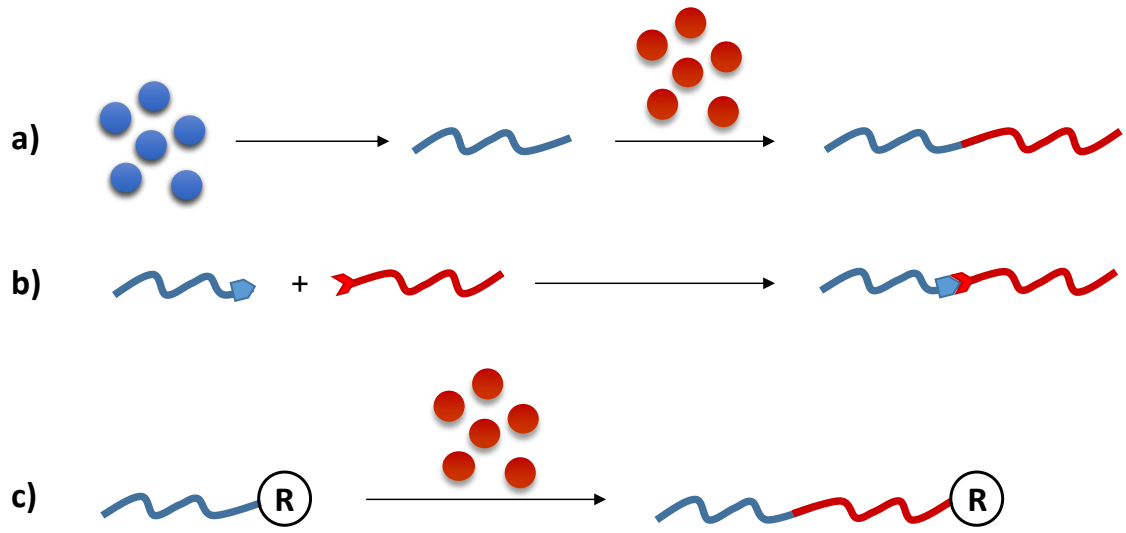

Figure 1.32: Synthetic approaches to diblock copolymers: Sequential polymerisation (a), coupling of preformed blocks (b) and use of a macroinitiator (c).

1.3.2 Aliphatic polycarbonates

When looking for biomedical applications, it is of vital importance the use of low cytotoxicity and biocompatible materials, being specially interesting those that are also biodegradable, as they may be degraded and removed after they have served their function.[114,115] In the polymers field, the most studied biodegradable ones are, by far, poly(esters). The main drawback of biodegradable poly(esters) is that their degradation can increase the levels of acidity, which may led to inflammation of human tissues[116] or degradation of small loaded molecules when used as polymeric

nanocarriers.[117,118] In comparison, aliphatic poly(carbonates) (APCs), whose constitutional units have carbonate bonds linking flexible aliphatic segments, are better candidates for drug delivery systems because no acidic compounds are produced during its degradation, and besides, its degradation rate is lower than for poly(esters), which may be useful for long-term *in vivo* circulation.[119,120]

The synthesis of APCs can be addressed by three methods: polycondensation, copolymerisation of epoxides with carbon dioxide and ring opening polymerisation (ROP) of cyclic carbonates. The synthesis of APCs by polycondensation was originally developed for the reaction between toxic phosgene or its derivatives and aliphatic diols, though further developments on this techniques led to the substitution of phosgene derivatives by dialkyl carbonates (Figure 1.33). This polycondensation offers poor control over the molecular weight and *Đ*. The catalyst, reaction temperature and the proportion between the dialkyl carbonate and the aliphatic diols have a great influence on the final polymer.

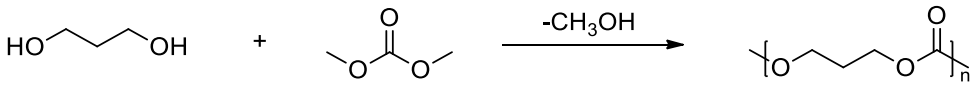

Figure 1.33: Synthesis of aliphatic polycarbonates by polycondensation.

Originally developed by Inoue *et al.* in 1969,[121] the copolymerisation of carbon dioxide with epoxides is a valuable and sustainable method, even at industrial scale (Figure 1.34). However, because most of the commercially available cyclic ethers are limited to three membered rings, the synthesis of APCs with constitutional repetitive units having higher aliphatic lengths is restricted.[122] The need of either heterogeneous (as zinc) or homogeneous (as aluminium-porphyrin complexes or zinc-phenoxide derivatives) metal catalysts also makes this strategy unattractive for biomedical applications.

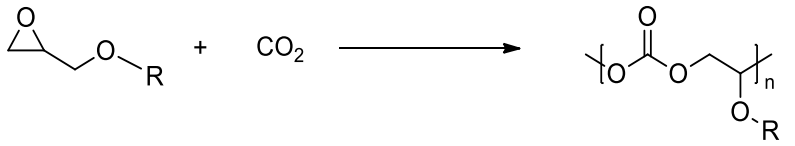

Figure 1.34: Synthesis of aliphatic polycarbonates by copolymerisation of CO_2 with epoxides.

ROP of cyclic carbonates allows the preparation of a great variety of APCs with good control over the molecular weight and *Đ* in short times and under mild conditions (Figure 1.35).[123]

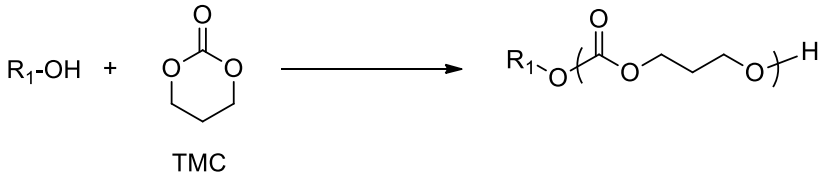

Figure 1.35: Synthesis of aliphatic polycarbonates by ROP of a cyclic carbonate, TMC.

The first ROP of a cyclic carbonate, trimethylene carbonate (TMC), was reported in 1932. Polymerisation was carried out in the melt state using potassium carbonate as the catalyst but side reactions such as decarboxylation in the polymeric backbone were detected.[124] Since this first example, several advances in the field have diminished the aforementioned side reactions and, now, ROP is actually considered a controlled polymerisation that affords polymers with controlled structure and molecular mass. ROP of cyclic carbonates can be carried out either in solution or melt state following diverse mechanisms, including cationic, anionic, coordination insertion, organocatalytic or enzymatic ones. Many catalysts have been used in the literature such as transition metals, alkyl halides, organocatalysts or enzymes.[122] Metal catalysts are highly active and offer good control over the ROP of cyclic carbonates, being one of the most used tin(II) 2-ethylhexanoate or tin(II) octoate ($Sn(Oct)_2$). Even though the use of $Sn(Oct)_2$ is approved by the U.S. Food and Drug Administration, it is still a rather toxic compound.[125] Therefore, for biomedical applications, it is especially interesting the use of organocatalysts. Pratt *et al.* tested the ROP of TMC using either 1.5.7-triazabicyclo-[4.4.0]dec-5-ene (TBD) or a combination of 1-(3,5-bis(trifluoromethyl)-phenyl)-3-cyclohexyl-2-thiourea (TU) and 1,8-diazabicyclo[5.4.0]undec-7-ene (DBU).[126] With TBD, ROP proceeded in short reaction times but the polymers showed broad dispersities, while the combination of TU/DBU showed excellent control over the polymerisation in relatively short times with low dispersities.

ROPs are initiated by a nucleophile, generally an alcohol. In this sense, the use of hydroxy-functionalised macromolecules, acting as macroinitiators, provides diblock

copolymers in a straight way. In particular, the use of poly(ethylene glycol) methyl ether (PEG-OH) with an hydroxyl terminal group as initiator of the ROP of cyclic carbonates is a common strategy to obtain amphiphilic diblock copolymers comprising an aliphatic polycarbonate hydrophobic block (Figure 1.36).

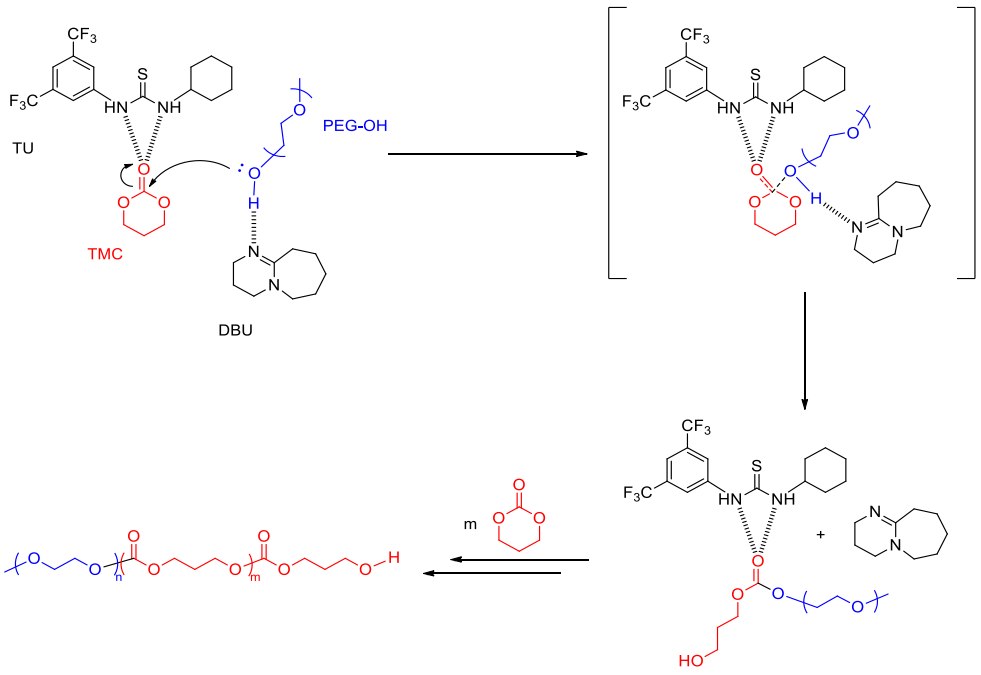

Figure 1.36: Mechanism of the ROP of TMC using PEG-OH as initiator and the organocatalytic system TU/DBU.

The use of bis-MPA for the synthesis of cyclic carbonates was firstly reported by Bish *et al.* in 1999.[127] Bis-MPA is a versatile molecule with two different functional groups, a carboxylic acid an two hydroxyl ones, which allows the introduction of functionalities in a polycarbonate chain in an simple way. Being a 1,3-diol, cyclic carbonates from bis-MPA can be easily prepared upon cyclisation with phosgene or ethyl chloroformate, a phosgene derivative (Figure 1.37). Additionally, esterification of the carboxyl group, either under acidic or basic conditions, can be used to incorporate functionality.

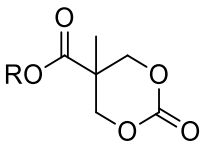

Figure 1.37: Structure of a cyclic carbonate derived from bis-MPA, R is the functional unit that will be introduced in the side chain of the polymeric backbone.

Bis-MPA based cyclic carbonates with allyl or propargyl esters are of particular interest because the ROP polymerisation of these monomers affords polycarbonate skeletons that can be further modified using highly efficient reactions such as thiol-ene or Cu(I)-catalysed alkyne-azide cycloaddition (CuAAC) from the collection of the so-called 'click chemistry' reactions. The allyl-functionalised cyclic carbonate, 5-methyl-5-allyloxycarbonyl-1,3-dioxan-2-one (MAC), has been used for the preparation of several polymers and copolymers. The ROP of MAC to yield the corresponding allyl functionalised polycarbonate (PC(A)) has been conducted under different conditions, such as in the molten state at 115 °C without catalyst or in toluene at 95 °C using a tin(II)-based catalyst, with poor control over the molecular weight and dispersity.[128] Various examples of amphiphilic diblock copolymers with a PC(A) block can be found in literature that have been synthesised using PEG-OH as initiator (Figure 1.38). Lv *et al.* reported the synthesis of a diblock copolymer comprised by hydrophilic PEG and a hydrophobic block formed by copolymerisation of MAC and dimethyltrimethylene carbonate (DTC) by enzymatic ROP using immobilized porcine pancreas lipase (IPPL) as catalyst.[129] Hu *et al.* reported the copolymerisation of L-lactide and MAC using PEG-OH as initiator and diethyl zinc as catalyst.[130] Tempelaar *et al.* reported the preparation of an amphiphilic diblock copolymer comprised by PEG and PC(A) by using the organocatalytic system sparteine/TU.[131] Yu *et al.* have recently reported the organocatalysed ROP of MAC using PEG-OH as initiator with TU/DBU as catalytic system.[132]

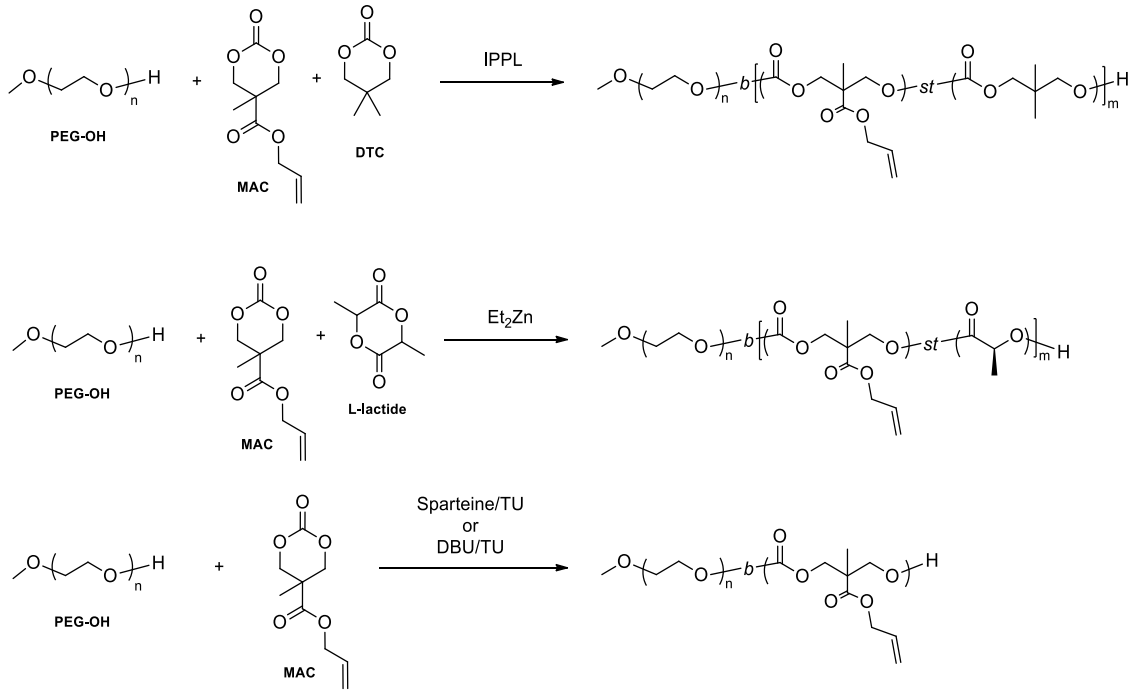

Figure 1.38: Synthesis of allyl functionalised amphiphilic diblock copolymers by enzymatic,[129] metallic[130] and organocatalysed[131,132] ROP of MAC initiated by PEG-OH.

The ROP of the propargyl ester of the bis-MPA based cyclic carbonate, 5-methyl-5-propargyloxycarbonyl-1,3-dioxan-2-one (MPC), to afford the corresponding propargyl functionalised polycarbonate (PC(P)) has also been described. Lu *et al.* reported on the copolymerisation of MPC and L-lactide in the molten state at 100 °C using benzyl alcohol as initiator and diethyl zinc as catalyst.[133] In 2008, Hedrick's group reported the copolymerisation of MPC with TMC in dichloromethane using the TU/DBU catalytic system and 4-pyrene-1-butanol as initiator.[126] The polymerisation of MPC catalysed by either DBU or TU/DBU and PEG-OH as initiator has been used to obtain copolymers with good control over the polymerisation degree and narrow dispersities by Dove,[134] Hu *et al.*[135] and Xia *et al.*[136,137] amongst others (Figure 1.39).

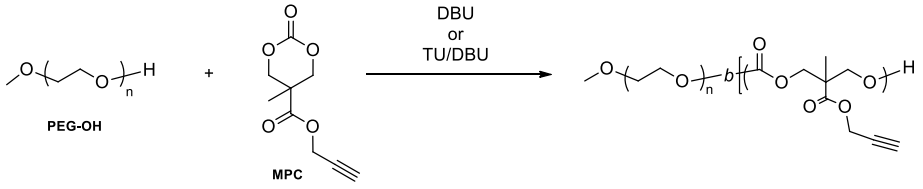

Figure 1.39: Synthesis of propargyl functionalised amphiphilic diblock copolymers by organocatalysed ROP of MPC initiated by PEG-OH.[134,135,136,137]

1.3.3 Post-polymerisation modifications

Introduction of functionalities such as light-responsive units in the side chain of a pre-formed polymeric backbone, is a very attractive strategy that allows the preparation of families of materials with diverse functionalities from the same polymeric scaffold. The main advantage of this post-polymerisation functionalisation is that all derivatives share the same polymerisation degree and dispersity. This is particularly relevant for the fabrication of polymeric nanocarriers as the morphology, size or dispersity of the self-assembled nanoparticles are directly related to the polymerisation degree or dispersity of the polymeric scaffold. Additionally, this approach also overcomes the limitations associated to monomers bearing specific functionalities, which often encounters that their availability and reactivity is limited.

1.3.3.1 Covalent functionalisation

"Click chemistry" is a term introduced by Sharpless in 2001 that gathers a series of reactions with quantitative yields under mild conditions, highly stereospecific and simple to perform experimentally. These features make click chemistry reactions very interesting for their application in post-polymerisation functionalisation strategies. Click chemistry reactions comprise [3+2] cycloadditions such as the Cu(I)-catalysed alkyne-azide cycloaddition (CuAAC), thiol-ene and thiol-yne reactions, Diels-Alder reaction or [4+1] cycloadditions between isocyanides and tetrazines amongst others.

CuAAC was independently reported by Fokin and Sharpless[138] and by Meldal *et al.*[139] in 2002 and it has become the most used click reaction. The non-catalysed cycloaddition gives a mixture of 1,4 and 1,5 disubstituted 1,2,3-triazoles, while the catalysed mechanism is regioselective and yields only the 1,4 disubstituted one (Figure 1.40). Most frequent Cu(I) sources are copper(I) bromide or iodide. Alternatively, Cu(II) salts such as copper(II) sulphate or copper(II) acetate can be used in the presence of a reductant agent such as sodium ascorbate for *in situ* reduction of Cu(II) to Cu(I).[140]

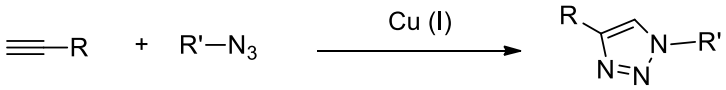

Figure 1.40: CuAAC general reaction scheme.

The development of the CuAAC reaction has widely broadened the scope of the post-polymerisation functionalisation approach, being nowadays one of the most used reactions in polymers chemistry.[140] Among numerous examples that can be found in the recent literature, the Liquid Crystals and Polymers Group has exploited the CuAAC reaction to functionalise either poly(propargyl methacrylate) or block copolymers with poly(methyl metacrylate) using azobenzene azides to process films with light induced optical anisotropy (Figure 1.41). [141,142,143]

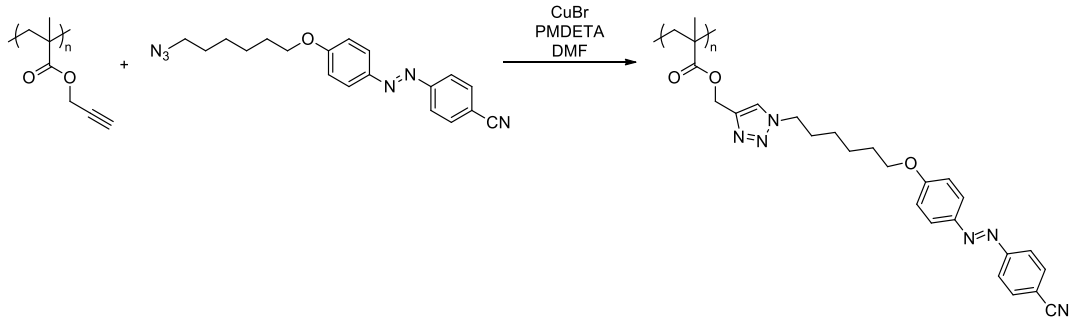

Figure 1.41: Scheme of CuAAC reaction from Royes *et al.* [141]

CuAAC has also been widely used in literature to introduce functionalities in amphiphilic diblock copolymers. For instance, BCs with PEG and an aliphatic polycarbonate with pendant propargyl radicals have been modified with azobenzene azides using the catalytic system Cu(II)/sodium ascorbate (Figure 1.42).

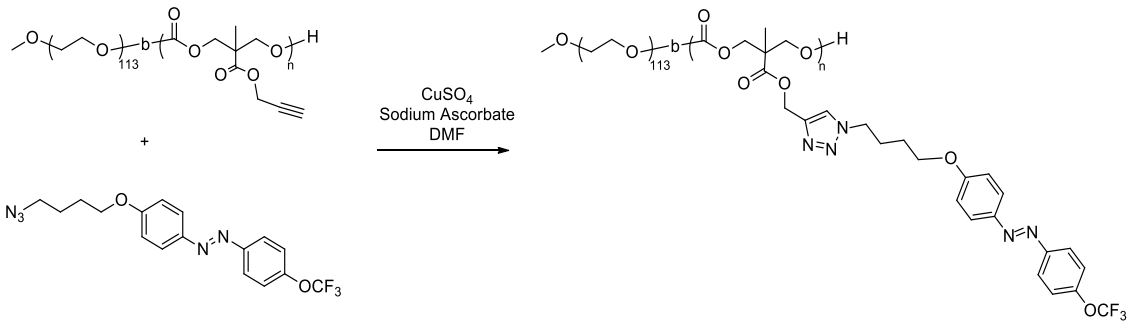

Figure 1.42: Scheme of CuAAC reaction used by Hu *et al.* [144]

The reaction of thiols and alkenes, known as thiol-ene reaction, is another of the click chemistry reactions widely used in polymer chemistry. The reaction is an anti-Markovnikov addition of the thiol to the alkene (Figure 1.43). With non-activated olefins, the addition proceeds by a radical mechanism initiated by radical initiators activated either with heat or light. With electron deficient olefins, the addition proceeds by a base catalysed nucleophilic mechanism (Michael addition).[145]

Figure 1.43: Thiol-ene general reaction scheme.

Justynska and Schlaad proved in 2004 the utility of free-radical thiol-ene reaction to modify a diblock copolymer comprised by PEG and polybutadiene with a variety of thiols having different functionalities as amines, carboxylic acids or esters.[146] Tempelaar *et al.* demonstrated the versatility of combining ROP of MAC and thiol-ene reactions to create functionalised aliphatic polycarbonates with a range of pendant functionalities in a facile and versatile way (Figure 1.44).[131]

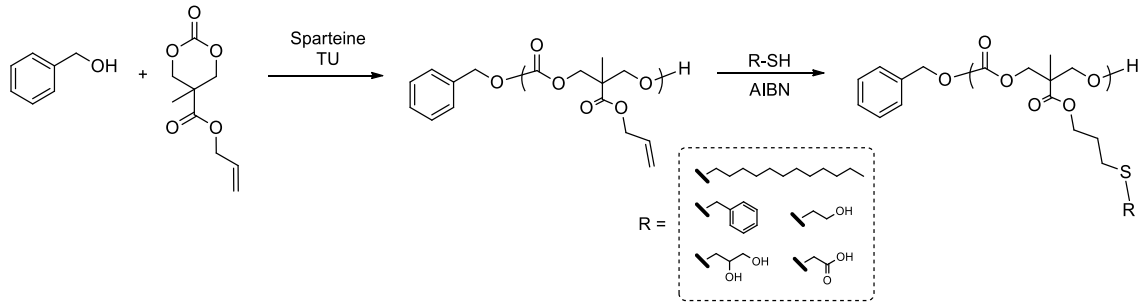

Figure 1.44: Synthesis of a functionalised amphiphilic diblock copolymer by combination of ROP and thiol-ene reaction.[131]

Nonetheless, when used in polymer functionalisation, the aforementioned reactions may not meet all the criteria to be classified as strict click chemistry reactions, as excess of some of the reactants or chromatographic purification may be necessary. Barner-Kowollik and colleagues reformulated click chemistry definition applied to polymer functionalisation, restricting some of the previously mentioned criteria such as quantitative conversions without using excesses of reactants, orthogonality, large scale purification, short reaction times and the formation of stable products.[147]

1.3.3.2 Supramolecular functionalisation

Supramolecular chemistry was defined by Lehn in his Nobel lecture in 1987 as "the chemistry of the intermolecular bond, covering the structures and functions of the entities formed by association of two or more chemical species".[148] The formation of supramolecular structures is governed by diverse non-covalent interactions, including van der Waals interactions, electrostatic interactions, hydrogen and halogen bonding or hydrophobic interactions, amongst others.[149]

The most frequently used interaction in supramolecular polymers is hydrogen bonding or H-bond.[150] H-bond is a highly directional interaction whose strength is influenced by various parameters. Indeed, the strength of a single H-bond depends on the nature of the H-bond donor and acceptor but the use of binding units combining several H-bonds is a way for strengthening the interaction. H-bonds are also strongly influence by the polarity of the medium, being stronger in apolar solvents than in polar ones, so H-bonds are drastically weakened in competitive solvents such as THF or water. Thus, it has been established that in aqueous environments the H-bonding units have to be surrounded by a hydrophobic microenvironment, which shields it from water and stabilizes the interaction.[151] Because of their fully reversible nature, H-bonds are also sensitive to temperature and pH, with the interaction weakening upon increasing the temperature or in mild acidic media.

Supramolecular polymers can be classified in two categories depending on whether the supramolecular interaction takes place in the main chain or in the side chain of the polymeric backbone (Figure 1.45).[152] In supramolecular main chain polymers, the non-covalent interactions control an equilibrium between the monomeric species and the supramolecular polymer. In the simplest example, a small molecule with complementary binding units located in its extremes is able to self-assemble into a linear supramolecular polymer (Figure 1.45). The polymerisation degree of the supramolecular polymer is mainly dominated by the binding constant of the complementary species, the monomer concentration and the assembly mechanism.[153] In supramolecular side chain polymers, non-covalent interactions

are used to modify or functionalise polymeric backbones with low synthetic effort (Figure 1.45).[152]

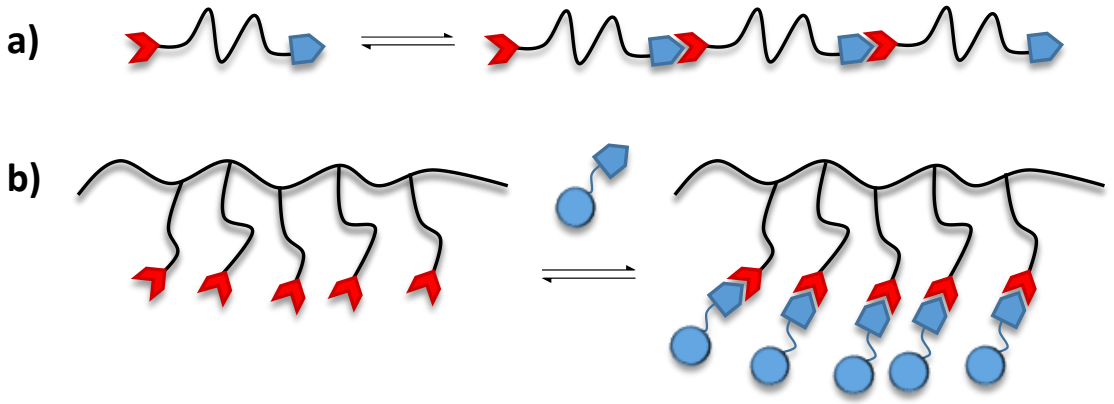

Figure 1.45: Types of supramolecular polymers: main chain (a) and side chain (b).

Fréchet, Kato and co-workers reported a pioneering work using H-bond to attach a series of mesogen units into the side chain of poly(siloxane)s and poly(acrylate)s.[154,155] The interaction between benzoic acid and pyridine was relatively weak as only one H-bond per mesogen unit was formed but proved the validity of the strategy for the preparation of side chain liquid crystalline polymers (Figure 1.46).

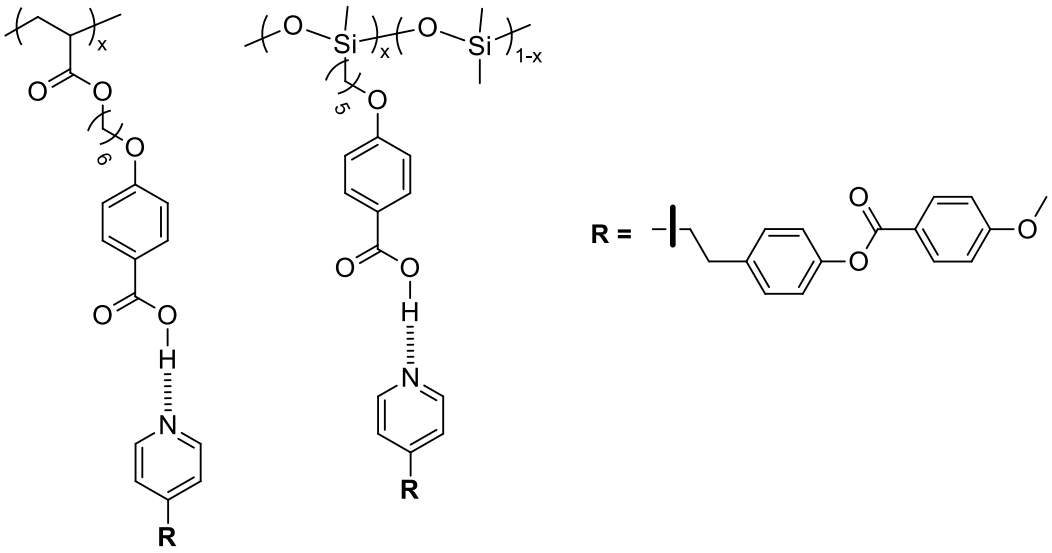

Figure 1.46: Supramolecular side chain polymers reported by Frechet, Kato and co-workers.[154,155]

DNA nitrogenous bases pairs, cytosine-guanine and adenine-thymine (or uracil in RNA), interact *via* two or three H-bond, leading to a reinforcement of the association if compared to a single bond interaction. Other non-naturally occurring

nitrogenous bases are able to stablish multiple H-bonds such as 2,6-diacylaminopyridine (DAP), which is complementary to thymine *via* a triple H-bond (Figure 1.47), or ureidopyrimidone, which is able to form dimers *via* a quadruple H-bond.[156,157]

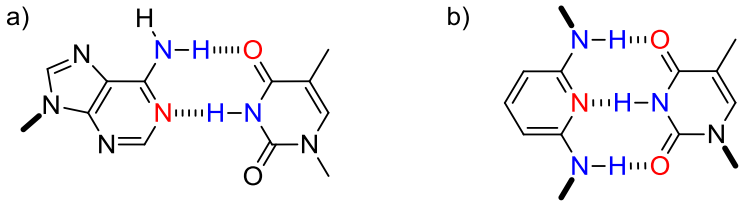

Figure 1.47: Complementary nitrogenous bases: adenine-thymine (a) and 2,6-diacylaminopyridine-thymine (b). In blue H-bond donor atoms and in red H-bond acceptor atoms.

Synthesis of nucleobase-containing polymers can be addressed by two strategies: direct polymerisation of monomers containing a nucleobase, or post-polymerisation functionalisation of a polymeric backbone (Figure 1.48). Van Hest and co-workers published a pioneering work consisting on polymerisation of methacrylate monomers from adenine, thymine, cytosine and guanine by atom transfer radical polymerisation.[158] Lately, Kim and co-workers synthesised a series of polymers where nucleobases were incorporated in the side chain of a polymeric scaffold *via* Steglich esterification reaction of pendant hydroxyl groups.[159]

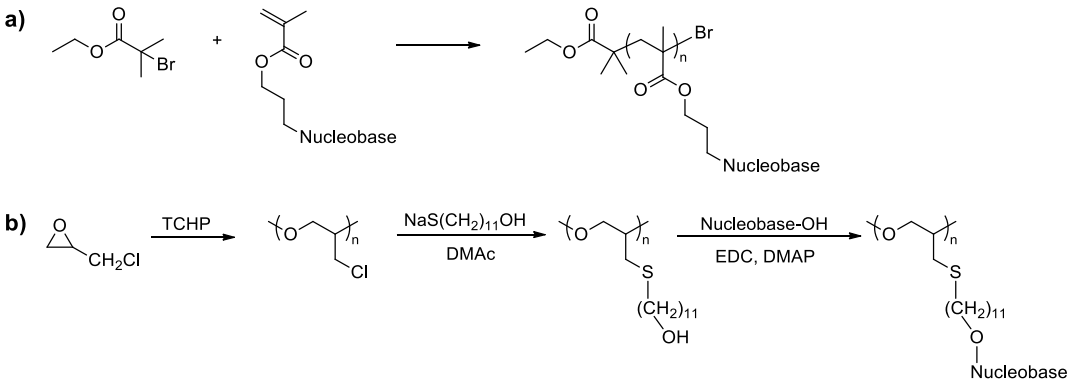

Figure 1.48: Preparation of nucleobase containing polymers by direct polymerisation of nucleobase derivatives (a)[158] or post-functionalisation of the polymeric backbone (b).[159]

Rotello and co-workers reported several side chain polymers bearing the adenine analogue DAP, which were modified with thymine derivatives of flavine showing a highly efficient recognition of the complementary pair.[160] They also reported on a

DAP partially functionalised styrenic polymer that was able to bind bisthymine derivatives. The polymers self-assembled into nanospheres in $CDCl_3$ that were dissembled and reassemble upon heating and cooling.[161]

In the Liquid Crystals and Polymers Group, the introduction of DAP pendant units in poly(methacrylate)s has been used to introduce light-responsive units by H-bond molecular recognition. In a first job, a PMMA macrochain transfer agent (mCTA) was used to polymerise a methacrylic monomer with DAP units. Azobenzene moieties where introduced by complexation of DAP units with complementary thymine or carboxylic acid derivatives. The photoorientational properties of these materials were demonstrated to be similar to those of azobenzene covalent polymers.[162]

Amphiphilic diblock copolymers with DAP units in the hydrophobic block were synthesised in a later work by using PEG-mCTAs with 2000 (PEG_{2k}) or 10000 (PEG_{10k}) g mol^{-1} average molar mass, which self-assembled into micelles when dispersed in water. Campthothecin loaded micelles showed similar antiviral activity to free campthothecin, proving the potential of these polymer nanocarriers as drug delivery systems.[104] Upon functionalisation of these amphiphilic diblock copolymers with an azobenzene bearing a thymine *via* H-bond, micelles or vesicles were formed in water depending on the PEG block length (Figure 1.49). It was demonstrated that UV light triggered the release of encapsulated small fluorescent probes in both types of self-assemblies (Figure 1.49). The behaviour of these systems was similar to covalent analogues proving the validity of the supramolecular approach in comparison to the covalent one.[105]

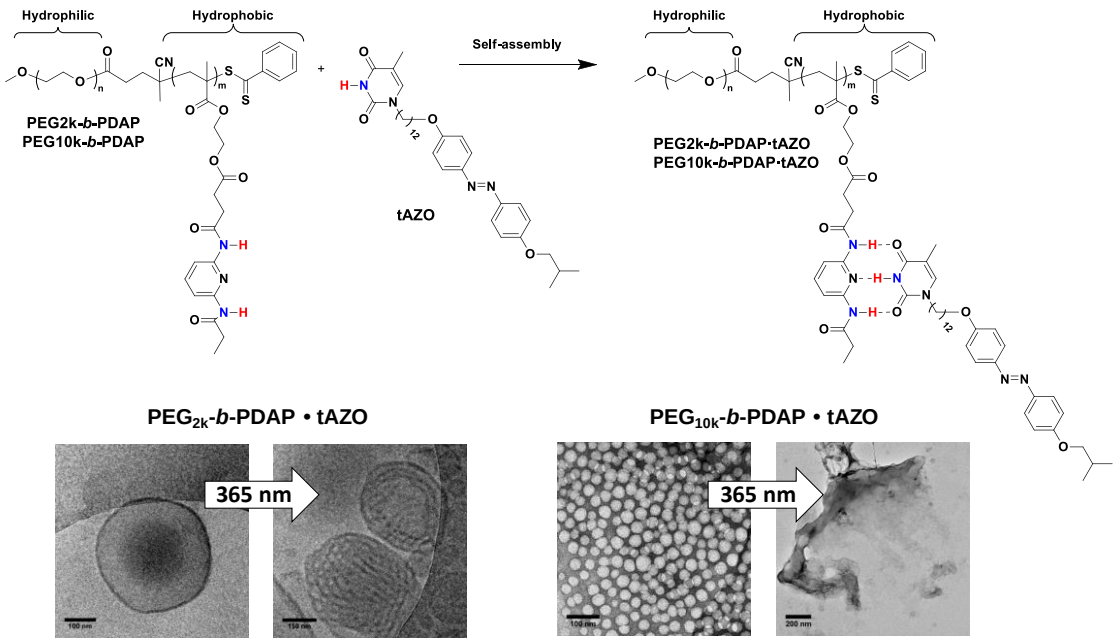

Figure 1.49: Synthesis of light-responsive supramolecular amphiphilic diblock copolymers and morphological changes in self-assemblies upon light irradiation.[105]

1.4 References

(1) Kriksin, Y. A.; Khalatur, P. G.; Erukhimovich, I. Ya.; ten Brinke, G.; Khokhlov, A. R. Microphase Separation of Diblock Copolymers with Amphiphilic Segment. *Soft Matter* **2009**, *5*, 2896-2904. https://doi.org/10.1039/b905923g.

(2) Lohse, D. J.; Hadjichristidis, N. Microphase Separation in Block Copolymers. *Curr. Opin. Colloid Interface Sci.* **1997**, *2*, 171–176. https://doi.org/10.1016/S1359-0294(97)80023-4.

(3) Feng, H.; Lu, X.; Wang, W.; Kang, N.-G.; Mays, J. Block Copolymers: Synthesis, Self-Assembly, and Applications. *Polymers* **2017**, *9*, 494. https://doi.org/10.3390/polym9100494.

(4) Barón, M.; Hellwich, K.-H.; Hess, M.; Horie, K.; Jenkins, A. D.; Jones, R. G.; Kahovec, J.; Kratochvíl, P.; Metanomski, W. V.; Mormann, W.; Stepto, R. F. T.; Vohlídal, J.; Wilks, E. S. Glossary of Class Names of Polymers Based on Chemical Structure and Molecular Architecture (IUPAC Recommendations 2009). *Pure Appl. Chem.* **2009**, *81*, 1131–1186. https://doi.org/10.1351/PAC-REC-08-01-30.

(5) Hadjichristidis, N.; Pitsikalis, M.; Pispas, S.; Iatrou, H. Polymers with Complex Architecture by Living Anionic Polymerization. *Chem. Rev.* **2001**, *101*, 3747–3792. https://doi.org/10.1021/cr9901337.

(6) Cho, B.-K. Mesophase Structure-Mechanical and Ionic Transport Correlations in Extended Amphiphilic Dendrons. *Science* **2004**, *305*, 1598–1601. https://doi.org/10.1126/science.1100872.

(7) Kim, J. K.; Yang, S. Y.; Lee, Y.; Kim, Y. Functional Nanomaterials Based on Block Copolymer Self-Assembly. *Prog. Polym. Sci.* **2010**, *35*, 1325–1349. https://doi.org/10.1016/j.progpolymsci.2010.06.002.

(8) Matsen, M. W.; Bates, F. S. Unifying Weak- and Strong-Segregation Block Copolymer Theories. *Macromolecules* **1996**, *29*, 1091–1098. https://doi.org/10.1021/ma951138i.

(9) Matsen, M. W.; Schick, M. Stable and Unstable Phases of a Diblock Copolymer Melt. *Phys. Rev. Lett.* **1994**, *72*, 2660–2663. https://doi.org/10.1103/PhysRevLett.72.2660.

(10) Mai, Y.; Eisenberg, A. Self-Assembly of Block Copolymers. *Chem. Soc. Rev.* **2012**, *41*, 5969. https://doi.org/10.1039/c2cs35115c.

(11) Smart, T.; Lomas, H.; Massignani, M.; Flores-Merino, M. V.; Perez, L. R.; Battaglia, G. Block Copolymer Nanostructures. *Nano Today* **2008**, *3*, 38–46. https://doi.org/10.1016/S1748-0132(08)70043-4.

(12) Cabral, H.; Miyata, K.; Osada, K.; Kataoka, K. Block Copolymer Micelles in Nanomedicine Applications. *Chem. Rev.* **2018**, *118*, 6844–6892. https://doi.org/10.1021/acs.chemrev.8b00199.

(13) Nagarajan, R. Molecular Packing Parameter and Surfactant Self-Assembly: The Neglected Role of the Surfactant Tail. *Langmuir* **2002**, *18*, 31–38. https://doi.org/10.1021/la010831y.

(14) Tritschler, U.; Pearce, S.; Gwyther, J.; Whittell, G. R.; Manners, I. 50th Anniversary Perspective : Functional Nanoparticles from the Solution Self-Assembly of Block Copolymers. *Macromolecules* **2017**, *50*, 3439–3463. https://doi.org/10.1021/acs.macromol.6b02767.

(15) Blanazs, A.; Armes, S. P.; Ryan, A. J. Self-Assembled Block Copolymer Aggregates: From Micelles to Vesicles and Their Biological Applications. *Macromol. Rapid Commun.* **2009**, *30*, 267–277. https://doi.org/10.1002/marc.200800713.

(16) Panyam, J.; Labhasetwar, V. Biodegradable Nanoparticles for Drug and Gene Delivery to Cells and Tissue. *Adv. Drug Deliv. Rev.* **2003**, *55*, 329–347. https://doi.org/10.1016/S0169-409X(02)00228-4.

(17) Chen, G.; Roy, I.; Yang, C.; Prasad, P. N. Nanochemistry and Nanomedicine for Nanoparticle-Based Diagnostics and Therapy. *Chem. Rev.* **2016**, *116*, 2826–2885. https://doi.org/10.1021/acs.chemrev.5b00148.

(18) Bueno, C. Z.; Oliveira, C. A.; Rangel-Yagui, C. O. Polymeric and Liposomal Nanomaterials. In *Nanobiomaterials*; Elsevier, 2018; pp 437–464. https://doi.org/10.1016/B978-0-08-100716-7.00017-9.

(19) Zhong, Y.; Meng, F.; Deng, C.; Zhong, Z. Ligand-Directed Active Tumor-Targeting Polymeric Nanoparticles for Cancer Chemotherapy. *Biomacromolecules* **2014**, *15*, 1955–1969. https://doi.org/10.1021/bm5003009.

(20) Stylianopoulos, T. EPR-Effect: Utilizing Size-Dependent Nanoparticle Delivery to Solid Tumors. *Ther. Deliv.* **2013**, *4*, 421–423. https://doi.org/10.4155/tde.13.8.

(21) Stockhofe, K.; Postema, J.; Schieferstein, H.; Ross, T. Radiolabeling of Nanoparticles and Polymers for PET Imaging. *Pharmaceuticals* **2014**, *7*, 392–418. https://doi.org/10.3390/ph7040392.

(22) Adams, M. L.; Lavasanifar, A.; Kwon, G. S. Amphiphilic Block Copolymers for Drug Delivery. *J. Pharm. Sci.* **2003**, *92*, 1343–1355. https://doi.org/10.1002/jps.10397.

(23) Halperin, A.; Alexander, S. Polymeric Micelles: Their Relaxation Kinetics. *Macromolecules* **1989**, *22*, 2403–2412. https://doi.org/10.1021/ma00195a069.

(24) Prasad, S.; Achazi, K.; Böttcher, C.; Haag, R.; Sharma, S. K. Fabrication of Nanostructures through Self-Assembly of Non-Ionic Amphiphiles for Biomedical Applications. *RSC Adv.* **2017**, *7*, 22121–22132. https://doi.org/10.1039/C6RA28654B.

(25) Astafieva, I.; Zhong, X. F.; Eisenberg, A. Critical Micellization Phenomena in Block Polyelectrolyte Solutions. *Macromolecules* **1993**, *26*, 7339–7352. https://doi.org/10.1021/ma00078a034.

(26) Aguiar, J.; Carpena, P.; Molina-Bolívar, J. A.; Carnero Ruiz, C. On the Determination of the Critical Micelle Concentration by the Pyrene 1:3 Ratio Method. *J. Colloid Interface Sci.* **2003**, *258*, 116–122. https://doi.org/10.1016/S0021-9797(02)00082-6.

(27) Fessi, H.; Puisieux, F.; Devissaguet, J. Ph.; Ammoury, N.; Benita, S. Nanocapsule Formation by Interfacial Polymer Deposition Following Solvent

Displacement. *Int. J. Pharm.* **1989**, *55*, R1–R4. https://doi.org/10.1016/0378-5173(89)90281-0.

(28) Leroux, J.; Alléman, E.; Doelker, E.; Gurny, R. New Approach for the Preparation of Nanoparticles by an Emulsification-Diffusion Method. *Eur. J. Pharm. Biopharm.* **1995**, *41*, 14–18.

(29) Ahn, J.; Ko, J.; Lee, S.; Yu, J.; Kim, Y.; Jeon, N. L. Microfluidics in Nanoparticle Drug Delivery; From Synthesis to Pre-Clinical Screening. *Adv. Drug Deliv. Rev.* **2018**, *128*, 29–53. https://doi.org/10.1016/j.addr.2018.04.001.

(30) *Block Copolymers in Nanoscience*, 1st ed.; Lazzari, M., Liu, G., Lecommandoux, S., Eds.; Wiley, 2006. https://doi.org/10.1002/9783527610570.

(31) Wei, M.; Gao, Y.; Li, X.; Serpe, M. J. Stimuli-Responsive Polymers and Their Applications. *Polym. Chem.* **2017**, *8*, 127–143. https://doi.org/10.1039/C6PY01585A.

(32) Karimi, M.; Ghasemi, A.; Sahandi Zangabad, P.; Rahighi, R.; Moosavi Basri, S. M.; Mirshekari, H.; Amiri, M.; Shafaei Pishabad, Z.; Aslani, A.; Bozorgomid, M.; Ghosh, D.; Beyzavi, A.; Vaseghi, A.; Aref, A. R.; Haghani, L.; Bahrami, S.; Hamblin, M. R. Smart Micro/Nanoparticles in Stimulus-Responsive Drug/Gene Delivery Systems. *Chem. Soc. Rev.* **2016**, *45*, 1457–1501. https://doi.org/10.1039/C5CS00798D.

(33) Torchilin, V. P. Multifunctional, Stimuli-Sensitive Nanoparticulate Systems for Drug Delivery. *Nat. Rev. Drug Discov.* **2014**, *13*, 813–827. https://doi.org/10.1038/nrd4333.

(34) Qin, S.; Geng, Y.; Discher, D. E.; Yang, S. Temperature-Controlled Assembly and Release from Polymer Vesicles of Poly(Ethylene Oxide)-Block- Poly(N-Isopropylacrylamide). *Adv. Mater.* **2006**, *18*, 2905–2909. https://doi.org/10.1002/adma.200601019.

(35) Kanamala, M.; Wilson, W. R.; Yang, M.; Palmer, B. D.; Wu, Z. Mechanisms and Biomaterials in pH-Responsive Tumour Targeted Drug Delivery: A Review. *Biomaterials* **2016**, *85*, 152–167. https://doi.org/10.1016/j.biomaterials.2016.01.061.

(36) Newell, K. J.; Tannock, I. F. Reduction of Intracellular pH as a Possible Mechanism for Killing Cells in Acidic Regions of Solid Tumors: Effects of Carbonylcyanide-3-Chlorophenylhydrazone. *Cancer Research* **1989**, *49* 4477-4482.

(37) Kataoka, K.; Matsumoto, T.; Yokoyama, M.; Okano, T.; Sakurai, Y.; Fukushima, S.; Okamoto, K.; Kwon, G. S. Doxorubicin-Loaded Poly(Ethylene Glycol)–Poly(β-Benzyl-l-Aspartate) Copolymer Micelles: Their Pharmaceutical Characteristics and Biological Significance. *J. Controlled Release* **2000**, *64*, 143–153. https://doi.org/10.1016/S0168-3659(99)00133-9.

(38) Khorsand, B.; Lapointe, G.; Brett, C.; Oh, J. K. Intracellular Drug Delivery Nanocarriers of Glutathione-Responsive Degradable Block Copolymers Having Pendant Disulfide Linkages. *Biomacromolecules* **2013**, *14*, 2103–2111. https://doi.org/10.1021/bm4004805.

(39) Zhang, H.; Wang, K.; Zhang, P.; He, W.; Song, A.; Luan, Y. Redox-Sensitive Micelles Assembled from Amphiphilic MPEG-PCL-SS-DTX Conjugates for the Delivery of Docetaxel. *Colloids Surf. B Biointerfaces* **2016**, *142*, 89–97. https://doi.org/10.1016/j.colsurfb.2016.02.045.

(40) Hüll, K.; Morstein, J.; Trauner, D. In Vivo Photopharmacology. *Chem. Rev.* **2018**, *118*, 10710–10747. https://doi.org/10.1021/acs.chemrev.8b00037.

(41) Zhao, Y. Light-Responsive Block Copolymer Micelles. *Macromolecules* **2012**, *45*, 3647–3657. https://doi.org/10.1021/ma300094t.

(42) Chatani, S.; Kloxin, C. J.; Bowman, C. N. The Power of Light in Polymer Science: Photochemical Processes to Manipulate Polymer Formation, Structure, and Properties. *Polym. Chem.* **2014**, *5*, 2187–2201. https://doi.org/10.1039/C3PY01334K.

(43) Beauté, L.; McClenaghan, N.; Lecommandoux, S. Photo-Triggered Polymer Nanomedicines: From Molecular Mechanisms to Therapeutic Applications. *Advanced Drug Delivery Reviews* **2019**, *138*, 148–166. https://doi.org/10.1016/j.addr.2018.12.010.

(44) Cheong, W. F.; Prahl, S. A.; Welch, A. J. A Review of the Optical Properties of Biological Tissues. *IEEE J. Quantum Electron.* **1990**, *26*, 2166–2185. https://doi.org/10.1109/3.64354.

(45) Juzenas, P.; Juzeniene, A.; Kaalhus, O.; Iani, V.; Moan, J. Noninvasive Fluorescence Excitation Spectroscopy during Application of 5-Aminolevulinic Acid in Vivo. *Photochem. Photobiol. Sci.* **2002**, *1*, 745–748. https://doi.org/10.1039/b203459j.

(46) Kaiser, W.; Garrett, C. G. B. Two-Photon Excitation in $CaF_2:Eu^{2+}$. *Phys. Rev. Lett.* **1961**, *7*, 229–231. https://doi.org/10.1103/PhysRevLett.7.229.

(47) Pawlicki, M.; Collins, H. A.; Denning, R. G.; Anderson, H. L. Two-Photon Absorption and the Design of Two-Photon Dyes. *Angew. Chem. Int. Ed.* **2009**, *48*, 3244–3266. https://doi.org/10.1002/anie.200805257.

(48) del Barrio, J.; Oriol, L.; Piñol, M. *Photoactive Functional Soft Materials: Preparation, Properties, and Applications*, 1st ed.; Li, Q., Ed.; Wiley, 2019. https://doi.org/10.1002/9783527816774.

(49) Ren, X.; Kondakova, M. E.; Giesen, D. J.; Rajeswaran, M.; Madaras, M.; Lenhart, W. C. Coumarin-Based, Electron-Trapping Iridium Complexes as Highly Efficient and Stable Phosphorescent Emitters for Organic Light-Emitting Diodes. *Inorg. Chem.* **2010**, *49*, 1301–1303. https://doi.org/10.1021/ic9022097.

(50) Bazzicalupi, C.; Caltagirone, C.; Cao, Z.; Chen, Q.; Di Natale, C.; Garau, A.; Lippolis, V.; Lvova, L.; Liu, H.; Lundström, I.; Mostallino, M. C.; Nieddu, M.; Paolesse, R.; Prodi, L.; Sgarzi, M.; Zaccheroni, N. Multimodal Use of New Coumarin-Based Fluorescent Chemosensors: Towards Highly Selective Optical Sensors for Hg^{2+} Probing. *Chem. Eur. J.* **2013**, *19*, 14639–14653. https://doi.org/10.1002/chem.201302090.

(51) Concellón, A.; Termine, R.; Golemme, A.; Romero, P.; Marcos, M.; Serrano, J. L. High Hole Mobility and Light-Harvesting in Discotic Nematic Dendrimers Prepared *via* 'Click' Chemistry. *J. Mater. Chem. C* **2019**, *7*, 2911–2918. https://doi.org/10.1039/C8TC06142D.

(52) Gaspar, A.; Matos, M. J.; Garrido, J.; Uriarte, E.; Borges, F. Chromone: A Valid Scaffold in Medicinal Chemistry. *Chem. Rev.* **2014**, *114*, 4960–4992. https://doi.org/10.1021/cr400265z.

(53) Jiang, J.; Qi, B.; Lepage, M.; Zhao, Y. Polymer Micelles Stabilization on Demand through Reversible Photo-Cross-Linking. *Macromolecules* **2007**, *40*, 790–792. https://doi.org/10.1021/ma062493j.

(54) Givens, R. S.; Matuszewski, B. Photochemistry of Phosphate Esters: An Efficient Method for the Generation of Electrophiles. *J. Am. Chem. Soc.* **1984**, *106*, 6860–6861. https://doi.org/10.1021/ja00334a075.

(55) Suzuki, A. Z.; Watanabe, T.; Kawamoto, M.; Nishiyama, K.; Yamashita, H.; Ishii, M.; Iwamura, M.; Furuta, T. Coumarin-4-Ylmethoxycarbonyls as Phototriggers for Alcohols and Phenols. *Org. Lett.* **2003**, *5*, 4867–4870. https://doi.org/10.1021/ol0359362.

(56) Schmidt, R.; Geissler, D.; Hagen, V.; Bendig, J. Kinetics Study of the Photocleavage of (Coumarin-4-Yl)Methyl Esters. *J. Phys. Chem. A* **2005**, *109*, 5000–5004. https://doi.org/10.1021/jp050581k.

(57) Givens, R. S.; Rubina, M.; Wirz, J. Applications of P-Hydroxyphenacyl (PHP) and Coumarin-4-ylmethyl Photoremovable Protecting Groups. *Photochem. Photobiol. Sci.* **2012**, *11*, 472-488. https://doi.org/10.1039/c2pp05399c.

(58) Fonseca, A. S. C.; Soares, A. M. S.; Gonçalves, M. S. T.; Costa, S. P. G. Thionated Coumarins and Quinolones in the Light Triggered Release of a Model Amino Acid: Synthesis and Photolysis Studies. *Tetrahedron* **2012**, *68*, 7892–7900. https://doi.org/10.1016/j.tet.2012.07.021.

(59) Fournier, L.; Gauron, C.; Xu, L.; Aujard, I.; Le Saux, T.; Gagey-Eilstein, N.; Maurin, S.; Dubruille, S.; Baudin, J.-B.; Bensimon, D.; Volovitch, M.; Vriz, S.; Jullien, L. A Blue-Absorbing Photolabile Protecting Group for in Vivo Chromatically Orthogonal Photoactivation. *ACS Chem. Biol.* **2013**, *8*, 1528–1536. https://doi.org/10.1021/cb400178m.

(60) Hammer, C. A.; Falahati, K.; Jakob, A.; Klimek, R.; Burghardt, I.; Heckel, A.; Wachtveitl, J. Sensitized Two-Photon Activation of Coumarin Photocages. J. Phys. Chem. Lett. 2018, 9, 1448–1453. https://doi.org/10.1021/acs.jpclett.7b03364.

(61) Goegan, B.; Terzi, F.; Bolze, F.; Cambridge, S.; Specht, A. Synthesis and Characterization of Photoactivatable Doxycycline Analogues Bearing Two-Photon-Sensitive Photoremovable Groups Suitable for Light-Induced Gene Expression. *ChemBioChem* **2018**, *19*, 1341–1348. https://doi.org/10.1002/cbic.201700628.

(62) Jin, Q.; Mitschang, F.; Agarwal, S. Biocompatible Drug Delivery System for Photo-Triggered Controlled Release of 5-Fluorouracil. *Biomacromolecules* **2011**, *12*, 3684–3691. https://doi.org/10.1021/bm2009125.

(63) Chen, J.; Li, G.; Liu, Q.; Liang, Y.; Liu, M.; Wu, H.; Gao, W. A Photocleavable Amphiphilic Prodrug Self-Assembled Nanoparticles with Effective Anticancer Activity In Vitro. *Nanomaterials* **2019**, *9*, 860. https://doi.org/10.3390/nano9060860.

(64) Karthik, S.; Jana, A.; Selvakumar, M.; Venkatesh, Y.; Paul, A.; Shah, Sk. S.; Singh, N. D. P. Coumarin Polycaprolactone Polymeric Nanoparticles: Light and Tumor Microenvironment Activated Cocktail Drug Delivery. *J. Mater. Chem. B* **2017**, *5*, 1734–1741. https://doi.org/10.1039/C6TB02944B.

(65) Ji, W.; Li, N.; Chen, D.; Qi, X.; Sha, W.; Jiao, Y.; Xu, Q.; Lu, J. Coumarin-Containing Photo-Responsive Nanocomposites for NIR Light-Triggered Controlled Drug Release via a Two-Photon Process. *J. Mater. Chem. B* **2013**, *1*, 5942. https://doi.org/10.1039/c3tb21206h.

(66) Babin, J.; Pelletier, M.; Lepage, M.; Allard, J.-F.; Morris, D.; Zhao, Y. A New Two-Photon-Sensitive Block Copolymer Nanocarrier. *Angew. Chem. Int. Ed.* **2009**, *48*, 3329–3332. https://doi.org/10.1002/anie.200900255.

(67) Kumar, S.; Allard, J.-F.; Morris, D.; Dory, Y. L.; Lepage, M.; Zhao, Y. Near-Infrared Light Sensitive Polypeptide Block Copolymer Micelles for Drug Delivery. *J. Mater. Chem.* **2012**, *22*, 7252–7257. https://doi.org/10.1039/c2jm16380b.

(68) Huang, Y.; Dong, R.; Zhu, X.; Yan, D. Photo-Responsive Polymeric Micelles. *Soft Matter* **2014**, *10*, 6121–6138. https://doi.org/10.1039/C4SM00871E.

(69) Sun, Z.; Liu, G.; Hu, J.; Liu, S. Photo- and Reduction-Responsive Polymersomes for Programmed Release of Small and Macromolecular Payloads. *Biomacromolecules* **2018**, *19*, 2071–2081. https://doi.org/10.1021/acs.biomac.8b00253.

(70) Benoit, C.; Talitha, S.; David, F.; Michel, S.; Anna, S.-J.; Rachel, A.-V.; Patrice, W. Dual Thermo- and Light-Responsive Coumarin-Based Copolymers with Programmable Cloud Points. *Polym. Chem.* **2017**, *8*, 4512–4519. https://doi.org/10.1039/C7PY00914C.

(71) Natansohn, A.; Rochon, P. Photoinduced Motions in Azo-Containing Polymers. *Chem. Rev.* **2002**, *102*, 4139–4176. https://doi.org/10.1021/cr970155y.

(72) Merino, E.; Ribagorda, M. Control over Molecular Motion Using the *Cis* – *Trans* Photoisomerisation of the Azo Group. *Beilstein J. Org. Chem.* **2012**, *8*, 1071–1090. https://doi.org/10.3762/bjoc.8.119.

(73) Hvilsted, S.; Sánchez, C.; Alcalá., R. The Volume Holographic Optical Storage Potential in Azobenzene Containing Polymers. *J. Mater. Chem.* **2009**, *19*, 6641-6648. https://doi.org/10.1039/b900930m.

(74) Yu, H.; Ikeda, T. Photocontrollable Liquid-Crystalline Actuators. *Adv. Mater.* **2011**, *23*, 2149–2180. https://doi.org/10.1002/adma.201100131.

(75) Li, M.-H.; Keller, P.; Li, B.; Wang, X.; Brunet, M. Light-Driven Side-On Nematic Elastomer Actuators. *Adv. Mater.* **2003**, *15*, 569–572. https://doi.org/10.1002/adma.200304552.

(76) Wang, G.; Tong, X.; Zhao, Y. Preparation of Azobenzene-Containing Amphiphilic Diblock Copolymers for Light-Responsive Micellar Aggregates. *Macromolecules* **2004**, *37*, 8911–8917. https://doi.org/10.1021/ma048416a.

(77) Beharry, A. A.; Woolley, G. A. Azobenzene Photoswitches for Biomolecules. *Chem. Soc. Rev.* **2011**, *40*, 4422-4437. https://doi.org/10.1039/c1cs15023e.

(78) Bandara, H. M. D.; Burdette, S. C. Photoisomerisation in Different Classes of Azobenzene. *Chem. Soc. Rev.* **2012**, *41*, 1809–1825. https://doi.org/10.1039/C1CS15179G.

(79) Yang, Y.; Hughes, R. P.; Aprahamian, I. Visible Light Switching of a BF_2-Coordinated Azo Compound. *J. Am. Chem. Soc.* **2012**, *134*, 15221–15224. https://doi.org/10.1021/ja306030d.

(80) Dong, M.; Babalhavaeji, A.; Samanta, S.; Beharry, A. A.; Woolley, G. A. Red-Shifting Azobenzene Photoswitches for in Vivo Use. *Acc. Chem. Res.* **2015**, *48*, 2662–2670. https://doi.org/10.1021/acs.accounts.5b00270.

(81) Siewertsen, R.; Neumann, H.; Buchheim-Stehn, B.; Herges, R.; Näther, C.; Renth, F.; Temps, F. Highly Efficient Reversible *Z–E* Photoisomerisation of a Bridged Azobenzene with Visible Light through Resolved S_1 ($n\pi^*$) Absorption Bands. *J. Am. Chem. Soc.* **2009**, *131*, 15594–15595. https://doi.org/10.1021/ja906547d.

(82) Sell, H.; Näther, C.; Herges, R. Amino-Substituted Diazocines as Pincer-Type Photochromic Switches. *Beilstein J. Org. Chem.* **2013**, *9*, 1–7. https://doi.org/10.3762/bjoc.9.1.

(83) Lentes, P.; Stadler, E.; Röhricht, F.; Brahms, A.; Gröbner, J.; Sönnichsen, F. D.; Gescheidt, G.; Herges, R. Nitrogen Bridged Diazocines: Photochromes Switching within the Near-Infrared Region with High Quantum Yields in Organic Solvents and in Water. *J. Am. Chem. Soc.* **2019**, *141*, 13592–13600. https://doi.org/10.1021/jacs.9b06104.

(84) Trads, J. B.; Hüll, K.; Matsuura, B. S.; Laprell, L.; Fehrentz, T.; Görldt, N.; Kozek, K. A.; Weaver, C. D.; Klöcker, N.; Barber, D. M.; Trauner, D. Sign Inversion in Photopharmacology: Incorporation of Cyclic Azobenzenes in Photoswitchable Potassium Channel Blockers and Openers. *Angew. Chem. Int. Ed.* **2019**, *58*, 15421–15428. https://doi.org/10.1002/anie.201905790.

(85) Yager, K. G.; Barrett, C. J. Chapter 17. Azobenzene Polymers as Photomechanical and Multifunctional Smart Materials. In *Intelligent Materials*;

Shahinpoor, M., Schneider, H.-J., Eds.; Royal Society of Chemistry: Cambridge, 2007; pp 424–446. https://doi.org/10.1039/9781847558008-00424.

(86) Garcia-Amorós, J.; Díaz-Lobo, M.; Nonell, S.; Velasco, D. Fastest Thermal Isomerisation of an Azobenzene for Nanosecond Photoswitching Applications under Physiological Conditions. *Angew. Chem. Int. Ed.* **2012**, *51*, 12820–12823. https://doi.org/10.1002/anie.201207602.

(87) Beharry, A. A.; Sadovski, O.; Woolley, G. A. Azobenzene Photoswitching without Ultraviolet Light. *J. Am. Chem. Soc.* **2011**, *133*, 19684–19687. https://doi.org/10.1021/ja209239m.

(88) Samanta, S.; McCormick, T. M.; Schmidt, S. K.; Seferos, D. S.; Woolley, G. A. Robust Visible Light Photoswitching with Ortho-Thiol Substituted Azobenzenes. *Chem. Commun.* **2013**, *49*, 10314-10316. https://doi.org/10.1039/c3cc46045b.

(89) Samanta, S.; Beharry, A. A.; Sadovski, O.; McCormick, T. M.; Babalhavaeji, A.; Tropepe, V.; Woolley, G. A. Photoswitching Azo Compounds in Vivo with Red Light. *J. Am. Chem. Soc.* **2013**, *135*, 9777–9784. https://doi.org/10.1021/ja402220t.

(90) Mendonça, C. R.; Neves, U. M.; De Boni, L.; Andrade, A. A.; dos Santos, D. S.; Pavinatto, F. J.; Zilio, S. C.; Misoguti, L.; Oliveira, O. N. Two-Photon Induced Anisotropy in PMMA Film Doped with Disperse Red 13. *Opt. Commun.* **2007**, *273*, 435–440. https://doi.org/10.1016/j.optcom.2007.01.035.

(91) Ishitobi, H.; Sekkat, Z.; Kawata, S. Photo-Orientation by Multiphoton Photoselection. *J. Opt. Soc. Am. B* **2006**, *23*, 868-873. https://doi.org/10.1364/JOSAB.23.000868.

(92) Maeda, M.; Ishitobi, H.; Sekkat, Z.; Kawata, S. Polarization Storage by Nonlinear Orientational Hole Burning in Azo Dye-Containing Polymer Films. *Appl. Phys. Lett.* **2004**, *85*, 351–353. https://doi.org/10.1063/1.1772522.

(93) Gascón-Moya, M.; Pejoan, A.; Izquierdo-Serra, M.; Pittolo, S.; Cabré, G.; Hernando, J.; Alibés, R.; Gorostiza, P.; Busqué, F. An Optimized Glutamate Receptor Photoswitch with Sensitized Azobenzene Isomerisation. *J. Org. Chem.* **2015**, *80*, 9915–9925. https://doi.org/10.1021/acs.joc.5b01402.

(94) Carroll, E. C.; Berlin, S.; Levitz, J.; Kienzler, M. A.; Yuan, Z.; Madsen, D.; Larsen, D. S.; Isacoff, E. Y. Two-Photon Brightness of Azobenzene Photoswitches Designed for Glutamate Receptor Optogenetics. *Proc. Natl. Acad. Sci.* **2015**, *112*, E776–E785. https://doi.org/10.1073/pnas.1416942112.

(95) Haase, M.; Schäfer, H. Upconverting Nanoparticles. *Angew. Chem. Int. Ed.* **2011**, *50*, 5808–5829. https://doi.org/10.1002/anie.201005159.

(96) Wu, X.; Chen, G.; Shen, J.; Li, Z.; Zhang, Y.; Han, G. Upconversion Nanoparticles: A Versatile Solution to Multiscale Biological Imaging. *Bioconjug. Chem.* **2015**, *26*, 166–175. https://doi.org/10.1021/bc5003967.

(97) Kano, K.; Tanaka, Y.; Ogawa, T.; Shimomura, M.; Okahata, Y.; Kunitake, T. Photoresponsive Membranes. Regulation of Membrane Properties by Photoreversible Cis–Trans Isomerisation of Azobenzenes. *Chem. Lett.* **1980**, *9*, 421–424. https://doi.org/10.1246/cl.1980.421.

(98) del Barrio, J.; Oriol, L.; Sánchez, C.; Serrano, J. L.; Di Cicco, A.; Keller, P.; Li, M.-H. Self-Assembly of Linear–Dendritic Diblock Copolymers: From Nanofibers to Polymersomes. *J. Am. Chem. Soc.* **2010**, *132*, 3762–3769. https://doi.org/10.1021/ja9083946.

(99) Blasco, E.; Barrio, J. del; Sánchez-Somolinos, C.; Piñol, M.; Oriol, L. Light Induced Molecular Release from Vesicles Based on Amphiphilic Linear-Dendritic Block Copolymers. *Polym. Chem.* **2013**, *4*, 2246-2254. https://doi.org/10.1039/c2py21025h.

(100) Blasco, E.; Serrano, J. L.; Piñol, M.; Oriol, L. Light Responsive Vesicles Based on Linear–Dendritic Block Copolymers Using Azobenzene–Aliphatic Codendrons. *Macromolecules* **2013**, *46*, 5951–5960. https://doi.org/10.1021/ma4009725.

(101) García-Juan, H.; Nogales, A.; Blasco, E.; Martínez, J. C.; Šics, I.; Ezquerra, T. A.; Piñol, M.; Oriol, L. Self-Assembly of Thermo and Light Responsive Amphiphilic Linear Dendritic Block Copolymers. *Eur. Polym. J.* **2016**, *81*, 621–633. https://doi.org/10.1016/j.eurpolymj.2015.12.021.

(102) Blasco, E.; Schmidt, B. V. K. J.; Barner-Kowollik, C.; Piñol, M.; Oriol, L. A Novel Photoresponsive Azobenzene-Containing Miktoarm Star Polymer: Self-Assembly and Photoresponse Properties. *Macromolecules* **2014**, *47*, 3693–3700. https://doi.org/10.1021/ma500254p.

(103) Blasco, E.; Schmidt, B. V. K. J.; Barner-Kowollik, C.; Piñol, M.; Oriol, L. Dual Thermo- and Photo-Responsive Micelles Based on Miktoarm Star Polymers. *Polym. Chem.* **2013**, *4*, 4506-4514. https://doi.org/10.1039/c3py00576c.

(104) Concellón, A.; Clavería-Gimeno, R.; Velázquez-Campoy, A.; Abian, O.; Piñol, M.; Oriol, L. Polymeric Micelles from Block Copolymers Containing 2,6-Diacylaminopyridine Units for Encapsulation of Hydrophobic Drugs. *RSC Adv.* **2016**, *6*, 24066–24075. https://doi.org/10.1039/C6RA01714B.

(105) Concellón, A.; Blasco, E.; Martínez-Felipe, A.; Martínez, J. C.; Šics, I.; Ezquerra, T. A.; Nogales, A.; Piñol, M.; Oriol, L. Light-Responsive Self-Assembled Materials by Supramolecular Post-Functionalization via Hydrogen Bonding of Amphiphilic Block Copolymers. *Macromolecules* **2016**, *49*, 7825–7836. https://doi.org/10.1021/acs.macromol.6b01112.

(106) Xia, Y.; Zeng, Y.; Hu, D.; Shen, H.; Deng, J.; Lu, Y.; Xia, X.; Xu, W. Light and pH Dual-Sensitive Biodegradable Polymeric Nanoparticles for Controlled Release of Cargos. *J. Polym. Sci. Part A Polym. Chem.* **2017**, *55*, 1773–1783. https://doi.org/10.1002/pola.28528.

(107) Dong, R.; Zhu, B.; Zhou, Y.; Yan, D.; Zhu, X. Reversible Photoisomerisation of Azobenzene-Containing Polymeric Systems Driven by Visible Light. *Polym. Chem.* **2013**, *4*, 912-915. https://doi.org/10.1039/c2py21060f.

(108) Wang, G.; Yuan, D.; Yuan, T.; Dong, J.; Feng, N.; Han, G. A Visible Light Responsive Azobenzene-Functionalized Polymer: Synthesis, Self-Assembly, and Photoresponsive Properties. *J. Polym. Sci. Part A Polym. Chem.* **2015**, *53*, 2768–2775. https://doi.org/10.1002/pola.27747.

(109) Zheng, X.; Bian, Q.; Ye, C.; Wang, G. Visible Light-, pH-, and Cyclodextrin-Responsive Azobenzene Functionalized Polymeric Nanoparticles. *Dyes Pigm.* **2019**, *162*, 599–605. https://doi.org/10.1016/j.dyepig.2018.10.063.

(110) Qian, S.; Li, S.; Xiong, W.; Khan, H.; Huang, J.; Zhang, W. A New Visible Light and Temperature Responsive Diblock Copolymer. *Polym. Chem.* **2019**, *10*, 5001–5009. https://doi.org/10.1039/C9PY01050E.

(111) Zhou, Y.; Ye, H.; Chen, Y.; Zhu, R.; Yin, L. Photoresponsive Drug/Gene Delivery Systems. *Biomacromolecules* **2018**, *19*, 1840–1857. https://doi.org/10.1021/acs.biomac.8b00422.

(112) Yan, K.; Chen, M.; Zhou, S.; Wu, L. Self-Assembly of Upconversion Nanoclusters with an Amphiphilic Copolymer for near-Infrared- and Temperature-Triggered Drug Release. *RSC Adv.* **2016**, *6*, 85293–85302. https://doi.org/10.1039/C6RA17622D.

(113) Lim Soo, P.; Eisenberg, A. Preparation of Block Copolymer Vesicles in Solution. *J. Polym. Sci. Part B Polym. Phys.* **2004**, *42*, 923–938. https://doi.org/10.1002/polb.10739.

(114) Ulery, B. D.; Nair, L. S.; Laurencin, C. T. Biomedical Applications of Biodegradable Polymers. *J. Polym. Sci. Part B Polym. Phys.* **2011**, *49*, 832–864. https://doi.org/10.1002/polb.22259.

(115) Nicolas, J.; Mura, S.; Brambilla, D.; Mackiewicz, N.; Couvreur, P. Design, Functionalization Strategies and Biomedical Applications of Targeted Biodegradable/Biocompatible Polymer-Based Nanocarriers for Drug Delivery. *Chem. Soc. Rev.* **2013**, *42*, 1147–1235. https://doi.org/10.1039/C2CS35265F.

(116) Guo, Q.; Lu, Z.; Zhang, Y.; Li, S.; Yang, J. In Vivo Study on the Histocompatibility and Degradation Behavior of Biodegradable Poly(Trimethylene Carbonate-Co-D,L-Lactide). *Acta Biochim. Biophys. Sin.* **2011**, *43*, 433–440. https://doi.org/10.1093/abbs/gmr034.

(117) Tinsley-Bown, A. M.; Fretwell, R.; Dowsett, A. B.; Davis, S. L.; G.H. Farrar. Formulation of Poly(d,l-Lactic-Co-Glycolic Acid) Microparticles for Rapid Plasmid

DNA Delivery. *J. Controlled Release* **2000**, *66*, 229–241. https://doi.org/10.1016/S0168-3659(99)00275-8.

(118) Walter, E.; Moelling, K.; Pavlovic, J.; Merkle, H. P. Microencapsulation of DNA Using Poly(Dl-Lactide-Co-Glycolide): Stability Issues and Release Characteristics. *J. Controlled Release* **1999**, *61*, 361–374. https://doi.org/10.1016/S0168-3659(99)00151-0.

(119) Artham, T.; Doble, M. Biodegradation of Aliphatic and Aromatic Polycarbonates. *Macromol. Biosci.* **2008**, *8*, 14–24. https://doi.org/10.1002/mabi.200700106.

(120) Dadsetan, M.; Christenson, E. M.; Unger, F.; Ausborn, M.; Kissel, T.; Hiltner, A.; Anderson, J. M. In Vivo Biocompatibility and Biodegradation of Poly(Ethylene Carbonate). *J. Controlled Release* **2003**, *93*, 259–270. https://doi.org/10.1016/j.jconrel.2003.08.010.

(121) Inoue, S.; Koinuma, H.; Tsuruta, T. Copolymerization of Carbon Dioxide and Epoxide with Organometallic Compounds. *Makromol. Chem.* **1969**, *130*, 210–220. https://doi.org/10.1002/macp.1969.021300112.

(122) Xu, J.; Feng, E.; Song, J. Renaissance of Aliphatic Polycarbonates: New Techniques and Biomedical Applications: Review. *J. Appl. Polym. Sci.* **2014**, *131*, 39822. https://doi.org/10.1002/app.39822.

(123) Okada, M. Chemical Syntheses of Biodegradable Polymers. *Prog. Polym. Sci.* **2002**, *27*, 87–133. https://doi.org/10.1016/S0079-6700(01)00039-9.

(124) Carothers, W. H.; Dorough, G. L.; Natta, F. J. van. Studies of Polymerization and Ring Formation. X. The Reversible Polymerization of Six-Membered Cyclic Esters. *J. Am. Chem. Soc.* **1932**, *54*, 761–772. https://doi.org/10.1021/ja01341a046.

(125) *Green Polymerization Methods: Renewable Starting Materials, Catalysis and Waste Reduction*; Mathers, R. T., Meier, M. A. R., Eds.; Wiley-VCH Verlag: Weinheim, Germany, 2011.

(126) Pratt, R. C.; Nederberg, F.; Waymouth, R. M.; Hedrick, J. L. Tagging Alcohols with Cyclic Carbonate: A Versatile Equivalent of (Meth)Acrylate for Ring-Opening Polymerization. *Chem. Commun.* **2008**, No. 1, 114–116. https://doi.org/10.1039/B713925J.

(127) Al-Azemi, T. F.; Bisht, K. S. Novel Functional Polycarbonate by Lipase-Catalyzed Ring-Opening Polymerization of 5-Methyl-5-Benzyloxycarbonyl-1,3-Dioxan-2-One. *Macromolecules* **1999**, *32*, 6536–6540. https://doi.org/10.1021/ma990639r.

(128) Tempelaar, S.; Mespouille, L.; Coulembier, O.; Dubois, P.; Dove, A. P. Synthesis and Post-Polymerisation Modifications of Aliphatic Poly(Carbonate)s Prepared by Ring-Opening Polymerisation. *Chem. Soc. Rev.* **2013**, *42*, 1312–1336. https://doi.org/10.1039/C2CS35268K.

(129) Lv, Y.; Yang, B.; Jiang, T.; Li, Y.-M.; He, F.; Zhuo, R.-X. Folate-Conjugated Amphiphilic Block Copolymers for Targeted and Efficient Delivery of Doxorubicin. *Colloids Surf. B Biointerfaces* **2014**, *115*, 253–259. https://doi.org/10.1016/j.colsurfb.2013.11.049.

(130) Hu, X.; Chen, X.; Xie, Z.; Liu, S.; Jing, X. Synthesis and Characterization of Amphiphilic Block Copolymers with Allyl Side-Groups. *J. Polym. Sci. Part A Polym. Chem.* **2007**, *45*, 5518–5528. https://doi.org/10.1002/pola.22297.

(131) Tempelaar, S.; Mespouille, L.; Dubois, P.; Dove, A. P. Organocatalytic Synthesis and Postpolymerization Functionalization of Allyl-Functional Poly(Carbonate)s. *Macromolecules* **2011**, *44*, 2084–2091. https://doi.org/10.1021/ma102882v.

(132) Yu, L.; Xie, M.; Li, Z.; Lin, C.; Zheng, Z.; Zhou, L.; Su, Y.; Wang, X. Facile Construction of Near-Monodisperse and Dual Responsive Polycarbonate Mixed Micelles with the Ability of PH-Induced Charge Reversal for Intracellular Delivery of Antitumor Drugs. *J. Mater. Chem. B* **2016**, *4*, 6081–6093. https://doi.org/10.1039/C6TB01865C.

(133) Lu, C.; Shi, Q.; Chen, X.; Lu, T.; Xie, Z.; Hu, X.; Ma, J.; Jing, X. Sugars-Grafted Aliphatic Biodegradable Poly(L-Lactide-Co-Carbonate)s by Click Reaction and Their Specific Interaction with Lectin Molecules. *J. Polym. Sci. Part A Polym. Chem.* **2007**, *45*, 3204–3217. https://doi.org/10.1002/pola.22070.

(134) Tempelaar, S.; Barker, I. A.; Truong, V. X.; Hall, D. J.; Mespouille, L.; Dubois, P.; Dove, A. P. Organocatalytic Synthesis and Post-Polymerization Functionalization of Propargyl-Functional Poly(Carbonate)s. *Polym. Chem.* **2013**, *4*, 174–183. https://doi.org/10.1039/C2PY20718D.

(135) Hu, D.; Peng, H.; Niu, Y.; Li, Y.; Xia, Y.; Li, L.; He, J.; Liu, X.; Xia, X.; Lu, Y.; Xu, W. Reversibly Light-Responsive Biodegradable Poly(Carbonate) Micelles Constructed via CuAAC Reaction. *J. Polym. Sci. Part A Polym. Chem.* **2015**, *53*, 750–760. https://doi.org/10.1002/pola.27499.

(136) Xia, Y.; Wang, N.; Qin, Z.; Wu, J.; Wang, F.; Zhang, L.; Xia, X.; Li, J.; Lu, Y. Polycarbonate-Based Core-Crosslinked Redox-Responsive Nanoparticles for Targeted Delivery of Anticancer Drug. *J. Mater. Chem. B* **2018**, *6*, 3348–3357. https://doi.org/10.1039/C8TB00346G.

(137) Xia, Y.; Zeng, Y.; Hu, D.; Shen, H.; Deng, J.; Lu, Y.; Xia, X.; Xu, W. Light and PH Dual-Sensitive Biodegradable Polymeric Nanoparticles for Controlled Release of Cargos. *J. Polym. Sci. Part A Polym. Chem.* **2017**, *55*, 1773–1783. https://doi.org/10.1002/pola.28528.

(138) Rostovtsev, V. V.; Green, L. G.; Fokin, V. V.; Sharpless, K. B. A Stepwise Huisgen Cycloaddition Process: Copper(I)-Catalyzed Regioselective Ligation of Azides and Terminal Alkynes. *Angew. Chem. Int. Ed.* **2002**, *41*, 2596–2599.

(139) Tornøe, C. W.; Christensen, C.; Meldal, M. Peptidotriazoles on Solid Phase: [1,2,3]-Triazoles by Regiospecific Copper(I)-Catalyzed 1,3-Dipolar Cycloadditions of Terminal Alkynes to Azides. *J. Org. Chem.* **2002**, *67*, 3057–3064. https://doi.org/10.1021/jo011148j.

(140) Blasco, E.; Sims, M. B.; Goldmann, A. S.; Sumerlin, B. S.; Barner-Kowollik, C. 50th Anniversary Perspective : Polymer Functionalization. *Macromolecules* **2017**, *50*, 5215–5252. https://doi.org/10.1021/acs.macromol.7b00465.

(141) Royes, J.; Rebolé, J.; Custardoy, L.; Gimeno, N.; Oriol, L.; Tejedor, R. M.; Piñol, M. Preparation of Side chain Liquid Crystalline Azopolymers by CuAAC Postfunctionalization Using Bifunctional Azides: Induction of Chirality Using Circularly Polarized Light. *J. Polym. Sci. Part A Polym. Chem.* **2012**, *50*, 1579–159o. https://doi.org/10.1002/pola.25929.

(142) Royes, J.; Provenzano, C.; Pagliusi, P.; Tejedor, R. M.; Piñol, M.; Oriol, L. A Bifunctional Amorphous Polymer Exhibiting Equal Linear and Circular Photoinduced Birefringences. *Macromol. Rapid Commun.* **2014**, 1890-1895. https://doi.org/10.1002/marc.201400355.

(143) Roche, A.; García-Juan, H.; Royes, J.; Oriol, L.; Piñol, M.; Audia, B.; Pagliusi, P.; Provenzano, C.; Cipparrone, G. Tuning the Thermal Properties of Azopolymers Synthesized by Post-Functionalization of Poly(Propargyl Methacrylate) with Azobenzene Azides: Influence on the Generation of Linear and Circular Birefringences. *Macromol. Chem. Phys.* **2018**, *219*, 1800318. https://doi.org/10.1002/macp.201800318.

(144) Hu, D.; Li, Y.; Niu, Y.; Li, L.; He, J.; Liu, X.; Xia, X.; Lu, Y.; Xiong, Y.; Xu, W. Photo-Responsive Reversible Micelles Based on Azobenzene-Modified Poly(Carbonate)s via Azide–Alkyne Click Chemistry. *RSC Adv* **2014**, *4*, 47929–47936. https://doi.org/10.1039/C4RA07345B.

(145) Hoyle, C. E.; Bowman, C. N. Thiol-Ene Click Chemistry. *Angew. Chem. Int. Ed.* **2010**, *49*, 1540–1573. https://doi.org/10.1002/anie.200903924.

(146) Justynska, J.; Schlaad, H. Modular Synthesis of Functional Block Copolymers. *Macromol. Rapid Commun.* **2004**, *25*, 1478–1481. https://doi.org/10.1002/marc.200400228.

(147) Barner-Kowollik, C.; Du Prez, F. E.; Espeel, P.; Hawker, C. J.; Junkers, T.; Schlaad, H.; Van Camp, W. “Clicking” Polymers or Just Efficient Linking: What Is

the Difference? *Angew. Chem. Int. Ed.* **2011**, *50*, 60–62. https://doi.org/10.1002/anie.201003707.

(148) Lehn, J.-M. Supramolecular Chemistry—Scope and Perspectives Molecules, Supermolecules, and Molecular Devices (Nobel Lecture). *Angew. Chem. Int. Ed. Engl.* **1988**, *27*, 89–112. https://doi.org/10.1002/anie.198800891.

(149) Ariga, K. Supermolecules. In *Biomaterials Nanoarchitectonics*; Elsevier, 2016; pp 25–40. https://doi.org/10.1016/B978-0-323-37127-8.00003-0.

(150) Brunsveld, L.; Folmer, B. J. B.; Meijer, E. W.; Sijbesma, R. P. Supramolecular Polymers. *Chem. Rev.* **2001**, *101*, 4071–4098. https://doi.org/10.1021/cr990125q.

(151) Krieg, E.; Bastings, M. M. C.; Besenius, P.; Rybtchinski, B. Supramolecular Polymers in Aqueous Media. *Chem. Rev.* **2016**, *116*, 2414–2477. https://doi.org/10.1021/acs.chemrev.5b00369.

(152) Weck, M. Side chain Functionalized Supramolecular Polymers. *Polym. Int.* **2007**, *56*, 453–460. https://doi.org/10.1002/pi.2200.

(153) Fox, J. D.; Rowan, S. J. Supramolecular Polymerizations and Main chain Supramolecular Polymers. *Macromolecules* **2009**, *42*, 6823–6835. https://doi.org/10.1021/ma901144t.

(154) Kato, T.; Frechet, J. M. J. Stabilization of a Liquid-Crystalline Phase through Noncovalent Interaction with a Polymer Side Chain. *Macromolecules* **1989**, *22*, 3818–3819. https://doi.org/10.1021/ma00199a060.

(155) Kumar, U.; Kato, T.; Frechet, J. M. J. Use of Intermolecular Hydrogen Bonding for the Induction of Liquid Crystallinity in the Side Chain of Polysiloxanes. *J. Am. Chem. Soc.* **1992**, *114*, 6630–6639. https://doi.org/10.1021/ja00043a004.

(156) Fouquey, C.; Lehn, J.-M.; Levelut, A.-M. Molecular Recognition Directed Self-Assembly of Supramolecular Liquid Crystalline Polymers from Complementary Chiral Components. *Adv. Mater.* **1990**, *2*, 254–257. https://doi.org/10.1002/adma.19900020506.

(157) Kan, L.; Zhang, P.; Jiang, H.; Zhang, S.; Liu, Z.; Zhang, X.; Ma, N.; Qiu, D.; Wei, H. Microphase Separation of a Quadruple Hydrogen Bonding Supramolecular Polymer: Effect of the Steric Hindrance of the Ureido-Pyrimidone on Their Viscoelasticity. *RSC Adv.* **2019**, *9*, 8905–8911. https://doi.org/10.1039/C8RA08861F.

(158) Spijker, H. J.; van Delft, F. L.; van Hest, J. C. M. Atom Transfer Radical Polymerization of Adenine, Thymine, Cytosine, and Guanine Nucleobase Monomers. *Macromolecules* **2007**, *40*, 12–18. https://doi.org/10.1021/ma0618o8s.

(159) Kim, J. C.; Kim, M.; Jung, J.; Lee, J.; Ree, B. J.; Kim, H.; Kim, I. J.; Kim, J. R.; Ree, M. Synthesis, Physicochemical Characteristics, and Biocompatibility of Self-Assemble Polymers Bearing Guanine, Cytosine, Uracil, and Thymine Moieties. *J. Polym. Sci. Part A Polym. Chem.* **2015**, *53*, 1151–1160. https://doi.org/10.1002/pola.27546.

(160) Ilhan, F.; Gray, M.; Rotello, V. M. Reversible Side Chain Modification through Noncovalent Interactions. "Plug and Play" Polymers. *Macromolecules* **2001**, *34*, 2597–2601. https://doi.org/10.1021/ma001700r.

(161) Thibault, R. J.; Hotchkiss, P. J.; Gray, M.; Rotello, V. M. Thermally Reversible Formation of Microspheres through Non-Covalent Polymer Cross-Linking. *J. Am. Chem. Soc.* **2003**, *125*, 11249–11252. https://doi.org/10.1021/ja034868b.

(162) Concellón, A.; Blasco, E.; Piñol, M.; Oriol, L.; Díez, I.; Berges, C.; Sánchez-Somolinos, C.; Alcalá, R. Photoresponsive Polymers and Block Copolymers by Molecular Recognition Based on Multiple Hydrogen Bonds. *J. Polym. Sci. Part A Polym. Chem.* **2014**, *52*, 3173–3184. https://doi.org/10.1002/pola.27373.

CHAPTER 2

NANOCARRIERS BASED ON AMPHIPHILIC BCs WITH COUMARIN ESTER UNITS

Published in *European Polymer Journal*, **2020**, pending pagination

2.1 Introduction and aims

Light-responsive polymeric nanoparticles assembled from amphiphilic BCs have emerged as attractive nanocarriers for externally regulated release of therapeutic agents to overcome toxicity, solubility or target selectivity limitations associated to classical drug formulations. While the working principle has been widely demonstrated using UV light, for biomedical applications of these systems NIR stimulation is preferred.

Development of amphiphilic BCs has been intimately linked with progress in controlled polymerisation techniques and efficient coupling chemistries that simplify access to very different chemically tuned structures. PEG, approved by the FDA, is a recurrently employed linear hydrophilic polymer since it is commercially available with different end-groups what makes possible its use as macroinitiator in different controlled polymerisations methodologies. Aliphatic biodegradable polycarbonates are an excellent and versatile choice as a hydrophobic polymer because they are easily affordable by ROP with a broad range of chemical handles in which light-responsive units can be integrated by post-polymerisation modification chemistries. Amongst different alternatives, the incorporation of functional moieties by molecular recognition through multiple H-bonding provides great versatility at minimum synthetic cost.

Based on these issues, the aim of the work presented in this chapter was the fabrication of NIR light triggered drug delivery systems from supramolecular biodegradable amphiphilic BCs focussing on the DEACM NIR sensitive group, previously validated by Zhao and co-workers.[1,2] To circumvent tedious synthesis of coumarin monomers, a modular synthetic approach was devised where the lateral anchoring of the light-responsive coumarin takes place by H-bond recognition using the DAP/thymine motif (Figure 2.1). Thus, organocatalysed ROP of a cyclic allyl carbonate was combined with two sequential post-polymerisation modification steps: (i) the covalent integration of the DAP nucleobase analogue by thiol-ene reaction, (ii) the noncovalent integration by H-bond of the light-responsive coumarin with a thymine unit.

Besides, a covalent model was prepared for comparative purposes (Figure 2.1). In this case, the organocatalysed ROP of a cyclic propargyl carbonate was combined with post-polymerisation modification by CuAAC.

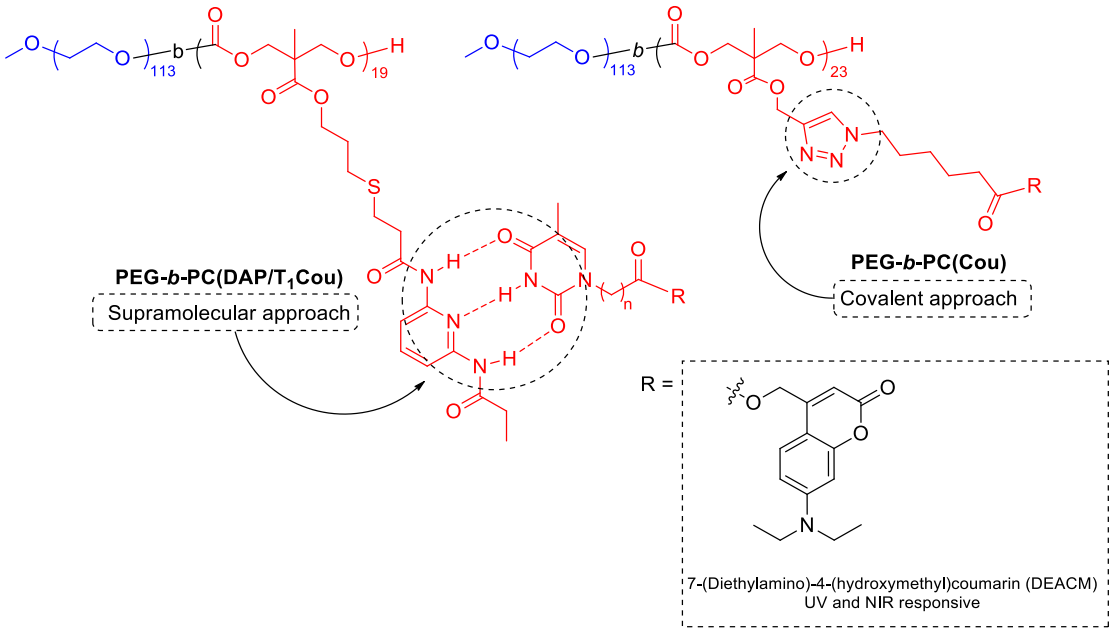

Figure 2.1: Structure of the amphiphilic diblock copolymers studied in this chapter.

According to the objective, the main tasks carried out in this chapter were:

- Synthesis and characterisation of the amphiphilic BC precursors with pendant allyloxy or propargyloxy groups.
- Synthesis and characterisation of the polymer with pendant DAP units and synthesis of the thymine with the DEACM unit. Preparation of the supramolecular amphiphilic BC by recognition between DAP and thymine units.
- Synthesis of the azide with the DEACM unit and synthesis and characterisation of covalent copolymer.
- Study of the self-assembly in water of the amphiphilic BCs. Characterisation of the self-assembled structures including optical properties.
- Encapsulation of a fluorescent probe to evaluate the release stimulated by UV or NIR light.

2.2 Synthesis and characterisation of supramolecular coumarin functionalised amphiphilic block copolymer

A BC precursor consisting on a PEG hydrophilic segment and a polycarbonate block with pendant double bonds, **PEG-*b*-PC(A)**, was prepared by ROP of the allylic cyclic carbonate **MAC** in dichloromethane using PEG-OH with an average polymerisation degree (*n*) of 113 as the macroinitiator, and the organocatalytic system TU/DBU (Figure 2.2). It has been described that the metal-free catalytic system TU/DBU promotes fast polymerisation rates and good control of the ROP for bis-MPA cyclic carbonates limiting concerns about metallic contaminants.[3,4,5] **MAC** was synthesised according to previously reported methods and its ^{1}H NMR is shown in Figure 2.3a.[6] ROP of **MAC** was carried out in dry dichloromethane at 35 °C for 8 h, with a [PEG-OH]:[**MAC**] relation of 1:26 and a [**MAC**]:[TU]:[DBU] relation of 1:0.05:0.01. **PEG-*b*-PC(A)** was analysed by size exclusion chromatography (SEC) that revealed a monomodal narrow distribution with $Đ$ = 1.05 (Figure 2.4). Polymerisation degree of the polycarbonate block was calculated by ^{1}H NMR end-group analysis by comparison of the signals *a*, the terminal methoxy group from PEG, and *e*, corresponding to the methylenic protons close to the ester group from the side chain of the polycarbonate block (Figure 2.3b). The polymerisation degree of the polycarbonate block was found to be 19.

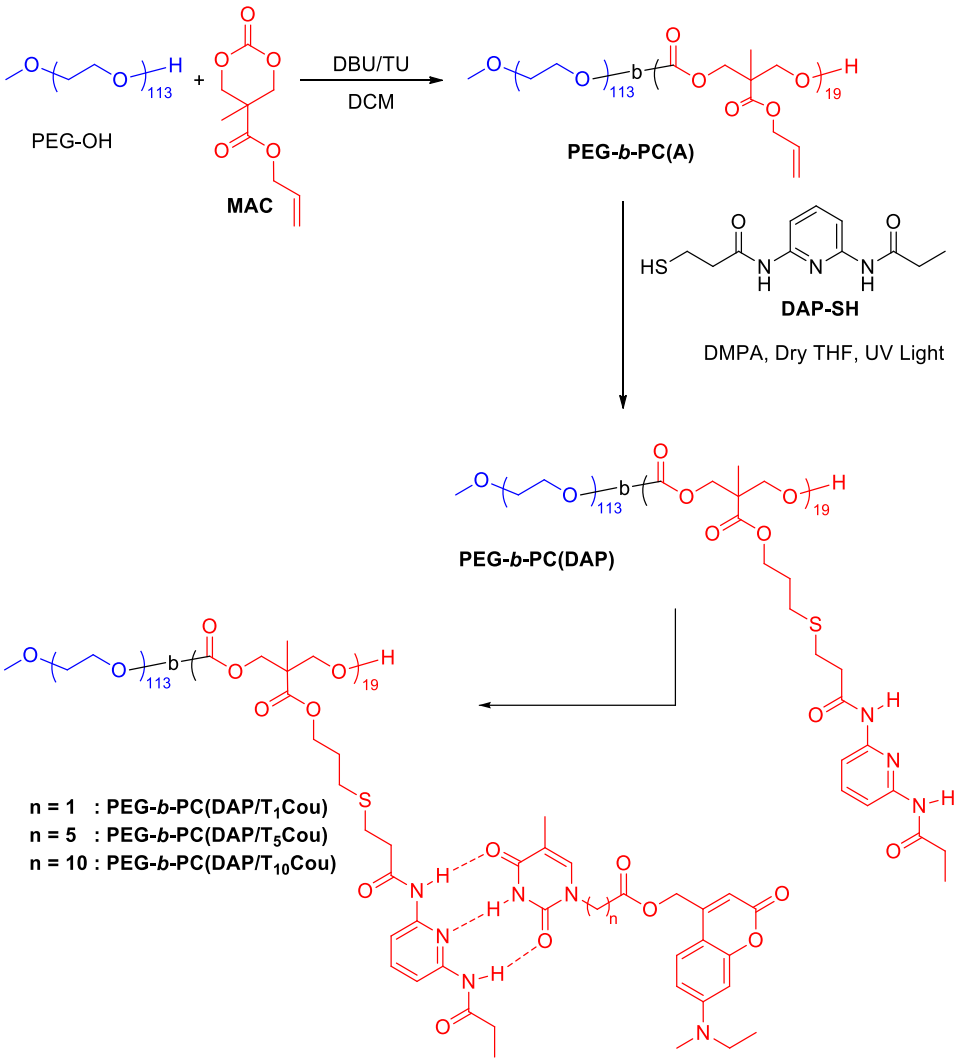

Figure 2.2: Synthetic pathway for the supramolecular copolymer.

The copolymer **PEG-*b*-PC(DAP)** with lateral DAP residues in the polycarbonate block was obtained by thiol-ene reaction between **PEG-*b*-PC(A)** and **DAP-SH** (synthetic details in Experimental Section). Both thermal (using AIBN as radical initiator) and light initiated (using DMPA as UV photoinitiator) thiol-ene reactions were tested with thiol:ene proportions ranging from 1:1 to 5:1. The progress of the functionalisation of the polymeric backbone was followed by the disappearance of the allyl signals at 5.89 and 5.28 ppm (signals *f* and *g*) in the ^{1}H NMR spectrum (Figure 2.3b), and by the appearance of new signals at 2.88 and 2.58 ppm (signals *h* and *g*) corresponding to the methylenic protons close to the thioether group (Figure 2.3c). Quantitative conversion of the vinyl groups according to ^{1}H NMR sensitivity was achieved only under UV light initiation with thiol:ene proportions equal or above to 2:1. SEC analysis for **PEG-*b*-PC(DAP)** revealed monomodal narrow

distribution with a *Đ* value of 1.05 (Figure 2.4). Besides, SEC traces of **PEG-*b*-PC(DAP)** showed a distribution peak shifted to lower retention time compared to **PEG-*b*-PC(A)**, due to the increase in the mass of the copolymer.

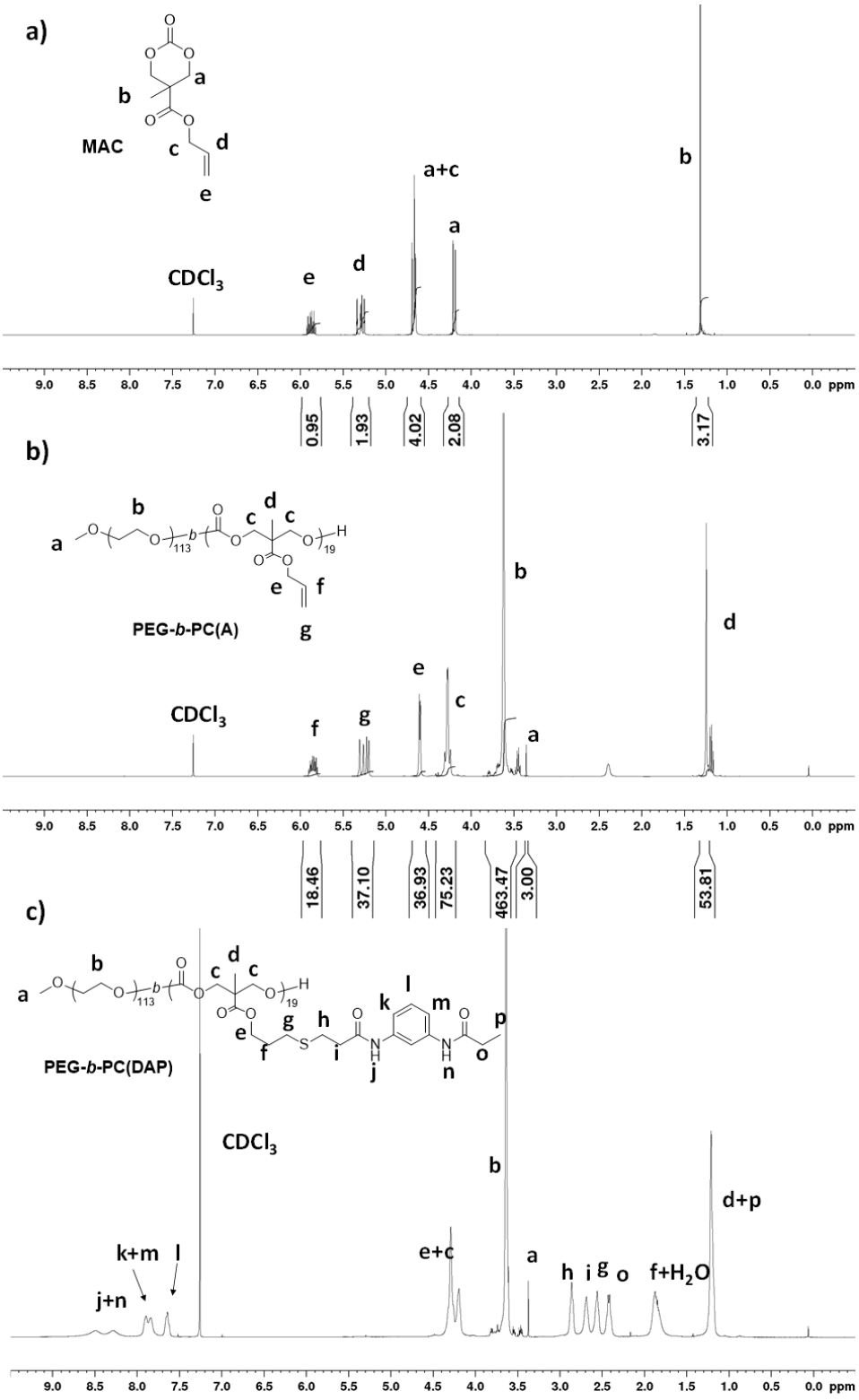

Figure 2.3: ^{1}H NMR (400 MHz, $CDCl_3$) spectra of **MAC** (a), **PEG-*b*-PC(A)** (b) and **PEG-*b*-PC(DAP)** (c).

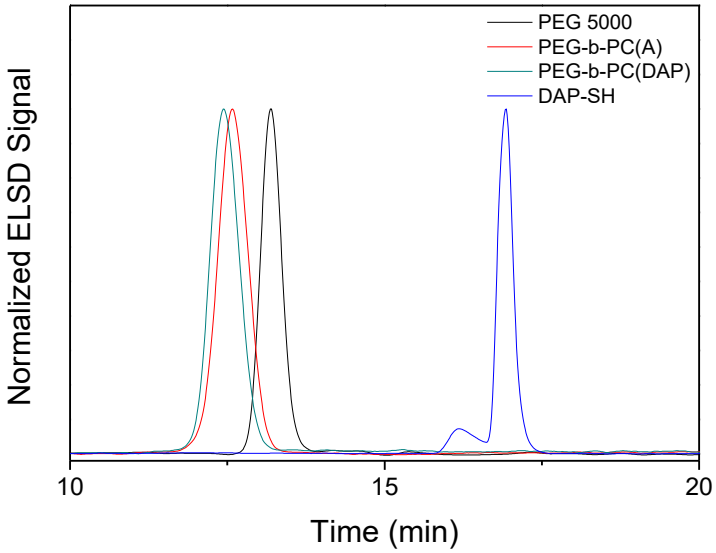

Figure 2.4: SEC traces from PEG, **PEG-*b*-PC(A)**, **PEG-*b*-PC(DAP)** and **DAP-SH**.

The corresponding coumarin functionalised supramolecular copolymers, were formed by DAP/T paring when dissolving **PEG-*b*-PC(DAP)** and the thymine-coumarin units, **T_nCou** (n = 1, 5, 10), in THF and subsequent slow evaporation of the solvent under continuous shaking at room temperature. Different spacers between the thymine unit and the light-responsive coumarin unit were tested and the corresponding supramolecular polymers were tagged as **PEG-*b*-PC(DAP/T_nCou)**, (n = 1, 5, 10) (Figure 2.2). Molar ratios of both precursors were calculated to functionalise 95% of the DAP units with **T_nCou**, to avoid an excess of **T_nCou**. Hydrogen bond formation in the bulk solid material was assessed by FTIR by the modification of the C=O and N-H amide bands, of **PEG-*b*-PC(DAP)**, **T_nCou** and **PEG-*b*-PC(DAP/T_nCou)** (see Figure 2.5 for **PEG-*b*-PC(DAP/T_1Cou)** as an example). Hydrogen bond formation was also observed by ^{1}H NMR in $CDCl_3$ solution, as the protons involved in the hydrogen bonds shifted to lower fields. The resonance at 8.85 ppm in **T_1Cou** (H_a) moved to 10.52 ppm in **PEG-*b*-PC(DAP/T_1Cou)** (Figure 2.6a and 2.6b) and resonance at 8.39 ppm corresponding to the DAP unit in **PEG-*b*-PC(DAP)** (H_b) shifted to 9.48 ppm in **PEG-*b*-PC(DAP/T_1Cou)** (Figure 2.6b and 2.6c).

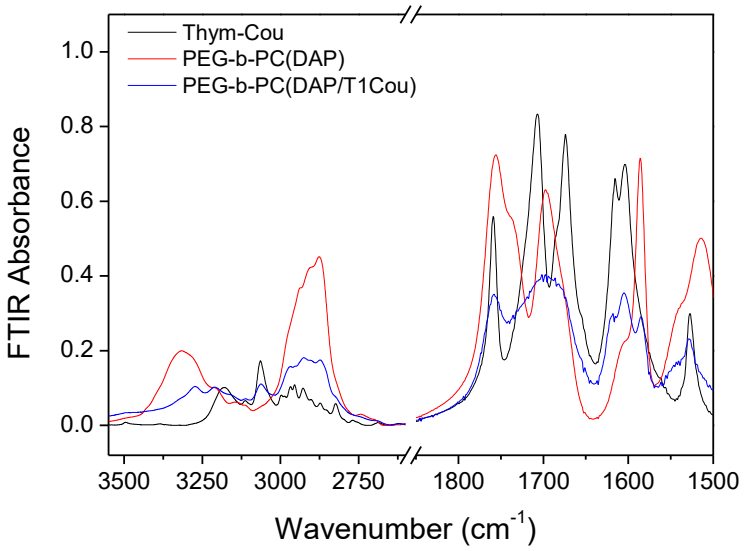

Figure 2.5: FTIR (in KBr) spectra corresponding to **T₁Cou**, **PEG-*b*-PC(DAP)** and **PEG-*b*-PC(DAP/T₁Cou)**.

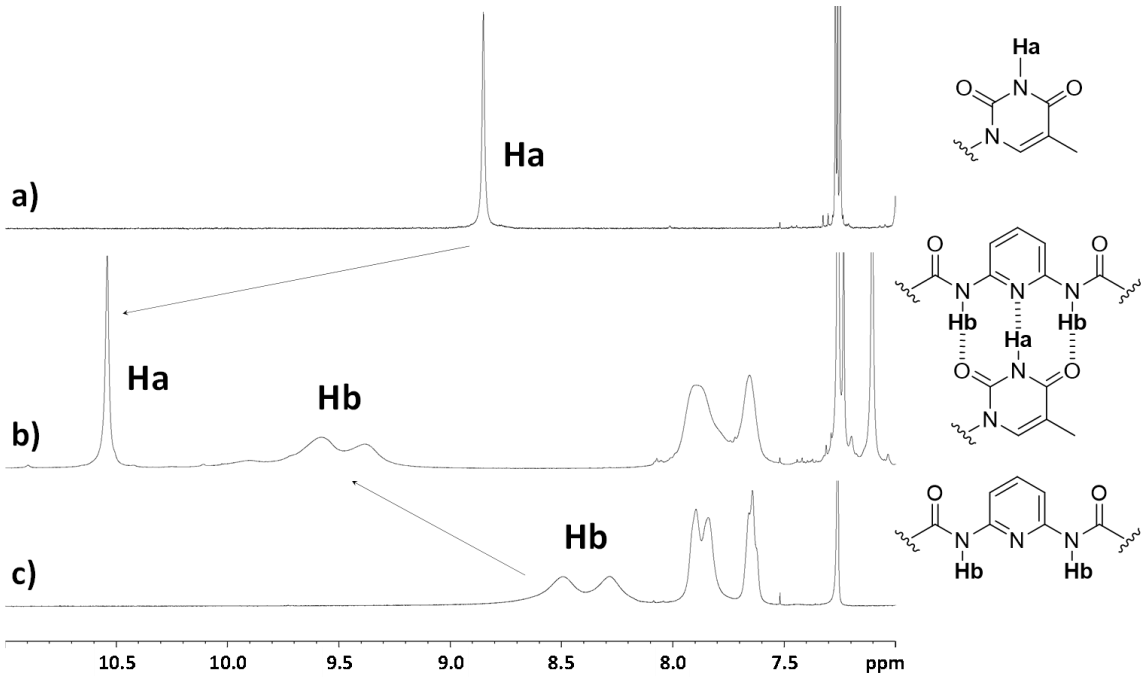

Figure 2.6: ^{1}H NMR (400 MHz, $CDCl_3$) spectra of **T₁Cou (a)**, **PEG-*b*-PC(DAP/T₁Cou)** (b) and **PEG-*b*-PC(DAP)** (c).

2.3 Synthesis and characterisation of covalent coumarin functionalised amphiphilic block copolymer

The reference covalent functionalised copolymer, **PEG-*b*-PC(Cou)**, was obtained by reaction of the alkynyl side groups of a precursor polymer, **PEG-*b*-PC(P)**, with the azide **N_3-Cou** *via* CuAAC (Figure 2.7).[7,8] In this case, the covalent incorporation of the coumarin by a photoinitiated thiol-ene post-polymerisation reaction was discarded to prevent its premature photolysis under UV illumination.

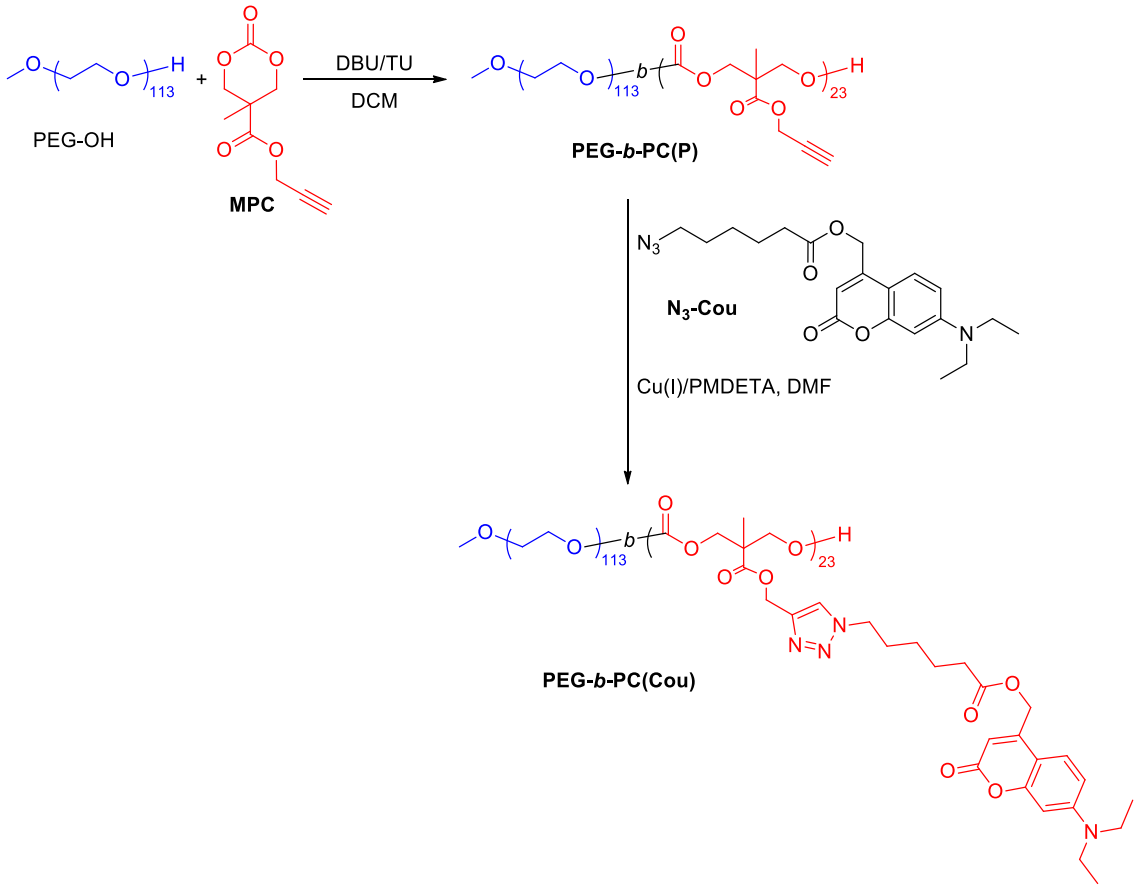

Figure 2.7: Synthetic pathway to covalent functionalised copolymer.

The synthesis of the precursor polymer was afforded by ROP of the propargyloxy functionalised cyclic carbonate **MPC,** realised following the same procedure used for **PEG-*b*-PC(A)**, with a [PEG-OH]:[**MPC**] relation of 1:30 and a [**MPC**]:[TU]:[DBU] relation of 1:0.05:0.01. **MPC** was synthesised according to previous reported methods and its ^{1}H NMR is shown in Figure 2.8a.[9] The polymerisation degree of the polycarbonate block was found to be 23, as calculated by ^{1}H NMR end-group analysis

from comparison of *a* and *e* signals (Figure 2.8b). SEC analysis showed a monomodal narrow distribution with $Đ$ = 1.08 (Figure 2.9).

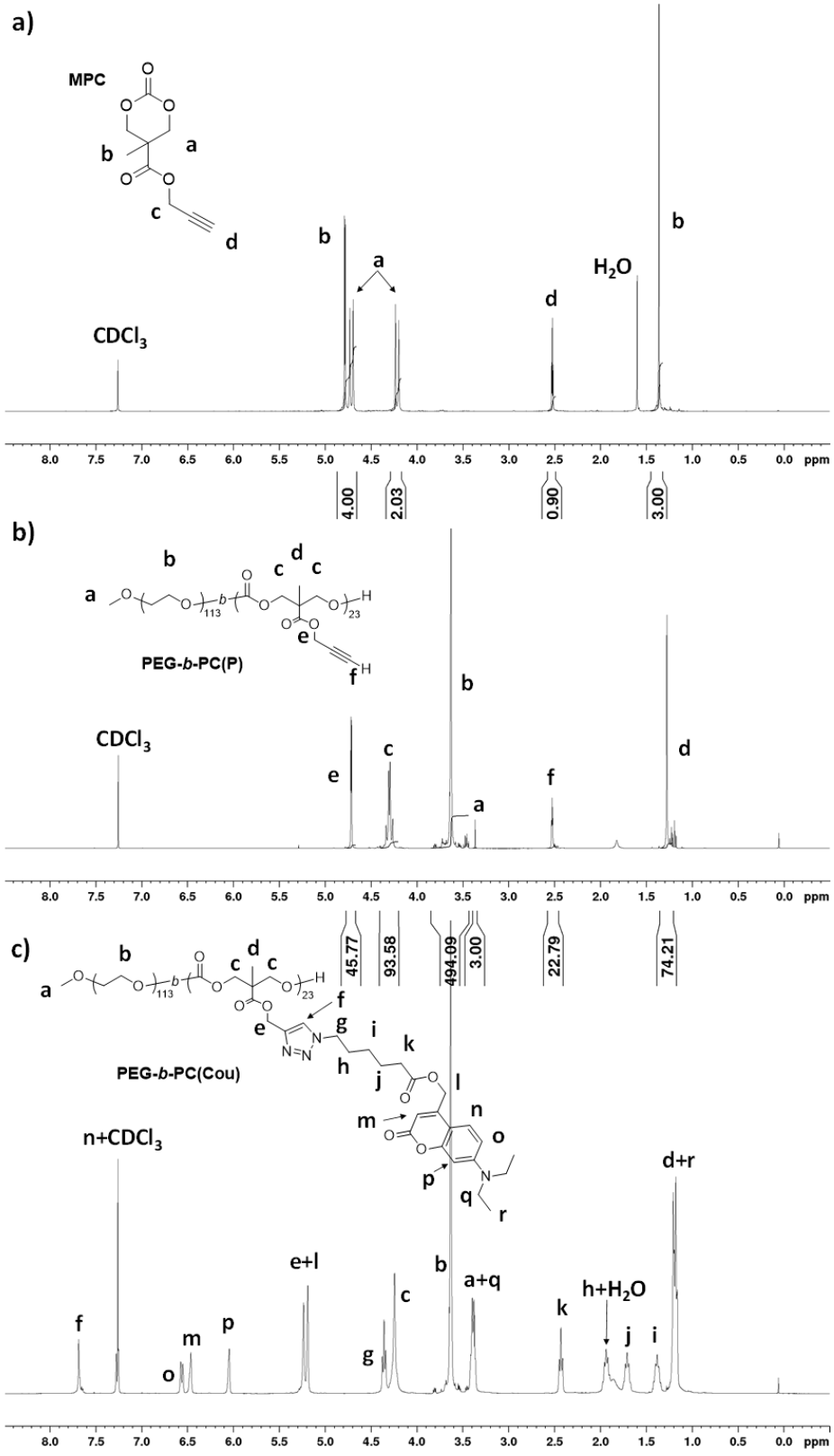

Figure 2.8: ^{1}H NMR (400 MHz, $CDCl_3$) spectra of **MPC** (a), **PEG-*b*-PC(P)** (b) and **PEG-*b*-PC(Cou)** (c).

Post-polymerisation of the pendant propargyl groups with the azide **N_3-Cou** (synthetic details in Experimental Section) was performed *via* CuAAC using the catalytic system CuBr/*N,N,N′,N″,N″*-pentamethyldiethylenetriamine (PMDETA) with a two-fold molar excess of **N_3-Cou**, looking for a quantitative functionalisation of the polymeric backbone. The CuAAC modification of **PEG-*b*-PC(P)** was assessed from the disappearance of the alkynyl proton (*f*, Figure 2.8b) and the shifting of the vicinal methylenic protons (*e*, Figure 2.8b and Figure 2.8c), and the appearance of the triazole proton resonance (*f*, Figure 2.8c). Also, the extension of the post-polymerisation modification was evaluated by FTIR in KBr disk from the disappearance of Csp–Hst and Csp–Cspst bands (Figure 2.10). Taking into account the sensitivity of both spectroscopic techniques, the post-polymerisation functionalisation was considered quantitative. SEC traces of **PEG-*b*-PC(Cou)** (dispersity value $Đ$ = 1.08) showed a distribution peak shifted to lower retention times compared to **PEG-*b*-PC(P)**, due to the increase in the mass of the functionalised copolymer (Figure 2.9).

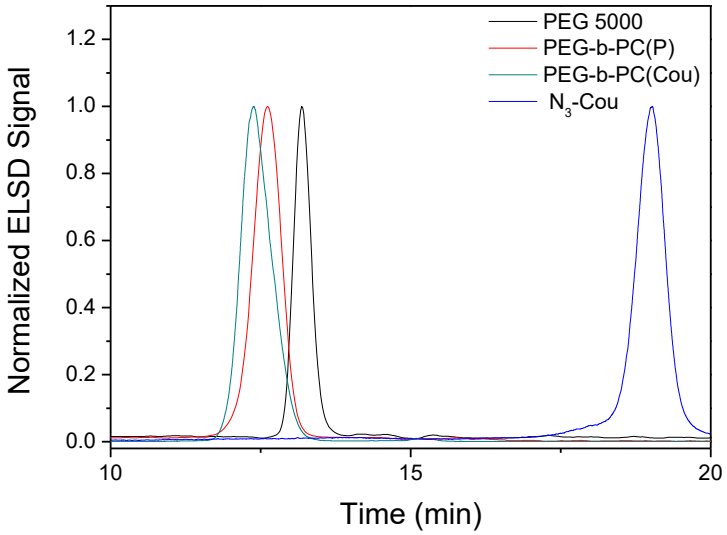

Figure 2.9: SEC traces of PEG, **PEG-*b*-PC(P)**, **PEG-*b*-PC(Cou)** and **N_3-Cou**.

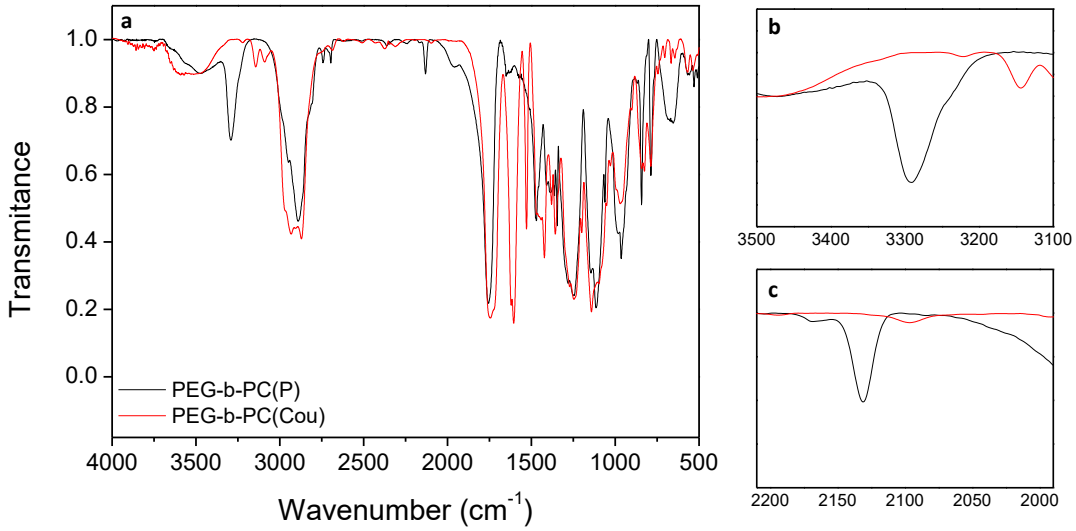

Figure 2.10: **PEG-*b*-PC(P)** and **PEG-*b*-PC(Cou)** FTIR spectra (KBr disk) (a), and zoom to Csp-H interval (b) and Csp-Csp interval (c).

Preliminary studies to gain information about the photoscission of the coumarin ester bond were carried out by irradiating **T_1Cou** and **PEG-*b*-PC(Cou)** solutions in DMSO-d^6 at a 10 μM concentration of coumarin ester units with UV light (365 nm, irradiance of 30 mW cm^{-2}). The hydrolysis process was followed by ^{1}H NMR from the shifting of the methylenic protons close to the ester group (H_a) and the disappearance of the methylenic protons from the coumarin unit (H_b) (Figure 2.11 and Figure 2.12). After 60 min of irradiation the scission of the photolabile coumarin ester bond was near to quantitative as confirmed by ^{1}H NMR, see Figure 2.11 for **T_1Cou** and Figure 2.12 for **PEG-*b*-PC(Cou)**.

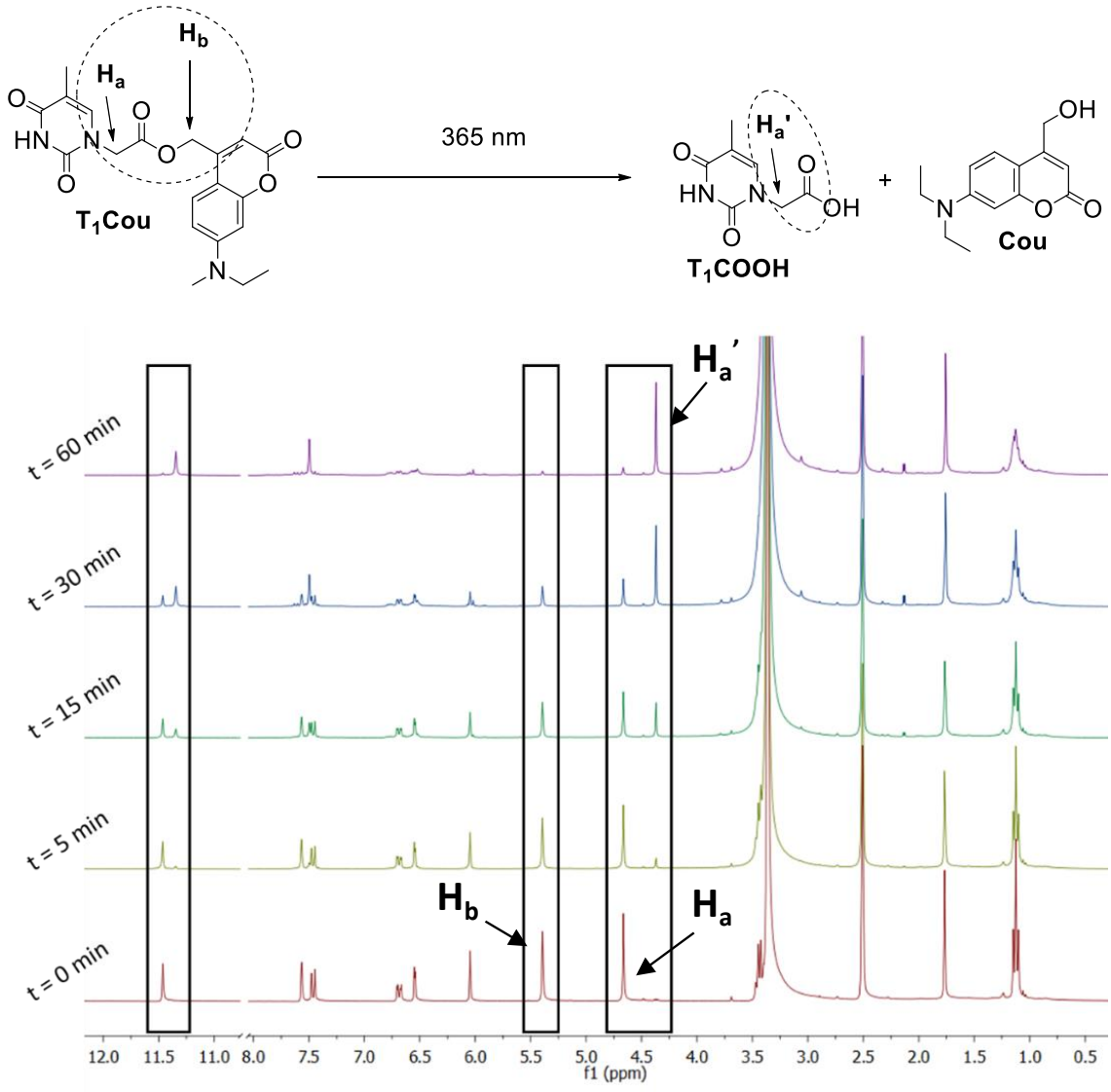

Figure 2.11: Photoscission of the coumarin ester unit from **T1Cou** (top) and ^{1}H NMR assessment of the photoscission of **T1Cou** under 365 nm (30 mW cm^{-2}) illumination in d^{6}-DMSO at different times at a 10 μM concentration of coumarin units (bottom).

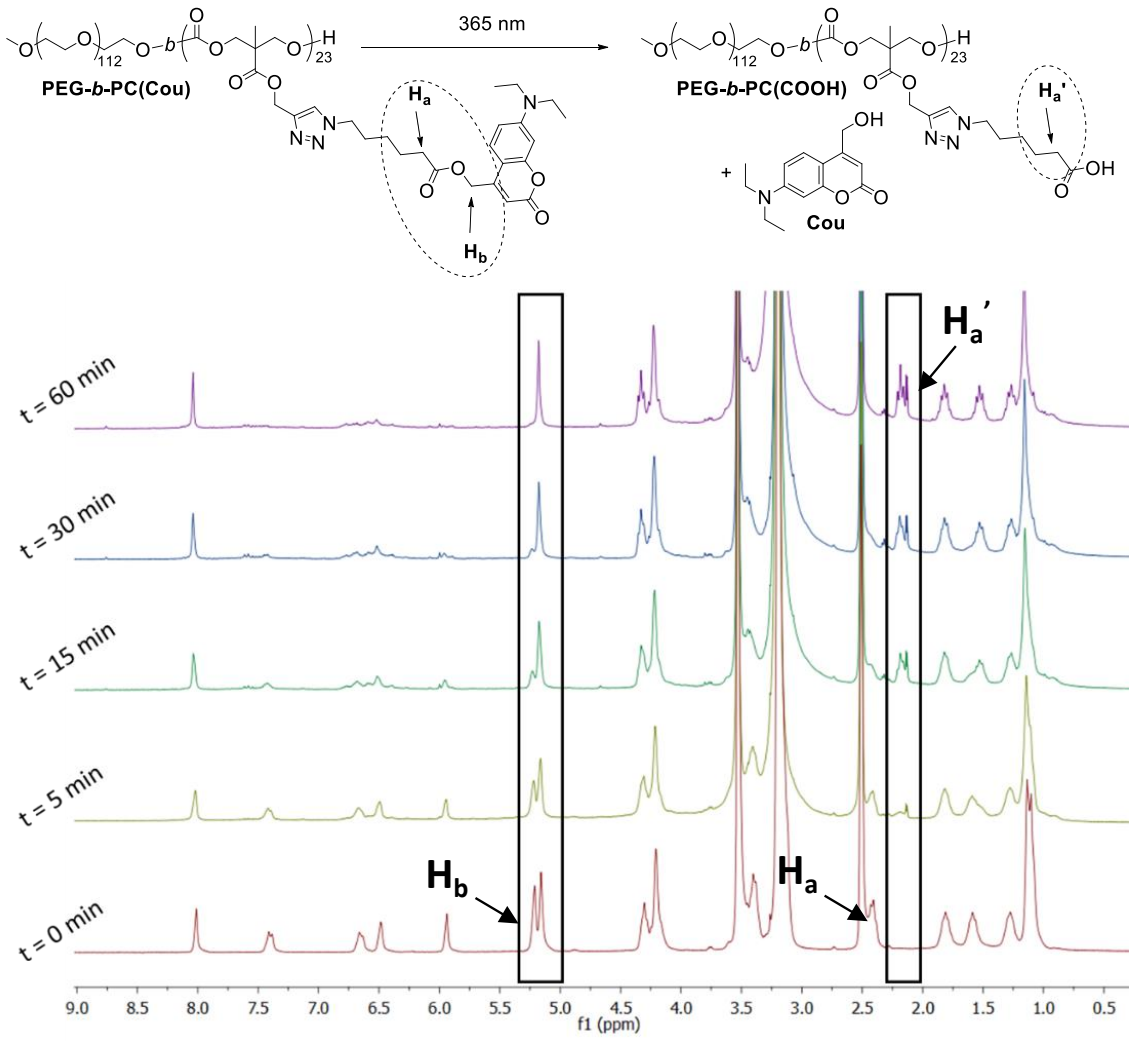

Figure 2.12: Photoscission of the coumarin ester unit from **PEG-*b*-PC(Cou)** (top) and ^{1}H NMR assessment of the photoscission of **PEG-*b*-PC(Cou)** under 365 nm (30 mW cm^{-2}) illumination in d^{6}-DMSO at different times at a 10 μM concentration of coumarin units (bottom).

2.4 Preparation and characterisation of self-assemblies in water

Self-assembly of **PEG-*b*-PC(DAP/T$_n$Cou)** and **PEG-*b*-PC(Cou)** was promoted by solvent switching starting from THF solutions of the copolymers and gradually adding water. The preparation of stable solutions of polymeric self-assemblies from the supramolecular polymers **PEG-*b*-PC(DAP/T$_n$Cou)** was strongly dependent on the length of the alkyl spacer connecting the coumarin to the thymine. Polymers with long spacers (n = 5, 10) formed a precipitate during the self-assembly process, while polymer with a shorter spacer (n = 1) formed a stable self-assemblies solution. Therefore, only supramolecular copolymer **PEG-*b*-PC(DAP/T$_1$Cou)**, and the covalent model, **PEG-*b*-PC(Cou)** were further investigated. Critical aggregation concentration (CAC) values determined by fluorescence spectroscopy experiments using Nile Red were 20 μg mL^{-1} for **PEG-*b*-PC(DAP/T$_1$Cou)** and 32 μg mL^{-1} for **PEG-*b*-PC(Cou)** (Figure 2.13). According to transmission electron microscopy (TEM) images, both **PEG-*b*-PC(DAP/T$_1$Cou)** and **PEG-*b*-PC(Cou)** formed spherical micelles with diameters around 25 nm (Figure 2.14). Micellar dispersions were analysed at room temperature by dynamic light scattering (DLS) showing monomodal size distribution curves with average hydrodynamic diameters (D_h) of 23 nm for **PEG-*b*-PC(DAP/T$_1$Cou)** and 28 nm for **PEG-*b*-PC(Cou)** (Figure 2.14). The samples were monitored up to three weeks showing almost constant D_h values along this period and not signs of precipitation (Figure 2.15). Overall results suggest a similar thermodynamic and temporal stability of the supramolecular and covalent BCs micellar self-assemblies, validating the hydrogen bond anchoring of the coumarin as a suitable strategy to access responsive nanocarriers from amphiphilic BCs.

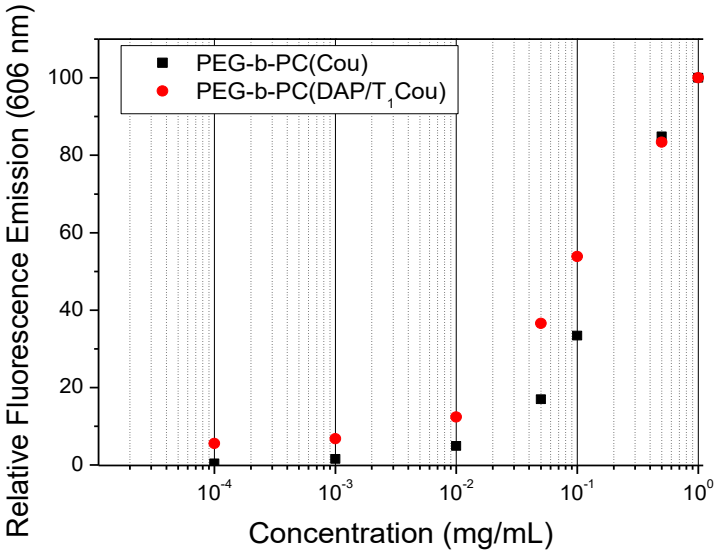

Figure 2.13: Normalised fluorescence emission of Nile Red at 606 nm (λ_{exc} = 550 nm) *versus* the copolymer concentration.

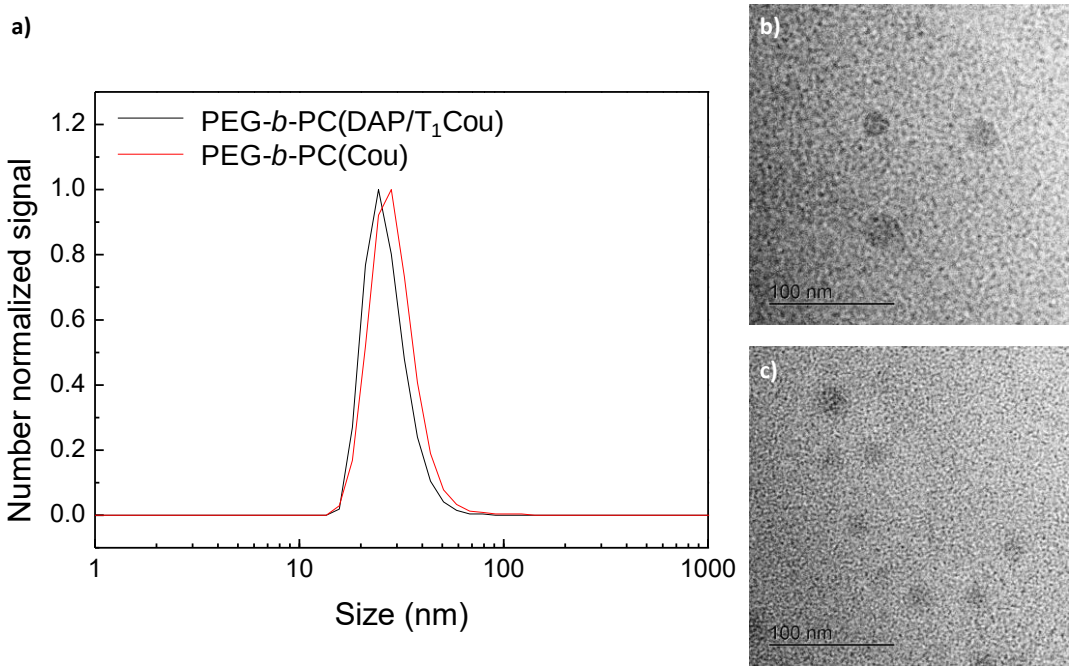

Figure 2.14: DLS traces of **PEG-*b*-PC(DAP/T1Cou)** and **PEG-*b*-PC(Cou)** (a), TEM images of **PEG-*b*-PC(DAP/T1Cou)** (b), and **PEG-*b*-PC(Cou)** (c).

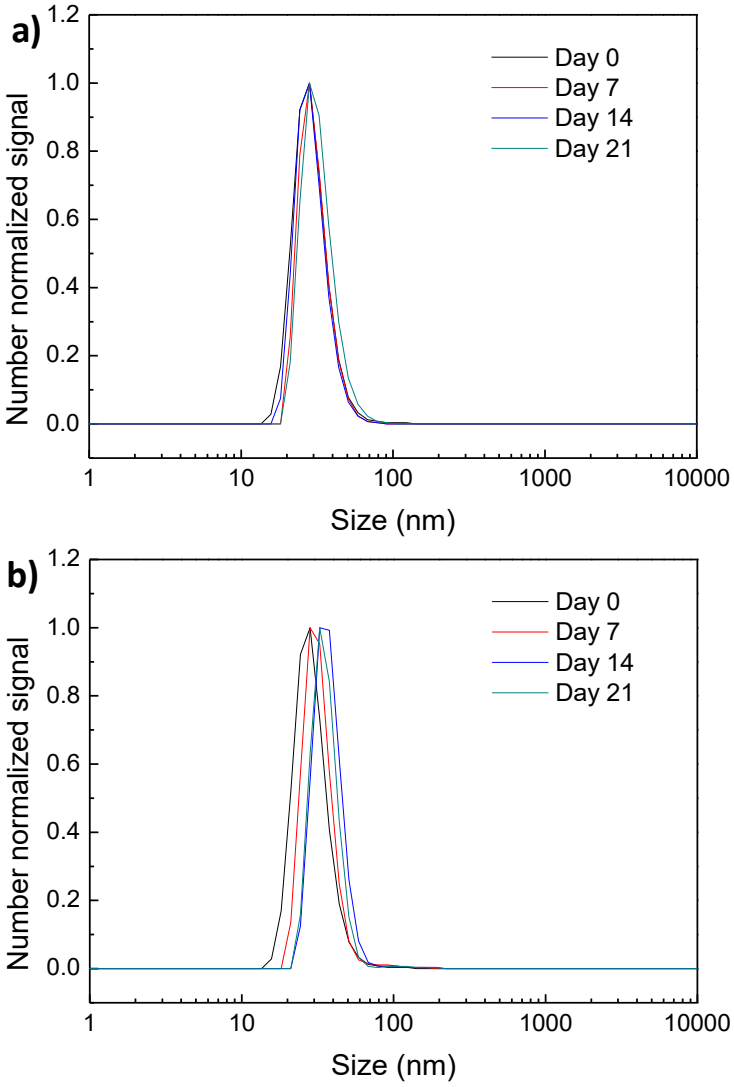

Figure 2.15: Temporal evolution of the number size distribution self-assemblies *versus* particle diameter for **PEG-*b*-PC(DAP/T$_1$Cou) (a)** and **PEG-*b*-PC(Cou)** (b).

UV-Vis and fluorescence spectra of the aqueous micelle dispersions were measured and compared with those in THF solution (Figure 2.16). Similar spectra profiles were recorded for **PEG-*b*-PC(DAP/T$_1$Cou)** and **PEG-*b*-PC(Cou)**, since the main spectral features are associated with the absorption/emission properties of the coumarin unit. A strong absorption band of the coumarin group was visible at 370 nm in THF. This band broaden and red shifted in the aqueous micelles dispersion, in particular in the supramolecular copolymer. A strong emission was observed at 450 nm in THF (λ_{exc}=370 nm) due to the coumarin. In the aqueous micellar dispersions, this emission was quenched due to the high local concentration of the coumarin inside of the micelle core.[1] A shift of the emission band was observed for the aqueous

micellar suspensions, from 450 to 489 nm for **PEG-*b*-PC(DAP/T$_1$Cou)** and to 475 nm for **PEG-*b*-PC(Cou)**.

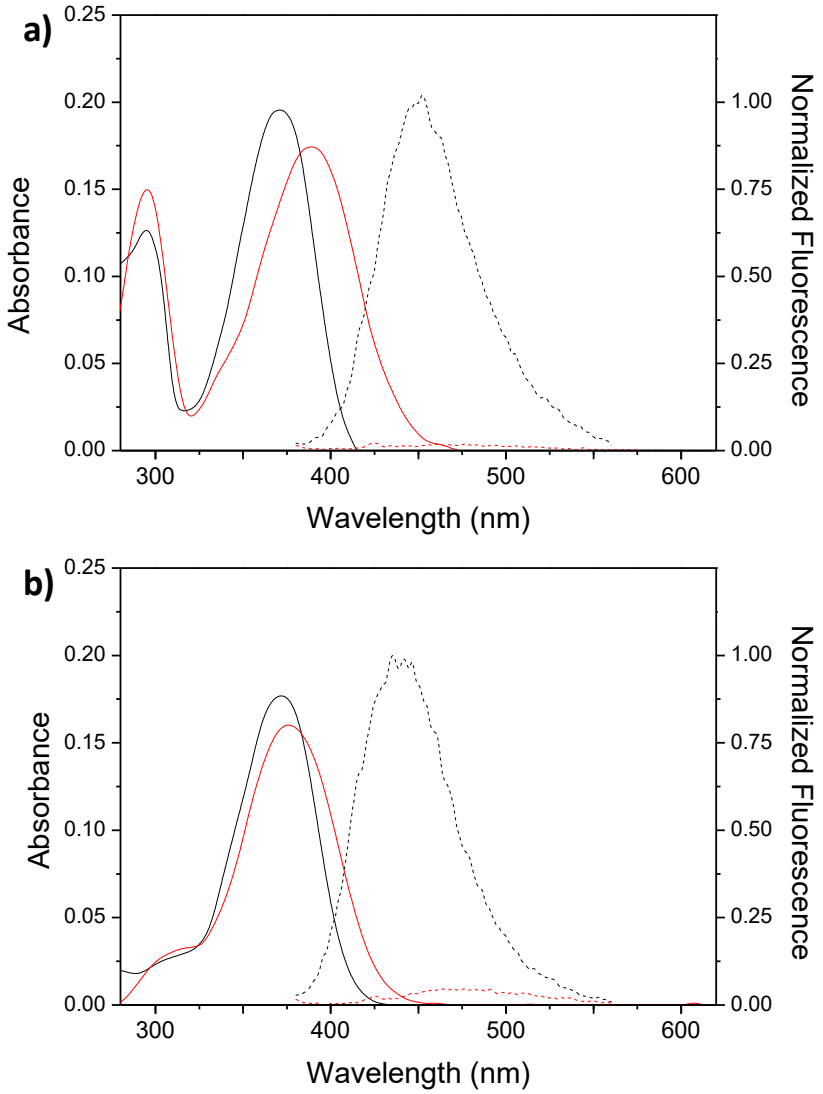

Figure 2.16: UV-Vis (solid line) and emission (λ_{exc} = 370 nm, dashed line) spectra in THF solution (black) and of the micellar dispersion in water (red) of **PEG-*b*-PC(DAP/T$_1$Cou)** (a) and **PEG-*b*-PC(Cou)** (b). Concentration of coumarin units was adjusted to about 10^{-4} M for UV-vis spectra and 10^{-6} M for emission spectra for both copolymers.

2.5 Release properties of photoresponsive micelles

Nile Red is a hydrophobic molecule which exhibit an intense emission at 620 nm (λ_{exc}=550 nm) in nonpolar media, while this emission is quenched in polar environments. The optical properties of Nile Red make it widely used as a fluorescent probe. The emission spectra of Nile Red loaded micellar dispersions from **PEG-*b*-PC(DAP/T$_1$Cou)** and **PEG-*b*-PC(Cou)** (Figure 2.17) showed two weak emission peaks when exciting at 370 nm. The highest energy one at approx. 480 nm corresponded to the above described emission of the coumarin. The lowest energy one at 620 nm was the Nile Red emission band due to a non-radiative energy transfer process from the excited coumarin to encapsulated Nile Red as they are both closely packed at the core of the micelle.[1] Consistently, the emission band located at 620 nm was not observed upon excitation at 370 nm of plain micelles that were not loaded with Nile Red (Figure 2.17). Nile Red loaded micelles showed almost identical sizes and morphologies than unloaded ones.

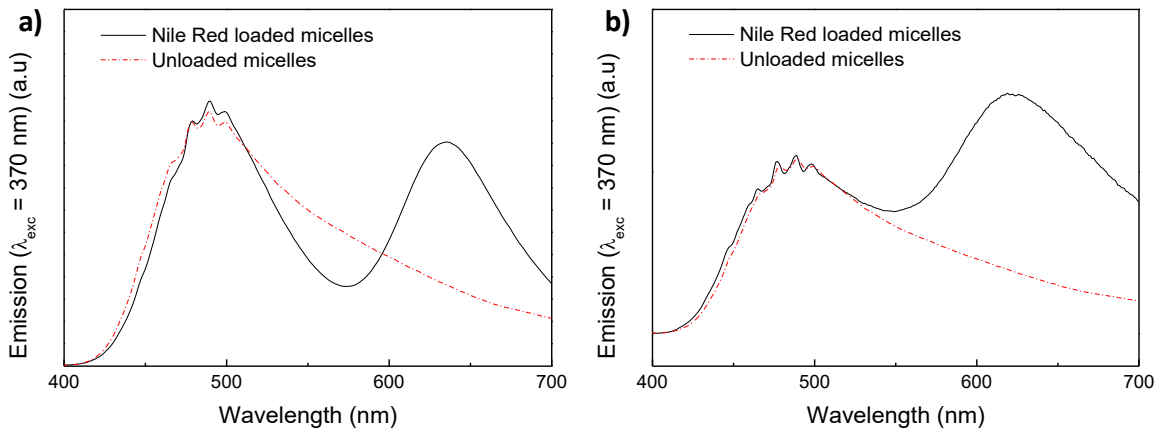

Figure 2.17: Fluorescence spectra (λ_{exc} = 370 nm) of Nile Red loaded and unloaded micelles from **PEG-*b*-PC(DAP/T$_1$Cou)** (a) and **PEG-*b*-PC(Cou)** (b).

Nile Red loaded micelles were irradiated at 365 nm (30 mW cm^{-2}) for different time intervals and changes on the emission spectra upon excitation of the coumarin unit at 370 nm or Nile Red at 550 nm were monitored. When micelles dispersions were irradiated at 365 nm (30 mW cm^{-2}), the coumarin emission band at 480 nm increased steadily due to photoscission and diffusion of the coumarins from the micelles core, and minimization of coumarin self-quenching (Figure 2.18).[1] After 40

min, an increase in the coumarin unit emission of a 60% for **PEG-*b*-PC(DAP/T$_1$Cou)** and 360% for **PEG-*b*-PC(Cou)** was measured. These changes on emission recorded after 40 min at 365 nm irradiation are in agreement with the photoscission of the coumarin unit and its release from the micelles core.

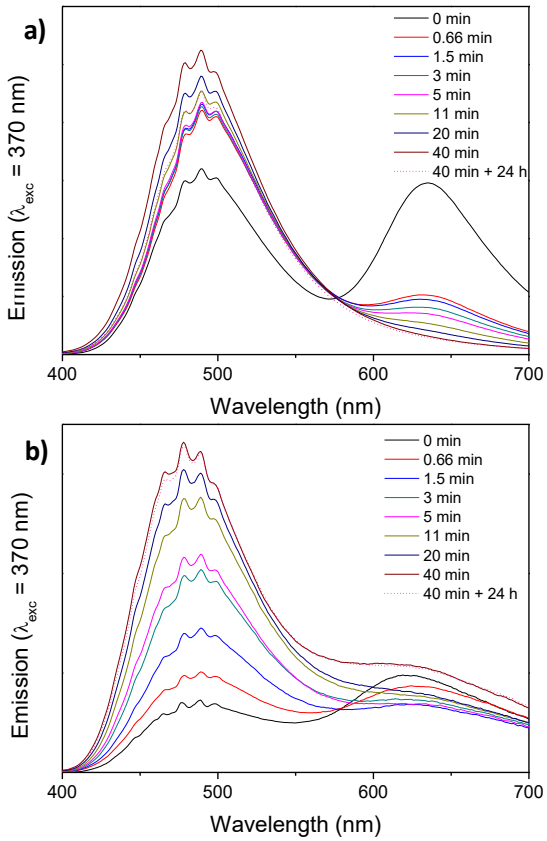

Figure 2.18: Emission spectra (λ_{exc} = 370 nm) of the Nile Red loaded **PEG–*b*–PC(DAP/T$_1$Cou)** (a) and **PEG–*b*–PC(Cou)** (b) micelles when exposed at 365 nm (30 mW cm^{-2}) for different times.

Changes on size and morphology of the Nile Red loaded micelles upon 365 nm illumination were tracked by TEM and DLS. The TEM images of irradiated micelles of **PEG-*b*-PC(DAP/T$_1$Cou)** showed a slight alteration of the surface while non-significant changes were detected in DLS measurements (Figure 2.19). Therefore, we conclude that the photodissociation of **T$_1$Cou** to generate the thymine unit, **T$_1$COOH** (Figure 2.11), and release of the coumarin unit, as deduced from the increase in its emission (Figure 2.18), did not induce acute changes in the morphology of the self-assemblies. To interpret these observations micelles of the copolymer **PEG-*b*-PC(DAP/T$_1$COOH)** (Figure 2.20) were prepared. Spherical micelles of similar sizes and morphology to **PEG-*b*-PC(DAP/T$_1$Cou)** were obtained,

suggesting that after the photocleavage of the thymine-coumarin unit, **T1Cou**, the polymeric aggregates allowed reassembly of the polymer into micelles of similar sizes (Figure 2.20).

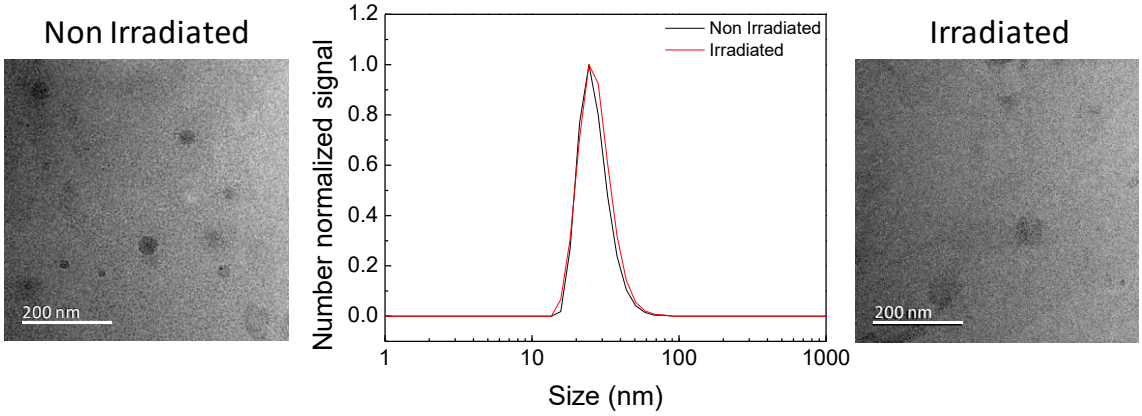

Figure 2.19: DLS traces and TEM images before (left) and after (right) 40 min 365 nm irradiation of **PEG-*b*-PC(DAP/T1Cou)** self-assemblies.

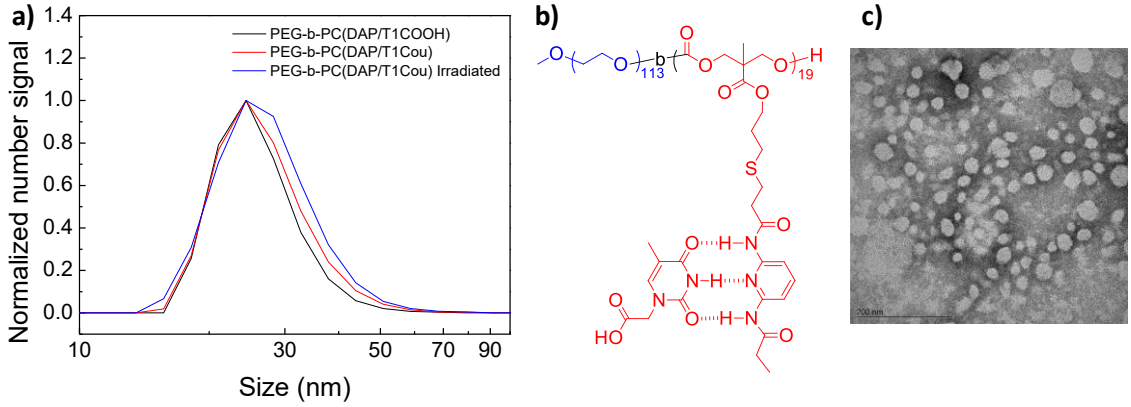

Figure 2.20: DLS traces of **PEG-*b*-PC(DAP/T1COOH)** and **PEG-*b*-PC(DAP/T1Cou)** before and after irradiation (a), structure of **PEG-*b*-PC(DAP/T1COOH)** (b) and TEM image of **PEG-*b*-PC(DAP/T1COOH)** (c).

After exposure at 365 nm for 40 min the initial spherical micelles of the covalent copolymer appeared as smashed and larger micellar structures (Figure 2.21). By DLS, the average D_h increased from 28 nm to 70 nm after UV light irradiation.

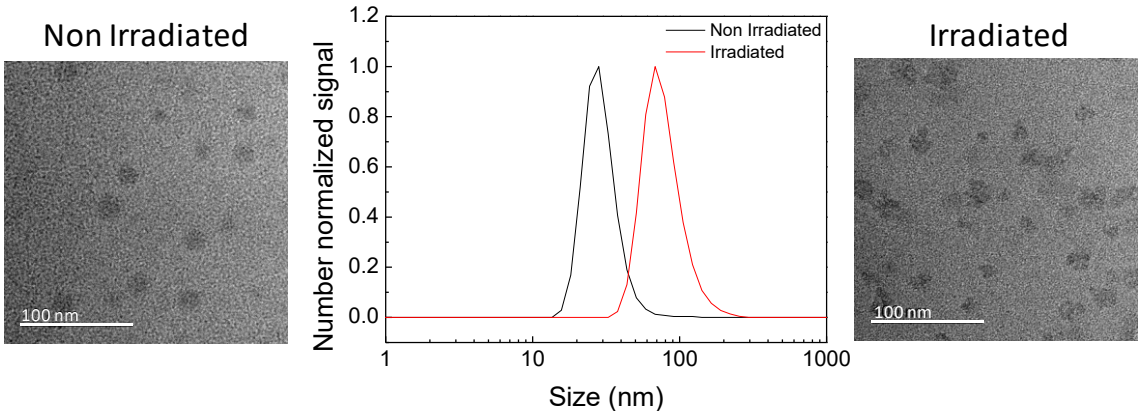

Figure 2.21: DLS traces and TEM images before (left) and after (right) 40 min 365 nm irradiation of **PEG-*b*-PC(Cou)** self-assemblies.

Figure 2.22 shows the evolution of the Nile Red emission upon 550 nm excitation of irradiated samples and the non-irradiated ones taken as reference. In the case of the non-irradiated micelles of supramolecular and covalent BCs, emission was almost constant in the studied range of time, evidencing that Nile Red is not released by a physical diffusion process. Under exposure at 365 nm (30 mW cm^{-2}), an abrupt decrease in emission was observed after 100 s for the covalent **PEG-*b*-PC(Cou)**, as Nile Red environment becomes more polar. In the case of **PEG-*b*-PC(DAP/T$_1$Cou)** the decrease in emission was more gradual, as expected from the less acute morphological changes in the supramolecular copolymer than in the covalent model. Because UV light irradiation did not induce a drastic disruption of the micellar morphology, it should be expected that a mainly hydrophobic core was maintained after coumarin release. Under this premise, decrease of the Nile Red emission should be more likely related with the release, at least partial, of the probe to the surrounding polar medium than with a shift in the polarity of the hydrophobic block induced by the photoscission of the coumarin ester unit. These results are in accordance with the previously described by Zhao and coworkers, which described Nile Red release under similar conditions on covalent copolymers. The final normalised Nile Red emission was similar for **PEG-*b*-PC(DAP/T$_1$Cou)** and

PEG-*b*-PC(Cou), though longer exposure times were required in the case of the supramolecular copolymer to achieve it due to a slower emission decrease.

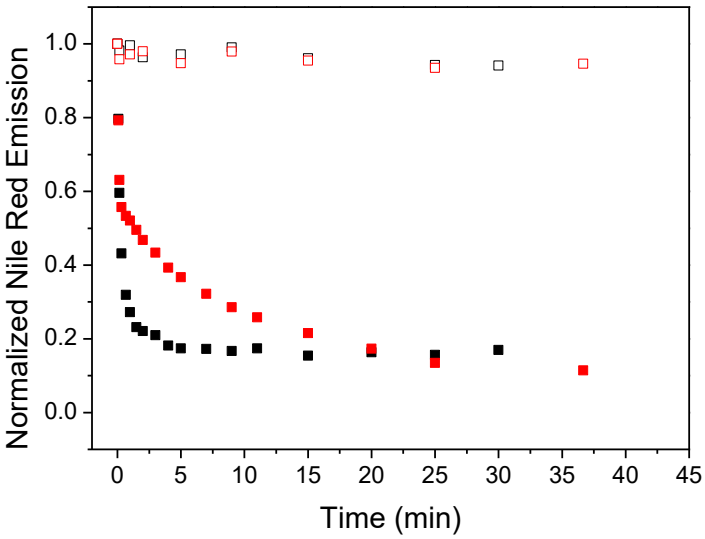

Figure 2.22: Normalised emission at 620 nm (λ_{exc} = 550 nm) of Nile Red vs UV irradiation time for **PEG-*b*-PC(DAP/T$_1$Cou)** (solid red for the irradiated sample and hollow red for reference) and **PEG-*b*-PC(Cou)** (solid black for the irradiated sample and hollow black for reference).

Once the behaviour of **PEG-*b*-PC(Cou)** and **PEG-*b*-PC(DAP/T$_1$Cou)** under UV-light stimulation was established, similar experiments were performed using NIR illumination. Samples were exposed to 730 nm light using a Chameleon Ultra II Ti:Sapphire laser (nominal power around 2 W at 730 nm) at laser power 10 or 20%. Emission of the Nile Red at 620 nm was monitored *in situ* (λ_{exc}=514 nm). Initially, a reference experiment without 730 nm light irradiation was carried out to determine the stability of the Nile Red upon excitation at 514 nm. A decrease of the emission intensity was detected, which was associated to photobleaching of Nile Red (Figure 2.23, reference in blue). When micelles in aqueous media were exposed to 730 nm light, the emission intensity decreased steadily when increasing the irradiation time. This decay was twice as fast when doubling the laser power (Figure 2.23). The NIR-induced response of the Nile Red micelles was slower than with UV irradiation. This is attributed to the lower efficiency inherent to two-photon processes. Again, different Nile Red emission profiles were observed for the covalent and supramolecular block copolymer, being slower for **PEG-*b*-PC(DAP/T$_1$Cou)** in agreement with Nile Red emission evolution observed under 365 nm stimulation.

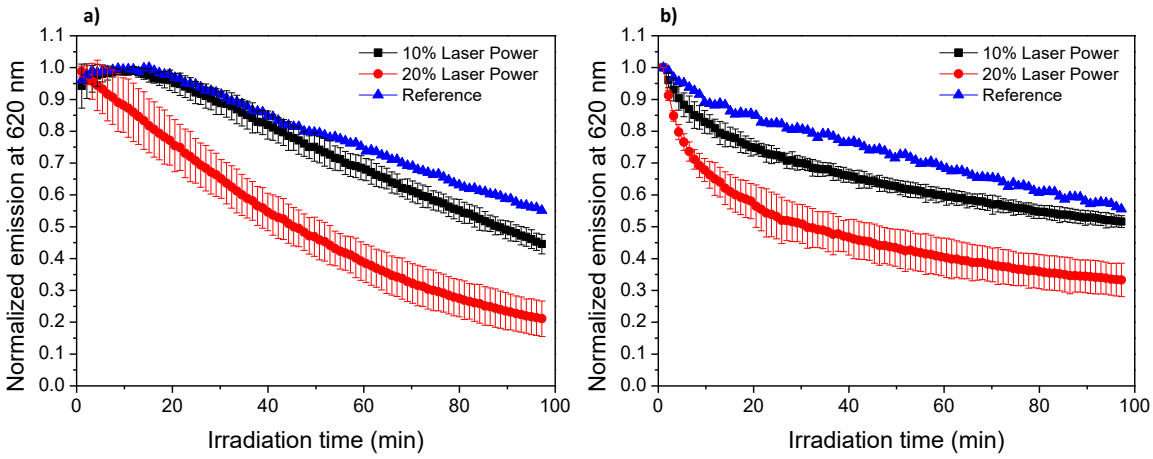

Figure 2.23: Evolution of normalised emission at 620 nm (λ_{exc}=514 nm) of Nile Red *versus* NIR (730 nm) irradiation time for **PEG-*b*-PC(DAP/TICou)** (a) and **PEG-*b*-PC(Cou)** (b).

2.6 Conclusions

Two amphiphilic BCs comprised by hydrophilic PEG and hydrophobic aliphatic polycarbonate have been synthesised by organocatalysed ROP. The introduction of the light-responsive unit, DEACM, has been approached either by supramolecular or covalent strategies. Both copolymers have proved their self-assembly capability when dispersed in water, forming micelles of about 25 nm diameter. Irradiation with 365 nm light induced the photoscission of the coumarin unit that led to morphological changes in the micelles.

Nile Red, a fluorescent molecular probe, has been loaded in the core of the micelles. Both UV and NIR light irradiation induced the release of encapsulated Nile Red, been this release more gradual for the supramolecular BC. NIR induced release took longer irradiation times in comparison to UV due to the lower efficiency of 2PA processes, though relative final Nile Red emission values were analogous for UV and NIR stimulated release. The introduction of the light-responsive unit by H-bond has proved to be a suitable strategy for the preparation of light-responsive nanocarriers with response to light equivalent to the reference covalent materials.

A synthetic approach that provides high flexibility in the functional polymeric materials design has been combined with the response to NIR light, which is of interest in biomedical applications for which UV light is not recommended.

2.7 Experimental section

2.7.1 Synthesis and characterisation of DAP-SH

The target compound was synthesised as shown in Figure 2.24 starting from *N*-(6-aminopyridin-2-yl)propionamide that was synthesised according to a previously reported procedure.[10]

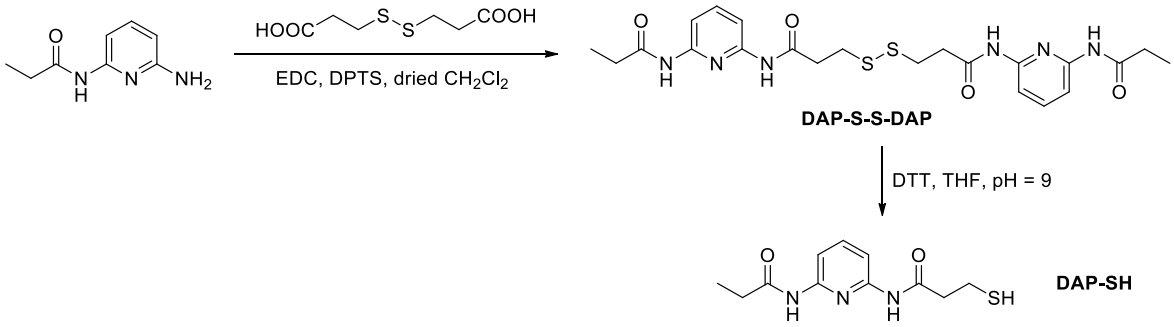

Figure 2.24: Synthesis of DAP-SH.

Synthesis of DAP-S-S-DAP. Diisopropyl carbodiimide (EDC) (4.63 g, 24.2 mmol) was added over a solution of *N*-(6-aminopyridin-2-yl)propionamide (6.00 g, 36.2 mmol), 3,3′-dithiodipropionic acid (2.54 g, 12.1 mmol) and 4-(dimethylamino)pyridinium 4-toluenesulfonate (DPTS) (3.52 g, 12.1 mmol) in dry dichlomethane (50 mL) under an Ar atmosphere. After stirring for 72 h, the reaction was washed with water (3×50 mL). The organic phase was dried over $MgSO_4$ and evaporated to dryness. The residue was purified by recrystallisation in toluene/ethanol (6:1), isolating the product as a white powder in 65% yield. FTIR (KBr, υ_{max}/cm^{-1}): 3323 (N-Hst), 1670 (C=Ost). ^{1}H NMR [400 MHz, d_6-DMSO, δ (ppm)]: 10.15 (s, 2H), 9.92 (s, 2H), 7.84 – 7.61 (m, 6H), 3.01 (t, 4H, *J* = 6.6 Hz), 2.83 (t, 4H, *J* = 6.6 Hz), 2.40 (q, 4H, *J* = 7.5 Hz), 1.06 (t, 6H, *J* = 7.5 Hz). ^{13}C NMR [100 MHz, d6-DMSO δ (ppm)]: 172.9, 170.1, 150.4, 150.1, 139.9, 109.1, 108.9, 35.8, 33.4, 29.3, 9.4.

Synthesis of DAP-SH. Trimethylamine was dropwise added over a solution of DAP-S-S-DAP (500 mg, 0.99 mmol) and dithiothreitol (DTT) (458 mg, 2.96 mmol) in dry THF (20 mL) under Ar atmosphere, until pH = 9.0. The solution was stirred overnight and evaporated to dryness. The residue was purified by flash column

chromatography over neutral alumina and dichloromethane/ethyl acetate (1:1) as eluent (R_f = 0.75) to give the target compound in quantitative yield. FTIR (KBr, υ_{max}/cm^{-1}): 3264 (N-Hst), 2555 (S-Hst), 1696 (C=Ost), 1664 (C=Ost). ^{1}H NMR [400 MHz, $(CD_3)_2CO$, δ (ppm)]: 9.18 (s, 1H), 9.03 (s, 1H), 7.93 – 7.85 (m, 2H), 7.75 – 7.69 (m, 1H), 2.87 – 2.74 (m, 4H), 2.44 (q, *J* = 7.6 Hz, 2H), 1.97 – 1.90 (m, 1H), 1.14 (t, *J* = 7.4 Hz, 3H). ^{13}C NMR [100 MHz, $(CD_3)_2CO$ δ (ppm)]: 173.2, 170.7, 151.5, 151.2, 140.8, 109.6, 109.5, 41.4, 30.6, 20.4, 9.6.

2.7.2 Synthesis and characterisation of T_nCou

T_nCou (n = 1, 5, 10) were synthesised as shown in Figure 2.25 by esterification of the corresponding thymine carboxylic acid derivative and 7-(diethylamino)-4-(hydroxymethyl)coumarin, synthesised according to a previously reported procedure.[11] Thymin-1-yl hexanoic acid and thymin-1-yl undecanoic acid were synthesised as previously reported.[12] Thymin-1-yl acetic acid was purchased from Sigma Aldrich and used as received.

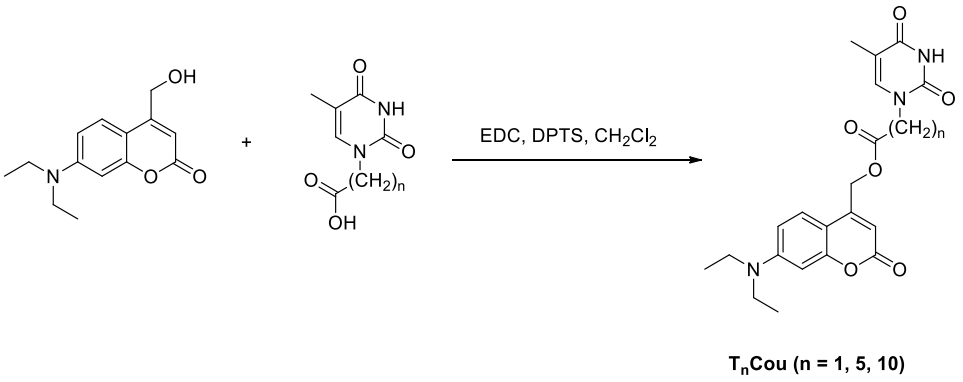

Figure 2.25: Synthesis of T_nCou.

On a typical esterification reaction, 7-(diethylamino)-4-(hydroxymethyl)coumarin (0.50 mmol), DPTS (0.19 mmol) and the corresponding thymin-1-yl acid (0.79 mmol) were dissolved in dry dichloromethane (10 mL) under Ar atmosphere. The flask was cooled in a salt-ice bath and EDC (0.79 mmol) was added. After stirring for 90 min, the ice bath was removed and the reaction stirred for 72 h more at room temperature. The reaction crude was diluted with dichloromethane (500 mL) and washed with water (2×100 mL) and brine (1×100 mL). The organic phase was dried over anhydrous $MgSO_4$, filtered and evaporated. The residue was purified by flash

column chromatography over silica gel using dichloromethane/ethyl acetate (8/2) as eluent.

T_1Cou: Yield = 62%. FTIR (KBr, υ_{max}/cm^{-1}): 3181 (N-H*st*), 3065 (Csp^2-H*st*), 1757 (C=O*st*),1713 (C=O*st*), 1676 (C=O*st*), 1607 (C=C*st*). ^{1}H NMR [400 MHz, $CDCl_3$, δ (ppm)]: 8.85 (s, 1H), 7.28- 7.23 (m, 1H), 7.00 - 6.97 (m, 1H), 6.60 -6.54 (m, 1H), 6.51 – 6.47 (m, 1H), 6.10 - 6.07 (m, 1H), 5.31 - 5.28 (m, 2H), 4.56 (s, 2H), 3.41 (q, *J* = 7.1 Hz, 4H), 1.94 -1.90 (m, 3H), 1.17 (t, *J* = 7.1 Hz, 6H). ^{13}C NMR [100 MHz, $CDCl_3$, δ (ppm)]: 167.0, 163.8, 161.6, 156.3, 150.8, 150.7, 148.2, 139.9, 124.4, 111.6, 108.8, 107.0, 105.8, 97.9, 62.8, 48.8, 44.8, 12.4, 12.3.

T_5Cou: Yield = 70%. FTIR (KBr, υ_{max}/cm^{-1}): 3160 (N-Hst), 3050 (Csp^2–H), 1753 (C=O*st*), 1716 (C=O*st*), 1698 (C=O*st*), 1610 (C=C*st*). ^{1}H NMR [400 MHz, $CDCl_3$, δ (ppm)]: 9.59 (s, 1H), 7.34- 7.25 (m, 1H), 7.03 - 6.96 (m, 1H), 6.66 -6.51 (m, 1H), 6.51 – 6.42 (m, 1H), 6.09 - 6.00 (s, 1H), 5.3 - 5.16 (m, 2H), 3.66 (t, *J* = 7.4 Hz, 2H), 3.38 (q, *J* = 7.1 Hz, 4H), 2.42 (t, *J* = 7.5 Hz, 2H), 1.90 - 1.84 (m, 3H), 1.78 -1.63 (m, 4H), 1.44 - 1.28 (m, 2H), 1.17 (t, *J* = 7.1 Hz, 6H). ^{13}C NMR [100 MHz, $CDCl_3$, δ (ppm)]: 172.5, 164.6, 161.8, 156.2, 151.1, 150.6, 149.5, 140.5, 124.3, 110.7, 108.7, 106.0, 105.9, 97.8, 61.2, 48.3, 44.7, 33.8, 28.8, 25.6, 24.3, 12.5, 12.3.

T_{10}Cou: Yield = 66%. FTIR (KBr, υ_{max}/cm^{-1}): 3156 (N-Hst), 3055 (Csp^2–H*st*), 1754 (C=O*st*), 1610 (C=C*st*). ^{1}H NMR [400 MHz, $CDCl_3$, δ (ppm)]: 9.05 (s, 1H), 7.32- 7.24 (m, 1H), 7.03 - 6.94 (s, 1H), 6.62 -6.54 (m, 1H), 6.53 – 6.47 (m, 1H), 6.13 - 6.08 (s, 1H), 5.23 - 5.18 (m, 2H), 3.66 (t, *J* = 7.4 Hz, 2H), 3.38 (q, *J* = 7.1 Hz, 4H), 2.42 (t, *J* = 7.5 Hz, 2H), 1.92 - 1.87 (s, 3H), 1.72 -1.59 (m, 4H), 1.35 - 1.21 (m, 12H), 1.17 (t, *J* = 7.1 Hz, 6H). ^{13}C NMR [100 MHz, $CDCl_3$, δ (ppm)]: 173.1, 164.5, 161.9, 156.3, 151.0, 150.7, 149.8, 140.6, 124.5, 110.6, 108.8, 106.3, 106.1, 97.8, 61.1, 48.6, 44.9, 34.2, 29.4, 29.3, 29.2, 29.2, 29.1, 26.5, 24.98, 12.5, 12.4.

2.7.3 Synthesis and characterisation of the coumarin N_3-Cou

The target compound was synthesised as shown in Figure 2.26 starting from 7-(diethylamino)-4-(hydroxymethyl)coumarin; which was synthesised according to a previously reported procedure.[11] 6-Azidohexanoic acid was synthesised as previously reported.[13]

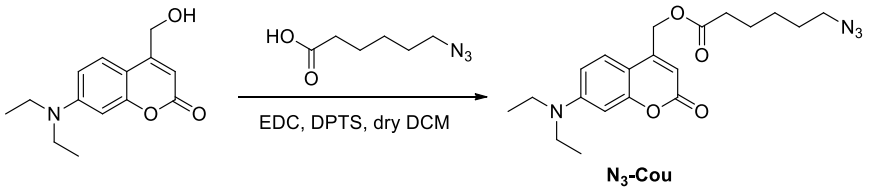

Figure 2.26: Synthesis of coumarin N_3-Cou.

7-(Diethylamino)-4-(hydroxymethyl)coumarin (750 mg, 3.03 mmol), DPTS (291 mg, 1.21 mmol) and 6-azidohexanoic acid (572 mg, 3.63 mmol) were dissolved in dry dichloromethane (10 mL) under Ar atmosphere. The flask was cooled in an acetone-ice bath and, then, EDC (695 mg, 3.63 mmol) was added and the mixture stirred for 30 min. The ice bath was removed and the reaction stirred for additional 72 h. The reaction crude was diluted with dichloromethane (100 mL) and washed with water (2×100 mL) and brine (100 mL). The organic phase was dried over anhydrous $MgSO_4$, filtered and evaporated. The residue was purified by flash column chromatography using silica and dichloromethane/ethyl acetate (8:2) as eluent to give the required compound in 82% yield. FTIR (KBr disk, υ/cm^{-1}): 3076 (Csp^2–H^{st}), 2096 ($N_3{}^{st}$), 1724 (C=O^{st}), 1618 (C=C^{st}). ^1H NMR (400 MHz, $CDCl_3$, δ, ppm): 7.28 (d, *J* = 9.0 Hz, 1H), 6.63–6.57 (m, 1H), 6.55–6.51 (m, 1H), 6.15–6.09 (s, 1H), 5.24- 5.20 (d, *J* = 1.2 Hz, 2H), 3.41 (q, *J* = 7.1 Hz, 4H), 3.27 (t, *J* = 6.8 Hz, 2H), 2.46 (t, *J* = 7.5 Hz, 2H), 1.81–1.53 (m, 4H), 1.52 – 1.37 (m, 2H), 1.20 (t, *J* = 7.1 Hz, 6H). ^{13}C NMR [100 MHz, $CDCl_3$, δ, ppm): 172.78, 161.92, 156.35, 150.58, 149.55, 124.54, 110.11, 109.02, 106.77, 98.24, 61.38, 51.30, 45.07, 33.99, 28.65, 26.35, 24.48, 12.49.

2.7.4 Synthesis of the block copolymers by ROP

Synthesis of the block copolymer PEG-*b*-PC(A). A solution of PEG-OH (2.00 g, 0.4 mmol), DBU (15.8 mg, 0.10 mmol) and TU (192.6 mg, 0.52 mmol) in dry dichloromethane (10 mL) was dried for 12 h over 4 Å molecular sieves under Ar atmosphere. This solution was added *via* cannula to Schlenk flask charged with the cyclic monomer MAC (2.08 g, 10.4 mmol) under Ar atmosphere. The mixture was stirred at 35 °C for 8 h. The reaction mixture was precipitated in cold diethyl ether (200 mL) three times, isolating the copolymer by filtration and re-dissolving it with dichloromethane (3 mL). Copolymer PEG-*b*-PC(A) was dried under vacuum overnight, isolating a white powder in a 48% yield. FTIR (KBr, υ_{max}/cm^{-1}): 2891

(Csp^3–H^{st}), 1761 (C=O^{st}). ^{1}H NMR (400 MHz, $CDCl_3$, δ, ppm): 5.97 - 5.77 (m, 18H), 5.37 - 5.16 (m, 37H), 4.65 - 4.56 (m, 36H), 4.35 - 4.20 (m, 76H), 3.82 - 3.46 (m, 463H), 3.36 (s, 3H), 1.24 (s, 54H).

Synthesis of the block copolymer PEG-*b*-PC(P). A solution of PEG-OH (1.5 g, 0.3 mmol), DBU (13.7 mg, 0.09 mmol) and TU (166.6 mg, 0.45 mmol) in dry dichloromethane (10 mL) was dried for 12 h over 4 Å molecular sieves under Ar atmosphere. This solution was added *via* cannula to Schlenk flask charged with the cyclic monomer MPC (1.78 g, 9.0 mmol) under Ar atmosphere. The mixture was allowed to stir at 35 °C for 8 h. The reaction mixture was precipitated in cold diethyl ether (200 mL) three times, isolating the copolymer by filtration and re-dissolving it with dichloromethane (3 mL). PEG-*b*-PC(P) was dried under vacuum overnight, isolating a white powder in a 55% yield. FTIR (KBr, υ_{max}/cm^{-1}): 3471 (O–H^{st}), 3290 (Csp–H^{st}), 2130 (Csp–Csp^{st}), 1754 (C=O^{st}). ^{1}H NMR (400 MHz, $CDCl_3$, δ, ppm): 4.66 (d, *J* = 2.4 Hz, 46H), 4.34–4.15 (m, 92H), 3.79–3.36 (m, 480H), 3.31 (s, 3H), 2.48 (t, *J* = 2.4 Hz, 23H), 1.22 (s, 69H).

2.7.5 Synthesis of PEG-b-PC(DAP)

A Schlenk flask was charged with DAP-SH (500 mg, 1.97 mmol) PEG-*b*-PC(A) (457 mg, 0.986 mmol of C=C) and DMPA (12.6 mg, 0.049 mmol) and flushed with Ar. Then, dry THF (5 mL) was added, and the solution stirred at 40 °C for 4 h under 365 nm illumination. The reaction crude was purified by preparative SEC using Biobeds SX-1 and THF as eluent and, the polymer precipitated into cold diethyl ether and isolated by filtration as a white powder (90% yield). FTIR (KBr, υ_{max}/cm^{-1}): 3316 (N-H^{st}), 2878 (Csp^3–H), 1752 (C=O), 1701 (C=O), 1589, 1447, 1294, 1236. ^{1}H NMR (400 MHz, $CDCl_3$, δ, ppm): 8.90 - 8.12 (m, broad signal), 7.98 - 7.75 (m), 7.72 - 7.57 (m), 4.40 - 4.11 (m), 3.82 - 3.43 (m), 3.37 (s), 2.95 - 2.80 (m), 2.76 - 2.63 (m), 2.63 - 2.50 (m), 2.49 - 2.36 (m), 2.00 - 1.73 (m), 1.27 - 1.14 (m)

2.7.6 Synthesis of the coumarin functionalised supramolecular block copolymers PEG-*b*-PC(DAP/T_nCou).

The same procedure was use for all T_nCou (n = 1, 5, 10) units, the example for n = 1 is shown below: A solution of T_1Cou (25.4 mg, 0.061 mmol) and PEG-*b*-PC(DAP) (30.0 mg, 0.065 mmol of DAP units) in dry THF (2 mL) was slowly evaporated at room temperature in an orbital shaker. The supramolecular polymer was dried under vacuum at 40 °C overnight.

2.7.7 Synthesis of the coumarin functionalised covalent block copolymer PEG-*b*-PC(Cou)

A Schlenk flask was charged with N_3-Cou (487 mg, 1.26 mmol), PEG-*b*-PC(P) (262 mg, 0.63 mmol of C≡C), CuBr (18.6 mg, 0.13 mmol) and PMDETA (22.52 mg, 0.13 mmol) and flushed with Ar. Then, deoxygenated and distilled *N,N*-dimethylformamide (5 mL) was added, and the solution stirred at 40 °C for 72 h. The reaction crude was diluted with dichloromethane and washed three times with distilled water. The organic fraction was dried over $MgSO_4$, filtered and evaporated to dryness. Residual azide was removed by preparative SEC using Biobeds SX-1 and THF as eluent and, the polymer precipitated into cold diethyl ether and isolated by filtration as a pale yellow powder (80% yield). FTIR (KBr, υ_{max}/cm^{-1}): 3045 (Csp^2–H^{st}), 1739 (C=O^{st}), 1607 (C=C^{st}). ^{1}H NMR (400 MHz, $CDCl_3$, δ, ppm): 7.68 (s), 7.26 (m), 6.6–6.52 (m), 6.40 (s), 5.98 (s), 5.25–5.07 (m), 4.30 (t, *J* = 7.2 Hz), 4.15 (s), 3.76–3.45 (m), 3.47–3.31 (m), 2.37 (t, *J* = 7.2 Hz), 1.93–1.81 (m), 1.70–1.58 (m), 1.38–1.24 (m), 1.2 –1.05 (m).

2.7.8 Preparation and characterisation of polymeric self-assemblies

Self-assembly Procedure. Milli-Q® water was gradually added to a solution of the copolymer (5 mg) in spectroscopic grade THF (1 mL) previously filtered through a 0.2 μm polytetrafluoroethylene (PTFE) filter. The self-assembly process was followed by measuring the loss of transmitted light intensity at 650 nm due to scattering as a function of water content. When a constant value of turbidity was

reached, the resulting suspension was filtered through a 5 μm cellulose acetate filter and dialyzed against water using a Spectra/Por dialysis membrane (MWCO, 1 kDa) for 2 days to remove THF, changing water 3 times. Water suspensions of the polymeric self-assemblies were diluted with Milli-Q® water to a final concentration 1 mg mL^{-1}.

Determination of the critical aggregation concentration and loading of Nile Red. Critical aggregation concentration (CAC) was determined by fluorescence spectroscopy using Nile Red. 87 μL of a solution of Nile Red in dichloromethane (3.7×10^{-5} M) was added into a vial and the solvent evaporated. Then, 600 μL of the aqueous suspension of the polymeric aggregates with concentrations ranging from 1.0×10^{-4} to 1.0 mg mL^{-1} were added and stirred overnight in orbital shaker. The emission spectrum of Nile Red was registered from 560 to 700 nm while exciting at 550 nm.

Preparation of TEM samples. A small amount of the micellar dispersion (1 mg mL^{-1} polymer concentration) was placed onto a holey carbon TEM grid (Plano S147-4), dried at room temperature with a tissue and imaged.

2.7.9 Irradiation experiments

Irradiation experiments with UV light (one-photon absorption process). Samples at a copolymer concentration of 1 mg mL^{-1} were placed in a quartz cuvette and irradiated at 365 nm and 30 mW cm^{-2} with a Dymax 2000-EC lamp equipped with a glass UV filter. At different time intervals the sample was removed from the lamp, measuring Nile Red and coumarin unit emission in a fluorescence spectrophotometer.

Irradiation experiments with NIR light (two-photon absorption process). Samples were studied on a Zeiss LSM 880 confocal microscope, with a 10× Plan Neofluar objective. A PDMS stencil with circular wells (4 mm ×3 50 μm, Alvéole) was stuck in a 23 mm glass bottom dish. Each well was filled with 5 μL of micellar solution (1 mg mL^{-1} polymer concentration). To avoid evaporation of the samples, the stencil was covered with a 20 mm diameter coverslip and a small amount of water was deposited on the outer ring of the dish, then, the dish itself was sealed

with parafilm. 3D stacks were alternatively acquired irradiating first at 730 nm for 1.08 min (coumarin photoscission) and then at 514 nm (Nile Red excitation) every 10 min up to 15 h. For illumination at 730 nm, a Chameleon Ultra II Ti:Sapphire laser was used. Its nominal power at 730 nm is around 2 W, the pulse width being 140 fs, at a frequency of 80 Mhz. The image size was set to 512×512 pixel (850×850 μm), and the dwell time was set to 8.2 μs, with a pinhole size of 100 μm. The light exposed volume of the sample corresponded to 6.8% of the total amount of solution.

2.8 References

(1) Babin, J.; Pelletier, M.; Lepage, M.; Allard, J.-F.; Morris, D.; Zhao, Y. A New Two-Photon-Sensitive Block Copolymer Nanocarrier. *Angew. Chem. Int. Ed.* **2009**, *48*, 3329–3332. https://doi.org/10.1002/anie.200900255.

(2) Kumar, S.; Allard, J.-F.; Morris, D.; Dory, Y. L.; Lepage, M.; Zhao, Y. Near-Infrared Light Sensitive Polypeptide Block Copolymer Micelles for Drug Delivery. *J. Mater. Chem.* **2012**, *22*, 7252–7257. https://doi.org/10.1039/c2jm16380b.

(3) Tempelaar, S.; Mespouille, L.; Dubois, P.; Dove, A. P. Organocatalytic Synthesis and Postpolymerization Functionalization of Allyl-Functional Poly(Carbonate)s. *Macromolecules* **2011**, *44*, 2084–2091. https://doi.org/10.1021/ma102882v.

(4) Qiao, Y.; Yang, C.; Coady, D. J.; Ong, Z. Y.; Hedrick, J. L.; Yang, Y.-Y. Highly Dynamic Biodegradable Micelles Capable of Lysing Gram-Positive and Gram-Negative Bacterial Membrane. *Biomaterials* **2012**, *33*, 1146–1153. https://doi.org/10.1016/j.biomaterials.2011.10.020.

(5) Pratt, R. C.; Nederberg, F.; Waymouth, R. M.; Hedrick, J. L. Tagging Alcohols with Cyclic Carbonate: A Versatile Equivalent of (Meth)Acrylate for Ring-Opening Polymerization. *Chem Commun* **2008**, No. 1, 114–116. https://doi.org/10.1039/B713925J.

(6) Hu, X.; Chen, X.; Xie, Z.; Liu, S.; Jing, X. Synthesis and Characterization of Amphiphilic Block Copolymers with Allyl Side-Groups. *J. Polym. Sci. Part A Polym. Chem.* **2007**, *45*, 5518–5528. https://doi.org/10.1002/pola.22297.

(7) Royes, J.; Rebolé, J.; Custardoy, L.; Gimeno, N.; Oriol, L.; Tejedor, R. M.; Piñol, M. Preparation of Side chain Liquid Crystalline Azopolymers by CuAAC Postfunctionalization Using Bifunctional Azides: Induction of Chirality Using Circularly Polarized Light. *J. Polym. Sci. Part A Polym. Chem.* **2012**, *50*, 1579–1590. https://doi.org/10.1002/pola.25929.

(8) Roche, A.; García-Juan, H.; Royes, J.; Oriol, L.; Piñol, M.; Audia, B.; Pagliusi, P.; Provenzano, C.; Cipparrone, G. Tuning the Thermal Properties of Azopolymers Synthesized by Post-Functionalization of Poly(Propargyl Methacrylate) with Azobenzene Azides: Influence on the Generation of Linear and Circular Birefringences. *Macromol. Chem. Phys.* **2018**, *219*, 1800318. https://doi.org/10.1002/macp.201800318.

(9) Lu, C.; Shi, Q.; Chen, X.; Lu, T.; Xie, Z.; Hu, X.; Ma, J.; Jing, X. Sugars-Grafted Aliphatic Biodegradable Poly(L-Lactide-Co-Carbonate)s by Click Reaction and Their Specific Interaction with Lectin Molecules. *J. Polym. Sci. Part A Polym. Chem.* **2007**, *45*, 3204–3217. https://doi.org/10.1002/pola.22070.

(10) Concellón, A.; Blasco, E.; Piñol, M.; Oriol, L.; Díez, I.; Berges, C.; Sánchez-Somolinos, C.; Alcalá, R. Photoresponsive Polymers and Block Copolymers by Molecular Recognition Based on Multiple Hydrogen Bonds. *J. Polym. Sci. Part A Polym. Chem.* **2014**, *52*, 3173–3184. https://doi.org/10.1002/pola.27373.

(11) Weinrich, T.; Gränz, M.; Grünewald, C.; Prisner, T. F.; Göbel, M. W. Synthesis of a Cytidine Phosphoramidite with Protected Nitroxide Spin Label for EPR Experiments with RNA: Synthesis of a Cytidine Phosphoramidite with Protected Nitroxide Spin Label for EPR Experiments with RNA. *Eur. J. Org. Chem.* **2017**, *2017*, 491–496. https://doi.org/10.1002/ejoc.201601174.

(12) Higley, M. N.; Pollino, J. M.; Hollembeak, E.; Weck, M. A Modular Approach toward Block Copolymers. *Chem. Eur. J.* **2005**, *11*, 2946–2953. https://doi.org/10.1002/chem.200401221.

(13) Kuil, J.; Branderhorst, H. M.; Pieters, R. J.; de Mol, N. J.; Liskamp, R. M. J. ITAM-Derived Phosphopeptide-Containing Dendrimers as Multivalent Ligands for Syk Tandem SH2 Domain. *Org. Biomol. Chem.* **2009**, *7*, 4088-4094. https://doi.org/10.1039/b905938e.

CHAPTER 3

NANOCARRIERS BASED ON AMPHIPHILIC BCs WITH AZOBENZENE

Published in *Polymers*, **2019**, *11*, 2060

3.1 Introduction and aims

It has already been emphasized the interest in the preparation of light-responsive polymeric nanoparticles for on demand delivery where release is stimulated out of the UV region. Azobenzene has been probably the most widely used light-responsive moiety as it can undergo a photoinduced reversible *trans*-to-*cis* isomerisation accompanied by a change in the geometry and polarity from which the light-induced release originates. There are numerous examples of amphiphilic BCs comprising azobenzene moieties that have been used for the fabrication light-responsive self-assemblies working under the application of UV light but those using visible-light stimulated azobenzene are still a challenge. Indeed, several cyclodextrin-azobenzene supramolecular systems can be compiled from the literature using visible light to regulate the guest-host interaction and consequently the release of payloads. However, the number of visible light activated systems using merely polymers with azobenzene covalently linked to the polymeric chain has been rather scarce and the majority either do not describe the loading/release ability of the self-assemblies or the release of molecular probes with visible light has not been definitely established as reviewed in the section 1.2.1.4 of **Chapter 1**.

The target of the work presented in this chapter was the development of polymeric self-assemblies with release abilities under visible light stimulation based on 2,2',5,5'-tetramethoxy-4-oxyazobenzene unit whose photo-response to visible light was established by Woolley and co-workers. As it was revised in **Chapter 1**, the *trans*-to-*cis* possible under green or red light because n-π* absorption maxima of both isomers are separated.

BCs were designed consisting of PEG as the hydrophilic segment bound to a hydrophobic aliphatic polycarbonate based on the bis-MPA building block where the azobenzene was grafted by a post-polymerisation modification (Figure 3.1). Amphiphilic diblock copolymers with pendant propargyloxy units in the side chain of the hydrophobic block were synthesised by ROP where azobenzene units were subsequently incorporated by CuAAC with azobenzene azides. Additionally, to establish direct comparisons, analogous amphiphilic BCs containing the

4-isobutyloxy-4'-oxyazobenzene unit, with response in the UV region and used as a proof-of-concept in earlier works, were also investigated.

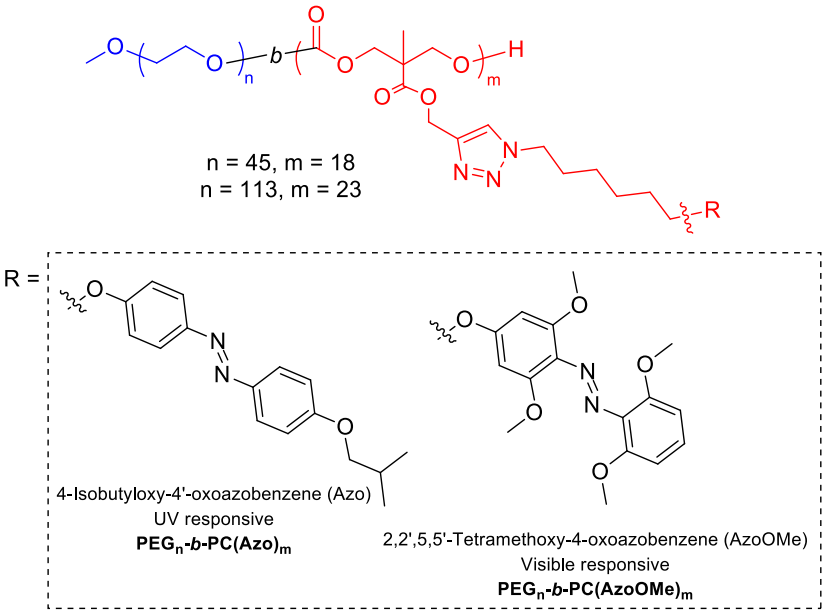

Figure 3.1: Structure of the amphiphilic diblock copolymers studied in this chapter.

According to the objective, the main tasks carried out in this chapter were:

- Synthesis and chemical characterisation of the polymers with pendant propargyloxy groups.
- Synthesis and chemical characterisation of the azobenzene azide derivatives.
- Synthesis of the light-responsive amphiphilic diblock copolymers *via* CuAAC.
- Study of the self-assembly in water of the amphiphilic diblock copolymers and characterisation of the self-assembled structures.
- Study of the response to light irradiation of the amphiphilic diblock copolymers in solution and of the self-assemblies.
- Encapsulation of fluorescent molecular probes and study of the light stimulated release.

3.2 Synthesis and characterisation of azobenzene functionalised amphiphilic diblock copolymers

Azobenzene functionalised amphiphilic BCs were obtained by organocatalysed ROP of **MPC** and further post-polymerisation functionalisation by CuAAC with azobenzene azides, either **N_3-Azo** or **N_3-AzoOMe** (Figure 3.2), following the strategy used in **Chapter 2** for the synthesis of the reference copolymer. ROP was promoted using PEG-OH as the macroinitiator and the organocatalytic system TU/DBU.

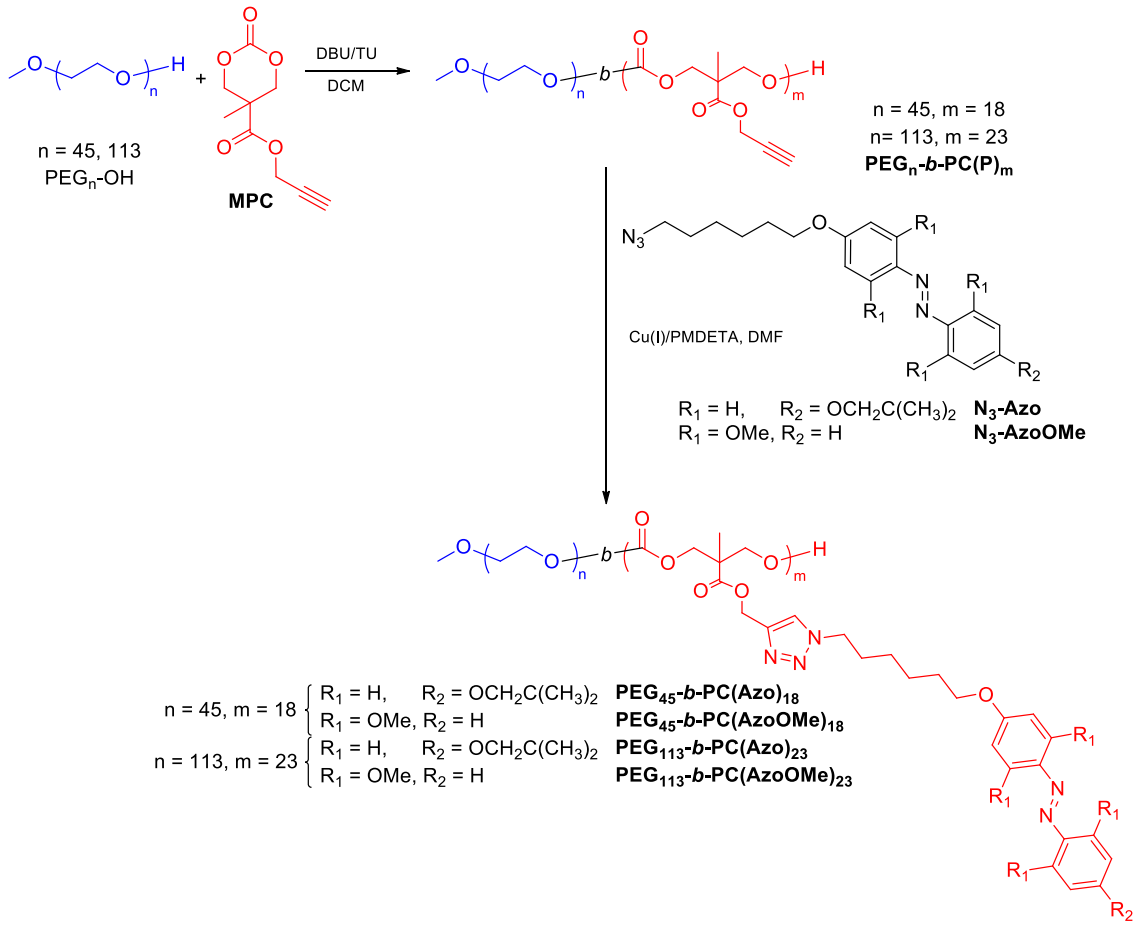

Figure 3.2: Route for the synthesis of the azobenzene functionalised amphiphilic block copolymers.

ROP of **MPC** was performed in dichloromethane ([**MPC**]$_0$ = 1.0 M) at 40 °C for 8 h using a [**MPC**]:[TU]:[DBU]=1:0.05:0.01 ratio. PEG$_n$-OH with average polymerisations degrees (n) of 113 and 45 were used while adjusting the [**MPC**]:[PEG$_n$-OH] ratio to get hydrophobic-to-hydrophilic ratios of about 80:20 (wt:wt) on the final diblock copolymers. Polymerisations were confirmed by ^{1}H

NMR by the disappearance of the methylenic protons of the **MPC** carbonate ring, at δ = 4.71 and 4.22 ppm, and the appearance of a new signal at 4.25 ppm corresponding to the polycarbonate backbone (Figure 3.3 and Figure 3.4). Average polymerisation degrees of the polycarbonate segment, *m*, were determined using ^{1}H NMR end group analysis by comparing relative integration of the terminal methoxy group of the PEG block (Figure 3.3a and Figure 3.4a, signal *a,* δ = 3.31 ppm) and the alkynyl side groups of the polycarbonate block (Figure 3.3a and Figure 3.4a, signal *f,* δ = 2.48 ppm). Values of *m* were found 23 and 18 when using PEG_{113}-OH and PEG_{45}-OH, which matched reasonably well with theoretical ones (30 and 23, respectively). Besides, SEC traces revealed unimodal distributions with $Đ$ = 1.06 for **PEG_{45}-*b*-PC(P)$_{18}$** and 1.08 for **PEG_{113}-*b*-PC(P)$_{23}$** (see Figure 3.5 and Figure 3.6).

Functionalisation of the polycarbonate block with azides **N_3-Azo** or **N_3-AzoOMe**, *via* CuAAC was approached using CuBr/PMDETA in DMF (Figure 3.2) under the same conditions used in **Chapter 2**.[1] Progress of the functionalisation was evaluated by ^{1}H NMR from the disappearance of the signal at δ = 2.48 ppm, corresponding this signal to the proton in the propargyl side group, and by the appearance of a new signal at 7.65 ppm from the proton in the triazole ring (see Figure 3.3b and c for copolymers with PEG_{45} segment). Extension of the functionalisation of the propargyl groups was also assessed by FTIR, from the disappearance of the Csp–H and Csp–Csp stretching bands at 3300 cm^{-1} and 2100 cm^{-1} respectively (see Figure 3.7 and Figure 3.8). Taking into account the sensitivity of both spectroscopic techniques, functionalisation of the propargyl groups was considered quantitative. SEC mass distribution peaks shifted to lower retention times in comparison to parent polymers **PEG_n-*b*-PC(P)$_n$** as expected due to the increase in the molecular mass (see Figure 3.5 and Figure 3.6) but dispersity values were about the same.

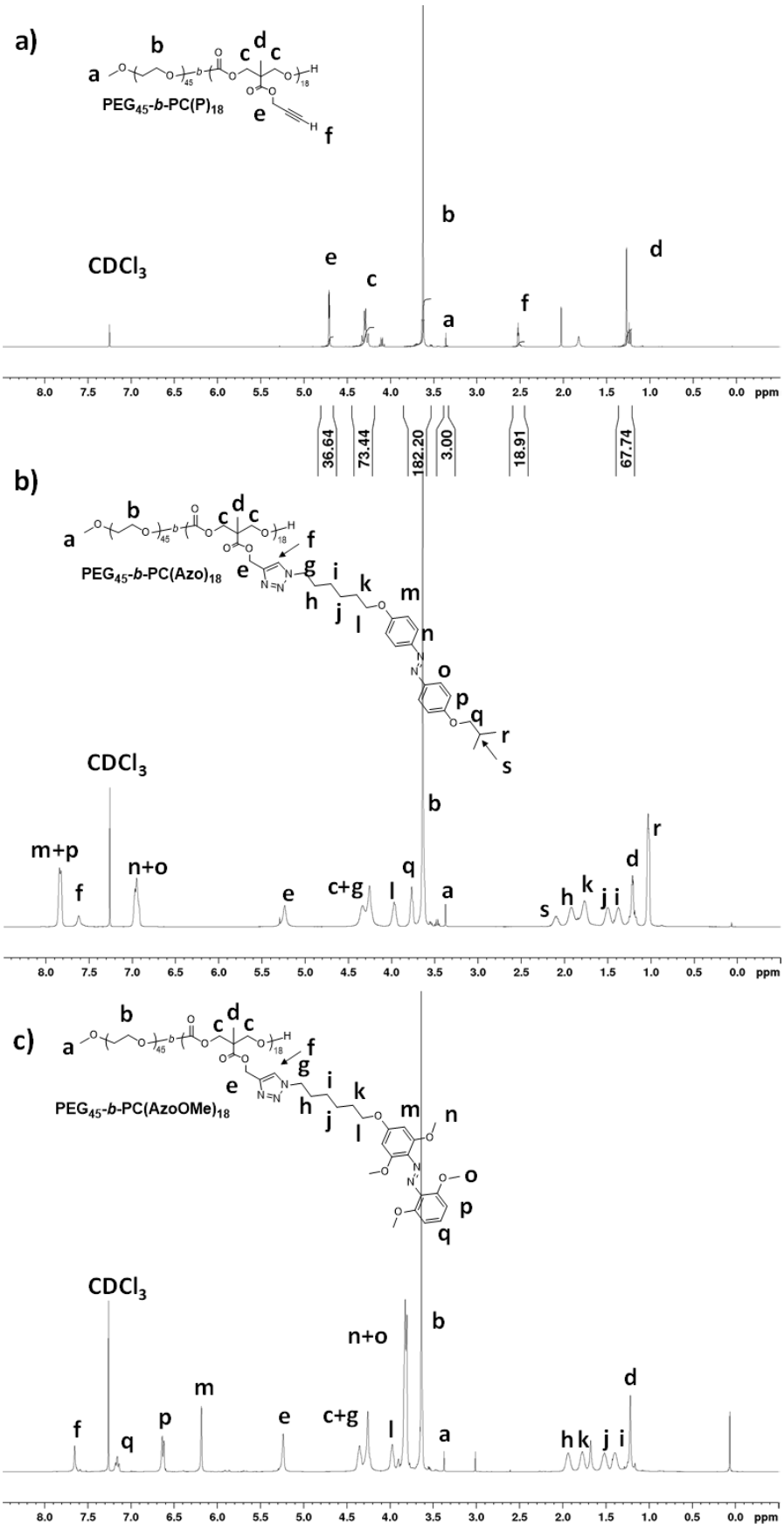

Figure 3.3: ^{1}H NMR (400 MHz, $CDCl_3$) spectra of **PEG_{45}-*b*-PC(P)$_{18}$** (a), **PEG_{45}-*b*-PC(Azo)$_{18}$** (b) and **PEG_{45}-*b*-PC(AzoOMe)$_{18}$** (c).

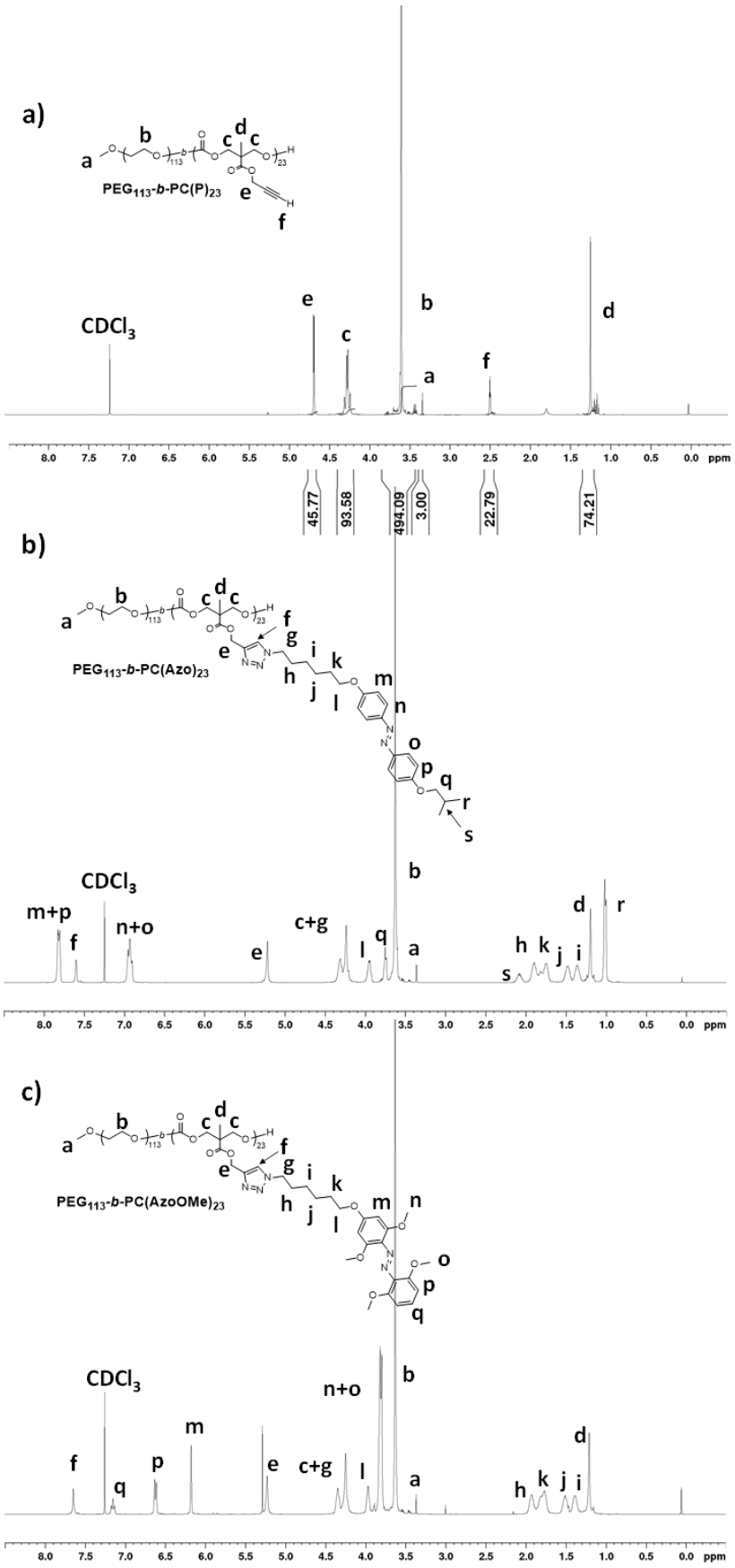

Figure 3.4: ^{1}H NMR (400 MHz, $CDCl_3$) spectra of **PEG_{113}-b-PC(P)$_{23}$** (a), **PEG_{113}-b-PC(Azo)$_{23}$** (b) and **PEG_{113}-*b*-PC(AzoOMe)$_{23}$** (c).

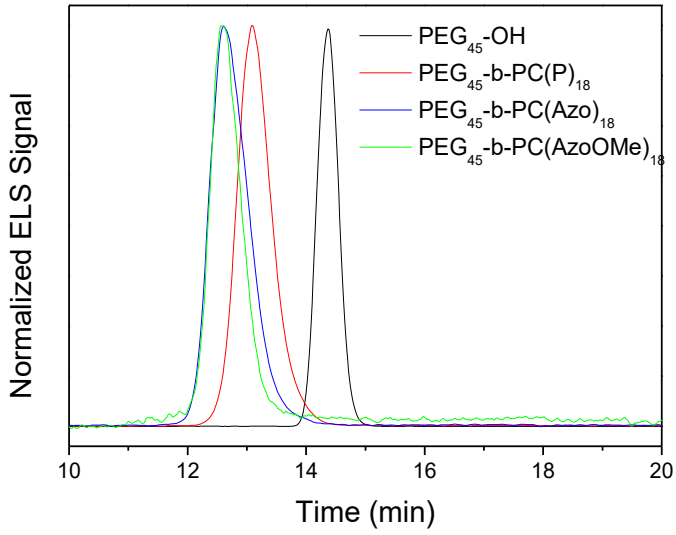

Figure 3.5: SEC traces for PEG$_{45}$-OH, **PEG$_{45}$-*b*-PC(P)$_{18}$**, **PEG$_{45}$-*b*-PC(Azo)$_{18}$** and **PEG$_{45}$-*b*-PC(AzoOMe)$_{18}$**.

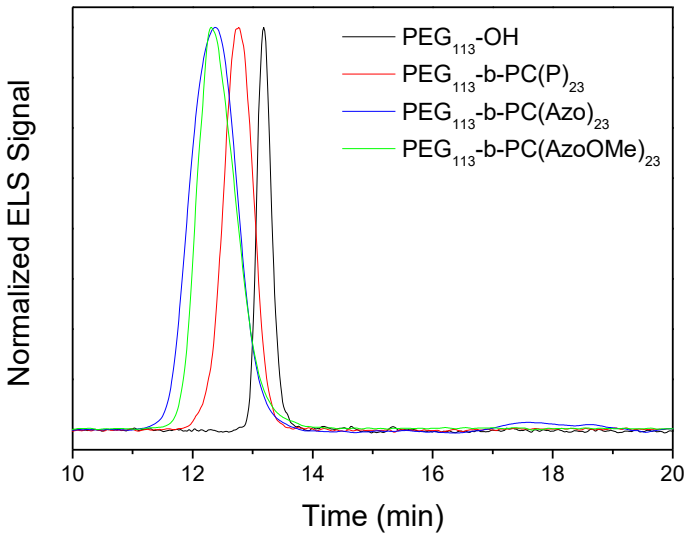

Figure 3.6: SEC traces for PEG$_{113}$-OH, **PEG$_{113}$-*b*-PC(P)$_{23}$**, **PEG$_{113}$-*b*-PC(Azo)$_{23}$** and **PEG$_{113}$-*b*-PC(AzoOMe)$_{23}$**.

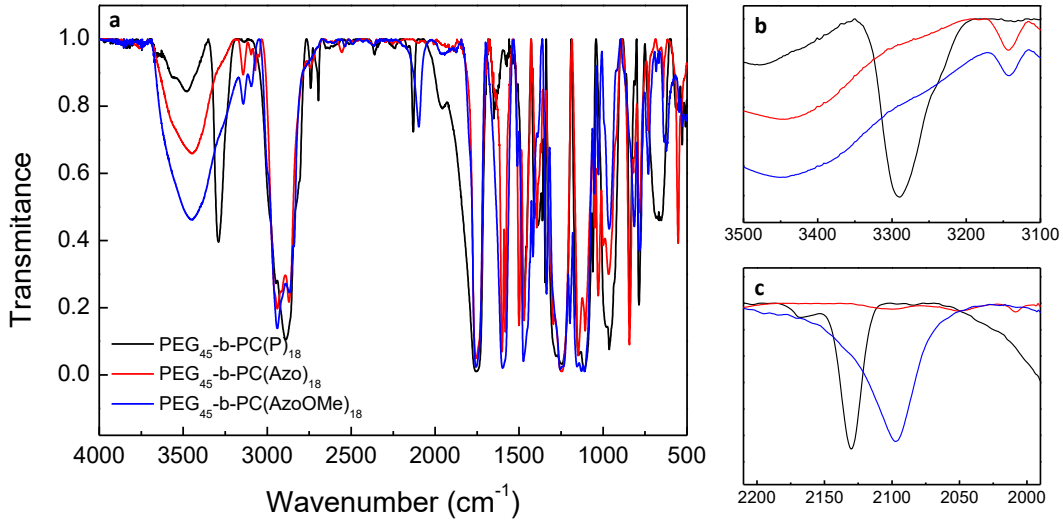

Figure 3.7: **PEG$_{45}$-*b*-PC(P)$_{18}$**, **PEG$_{45}$-*b*-PC(Azo)$_{18}$** and **PEG$_{45}$-*b*-PC(AzoOMe)$_{18}$** FTIR spectra (KBr disk) (a), and zoom to Csp-H interval (b) and Csp-Csp interval (c).

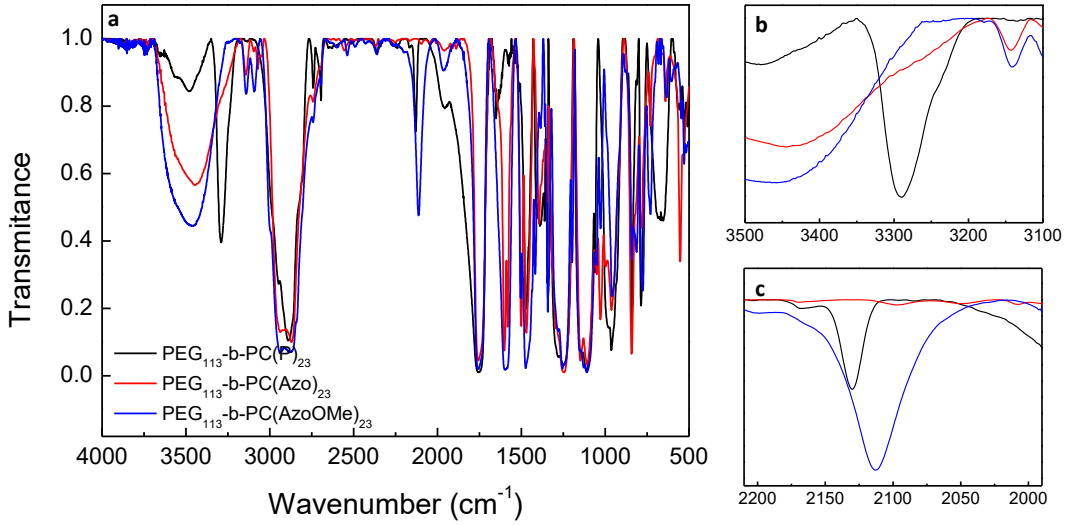

Figure 3.8: **PEG$_{113}$-*b*-PC(P)$_{23}$**, **PEG$_{113}$-*b*-PC(Azo)$_{23}$** and **PEG$_{113}$-*b*-PC(AzoOMe)$_{23}$** FTIR spectra (KBr disk) (a), and zoom to Csp-H interval (b) and Csp-Csp interval (c).

3.3 Thermal characterisation

Thermal stability of the diblock copolymers was evaluated by TGA (Figure 3.9) and data are summarized in Table 3.1. In general terms, copolymers with the longer PEG segment, **PEG_{113}-*b*-PC(Azo)$_{23}$** and **PEG_{113}-*b*-PC(AzoOMe)$_{23}$**, presented decomposition temperatures above 200 °C, while those with shorter one, **PEG_{45}-*b*-PC(Azo)$_{18}$** and **PEG_{45}-*b*-PC(AzoOMe)$_{18}$**, just below 200 °C. Besides the AzoOMe unit decreases the stability in comparison to Azo unit. Evolution of volatiles due to the presence of residual solvents or water was not observed.

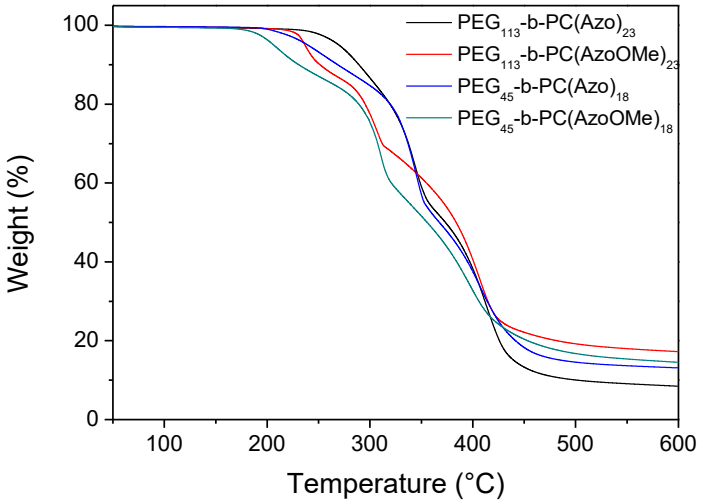

Figure 3.9: TGA curves registered at 10 °C min^{-1} heating rate under nitrogen atmosphere.

Table 3.1: Thermal stability and transition temperatures of azobenzene block copolymers.

Polymer	Hydrophobic content (wt %) [1]	TGA (°C) [2]	T_g (°C) [3]	T_m (°C) [ΔH_m (J g^{-1})] [4]	T_{M-I} (°C) [ΔH_{M-I} (J g^{-1})] [5]
PEG_{45}-*b*-PC(Azo)$_{18}$	84	195	31	63 [12.9]	73 [4.5]
PEG_{113}-*b*-PC(Azo)$_{23}$	73	258	-	45 [17.5], 61 [-][6]	73 [10.6] [6]
PEG_{45}-*b*-PC(AzoOMe)$_{18}$	85	185	39	-	-
PEG_{113}-*b*-PC(AzoOMe)$_{23}$	75	226	19	-	-

[1] Hydrophobic weight content in %. [2] Decomposition temperature determined by TGA given in °C at the onset of the weight loss curve. [3] Glass transition temperature (T_g) of the azobenzene polycarbonate determined by DSC during the second heating scan at 10 °C min^{-1}. [4] Melting temperature (T_m) and associated melting enthalpy (ΔH_m) determined by DSC during the second heating scan at 10 °C min^{-1}. [5] Mesophase-to-isotropic liquid transition temperature (T_{M-I}) and associated enthalpy (ΔH_{M-I}) calculated from the second heating scan at 10 °C min^{-1}.[6] Peaks at 61 °C (T_m) and 73 °C (T_{M-I}) overlap, the combined enthalpy value was 10.6 J g^{-1}.

Thermal transitions were determined by DSC analysis in the range of -50 °C to 120 °C and relevant data are collected in Table 3.1. Neat PEG_{45}-OH and PEG_{113}-OH are semicrystalline polymers whose melting temperatures were recorded at 49 °C (ΔH_m = 161 J/g) and 54 °C (ΔH_m = 158 J/g), respectively (Figure 3.10b and Figure 3.11c). In all the block copolymers crystallisation of the PEG segments was hindered, in particular, for block copolymers of the PEG_{45} series. Only on the first heating scan of **PEG_{113}-*b*-PC(Azo)$_{23}$** an endothermic peak was registered at 50 °C (with ΔH = 31.8 J g^{-1}) which correlates well with melting of PEG. Glass transitions, which have been reported about -49 °C, were not detected.[2]

When inspected by polarizing optical microscopy (POM), **PEG_n-*b*-PC(Azo)$_m$** polymers showed birefringent textures upon heating associated to liquid crystalline properties, as the corresponding homopolymer **PC(Azo)** (see structure in Figure 3.12), which was a liquid crystalline material that exhibited a highly viscous mesophase from 69 °C (melting temperature after cold crystallisation above T_g at 46 °C) to 77 °C (mesophase to isotropic transition temperature) difficult to identify by POM (Figure 3.12). For the pristine **PEG_{45}-*b*-PC(Azo)$_{18}$** some residual PEG crystallisation was observed from the first heating curve. However, the melting transition of the PEG block was not observed after cooling and re-heating of the sample suggesting not crystallisation. Instead, a glass transition and two endothermic peaks originated from the liquid crystalline polycarbonate block were observed. On the contrary, the heating curve of **PEG_{113}-*b*-PC(Azo)$_{23}$** showed the thermal events associated to each block, namely, melting of PEG segment at 45 °C (probably masking the glass transition of PC(Azo) block), melting of the PC(Azo) block at 61 °C and the mesophase to isotropic transition at 73 °C.

Block copolymers of the **PEG_n-*b*-PC(AzoOMe)$_m$** series were amorphous as they only exhibited a glass transition on the second heating scan attributed to the polycarbonate block.

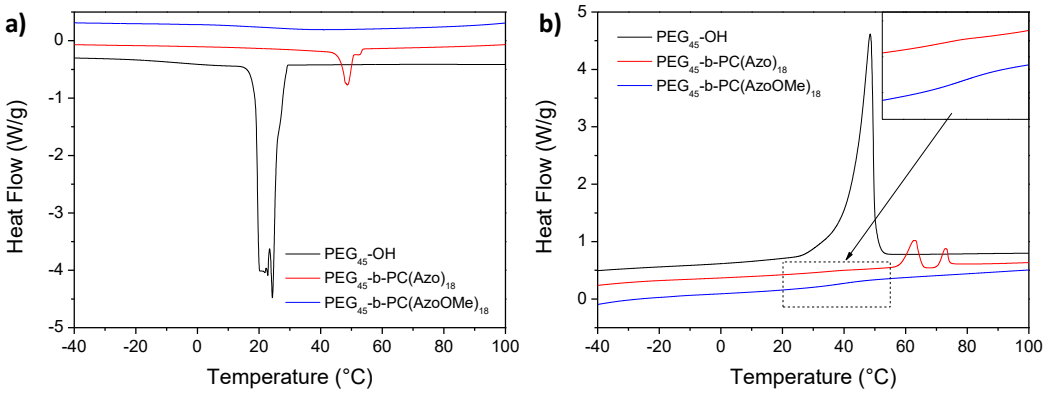

Figure 3.10: DSC curves registered on cooling (a) and subsequent heating (b) at a 10 °C min^{-1} scanning rate of PEG$_{45}$-OH, **PEG$_{45}$-*b*-PC(Azo)$_{18}$** and **PEG$_{45}$-*b*-PC(AzoOMe)$_{18}$**.

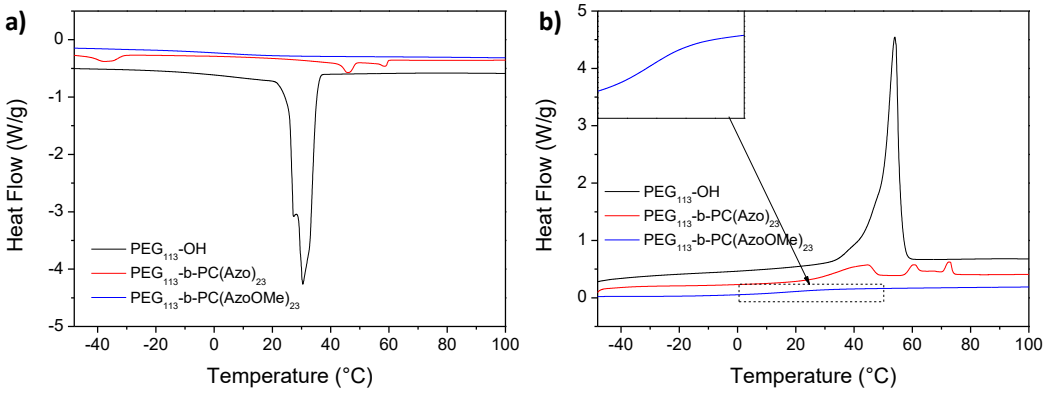

Figure 3.11: DSC curves registered on cooling (a) and subsequent heating (b) at a 10 °C min^{-1} scanning rate of PEG$_{113}$-OH, **PEG$_{113}$-*b*-PC(Azo)$_{23}$** and **PEG$_{113}$-*b*-PC(AzoOMe)$_{23}$**.

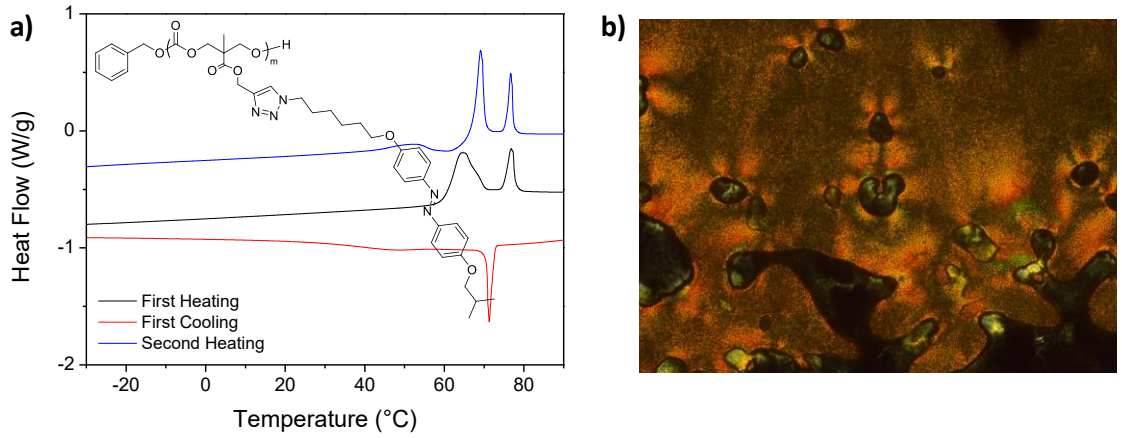

Figure 3.12: Structure of **PC(Azo)** and DSC curves registered at a 10 °C min^{-1} scanning rate (a) and POM image captured at 73 °C for **PC(Azo)** (b).

3.4 Self-Assembly in water and morphological analysis

Self-assembly of **PEG$_n$-*b*-PC(Azo)$_m$** and **PEG$_n$-*b*-PC(AzoOMe)$_m$** polymers was promoted by the co-solvent method when water was gradually added to THF solutions of the polymers. The process was monitored by turbidimetry recording the decrease of transmitted light through the sample that occurs upon self-assembly. Morphology and size of the self-assembled structures were determined by transmission electron microscopy (TEM), transmission electron cryomicroscopy (Cryo-TEM) and dynamic light scattering (DLS).

TEM images collected for copolymers of the PEG$_{113}$ series (**PEG$_{113}$-*b*-PC(Azo)$_{23}$** and **PEG$_{113}$-*b*-PC(AzoOMe)$_{23}$**), which comprise about 75% hydrophobic content in mass percentage showed the formation of spherical micelles (Figure 3.13) with the azobenzene segments forming the compact core. Average hydrodynamic diameters, D_h, measured by DLS were 24 nm for **PEG$_{113}$-*b*-PC(Azo)$_{23}$** and 30 nm for **PEG$_{113}$-*b*-PC(AzoOMe)$_{23}$**, matching with the values estimated from the TEM images (Figure 3.13). Critical aggregation concentrations (CAC) were determined by fluorescence spectroscopy using Nile Red as a probe, obtaining values of 17 and 22 μg mL^{-1} for **PEG$_{113}$-*b*-PC(Azo)$_{23}$** and **PEG$_{113}$-*b*-PC(AzoOMe)$_{23}$** (Figure 3.14).

For block copolymers of the PEG$_{45}$ series (**PEG$_{45}$-*b*-PC(Azo)$_{18}$** and **PEG$_{45}$-*b*-PC(AzoOMe)$_{18}$**) having approx. 85% hydrophobic mass percentage, vesicles were visualized by TEM and Cryo-TEM (Figure 3.15) with the azobenzene hydrophobic segments confined inside the vesicle's membrane hydrophobic region. A D_h of 350 nm for **PEG$_{45}$-*b*-PC(Azo)$_{18}$** and 220 nm for **PEG$_{45}$-*b*-PC(AzoOMe)$_{18}$** were determined by DLS (Figure 3.15). The CACs for **PEG$_{45}$-*b*-PC(Azo)$_{18}$** and **PEG$_{45}$-*b*-PC(AzoOMe)$_{18}$** were found to be 32 and 33 μg mL^{-1} respectively (Figure 3.16). The increase of CAC on increasing the hydrophobicity of the BCs, also associated to a change from micelles to vesicles, has been observed for other BCs[3] and could be related with the shorter length of the PEG block on the vesicles. The longer PEG chain length on the micellar self-assemblies will lead to a higher coverage of the micelle core increasing their stability and, consequently, displaying lower CAC values.[4]

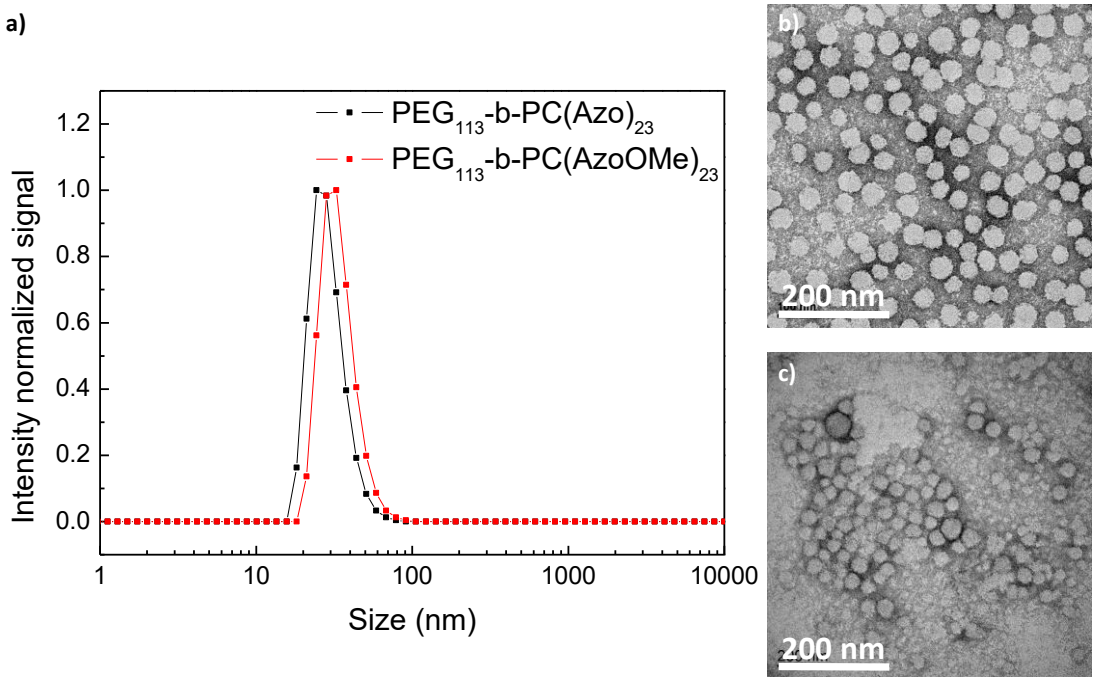

Figure 3.13: Analysis of the self-assembled structures of PEG_{113} amphiphilic block copolymers series. DLS distribution curves of **PEG_{113}-*b*-PC(Azo)$_{23}$** and **PEG_{113}-*b*-PC(AzoOMe)$_{23}$** (a). TEM image of **PEG_{113}-*b*-PC(Azo)$_{23}$** (b) and **PEG_{113}-*b*-PC(AzoOMe)$_{23}$** (c).

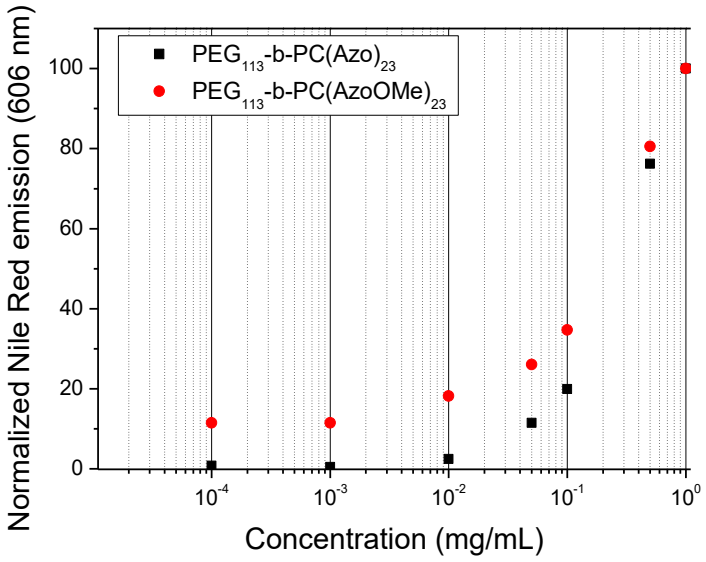

Figure 3.14: Normalised fluorescence emission of Nile Red at 606 nm (λ_{exc} = 550 nm) *versus* the **PEG_{113}-*b*-PC(Azo)$_{23}$** and **PEG_{113}-*b*-PC(AzoOMe)$_{23}$** concentration. CAC was determined from the intersection of the two extrapolated lines.

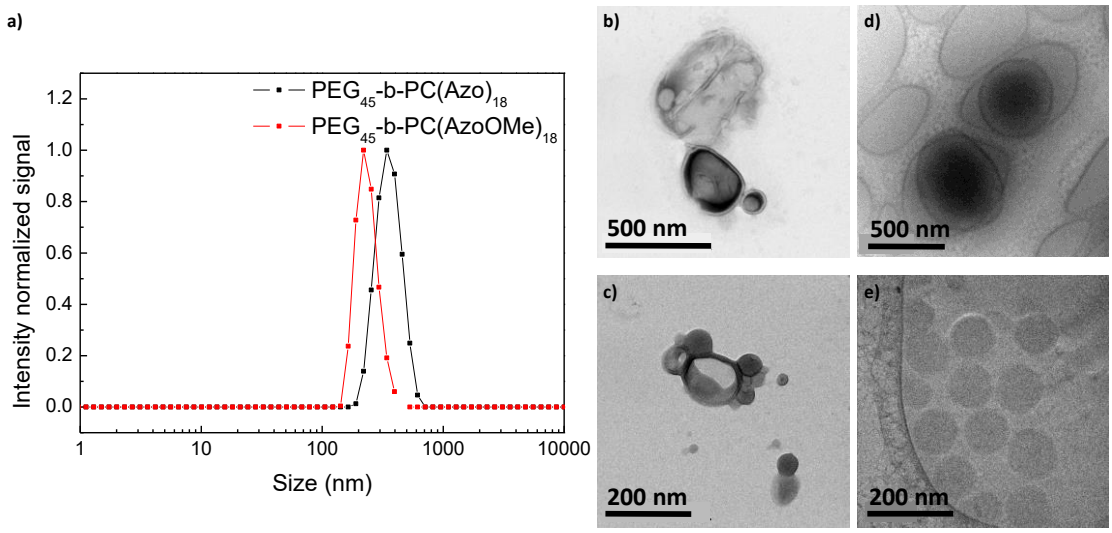

Figure 3.15: Analysis of the self-assembled structures of PEG_{45} amphiphilic block copolymers series. DLS distribution curves of **PEG_{45}-*b*-PC(Azo)$_{18}$** and **PEG_{45}-*b*-PC(AzoOMe)$_{18}$** (a). TEM images of **PEG_{45}-*b*-PC(Azo)$_{18}$** (b) and **PEG_{45}-*b*-PC(AzoOMe)$_{18}$** (c). Cryo-TEM image of **PEG_{45}-*b*-PC(Azo)$_{18}$** (d) and **PEG_{45}-*b*-PC(AzoOMe)$_{18}$** (e).

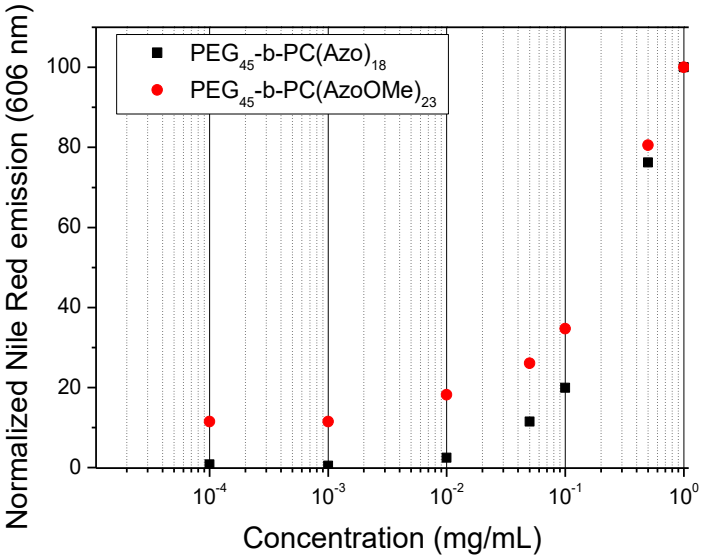

Figure 3.16: Normalised fluorescence emission of Nile Red at 606 nm (λ_{exc} = 550 nm) *versus* the **PEG_{45}-*b*-PC(Azo)$_{18}$** and **PEG_{45}-*b*-PC(AzoOMe)$_{18}$** concentration. CAC was determined from the intersection of the two extrapolated lines.

3.5 Light responsiveness of PEG_n-*b*-$PC(Azo)_m$ self-assemblies

UV-Vis spectra of the **PEG_n-*b*-$PC(Azo)_m$** series polymers were registered both in THF solution, at a concentration of 10^{-4} M relative to the azobenzene moieties, and the self-assemblies aqueous dispersions, at a concentration of 1 mg of BC per mL. The solution spectra displayed two absorption bands arising from the *trans*-azobenzene isomer, a strong one located at 360 nm corresponding to the π-π* transition and a weak one centered at 450 nm which corresponds to the forbidden n-π* transition (Figure 3.17). After 15 s exposure to an UV light lamp (Irradiance in the sample of 3.5 μW cm^{-2} at 365 nm), a drastic decrease of the absorbance at 360 nm accompanied by the apparition of a new less intense π-π* band centered at 330 nm corresponding to *cis*-azobenzene unit was observed, alongside with an increase in the absorbance at 450 nm due to the *trans-cis* photoisomerisation. These spectral features agree well with those reported for LDBCs decorated with the same azobenzene moiety.[5]

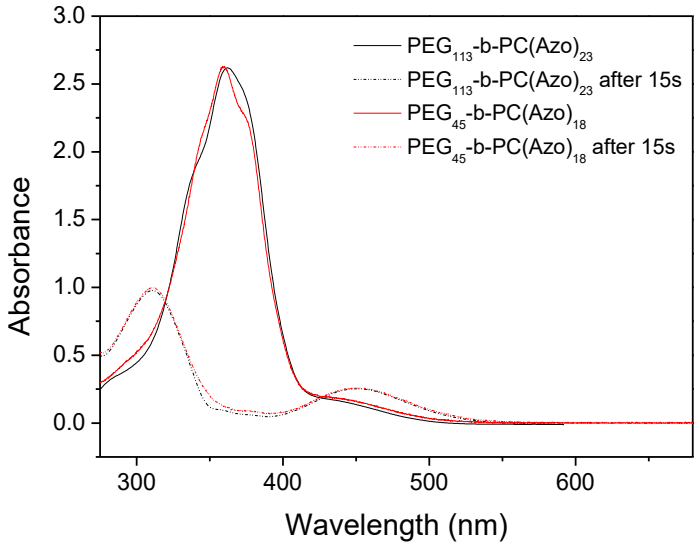

Figure 3.17: UV-Vis spectra of a 10^{-4} M (referred to the repetitive azobenzene unit) **PEG_{113}-*b*-$PC(Azo)_{23}$** and **PEG_{45}-*b*-$PC(Azo)_{18}$** solution in THF, before and after 15 s UV (3.5 μW cm^{-2} at 365 nm) illumination.

The spectra of the self-assemblies (both micelles and vesicles) aqueous dispersions showed a blue shift of the π-π* band maximum from 360 nm to 320 nm indicative of the prevalent formation of H-aggregates of azobenzene units (Figure 3.18).

Moreover, two weak shoulders were observed, one at 360 nm associated to the non-aggregated azobenzenes and one at 375 nm arising the formation of J-aggregates.[5,6,7] Upon UV illumination, a decrease on the intensity of the π- π* band with a concurrent increase in the absorbance at 450 nm was monitored due to the *trans-cis* photoisomerisation and changes of the azobenzene aggregation. No further evolution on the spectra was observed after 5 min of illumination inferring that a photostationary state was reached at this point. After storing the irradiated sample at room temperature for 24 h in the dark, the initial spectra were not recovered as the broad π- π* band was centered at 360 nm (instead of 320 nm), suggesting an azobenzene aggregation different to the observed on the non-irradiated self-assemblies.

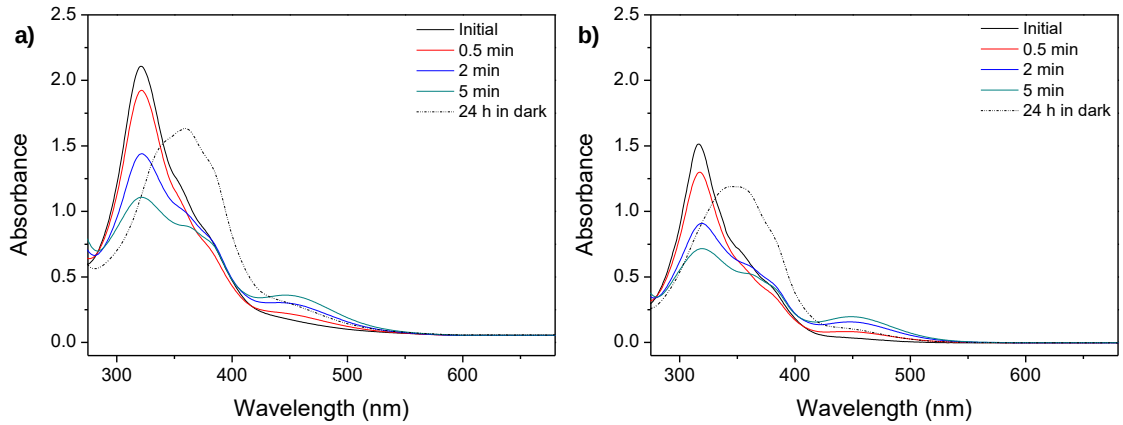

Figure 3.18: UV-Vis spectra of 1 mg BC mL^{-1} self-assemblies water suspensions upon UV light (3.5 μW cm^{-2} at 365 nm) illumination for different times and subsequent storage at room temperature for 24 h in the dark: (a) **PEG$_{45}$-*b*-PC(Azo)$_{18}$** vesicles and (b) **PEG$_{113}$-*b*-PC(Azo)$_{23}$** micelles.

Once the *trans-cis* photoisomerisation of the 4-isobutyloxy-4'-oxyazobenzene moieties confined into the hydrophobic regions of the self-assemblies was corroborated, morphological changes of the micelles and vesicles after UV light illumination were studied by TEM and DLS. After 10 min of exposure to UV light **PEG$_{113}$-*b*-PC(Azo)$_{23}$** micelles were still visible across the TEM grid, although its morphology was less defined and were accompanied by organic material without a defined morphology, in a similar way to previous reported azobenzene light-responsive micelles[8] (Figure 3.19). A slight increase in the size of the micelles was measured by DLS, with D_h going up from 24 nm to 30 nm (Figure 3.19).

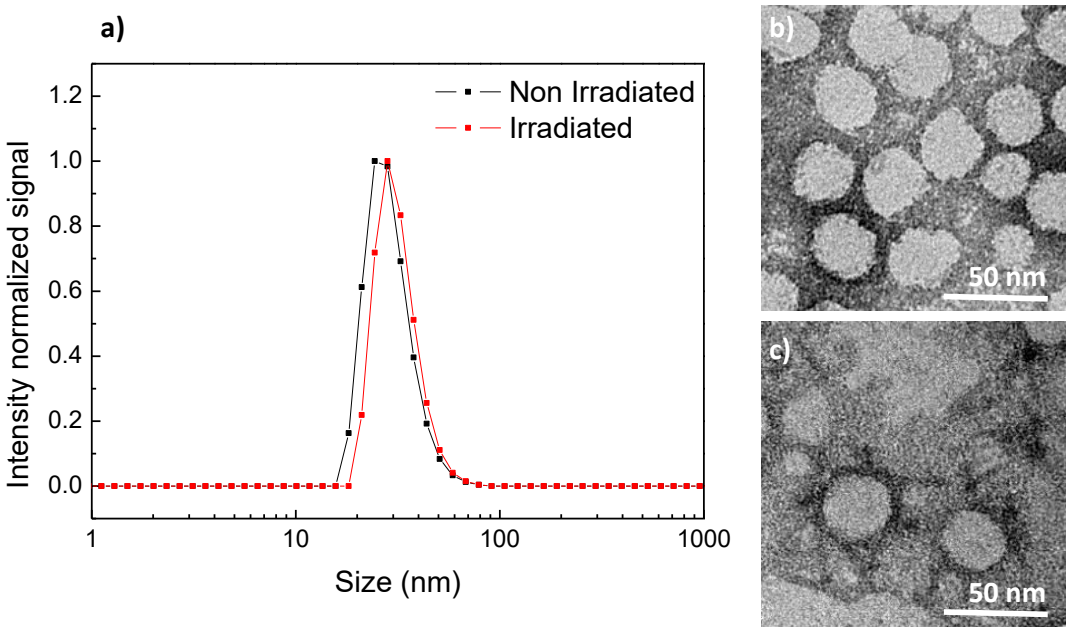

Figure 3.19: DLS traces (a) and TEM images before (b) and after 10 min UV light (3.5 μW cm^{-2} at 365 nm) irradiation (c) of **PEG$_{113}$-*b*-PC(Azo)$_{23}$** self-assemblies.

Upon UV illumination, vesicles from **PEG$_{45}$-*b*-PC(Azo)$_{18}$** appeared distorted and wrinkled in the TEM images as in the related linear-dendritic block copolymers previously described with this 4-isobutyloxy-4'-oxyazobenzene unit.[5,9] These vesicles were found to coexist with smaller vesicles that were not observed in non-irradiated samples (Figure 3.20). Alteration of the vesicles was confirmed by Cryo-TEM inspection, where the continuous and smooth vesicle became non-continuous and folded (Figure 3.21). In accordance, by DLS an increase in the size dispersity of the self-assemblies and the appearance of a second smaller size population was observed (Figure 3.21).

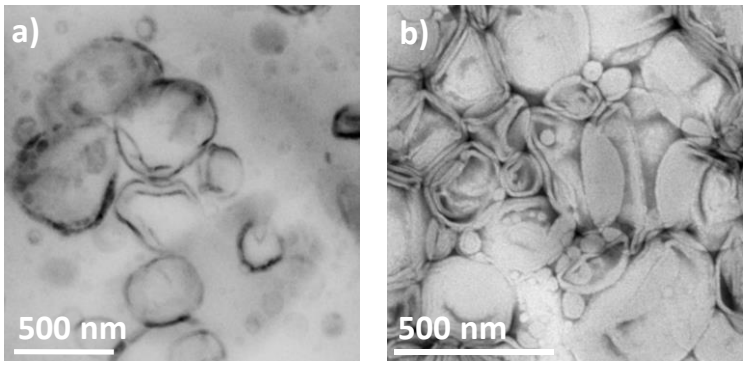

Figure 3.20: TEM images of **PEG$_{45}$-*b*-PC(Azo)$_{18}$** self-assemblies before (a) and after 10 min low intensity UV light (3.5 μW cm^{-2} at 365 nm) irradiation (b).

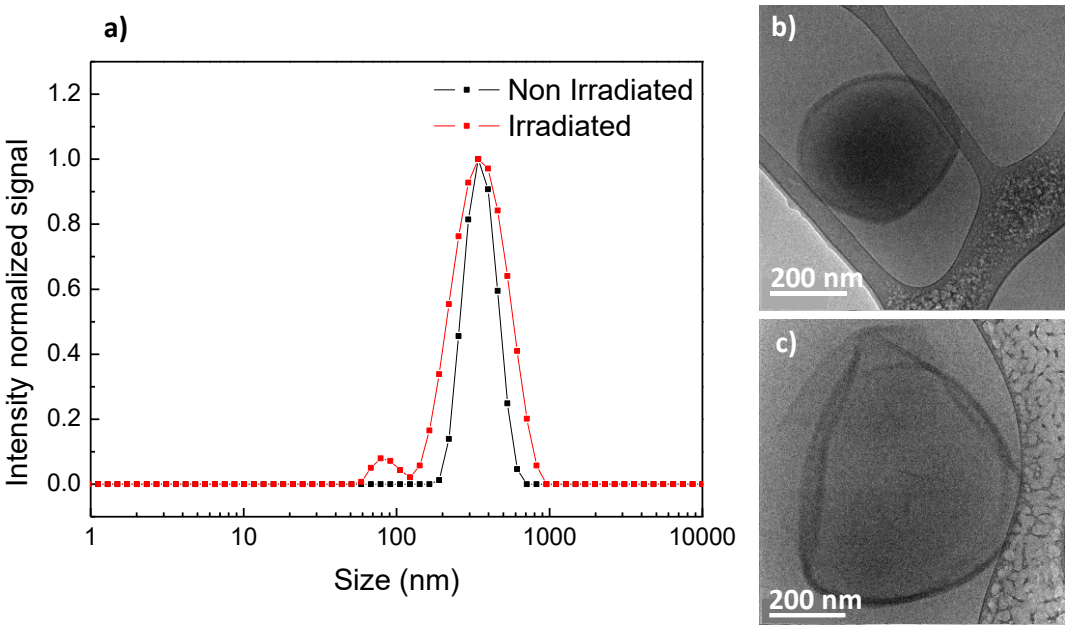

Figure 3.21: DLS traces (a) and Cryo-TEM images before (b) and after 10 min UV light (3.5 μW cm^{-2} at 365 nm) irradiation (c) of **PEG_{45}-*b*-PC(Azo)$_{18}$** self-assemblies.

3.6 Light responsiveness of PEG_n-*b*-PC(AzoOMe)$_m$ self-assemblies

The UV-vis spectra of tetra-*ortho*-methoxy substituted azobenzenes polymers, **PEG_{45}-*b*-PC(AzoOMe)$_{18}$** and **PEG_{113}-*b*-PC(AzoOMe)$_{23}$**, in solution showed a main band corresponding to the π-π* electronic transition centred at 320 nm and a second absorption band due to n-π* transition located at 470 nm (Figure 3.22).Due to the non-planar molecular geometry of the AzoOMe moiety, this n-π* transition absorption band is significantly more intense and red-shifted compared to PC(Azo) series (470 nm *versus* 450 nm).[10] This n-π* band is extended beyond 600 nm and, consequently, the photoisomerisation could be induced with red light.[11]

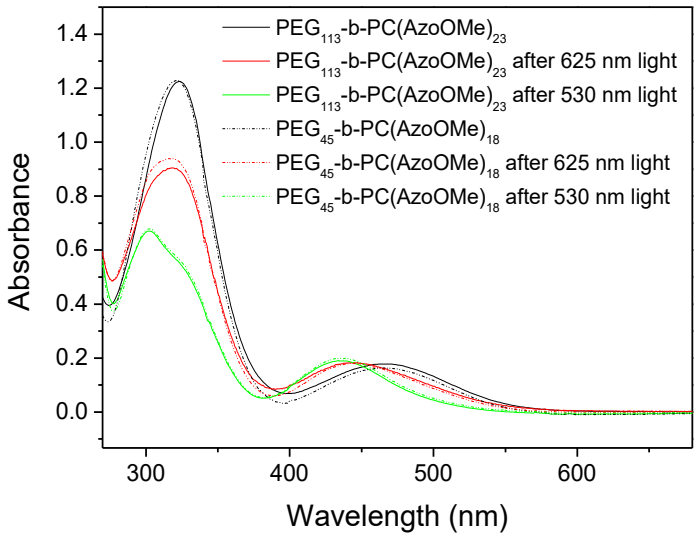

Figure 3.22: UV-Vis spectra of a 10^{-4} M (referred to the repetitive azobenzene unit) **PEG_{113}-*b*-PC(AzoOMe)$_{23}$** and **PEG_{45}-*b*-PC(AzoOMe)$_{18}$** solution in THF and photostationary state reached after 40 min under 625 nm light (30 μW cm^{-2}) and after 30 s under 530 nm (30 μW cm^{-2}) light.

The *trans-cis* isomerisation of the AzoOMe unit was induced using a LED of either 625 nm or 530 nm wavelength (Irradiance in the sample of 30 μW cm^{-2}). When BCs THF solutions were exposed to 625 nm light a photostationary state was reached after 40 min. Spectra showed a remarkable decrease in the intensity of π-π* band and a blue shift of the n-π* band, from 470 to 445 nm, attributed to the *trans*-to-*cis* photoisomerisation of the photoactive units (Figure 3.22). The same trend was

observed under 530 nm irradiation although in a shorter timescale, *i.e.* the photostationary state was reached only after 30 s, due to a higher absorption at the irradiation wavelength. Besides, the decrease in the intensity of the π-π* band was more acute and the n-π* band was shifted up to 435 nm. The evolution of spectra upon illumination showed the presence of two isosbestic points at 390 and 460 nm giving evidence of an equilibrium between two different species during the photoisomerisation without the occurrence of other competitive processes.[12] The *cis*-azobenzene fraction (γ), on the photostationary state can be estimated from the absorbance at 330 nm using the expression $\gamma = 1.05 \cdot (1-A/A_0)$ being A_0 and A absorbance before and after irradiation.[13,14] Under 625 nm light a *cis* content of approx. 30% at the photostationary state was found for both copolymers, while under 530 nm light *cis* content raised up to approx. 55%.

Compared to solution, UV-Vis spectra of the self-assembled structures showed a shift of the n-π* band to higher frequencies, from 470 to 450 nm (Figure 3.23). Under visible light illumination both micelles and vesicles showed similar behaviour. When self-assemblies were illuminated with 625 nm light (Figure 3.23a and b), the photostationary state was reached in irradiation times between 120 and 150 min, which are longer illumination times when compared to solution, probably due to the blue-shifting of the n-π* band with respect to THF solutions and the confinement of azobenzene moieties in the hydrophobic regions of the self-assemblies (Figure 3.23). At the photostationary state the *cis* content was similar for both micelles and vesicles, about 40%. Once the light was turn off and the irradiated samples were stored in the dark for 24 h, the initial situation was only partially recovered, as a *cis* content of approx. 20% and 5% was found for micelles and vesicles, respectively (Figure 3.23).

By irradiating the aqueous dispersions with 530 nm light, the photostationary states were reached at the same timescale than in THF solution (Figure 3.23c and 3.23d) but rendering lower *cis* contents in comparison to those obtained with 625 nm light: 26% and 29% for micelles and vesicles, respectively. It was remarkable the low thermal reversibility of the light induced changes after storing the samples 24 h in the dark for both types of self-assemblies (Figure 3.23c and 3.23d).

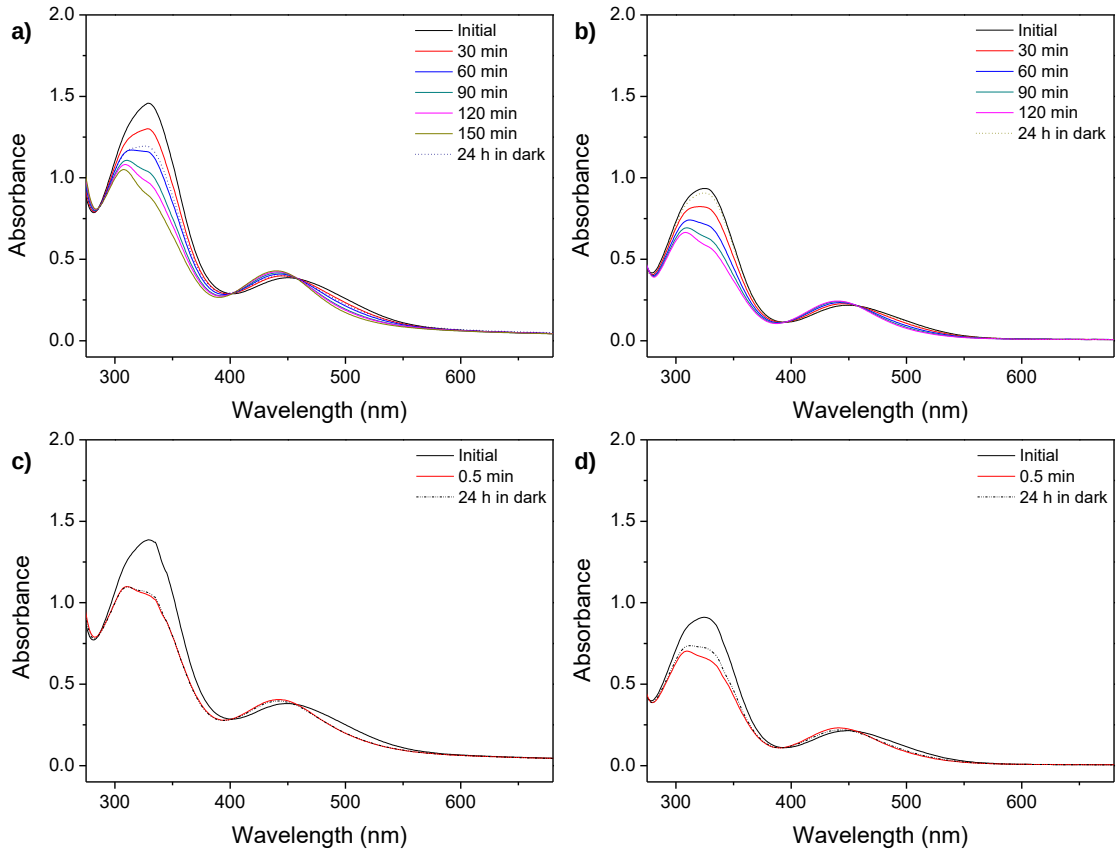

Figure 3.23: UV-Vis spectra of a 1 mg BC mL^{-1} self-assemblies water suspensions of **PEG$_{113}$-*b*-PC(AzoOMe)$_{23}$** (a) and **PEG$_{45}$-*b*-PC(AzoOMe)$_{18}$** (b) under 625 nm (30 μW cm^{-2}) light illumination for different times and subsequent storage for 24 h in the dark and **PEG$_{113}$-*b*-PC(AzoOMe)$_{23}$** (c) and **PEG$_{45}$-*b*-PC(AzoOMe)$_{18}$** (d) under 530 nm (30 μW cm^{-2}) light illumination for different times and subsequent storage for 24 h in the dark.

According to TEM images and DLS analysis, micelles of **PEG$_{113}$-*b*-PC(AzoOMe)$_{23}$** remained stable after 120 min under 625 nm light exposure (Figure 3.24c). However, they were affected by the action of 530 nm light. After 5 min, a slight modification in size was registered by DLS, with the average diameter decreasing from 30 to 27 nm (Figure 3.24a). On the TEM images the unmodified micelles coexisted with smaller ones (Figure 3.24d).

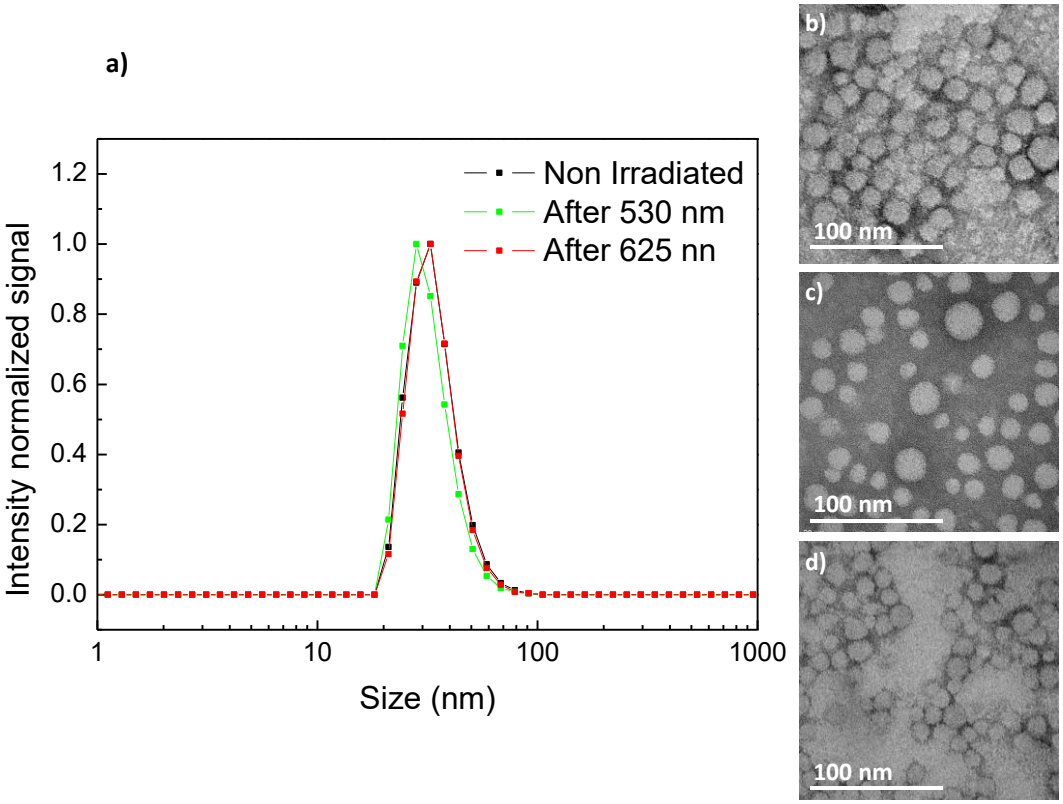

Figure 3.24: DLS traces (a) and TEM images before (b), after 2 hours 625 nm (30 μW cm^{-2}) irradiation (c) and after 5 min 530 nm (30 μW cm^{-2}) light irradiation (d) of **PEG_{113}-*b*-PC(AzoOMe)$_{23}$** micelles.

When the vesicles dispersion of **PEG_{45}-*b*-PC(AzoOMe)$_{18}$** was exposed to 625 nm light up to 120 min, the effect of illumination on the self-assemblies was negligible according to TEM images (Figure 3.25) and DLS measurements (Figure 3.26). However, after 5 min under 530 nm light a remarkable increase in the size dispersity of the self-assemblies was monitored by DLS (Figure 3.26) as a consequence of the *trans-cis* isomerisation. Disruption of the vesicle morphology was confirmed by TEM (Figure 3.25) and Cryo-TEM (Figure 3.26), as the number of vesicle diminishes after 530 nm light irradiation.

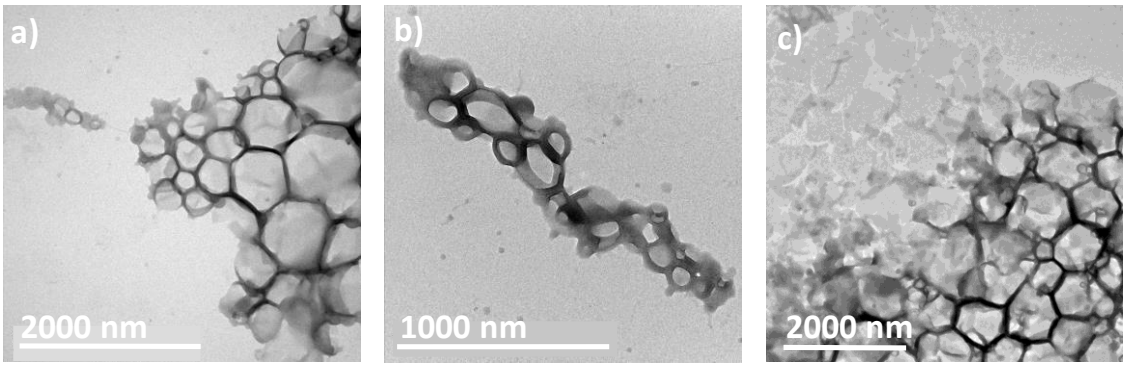

Figure 3.25: TEM images of **PEG$_{45}$-*b*-PC(AzoOMe)$_{18}$** self-assemblies before (a), after 120 min 625 nm (30 µW cm^{-2}) light irradiation (b) and after 5 min 530 nm (30 µW cm^{-2}) light irradiation (c).

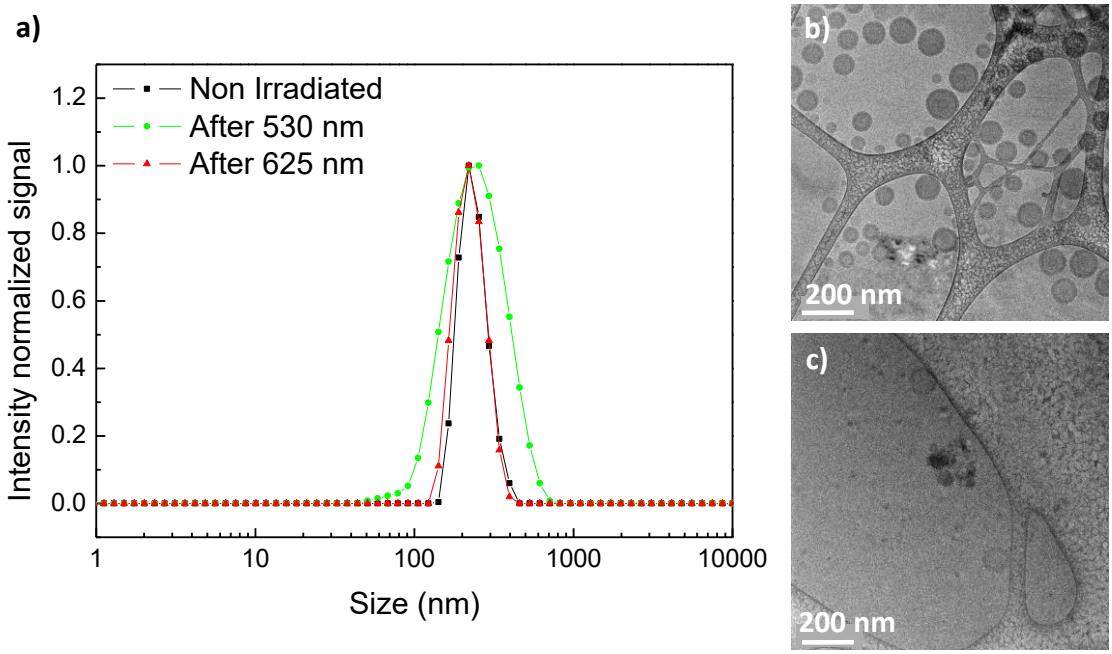

Figure 3.26: DLS traces (a) and Cryo-TEM images before (b) and after 5 min 530 nm (30 µW cm^{-2}) light irradiation (c) of **PEG$_{45}$-*b*-PC(AzoOMe)$_{18}$** vesicles.

3.7 Encapsulation and light-induced release of molecular probes

After having evaluated the light-response of micelles and vesicles, their potential capability as light-responsive nanocarriers was tested by using fluorescent molecular probes. Micelles were loaded at the internal core with the well-known hydrophobic fluorescent probe, Nile Red, while vesicles were loaded with Nile Red, and with a hydrophilic fluorescent probe, Rhodamine B. The changes on the emission intensity registered at different light exposure times (Figure 3.27 and Figure 3.28).

Nile Red loaded **PEG_{113}-*b*-PC(Azo)$_{23}$** micelles showed an intense and broad emission band located at 610 nm (when exciting at 550 nm) that sharply decreased during the UV illumination process (Figure 3.27). The emission was only partially recovered after 24 h in dark, which seems to evidence that Nile Red is released from the hydrophobic micelle core [9].

Nile Red and AzoOMe n-π*absorption bands are partially overlapped, being this overlapping smaller for the *cis* isomer as its n-π*absorption band is blue-shifted in comparison to the *trans* one (Figure 3.23). Moreover, the *trans*-isomer can also absorb the light emitted by Nile Red. Under exposure to 625 nm light, the emission of Nile Red loaded **PEG_{113}-*b*-PC(AzoOMe)$_{23}$** micelles increased steadily in the same time interval that *trans*-*cis* isomerisation takes place, because Nile Red emission was enhanced due to the decrease of the percentage of the *trans* isomer. After 120 min under 625 nm light irradiation, once the photostationary state was reached, Nile Red emission remained constant, which seems to evidence that it was not released to the surrounding media by the effect of 625 nm irradiation (Figure 3.27). After 24 h in the dark, the thermal *cis*-to-*trans* relaxation took place and consequently the percentage of *trans* isomer increased and the emission of Nile Red decreased (Figure 3.27).

Under exposure to 530 nm light for 30 s an initial increase in Nile Red emission was observed due to the *trans*-to-*cis* isomerisation. However, under longer exposure times (photostationary state was detected at around 30 s, see above), a steady decrease in Nile Red emission was detected that might be a consequence of Nile Red release to the aqueous media (Figure 3.27). 530 nm light seems to induce not only

morphological changes in the micelles but also the release of hydrophobic molecular cargoes encapsulated in the micelles core. After 24 h in the dark Nile Red emission remained almost constant, in accordance with the low thermal reversibility observed under these experimental conditions (see above).

Encapsulation and light induced release was also tested for vesicles using either hydrophilic or hydrophobic fluorescent probes, Nile Red and Rhodamine B respectively. Nile Red loaded **PEG_{45}-*b*-PC(Azo)$_{18}$** vesicles showed similar features under UV light exposure to those described for the corresponding micelles, which is compatible with partial release of Nile Red from the membrane to the aqueous surrounding media under UV light (Figure 3.28). Emission of Nile Red loaded **PEG_{45}-*b*-PC(AzoOMe)$_{18}$** vesicles increased under 625 nm light in the same time interval where *trans-cis* takes place (Figure 3.28). Again, when the photostationary state was reached after 120 min, a constant emission value was measured. As in the case of micelles, irradiation with 625 nm seems to be not efficient to provoke the release of the encapsulated hydrophobic cargo. Under 530 nm illumination it is observed again the same behaviour as in **PEG_{113}-*b*-PC(AzoOMe)$_{23}$** micelles, an initial increase for the first 30 s during *trans-cis* isomerisation and then a continuous decrease, associated to Nile Red release to aqueous media (Figure 3.28).

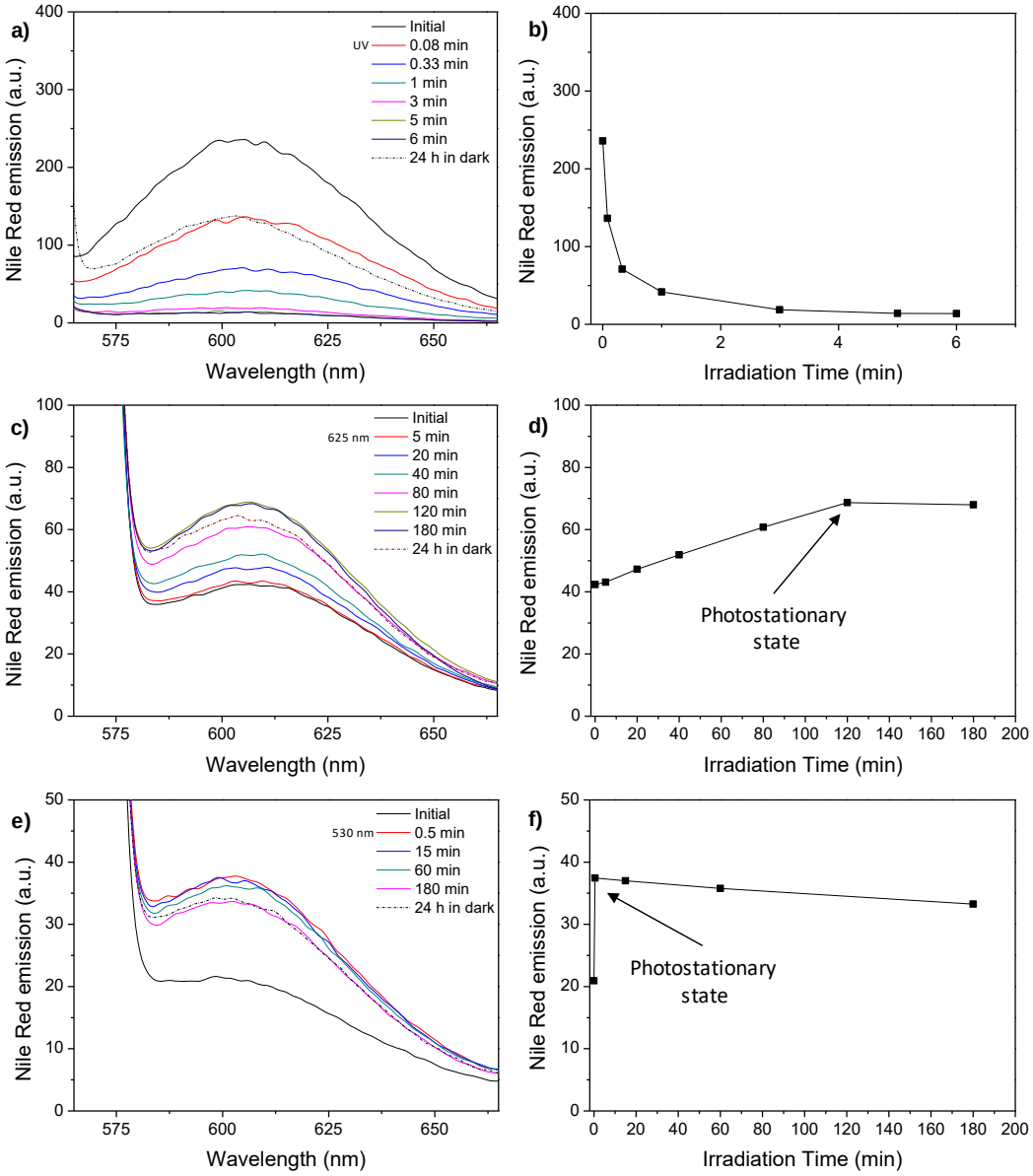

Figure 3.27: Emission spectra (excitation wavelength 550 nm) of the Nile Red loaded micelles recorded after light illumination and for different time intervals and subsequent storage for 24 h in the dark, and the corresponding release profiles, for **PEG$_{113}$-*b*-PC(Azo)$_{23}$** micelles under UV light (a and b), **PEG$_{113}$-*b*-PC(AzoOMe)$_{23}$** micelles under 625 nm (30 µW cm^{-2}) light (c and d) and **PEG$_{113}$-*b*-PC(AzoOMe)$_{23}$** micelles under 530 nm (30 µW cm^{-2}) light (e and f).

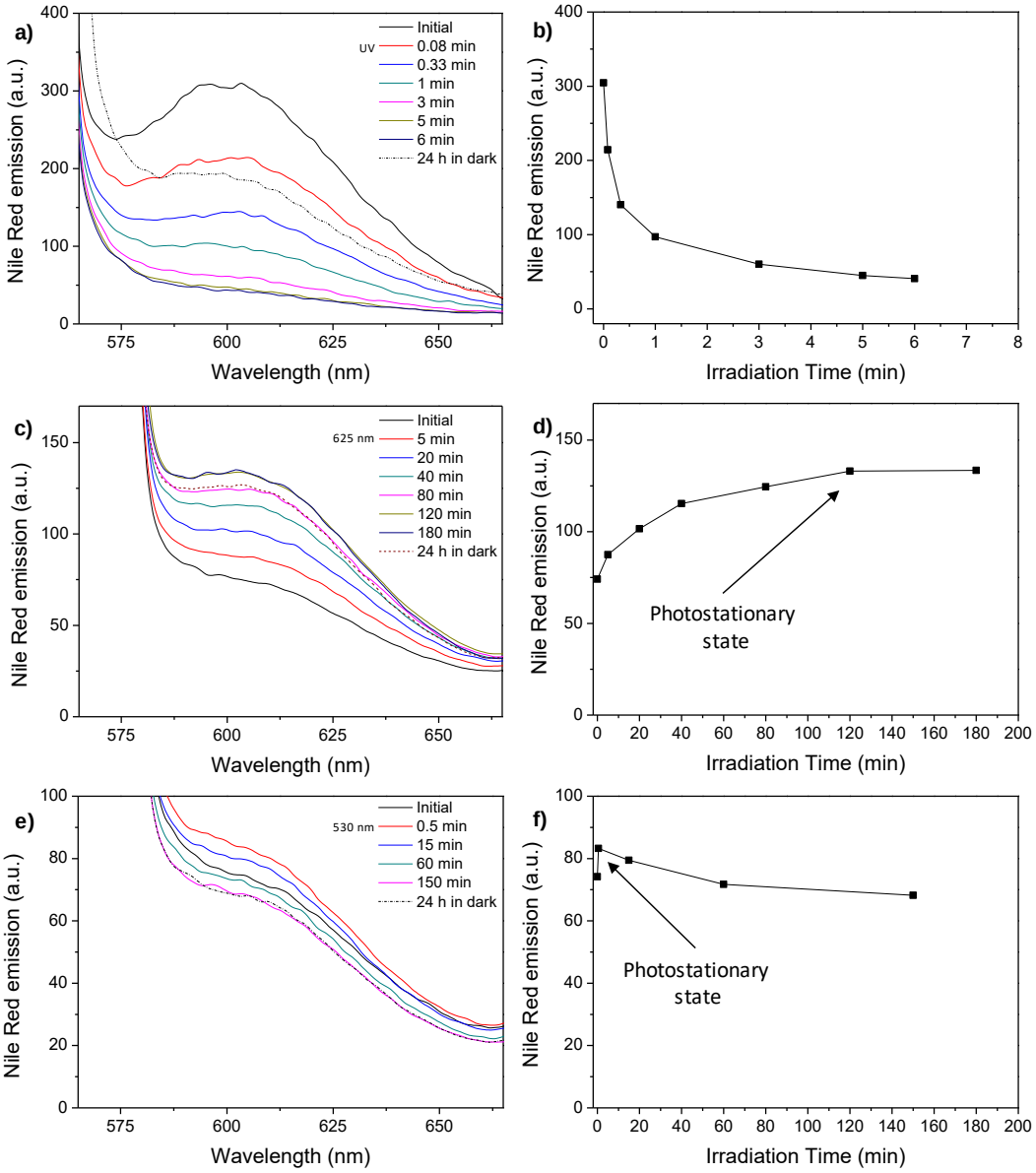

Figure 3.28: Emission spectra (excitation wavelength 550 nm) of the Nile Red loaded micelles recorded after light illumination and for different time intervals and subsequent storage for 24 h in the dark, and the corresponding release profiles, for **PEG$_{45}$-*b*-PC(Azo)$_{18}$** vesicles under UV light (a and b), **PEG$_{45}$-*b*-PC(AzoOMe)$_{18}$** vesicles under 625 nm (30 μW cm^{-2}) light (c and d) and **PEG$_{45}$-*b*-PC(AzoOMe)$_{18}$** vesicles under 530 nm (30 μW cm^{-2}) light (e and f).

Vesicles of **PEG$_{45}$-*b*-PC(Azo)$_{18}$** and **PEG$_{45}$-*b*-PC(AzoOMe)$_{18}$** were loaded with Rhodamine B which, given its hydrophilic character, would be trapped inside the aqueous cavity of the vesicle. The encapsulation and light induced release of Rhodamine B was monitored by confocal microscopy. Images of the initial samples showed fluorescence dots were on a dark background verifying the entrapment of the fluorescent probe inside the vesicles (Figure 3.29 and Figure 3.30). The number of encapsulated molecules was determined by HPLC, being 0.1 molecules of

Rhodamine B per block copolymer chain. Images collected for vesicles of **PEG$_{45}$-*b*-PC(Azo)$_{18}$** after being exposed for 10 min to UV light exhibited a fluorescent background as a consequence of the photoinduced release of Rhodamine B from the vesicles inner cavity to the surrounding media (Figure 3.29).[5,15]

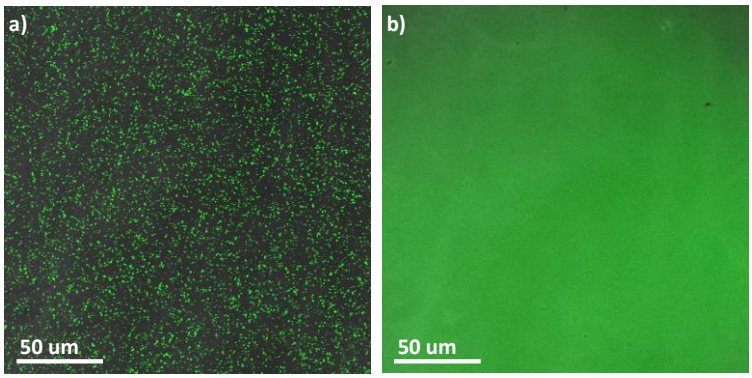

Figure 3.29: Fluorescence microscopy images of Rhodamine B loaded **PEG$_{45}$-*b*-PC(Azo)$_{18}$** vesicles before (a) and after 10 min low intensity UV (3.5 μW cm^{-2} at 365 nm) light irradiation (b).

For vesicles of **PEG$_{45}$-*b*-PC(AzoOMe)$_{18}$** differences were very clear depending on the illumination wavelength. After 120 min at 625 nm light illumination, the fluorescence dots were still visible and the background remained dark, that is to say, the isomerisation induced by 625 nm illumination did not induce the release of the encapsulated Rhodamine B (Figure 3.30). However, in the sample illuminated with 530 nm light for 5 min, the fluorescence is extended all over the background, being still visible some fluorescence dots (Figure 3.30).

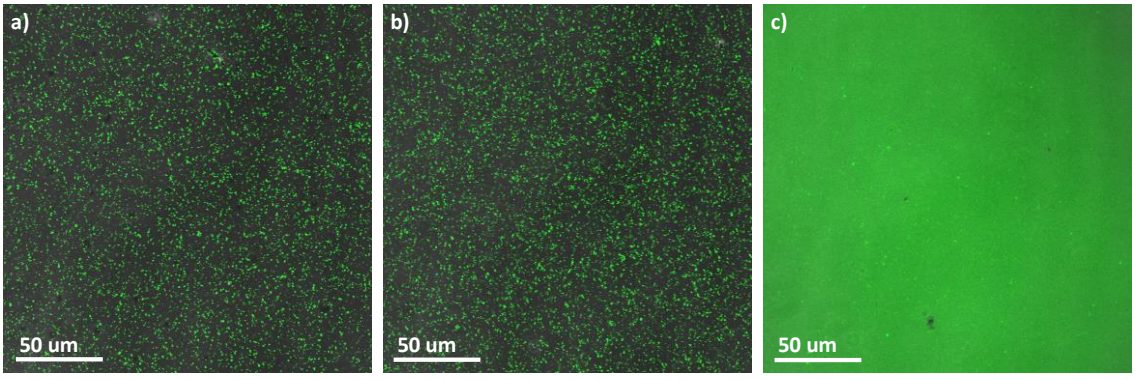

Figure 3.30: Fluorescence microscopy images of Rhodamine B loaded **PEG$_{45}$-*b*-PC(AzoOMe)$_{18}$** vesicles before (a), after 2 hours 625 nm (30 μW cm^{-2}) light irradiation (b) and after 5 min 530 nm (30 μW cm^{-2}) light irradiation (c).

Light-induced release of Rhodamine B from the vesicles was also studied by dialysis experiments. Rhodamine B loaded vesicles from **PEG$_{45}$-*b*-PC(Azo)$_{18}$** and

PEG$_{45}$-*b*-PC(AzoOMe)$_{18}$ were irradiated with UV light for 10 min or 530 nm light for 5 min respectively, dialysed against Milli-Q water (Slide-A-Lyzer 2kDa, ThermoScientific), and the fluorescence of the dialysis water measured at different times. A continuous increase in Rhodamine B emission was measured for times up to 56 h (Figure 3.31). A blank experiment without irradiating before the dialysis was also performed, observing some Rhodamine B fluorescence in the dialysis water, but much weaker than in the illuminated samples. Thus, we conclude that for **PEG$_{45}$-*b*-PC(Azo)$_{18}$** UV light irradiation, and for **PEG$_{45}$-*b*-PC(AzoOMe)$_{18}$** 530 nm illumination, triggers effectively the release of Rhodamine B from the vesicles inner cavity to the surrounding aqueous media.

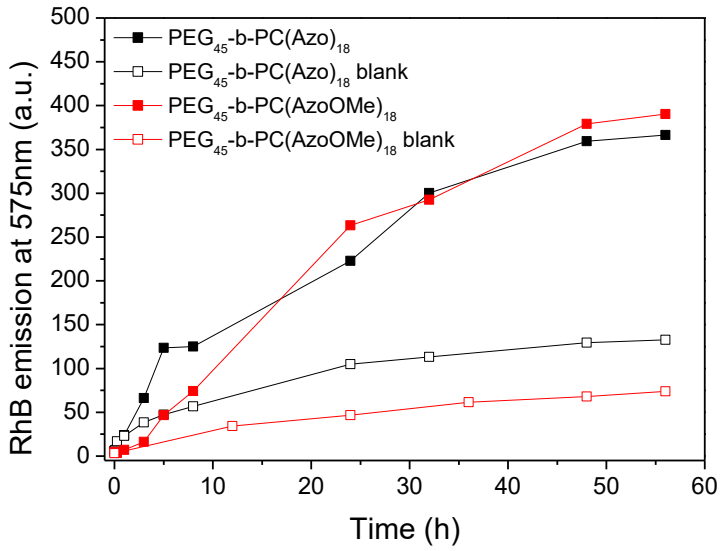

Figure 3.31: Rhodamine B release profiles for **PEG$_{45}$-*b*-PC(Azo)$_{18}$** and **PEG$_{45}$-*b*-PC(AzoOMe)$_{18}$** upon irradiation with UV (3.5 μW cm^{-2} at 365 nm) light or 530 nm (30 μW cm^{-2}) light respectively.

3.8 Conclusions

A series of amphiphilic diblock copolymers bearing either 4-isobutyloxy-4'-oxyazobenzene or 2,2',5,5'-tetramethoxy-4-oxyazobenzene units in the side chain of the hydrophobic block have been synthesised by combination of ROP and CuAAC. The synthesised amphiphilic BCs are able to self-assemble when dispersed in water. The length of the hydrophilic block has a drastic influence in the morphology of the self-assemblies. Vesicles are formed for the copolymers with a PEG segment of n = 45, whereas those with a PEG segment of n = 113 self-assemble into spherical micelles. Micelles have been loaded with a hydrophobic fluorescent probe, Nile Red, and vesicles with Nile Red and a hydrophilic fluorescent probe, Rhodamine B. Morphological changes in the self-assemblies from **PEG$_{113}$-*b*-PC(Azo)$_{23}$** and **PEG$_{45}$-*b*-PC(Azo)$_{18}$** have been induced upon the application of UV light, triggering the release of encapsulated Nile Red and Rhodamine B. Unfortunately, 625 nm light irradiation does not induce appreciable morphological changes in the self-assemblies from **PEG$_{113}$-*b*-PC(AzoOMe)$_{23}$** and **PEG$_{45}$-*b*-PC(AzoOMe)$_{18}$**. Nonetheless, 530 nm light irradiation induce morphological changes in the self-assembled structures from **PEG$_{113}$-*b*-PC(AzoOMe)$_{23}$** and **PEG$_{45}$-*b*-PC(AzoOMe)$_{18}$** and triggers the effective release of encapsulated molecules in an equivalent way to **PEG$_{113}$-*b*-PC(Azo)$_{23}$** and **PEG$_{45}$-*b*-PC(Azo)$_{18}$** under UV light, proving the validity of substituting the UV-responsive 4-isobutyloxy-4'-oxyazobenzene by 2,2',5,5'-tetramethoxy-4-oxyazobenzene

3.9 Experimental section

3.9.1 Synthesis and characterisation of N_3-Azo and N_3-AzoOMe

Azide azobenzenes were synthesised as illustrated in Figure 28 from the corresponding 4-hydroxyazobencenes *via* Mitsunobu reaction with 6-azidohexan-1-ol. 4-isobutyloxy-4'-hydroxyazobenzene,[5] 2,2',5,5'-tetramethoxy-4-hydroxy-azobenzene[14] and 6-azidohexan-1-ol[16] were synthesised according to previously reported procedures.

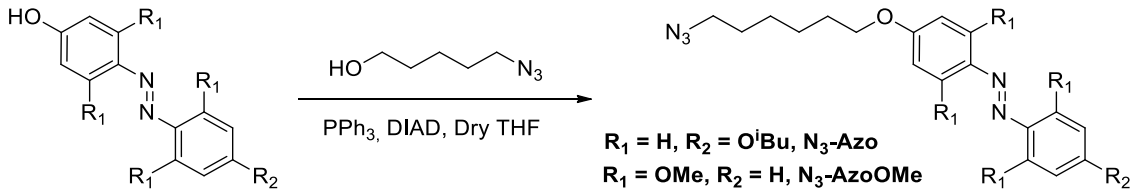

Figure 3.32: General synthesis of azides **N_3-Azo** y **N_3-AzoOMe**

Synthesis and characterisation of N_3-Azo. 4-Isobutyloxy-4'-hydroxyazobenzene (1.50 g, 5.54 mmol), 6-azidohexanol (786 mg, 5.54 mmol) and diisopropyl azodicarboxylate (DIAD) (1.12 g, 5.54 mmol) were dissolved in dry THF (50 mL) under Ar atmosphere and cooled down in an acetone-ice bath. Then, a triphenylphospine (PPh_3) (1.45 g, 5.54 mmol) solution in anhydrous THF (10 mL) was added dropwise. The reaction mixture was stirred for 24 h. Solvent was evaporated to dryness and the product purified by recrystallisation in ethanol. Product was isolated by filtration as a pale orange solid. Yield 80%. FTIR (KBr, υ_{max}/cm^{-1}): 3050 (Csp^2-H^{st}), 2938 (Csp^3-H^{st}), 2102 (N_3^{st}), 1560 (CAr-CArst), 1471 (N=Nst), 1239 (C-Ost). ^{1}H NMR [400 MHz, $CDCl_3$, δ, ppm]: 7.94 - 7.79 (m, 4H), 7.07 - 6.91 (m, 4H), 4.03 (t, *J* = 6.4 Hz, 2H), 3.80 (d, *J* = 6.6 Hz, 2H), 3.29 (t, *J* = 6.8 Hz, 2H), 2.17 - 2.06 (m, 1H), 1.90 - 1.78 (m, 2H), 1.72 - 1.58 (m, 2H), 1.57 - 1.38 (m, 4H), 1.05 (d, *J* = 6.8 Hz, 6H). ^{13}C NMR [100 MHz, $CDCl_3$, ppm]: 161.45, 161.15, 147.15, 147.05 124.32, 114.82. 114.18, 74.81, 68.16, 51.51, 29.22, 28.93, 28.42, 26.65, 25.80, 19.37.

Synthesis and characterisation of N_3-AzoOMe. 2,2',5,5'-Tetramethoxy-4-hydroxyazobenzene, (400 mg, 1.26 mmol), DPTS (146 mg,

0.51 mmol) and 6-azidohexanoic acid (239 mg, 1.52 mmol) were dissolved in dry dichloromethane (10 mL) under Ar atmosphere. The flask was cooled in an acetone-ice bath. Then, EDC (290 mg, 1.52 mmol) was added under Ar atmosphere. After half an hour, the ice bath was removed and the reaction was stirred for 72 h at room temperature. Crude reaction was diluted with dichloromethane (100 mL) and washed with water (2x100 mL) and brine (100 mL). The organic phase was dried over anhydrous $MgSO_4$, filtered off and evaporated. The residue was purified by silica column chromatography, using dichloromethane/ethyl acetate (8/2) as eluent. Yield 45%. FTIR (KBr, υ_{max}/cm^{-1}): 3009 (Csp^2-H^{st}), 2942 (Csp^3-H^{st}), 2092 (N_3^{st}), 1581 (CAr-CArst), 1472 (N=Nst), 1255 (C-Ost). NMR ^1H [400 MHz, $CDCl_3$, δ (ppm)]: 7.18 (t, J = Hz, 1H), 6.65 (d, J = Hz, 2H), 6.21 (s, 2H), 4.01 (t, J = Hz, 2H), 3.87 (s, 6H), 3.84 (s, 6H), 3.30 (t, J = Hz, 2H), 1.90 - 1.75 (m, 2H), 1.73 - 1.60 (m, 2H), 1.60 - 1.39 (m, 4H). NMR ^{13}C [100 MHz, $CDCl_3$, δ (ppm)]: 161.03, 154.49, 152.28, 134.82, 128.71, 128.52, 105.2, 91.92, 67.75, 56.62, 51.33, 29.06, 28.75, 26.49, 25.64.

3.9.2 General procedure for the synthesis of PEG_n-*b*-PC_n block copolymers

A solution of PEG_n-OH (1 mol), DBU (1% mol to monomer) and TU (5% mol to monomer) in dry dichloromethane ($[MPC]_0$= 1.0 M) was previously dried for 12 h over activated 4 Å molecular sieves under Ar atmosphere. This solution was added *via* cannula to a Schlenk flask charged with MPC (23 mol for PEG_{45}-OH, 30 mol for PEG_{113}-OH) under Ar atmosphere. The reaction was stirred at 35 °C for 8 h, then concentrated under vacuum. PEG_{113}-*b*-$PC(P)_{23}$ was precipitated in cold diethyl ether and isolated as a white power by vacuum filtration. PEG_{45}-*b*-$PC(P)_{18}$, which was soluble in cold diethyl ether, was isolated by silica column chromatography using dichloromethane/ethyl acetate (8/2) as eluent. e.g. PEG_{113}-*b*-$PC(P)_{23}$: FTIR (KBr, υ_{max}/cm^{-1}): 3471 (O-H^{st}), 3290 (Csp-H^{st}), 2887 (Csp^3-H^{st}), 2130 (Csp-Cspst), 1754 (C=Ost). ^1H NMR (400 MHz, $CDCl_3$, δ, ppm]: 4.66 (d, *J* = 2.4 Hz), 4.34 – 4.15 (m), 3.79 – 3.36 (m), 3.31 (s), 2.48 (t, *J* = 2.4 Hz), 1.22 (s). SEC data: PEG_{113}-*b*-$PC(P)_{23}$ M_n = 9460, $Đ$ = 1.06 PEG_{45}-*b*-$PC(P)_{18}$ M_n = 6810, $Đ$ = 1.08.

3.9.3 General procedure for the side chain functionalisation by CuAAC

A Schlenk flask charged with the azide N_3-Azo or N_3-AzoOMe (2 mol), the propargyl functionalised copolymer PEG_n-*b*-PC_m (1 mol of propargyl group), CuBr (0.3 mol) and PMDETA (0.3 mol) was flushed with Ar. Then, deoxygenated and distilled DMF (5 mL) was added. The reaction was maintained at 40 °C for 5 days. The crude reaction was diluted with dichloromethane and washed three times with distilled water. The organic fraction was dried over $MgSO_4$ and evaporated to dryness. Residual azide was removed by preparative SEC using Biobeds SX-1 and dichloromethane as eluent. Copolymer containing fractions were precipitated into cold diethyl ether and the solid isolated by filtration. Isolated yield 75-80%.

Characterisation data of PEG_n-*b*-$PC(Azo)_m$, e.g. PEG_{113}-*b*-$PC(Azo)_{23}$: FTIR (KBr, υ_{max}/cm^{-1}): 3141 (Csp^2-H^{st}), 2938 (Csp^3-H^{st}), 1763 (C=O^{st}), 1601 (CAr-CAr^{st}), 1499, 1474 (N=N^{st}), 1143 (C-O^{st}). ^{1}H NMR [400 MHz, $CDCl_3$, δ, ppm]: 7.89 – 7.78 (m), 7.64 (s), 7.03 – 6.89 (m), 5.24 (s), 4.44 – 4.17 (m), 4.04 – 3.91 (m), 3.80 – 3.72 (m), 3.70 - 3.58 (s, broad), 3.39 (s), 2.17 – 2.05 (m), 2.01 – 1.70 (m), 1.59 – 1.32 (m), 1.20 (s), 1.10 – 0.97 (m). SEC data: PEG_{113}-*b*-$PC(Azo)_{23}$ M_n = 12400, *Đ* = 1.11 PEG_{45}-*b*-$PC(Azo)_{18}$ M_n = 9530, *Đ* = 1.10.

Characterisation data of PEG_n-*b*-$PC(AzoOMe)_m$, e.g. PEG_{113}-*b*-$PC(AzoOMe)_{23}$: FTIR (KBr, υ_{max}/cm^{-1}): 3142 (Csp^2-H^{st}), 2938 (Csp^3-H^{st}), 2105, 1743 (C=O^{st}), 1598 (CAr-CAr^{st}), 1473 (N=N^{st}), 1240, 1148 (C-O^{st}). ^{1}H NMR [400 MHz, $CDCl_3$, δ, ppm]: 7.65 (s), 7.20 - 7.11 (m), 6.66 - 6.58 (m), 6.18 (s), 5.23 (s), 4.40 - 4.31 (m), 4.30 - 4.18 (m), 4.02 - 3.93 (m), 3.86 - 3.76 (m), 3.68 - 3.57 (s, broad), 3.37 (s), 2.00 - 1.88 (m), 1.86 -1.68 (m), 1.57 - 1.44 (m), 1.44 - 1.32 (m), 1.21 (s). SEC data: PEG_{113}-*b*-$PC(AzoOMe)_{23}$ M_n = 9950, *Đ* = 1.08 PEG_{45}-*b*-$PC(AzoOMe)_{18}$ M_n = 8030, *Đ* = 1.11.

3.9.4 Thermal characterisation

Thermogravimetric analysis (TGA): TGA was performed at 10 °C min^{-1} under nitrogen atmosphere using a TGA Q5000IR from TA Instruments. TGA data were given as the onset of the decomposition curve.

Differential scanning calorimetry (DSC): DSC was performed using a DSC Q2000 from TA Instruments with samples (approx. 3 mg) sealed in aluminium pans at a scanning rate of 10 or 20 °C min^{-1} under a nitrogen atmosphere. Melting temperatures were read at the maximum of the transition peaks, and glass transition temperatures were read at the midpoint of the heat capacity increase.

3.9.5 Preparation and characterisation of self-assemblies

Self-assembly Procedure. Milli-Q® water was gradually added to a solution of the copolymer (5 mg) in spectroscopic grade THF (1 mL) previously filtered through a 0.2 μm polytetrafluoroethylene (PTFE) filter. The self-assembly process was followed by measuring the loss of transmitted light intensity at 650 nm due to scattering as a function of water content. When a constant value of turbidity was reached, the resulting suspension was filtered through a 5 μm cellulose acetate filter and dialyzed against water using a Spectra/Por dialysis membrane (MWCO, 1 kDa) for 2 days to remove THF, changing water 3 times. Water suspensions of the polymeric self-assemblies were diluted with Milli-Q® water to a final concentration 1 mg mL^{-1}.

Determination of the critical aggregation concentration and loading of Nile Red. Critical aggregation concentration (CAC) was determined by fluorescence spectroscopy using Nile Red. 87 μL of a solution of Nile Red in dichloromethane (3.7×10^{-5} M) was added into a vial and the solvent evaporated. Then, 600 μL of the aqueous suspension of the polymeric aggregates with concentrations ranging from 1.0×10^{-4} to 1.0 mg mL^{-1} were added and stirred overnight in orbital shaker. The emission spectrum of Nile Red was registered from 560 to 700 nm while exciting at 550 nm.

Preparation of TEM samples. 10 μL of a 1.0 mg mL^{-1} self-assemblies water dispersion was deposited onto carbon-coated copper grid and the water removed by capillarity using filter paper. The samples were stained with uranyl acetate removing the excess by capillarity using filter paper. The grids were dried overnight under vacuum.

Preparation of Cryo-TEM samples. 3 μL of a 1.0 mg mL^{-1} vesicular water dispersion was placed on a TEM Quantifoil carbon grid, excess of solvent was blotted away with filter paper and the grid freeze-plunged into liquid ethane using a FEI Vitrobot (FEI Company). Samples were maintained under liquid nitrogen with a Gatan TEM cryo-holder (FEI Company).

3.9.6 Irradiation experiments

Irradiation experiments with UV light. Samples, either THF solutions at a concentration of 10^{-4} M (referred to the repetitive azobenzene unit) or aqueous suspensions of self-assemblies at a concentration of 1 mg BC mL^{-1}, were irradiated in a quartz UV cuvette, path length of 10 mm for THF solutions and 1 mm for aqueous suspensions, with a compact low-pressure fluorescent lamp Philips PL-S 9W emitting between 350 and 400 nm. Irradiance in the sample at 365 nm was 3.5 μW cm^{-2}.

Irradiation experiments with visible light. Samples, either THF solutions at a concentration of 10^{-4} M (referred to the repetitive azobenzene unit) or aqueous suspensions of self-assemblies at a concentration of 1 mg mL^{-1}, were irradiated in a quartz UV cuvette, path length of 10 mm for THF solutions and 1 mm for aqueous suspensions, with green (530 nm) or red light (625 nm) using a Mightex LCS-0530-15-22 or a Mightex LCS-0625-07-22 high power LED respectively. Irradiance in the sample at 530 or 625 nm was 30 μW cm^{-2}.

3.9.7 Encapsulation and light-stimulated release of Rhodamine B

Encapsulation of Rhodamine B. Rhodamine B loaded vesicles were prepared as described in **3.9.5 Self-assembly procedure** by adding a solution of Rhodamine B in water (the concentration was adjusted to have a final feed stock of 5 molecules of Rhodamine B per molecule of block copolymer) to a solution of the copolymer (5 mg) in spectroscopic grade THF (1 mL). Non-encapsulated Rhodamine B was removed during dialysis.

Rhodamine B concentration was determined by high performance liquid chromatography (HPLC) using a Waters 600 controller pump system with a mixture acetonitrile/100 mM ammonium acetate in water (8:2) as the mobile phase at a 1 mL min^{-1} flow rate, a column Waters Spherisorb 5µm C8 (4.6 × 250 mm, particle size 5 µm and pore size 80 Å) as stationary phase and a Waters 2998 PDA detector at 550 nm. Rhodamine B loaded self-assemblies water suspensions (250 µL) were diluted with acetonitrile (250 µL), sonicated for 10 min and injected into the HPLC system.

Light stimulated release of Rhodamine B. 0.6 mL aliquots of Rhodamine B loaded vesicular suspensions were placed in a glass vial and irradiated as described in **3.9.6 Irradiation experiments**. Aliquots where then placed into a Slide-A-Lyzer™ 2K MWCO and 0.5 mL Dialysis Cassettes, dialysed against fresh Milli-Q water and the fluorescence of the dialysis water measured at different times.

3.10 References

(1) Roche, A.; García-Juan, H.; Royes, J.; Oriol, L.; Piñol, M.; Audia, B.; Pagliusi, P.; Provenzano, C.; Cipparrone, G. Tuning the Thermal Properties of Azopolymers Synthesized by Post-Functionalization of Poly(Propargyl Methacrylate) with Azobenzene Azides: Influence on the Generation of Linear and Circular Birefringences. *Macromol. Chem. Phys.* **2018**, *219*, 1800318. https://doi.org/10.1002/macp.201800318.

(2) Rufino, T. do C.; Felisberti, M. I. Confined PEO Crystallisation in Immiscible PEO/PLLA Blends. *RSC Adv.* **2016**, *6*, 30937–30950. https://doi.org/10.1039/C6RA02406H.

(3) Chen, W.; Meng, F.; Cheng, R.; Zhong, Z. PH-Sensitive Degradable Polymersomes for Triggered Release of Anticancer Drugs: A Comparative Study with Micelles. *J. Controlled Release* **2010**, *142*, 40–46. https://doi.org/10.1016/j.jconrel.2009.09.023.

(4) Owen, S. C.; Chan, D. P. Y.; Shoichet, M. S. Polymeric Micelle Stability. *Nano Today* **2012**, *7*, 53–65. https://doi.org/10.1016/j.nantod.2012.01.002.

(5) Blasco, E.; Barrio, J. del; Sánchez-Somolinos, C.; Piñol, M.; Oriol, L. Light Induced Molecular Release from Vesicles Based on Amphiphilic Linear-Dendritic Block Copolymers. *Polym. Chem.* **2013**, *4*, 2246. https://doi.org/10.1039/c2py21025h.

(6) Tejedor, R. M.; Serrano, J.-L.; Oriol, L. Photocontrol of Supramolecular Architecture in Azopolymers: Achiral and Chiral Aggregation. *Eur. Polym. J.* **2009**, *45*, 2564–2571. https://doi.org/10.1016/j.eurpolymj.2009.05.010.

(7) Menzel, H.; Weichart, B.; Schmidt, A.; Paul, S.; Knoll, W.; Stumpe, J.; Fischer, T. Small-Angle X-Ray Scattering and Ultraviolet-Visible Spectroscopy Studies on the Structure and Structural Changes in Langmuir-Blodgett Films of Polyglutamates with Azobenzene Moieties Tethered by Alkyl Spacers of Different Length. *Langmuir* **1994**, *10*, 1926–1933. https://doi.org/10.1021/la00018a052.

(8) Blasco, E.; Schmidt, B. V. K. J.; Barner-Kowollik, C.; Piñol, M.; Oriol, L. Dual Thermo- and Photo-Responsive Micelles Based on Miktoarm Star Polymers. *Polym. Chem.* **2013**, *4*, 4506. https://doi.org/10.1039/c3py00576c.

(9) Blasco, E.; Serrano, J. L.; Piñol, M.; Oriol, L. Light Responsive Vesicles Based on Linear–Dendritic Block Copolymers Using Azobenzene–Aliphatic Codendrons. *Macromolecules* **2013**, *46*, 5951–5960. https://doi.org/10.1021/ma4009725.

(10) Beharry, A. A.; Sadovski, O.; Woolley, G. A. Azobenzene Photoswitching without Ultraviolet Light. *J. Am. Chem. Soc.* **2011**, *133*, 19684–19687. https://doi.org/10.1021/ja209239m.

(11) Dong, M.; Babalhavaeji, A.; Samanta, S.; Beharry, A. A.; Woolley, G. A. Red-Shifting Azobenzene Photoswitches for in Vivo Use. *Acc. Chem. Res.* **2015**, *48*, 2662–2670. https://doi.org/10.1021/acs.accounts.5b00270.

(12) Li, X.; Fang, L.; Hou, L.; Zhu, L.; Zhang, Y.; Zhang, B.; Zhang, H. Photoresponsive Side chain Liquid Crystalline Polymers with Amide Group-Substituted Azobenzene Mesogens: Effects of Hydrogen Bonding, Flexible Spacers, and Terminal Tails. *Soft Matter* **2012**, *8*, 5532. https://doi.org/10.1039/c2sm25163a.

(13) Wang, G.; Yuan, D.; Yuan, T.; Dong, J.; Feng, N.; Han, G. A Visible Light Responsive Azobenzene-Functionalized Polymer: Synthesis, Self-Assembly, and Photoresponsive Properties. *J. Polym. Sci. Part A Polym. Chem.* **2015**, *53*, 2768–2775. https://doi.org/10.1002/pola.27747.

(14) Wang, G.; Wang, X. A Novel Hyperbranched Polyester Functionalized with Azo Chromophore: Synthesis and Photoresponsive Properties. *Polym. Bull.* **2002**, *49*, 1–8. https://doi.org/10.1007/so0289-002-0073-4.

(15) Concellón, A.; Blasco, E.; Martínez-Felipe, A.; Martínez, J. C.; Šics, I.; Ezquerra, T. A.; Nogales, A.; Piñol, M.; Oriol, L. Light-Responsive Self-Assembled Materials by Supramolecular Post-Functionalization via Hydrogen Bonding of Amphiphilic Block Copolymers. *Macromolecules* **2016**, *49*, 7825–7836. https://doi.org/10.1021/acs.macromol.6b01112.

(16) Blasco, E.; Barrio, J. del; Piñol, M.; Oriol, L.; Berges, C.; Sánchez, C.; Alcalá, R. Azobenzene-Containing Linear–Dendritic Block Copolymers Prepared by Sequential ATRP and Click Chemistry. *Polymer* **2012**, *53*, 4604–4613. https://doi.org/10.1016/j.polymer.2012.08.022.

CHAPTER 4

NANOCARRIERS BASED ON AMPHIPHILIC BCs WITH AZOBENZENE UNITS AND ALIPHATIC CHAINS

4.1 Introduction and aims

Amongst different morphologies self-assembled from amphiphilic BCs, polymer vesicles are versatile nanocarriers candidates as they offer the possibility to encapsulate either hydrophilic compounds in their aqueous cavities or the insertion of hydrophobic compounds in their membranes but also the simultaneous encapsulation of both. In **Chapter 3**, it has been demonstrated the subtle influence of the hydrophobic/hydrophilic balance and the decisive influence of the hydrophilic block length on the self-assemblies morphology. Thus, it was established that the formation of vesicles over micelles was favoured by shortening the length of the hydrophilic PEG block. Besides, the tetra-*ortho*-methoxy substituted azobenzenes unit was successfully used to fabricate light-responsive systems for which release of payloads can be stimulated by using visible light.

Former studies on UV-responsive vesicles from amphiphilic LDBCs showed that it is possible to adjust the payload release profile if the azobenzene units located at the hydrophobic block were partially substituted by long aliphatic chains. Decreasing the number of photoactive moieties accelerated the *trans-cis* isomerization at the inner membrane probably by frustrating the aggregation tendency of azobenzenes and providing higher mobility. Therefore, even if a minimum percentage of azobenzene units was required to maintain the light responsiveness of the polymeric vesicles, the release rate was remarkably increased by decreasing the azobenzene/aliphatic chain ratio at the periphery of the dendron.

The objective of this chapter was to modulate the light responsiveness of the vesicles containing tetra-*ortho*-methoxy substituted azobenzenes by using monomers containing long alkyl chains to dilute the azo content on the hydrophobic block of the nanocarriers. The BC **PEG$_{45}$-*b*-PC(AzoOMe)$_{18}$** reported in **Chapter 3** was taken as reference for the incorporation of alkyl chains to have hydrophobic polycarbonate blocks with azobenzene/aliphatic chain in 75:25, 50:50 or 25:75 molar ratios. Again, to stablish a direct comparison, corresponding polymers from **PEG$_{45}$-*b*-PC(Azo)$_{18}$** with the 4-isobutyloxy-4'oxoazobenzene used for the proof-of-concept in previous works were also synthesised.

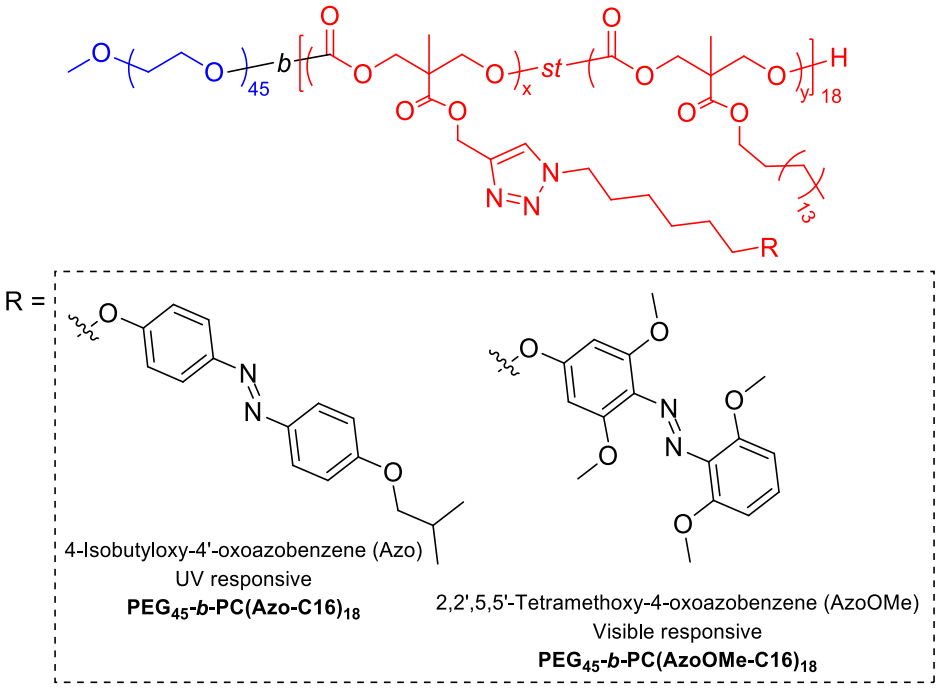

Figure 4.1: Structure of the amphiphilic diblock copolymers studied in this chapter.

According to the objective, the main tasks carried out in this chapter were:

- Synthesis and chemical characterisation of the polymer precursors with side chain propargyloxy groups and aliphatic chains.
- Synthesis of the light-responsive amphiphilic diblock copolymers *via* CuAAC.
- Study of the self-assembly in water of the amphiphilic diblock copolymers and characterisation of the self-assembled structures.
- Study of the response to light irradiation of the amphiphilic diblock copolymers in solution and of the self-assemblies.
- Encapsulation of small fluorescent probes and study of the light stimulated release.

4.2 Synthesis and characterisation of the diblock copolymers

The synthesis of the amphiphilic BCs was addressed by sequential organocatalysed ring opening polymerisation (ROP) and post-functionalisation by Cu(I)-catalysed alkyne-azide cycloaddition (CuAAC) in a similar way to that used in **Chapter 3**. The hydrophobic block consisted of two carbonate repeating units statistically distributed formed by polymerising the propargyloxy, **MPC**, and the aliphatic 5-methyl-5-hexadecyloxycarbonyl-1,3-dioxan-2-one (**MCC**) substituted monomers (Figure 4.2). Synthesis of **MCC** was afforded following the same procedure used for the synthesis of **MPC**.

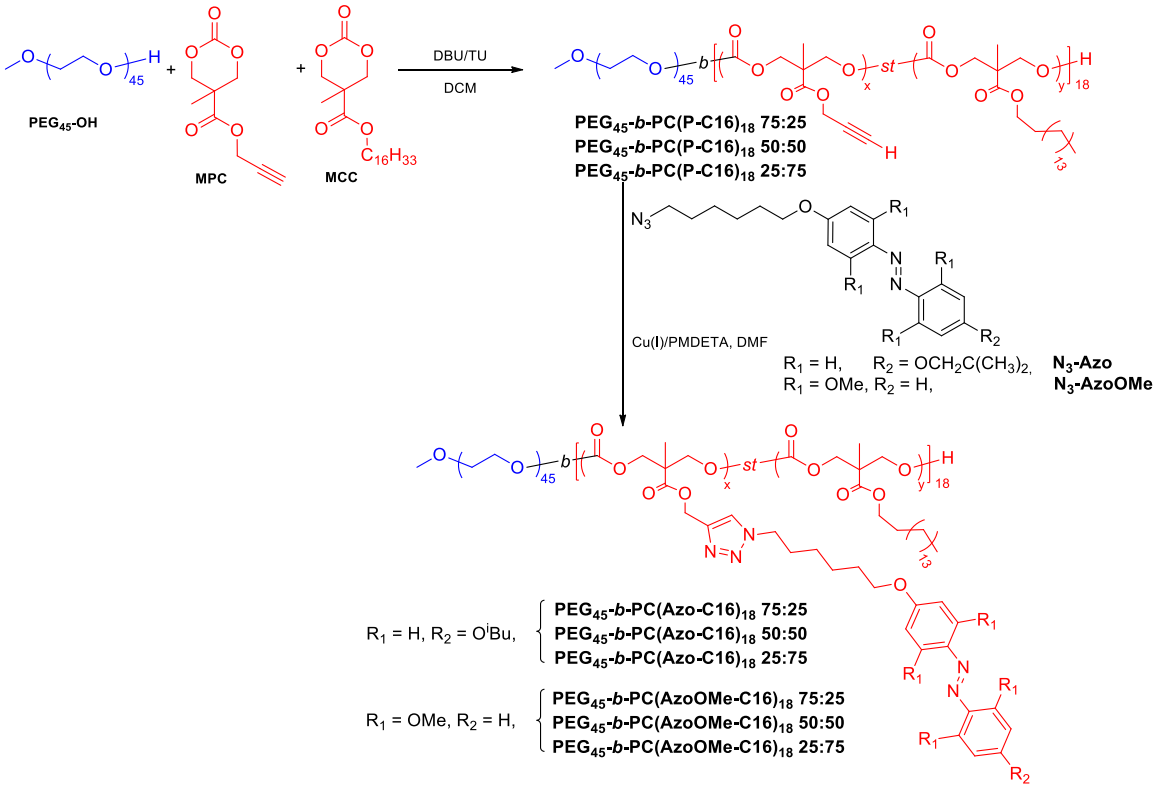

Figure 4.2: Route for the synthesis of the azobenzene-alkoxy co-functionalised amphiphilic BCs.

ROP of **MPC** and **MCC** mixtures was carried out in similar conditions to that reported in **Chapter 3**. ROP was conducted for 8 h in dichloromethane at 40 °C using a mixture of **MPC**/**MCC** in feed molar ratios of 75/25, 50/50 or 25/75. PEG_{45}-OH was used to initiate the polymerisation using a macroinitiator/monomer molar ratio [PEG_{45}-OH]:([**MPC**]+[**MCC**]) = 1:23 to target a polymerisation degree of the polycarbonate block of 18, according to previous results. Copolymerisations

were performed with a relation of ([**MPC**]+[**MCC**]):[TU]:[DBU] = 1:0.05:0.01 and a concentration of ([**MPC**]+[**MCC**]) = 1.0 M. The copolymers were tagged as **PEG$_{45}$-*b*-PC(P-C16)$_{18}$ X/Y**, where **X** and **Y** represent the molar percentage of the polycarbonates repeating units derived from **MPC** and **MCC** respectively.

The progress of copolymerisations was monitored by ^{1}H NMR from the disappearance of the signal corresponding to the methylenic protons in the carbonate rings at δ = 4.71 and 4.22 ppm and the appearance of a signal from the polycarbonate chain (signals *c* and *c'*) at around 4.25 ppm (see Figure 4.3, Figure 4.4 and Figure 4.5). The inclusion of both monomers in the polycarbonate block was confirmed by the presence of signals from both repeating units, *e* at 4.72 ppm for the methylenic protons of the propargylic radical from **MPC**, and *g* at 4.10 ppm for the methylenic protons close to the ester group for the alkoxy radical from **MCC** (Figure 4.3, Figure 4.4 and Figure 4.5). The polymerisation degree of the polycarbonate blocks was calculated by ^{1}H NMR end group analysis by comparison of the signal corresponding to the terminal methoxy group from the PEG block, *a*, at 3.31 ppm and the signals from the polycarbonate block, *c* and *c'* (Figure 4.3, Figure 4.4 and Figure 4.5). Monomers were incorporated to the polycarbonate block in approximately the same relation than the molar proportion between **MCC** and **MPC** introduced in the polymerisations (Table 4.1).

Polymerisation degree of the polycarbonate block was found to be 18 for all copolymers, the same than the reported previously in **Chapter 3** for **PEG$_{45}$-*b*-PC(P)$_{18}$**. SEC analysis revealed monomodal narrow distributions (Figure 4.6, Figure 4.7 and Figure 4.8), *Đ* values are sumarized in Table 4.1.

Table 4.1: Characterisation of propargyloxy functionalised copolymers.

Polymer	Theoretical MPC:MCC [1]	Final MPC:MCC [2]	M_n [3]	M_n [4]	$Đ$ [4]
PEG_{45}-*b*-PC(P-C16)$_{18}$ 75/25	75:25	73:27	6504	7742	1.07
PEG_{45}-*b*-PC(P-C16)$_{18}$ 50/50	50:50	47:53	7254	8379	1.06
PEG_{45}-*b*-PC(P-C16)$_{18}$ 25/75	25:75	28:72	8003	8818	1.06

[1] Fed molar relation of the monomers, **MPC** and **MCC**. [2] Incorporated molar relation of monomers **MPC** and **MCC** estimated by relative integration of the signals from the methylenic protons close to the polycarbonate block (*e* and *g*, Figure 4.3, Figure 4.4 and Figure 4.5). [3] Molar mass (g mol^{-1}) calculated by ^{1}H NMR end group analysis assuming for the PEG segment a 2000 g mol^{-1} molar mass. [4] M_n and $Đ$ calculated by SEC using PMMA standards and ELSD detector.

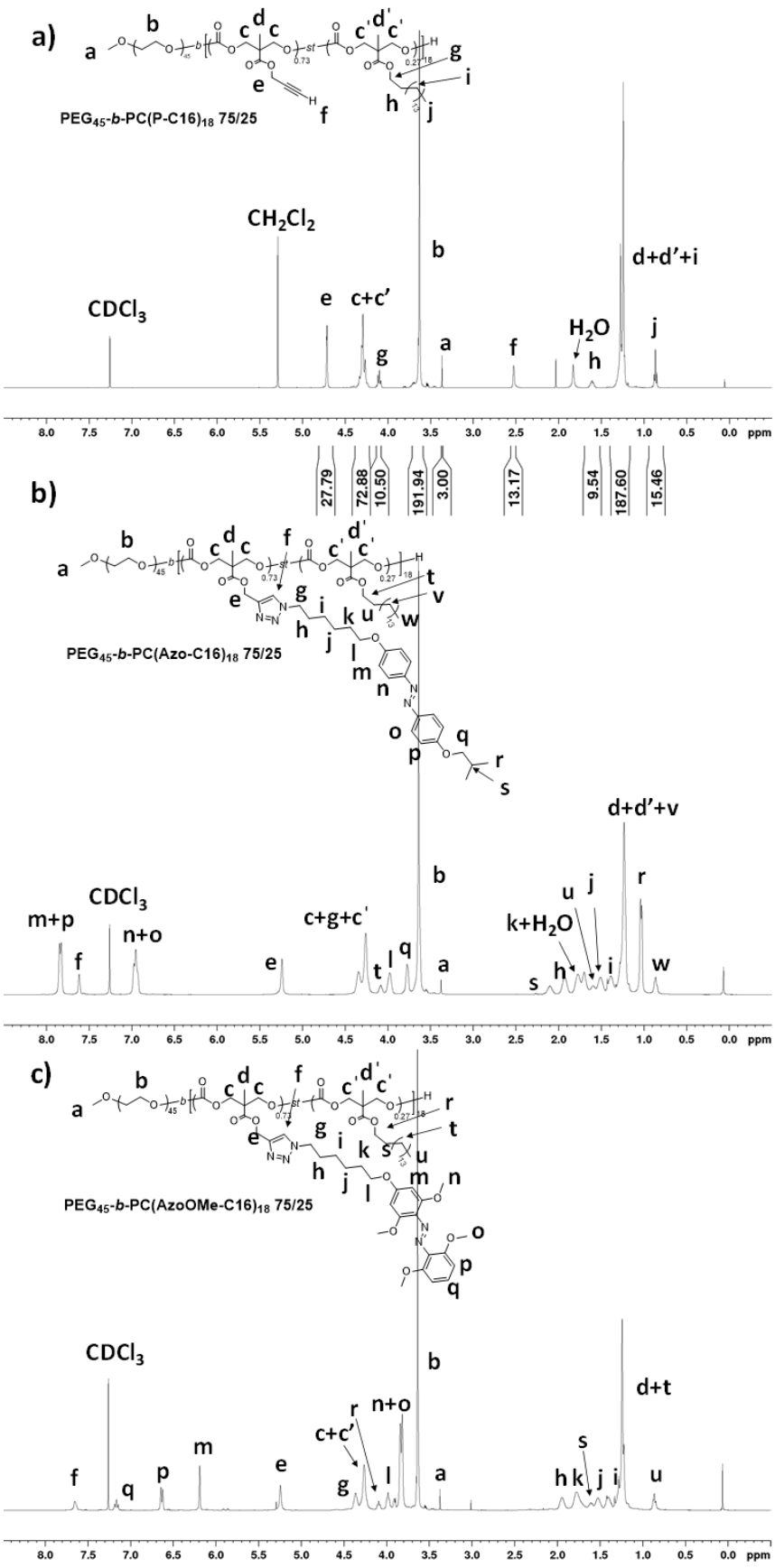

Figure 4.3: ^{1}H NMR (400 MHz, $CDCl_3$) spectra of **PEG$_{45}$-*b*-PC(P-C16)$_{18}$ 75/25** (a), **PEG$_{45}$-*b*-PC(Azo-C16)$_{18}$ 75/25** (b) and **PEG$_{45}$-*b*-PC(AzoOMe-C16)$_{18}$ 75/25** (c).

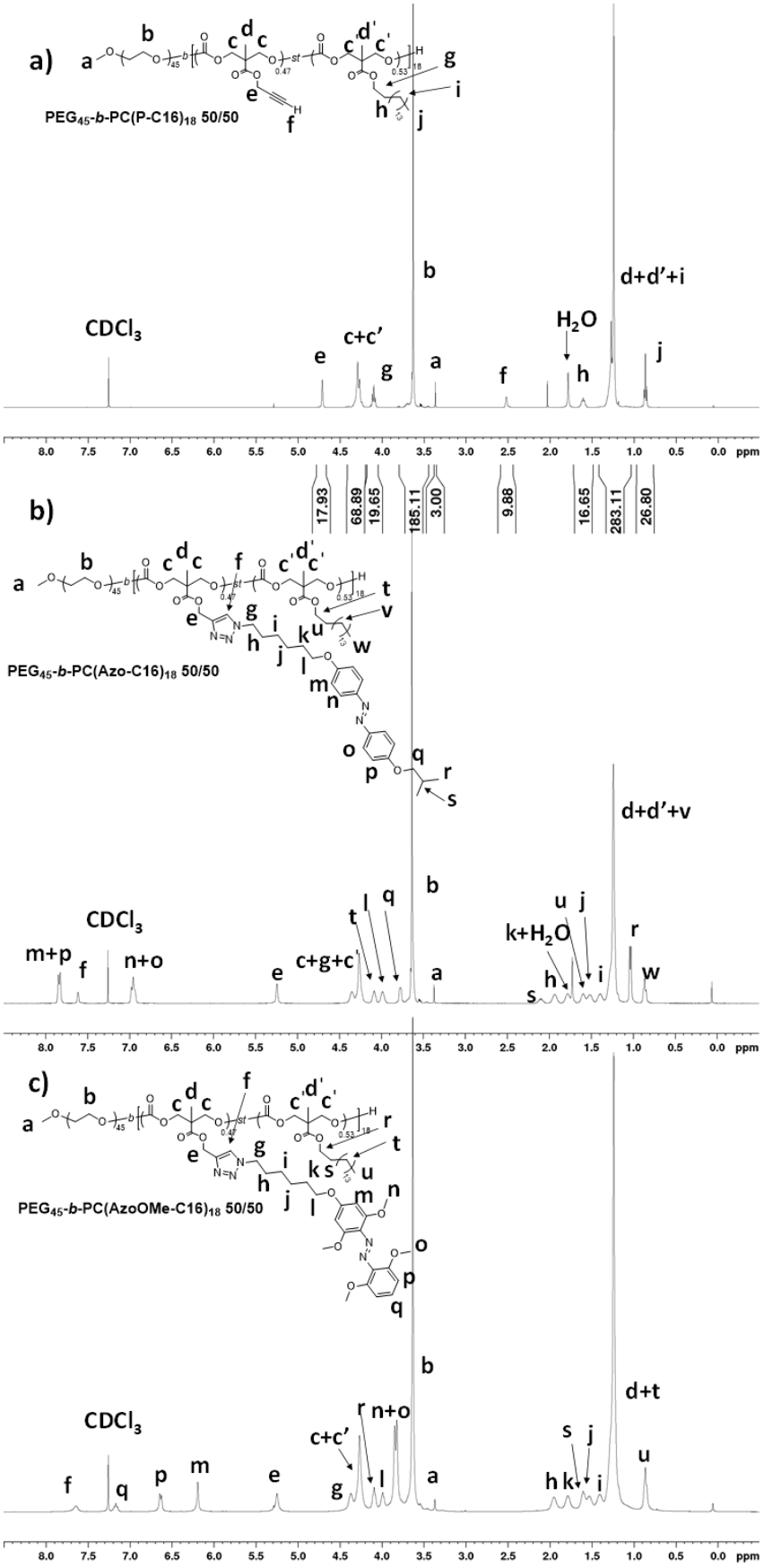

Figure 4.4: ^{1}H NMR (400 MHz, $CDCl_3$) spectra of **PEG_{45}-*b*-PC(P-C16)$_{18}$ 50/50** (a), **PEG_{45}-*b*-PC(Azo-C16)$_{18}$ 50/50** (b) and **PEG_{45}-*b*-PC(AzoOMe-C16)$_{18}$ 50/50** (c).

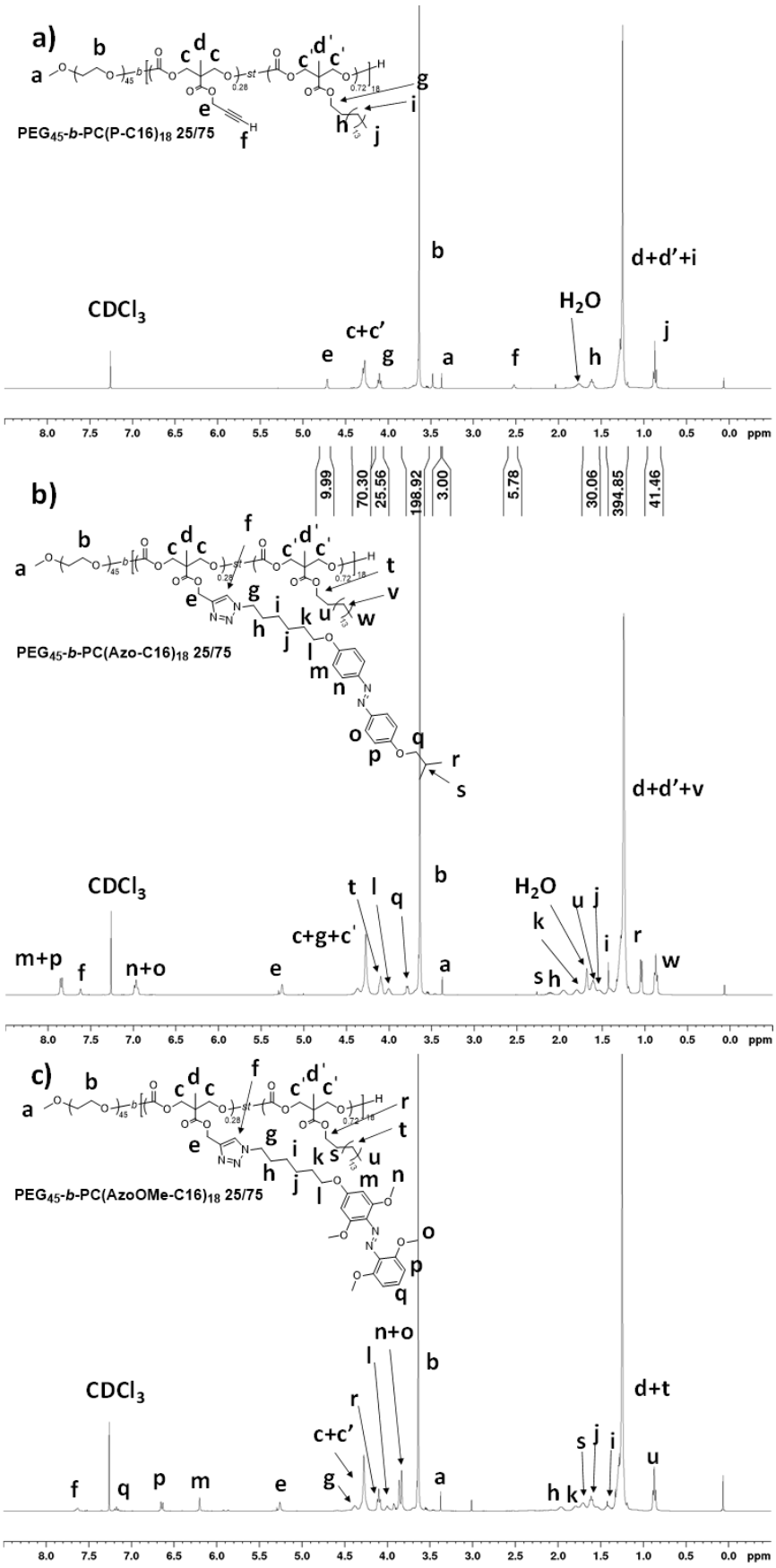

Figure 4.5: ^{1}H NMR (400 MHz, $CDCl_3$) spectra of **PEG_{45}-*b*-PC(P-C16)$_{18}$ 25/75** (a), **PEG_{45}-*b*-PC(Azo-C16)$_{18}$ 25/75** (b) and **PEG_{45}-*b*-PC(AzoOMe-C16)$_{18}$ 25/75** (c).

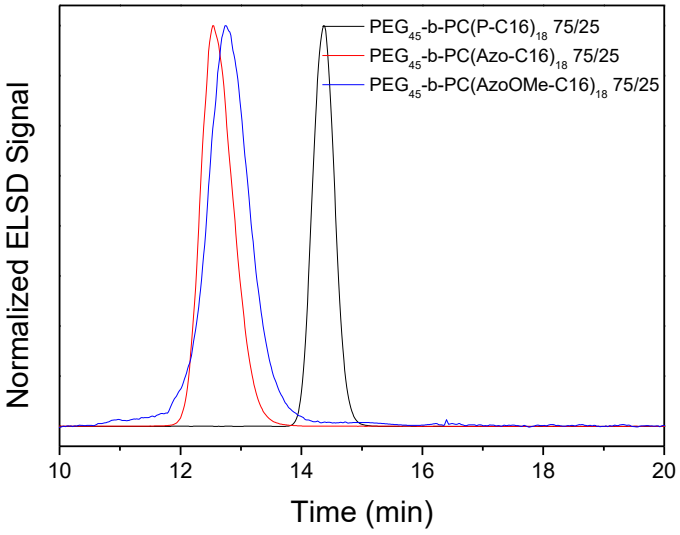

Figure 4.6: SEC traces from **PEG$_{45}$-*b*-PC(P-C16)$_{18}$ 75/25**, **PEG$_{45}$-*b*-PC(Azo-C16)$_{18}$ 75/25** and **PEG$_{45}$-*b*-PC(AzoOMe-C16)$_{18}$ 75/25**.

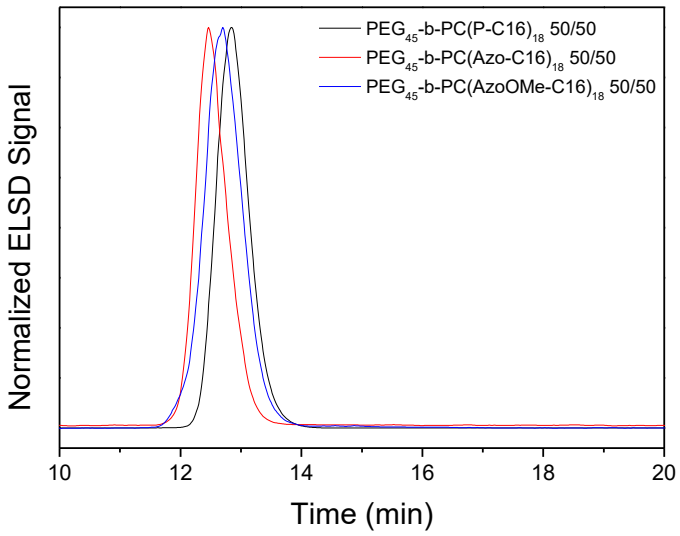

Figure 4.7: SEC traces from **PEG$_{45}$-*b*-PC(P-C16)$_{18}$ 50/50**, **PEG$_{45}$-*b*-PC(Azo-C16)$_{18}$ 50/50** and **PEG$_{45}$-*b*-PC(AzoOMe-C16)$_{18}$ 50/50**.

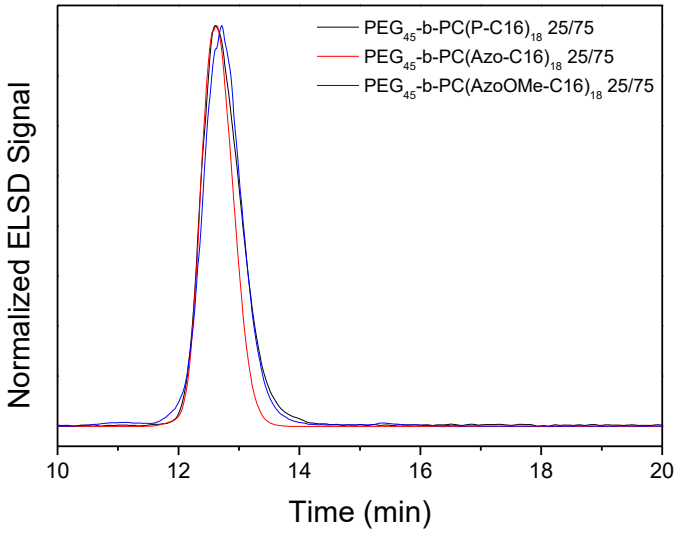

Figure 4.8 SEC traces from **PEG$_{45}$-*b*-PC(P-C16)$_{18}$ 25/75**, **PEG$_{45}$-*b*-PC(Azo-C16)$_{18}$ 25/75** and **PEG$_{45}$-*b*-PC(AzoOMe-C16)$_{18}$ 25/75**.

The introduction of the light-responsive units was accomplished *via* CuAAC between the pendant propargyloxy radicals of the polymeric backbone and the azobenzene azides **N$_3$-Azo** or **N$_3$-AzoOMe**, using the catalytic system CuBr/PMDETA (Figure 4.2). The copolymers with Azo unit were tagged as **PEG$_{45}$-*b*-PC(Azo-C16)$_{18}$ X/Y** whereas those with AzoOMe unit as **PEG$_{45}$-*b*-PC(AzoOMe-C16)$_{18}$ X/Y**. Introduction of the light-responsive units was confirmed by ^{1}H NMR by the appearance of a new signal corresponding to the triazole ring, at 7.65 ppm, and the disappearance of the signal from the alkynyl protons, at 2.48 ppm (Figure 4.3, Figure 4.4 and Figure 4.5). According to FTIR technique, and taking into account its sensitivity, a complete functionalisation of the polymeric backbone was achieved as deduced from the disappearance of the disappearance of the Csp–Hst and Csp–Cspst bands at 3300 cm^{-1} and 2100 cm^{-1} (Figure 4.9, Figure 4.10 and Figure 4.11). As expected from the increase in the molar mass, SEC traces were shifted to lower retentions times. For the light-responsive copolymers derived from **PEG$_{45}$-*b*-PC(P-C16)$_{18}$ 75/25** a slight increase in $Đ$ was detected while no appreciable changes in $Đ$ were detected for the copolymers derived from **PEG$_{45}$-*b*-PC(P-C16)$_{18}$ 50/50** and **PEG$_{45}$-*b*-PC(P-C16)$_{18}$ 25/75** (Figure 4.6, Figure 4.7 and Figure 4.8). Hydrophobic polycarbonates block mass contents are comprised between 74 and 83% (Table 4.2).

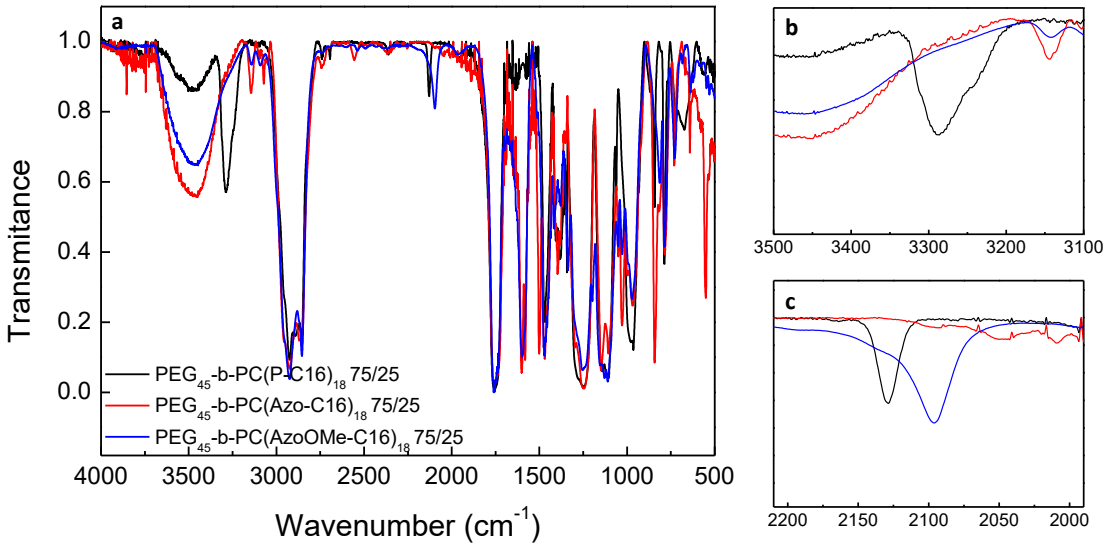

Figure 4.9: **PEG$_{45}$-*b*-PC(P-C16)$_{18}$ 75/25**, **PEG$_{45}$-*b*-PC(Azo-C16)$_{18}$ 75/25** and **PEG$_{45}$-*b*-PC(AzoOMe-C16)$_{18}$ 75/25** FTIR spectrum (KBr disk) (a), and zoom to Csp-H zone (b) and Csp-Csp zone (c).

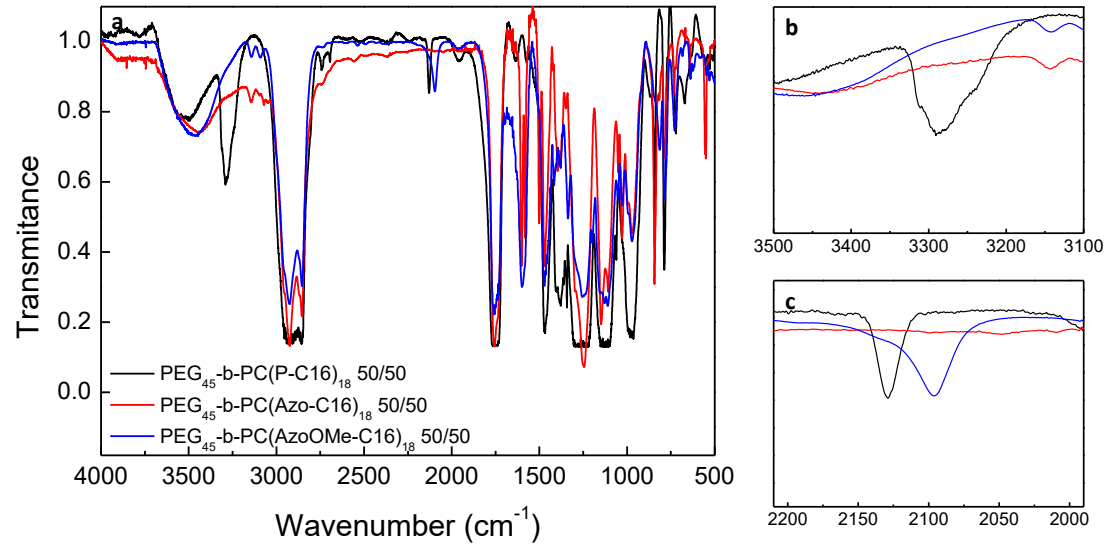

Figure 4.10: **PEG$_{45}$-*b*-PC(P-C16)$_{18}$ 50/50**, **PEG$_{45}$-*b*-PC(Azo-C16)$_{18}$ 50/50** and **PEG$_{45}$-*b*-PC(AzoOMe-C16)$_{18}$ 50/50** FTIR spectrum (KBr disk) (a), and zoom to Csp-H zone (b) and Csp-Csp zone (c).

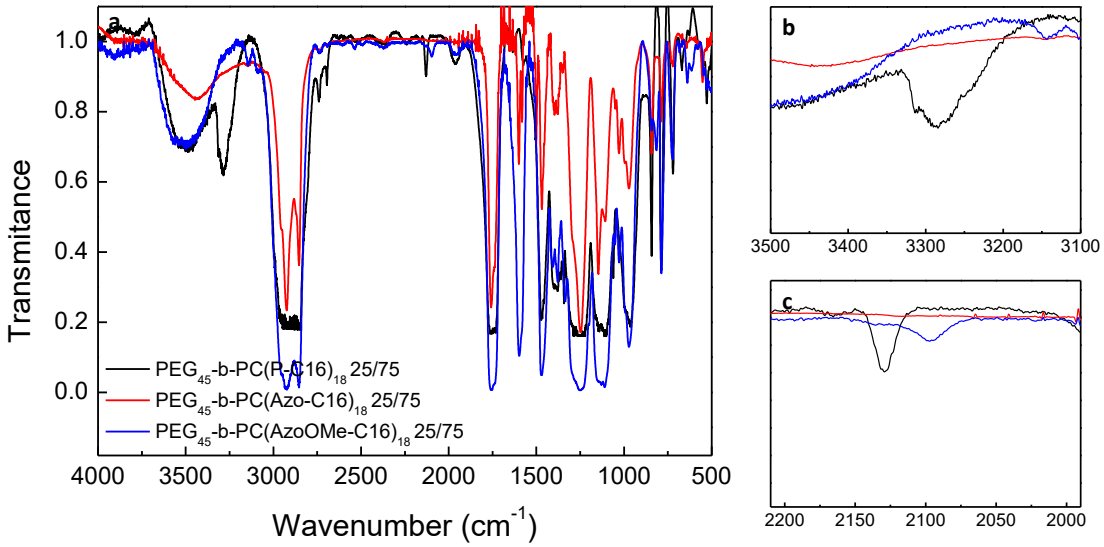

Figure 4.11: **PEG$_{45}$-*b*-PC(P-C16)$_{18}$ 25/75**, **PEG$_{45}$-*b*-PC(Azo-C16)$_{18}$ 25/75** and **PEG$_{45}$-*b*-PC(AzoOMe-C16)$_{18}$ 25/75** FTIR spectrum (KBr disk) (a), and zoom to Csp-H zone (b) and Csp-Csp zone (c).

4.3 Thermal characterisation

Thermal stability of the diblock copolymers was evaluated by TGA (Figure 4.12) and data are collected in Table 4.2. Copolymers presented good stability, with decomposition temperatures above 230 °C, higher than the equivalent copolymers without aliphatic chains in the side chain of the hydrophobic block.

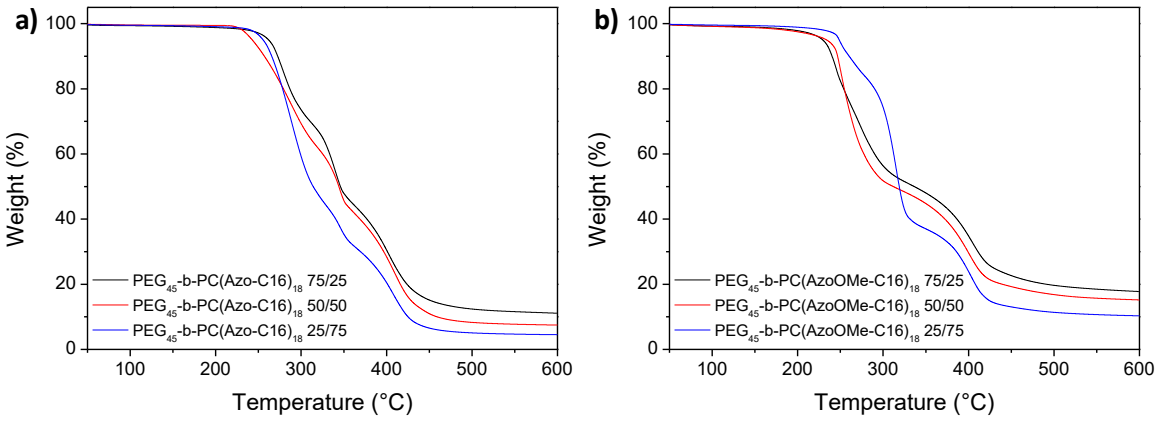

Figure 4.12: TGA curves registered at 10 °C min^{-1} heating rate under nitrogen atmosphere.

Thermal properties were determined by DSC from -50 °C to 120 °C at a rate of 10 °C/min. To have a common thermal history, thermal transitions were registered during the second heating scans and are summarized in Table 4.2. DSC curves of **PEG_{45}-*b*-PC(Azo-C16)$_{18}$** and **PEG_{45}-*b*-PC(AzoOMe-C16)$_{18}$** series are collected in Figure 4.13 and Figure 4.14. As it was observed in **Chapter 3**, in no case were transitions associated with the PEG block observed, neither T_g nor T_m. In particular, this confirms that crystallisation of PEG is restricted when low molecular mass PEG blocks are incorporated. Therefore, only transitions corresponding to the polycarbonate block were registered.

Table 4.2: Thermal stability and transition temperatures of azobenzene block copolymers.

Polymer	Hydrophobic content (wt %) [1]	TGA (°C) [2]	T_g (°C) [3]	T_m (°C) [ΔH_m (J g^{-1})] [4]	T_{M-I} (°C) [ΔH_{M-I} (J g^{-1})] [5]
PEG_{45}-*b*-PC(Azo)$_{18}$	84	195	31	63 [12.9]	73 [4.5]
PEG_{45}-*b*-PC(Azo-C16)$_{18}$ 75:25	82	261	17	48[3.1][6]	63 [11.2][6]
PEG_{45}-*b*-PC(Azo-C16)$_{18}$50:50	78	231	-	21, 29 [24.2][7]	57 [1.0]
PEG_{45}-*b*-PC(Azo-C16)$_{18}$25:75	74	258	-	18 [19.1], 31 [7.2]	-
PEG_{45}-*b*-PC(AzoOMe)$_{18}$	85	185	39	-	-
PEG_{45}-*b*-PC(AzoOMe-C16)$_{18}$75:25	83	231	22	-	-
PEG_{45}-*b*-PC(AzoOMe-C16)$_{18}$50:50	79	241	-1	-	-
PEG_{45}-*b*-PC(AzoOMe-C16)$_{18}$25:75	75	241	-	20 [19.6]	-

[1] Hydrophobic weight content in %. [2] Decomposition temperature determined by TGA given in °C at the onset of the weight loss curve. [3] Glass transition temperature (T_g) of the azobenzene polycarbonate determined by DSC during the second heating scan at 10 °C min^{-1}. [4] Melting temperature (T_m) and associated melting enthalpy (ΔH_m) determined by DSC during the second heating scan at 10 °C min^{-1}. [5] Mesophase-to-isotropic liquid transition temperature (T_{M-I}) and associated enthalpy (ΔH_{M-I}) calculated from the second heating scan at 10 °C min^{-1}. [6] Cold crystallisation and recrystallisation processes at 33 °C (-6.5 J g^{-1}) and 54 °C (-6.4 J g^{-1}). [7] Overlapped peaks.

The DSC curve of polymer **PEG_{45}-*b*-PC(AzoOMe)$_{18}$** shows only a T_g at 39 °C indicating the amorphous character of the azobenzene polycarbonate (Figure 4.13). Upon incorporating aliphatic chains, the T_g weakened and appeared at lower temperatures, 22 °C and -1 °C for **PEG_{45}-*b*-PC(AzoOMe-C16)$_{18}$ 75:25** and **PEG_{45}-*b*-PC(AzoOMe-C16)$_{18}$ 50:50**, respectively. Not T_g was observed for **PEG_{45}-*b*-PC(AzoOMe-C16)$_{18}$ 25:75**, instead an endothermic peak was registered at 20 °C. This melting transition, T_m, can be attributed to the crystallisation of the long flexible hexadecyloxy side chains.[1] In fact, BCs of PEG and a bis-MPA based polycarbonates with decadecyloxy have been described as crystalline with melting temperatures just above 50 °C, depending on the length of the polycarbonate block.[2]

As described in **Chapter 3**, **PEG_{45}-*b*-PC(Azo)$_{18}$** is a liquid crystalline BC that exhibits a T_g at 31 °C and a liquid crystal phase between 63 °C, T_m, and 73 °C, T_{M-I}. The influence of the aliphatic chains on the thermal properties can be rationalized in the same terms as above. Transition temperatures, T_g, T_m and T_{M-I}, are lowered being the decrease more remarkable on T_m (Figure 4.14). Besides, the development of

liquid crystallinity is restricted for the highest contents of aliphatic chains and the degree of crystallinity increases due to crystallisation of the side chains.

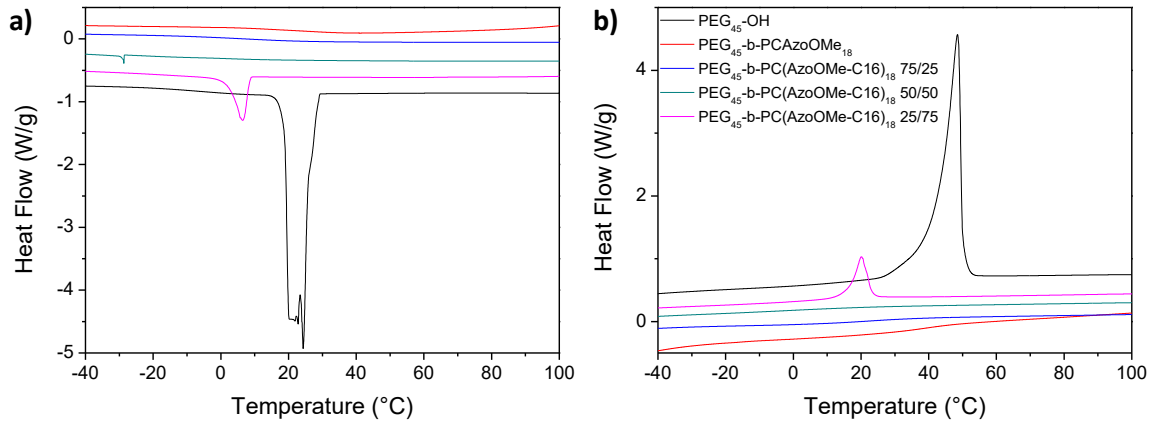

Figure 4.13: DSC curves registered on cooling (a) and subsequent heating (b) at a 10 °C min^{-1} scanning rate of PEG_{45}-OH, **PEG_{45}-*b*-PC(AzoOMe)$_{18}$** and **PEG_{45}-*b*-PC(AzoOMe-C16)$_{18}$**.series.

.

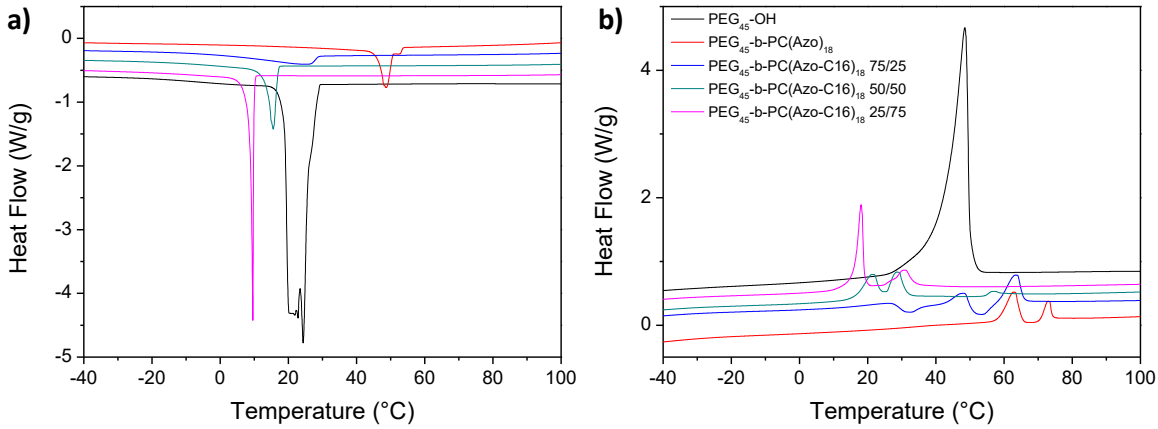

Figure 4.14: DSC curves registered on cooling (a) and subsequent heating (b) at a 10 °C min^{-1} scanning rate of PEG_{45}-OH, **PEG_{45}-*b*-PC(Azo)$_{18}$** and **PEG_{45}-*b*-PC(Azo-C16)$_{18}$**.series.

4.4 Self-Assembly in water and morphological analysis

Self-assembled structures from **PEG$_{45}$-*b*-PC(Azo-C16)$_{18}$** and **PEG$_{45}$-*b*-PC(AzoOMe-C16)$_{18}$** series were prepared by the co-solvent method using the pair THF/water. Morphology and size of the self-assemblies was determined by transmission electron cryomicroscopy (Cryo-TEM) and dynamic light scattering (DLS).

Cryo-TEM images revealed the formation of well-defined vesicular structures with sizes between 100 and 400 nm for the BCs of **PEG$_{45}$-*b*-PC(Azo-C16)$_{18}$** series (Figure 4.15). A homogeneous and smooth membrane was observed with a thickness of approximately 15 nm in all cases, fitting with previously reported thickness of typical bilayer arrangements in polymeric vesicles.[3] The fact that all copolymers have the same membrane thickness could be expected as it is dependent on the length of the hydrophobic block.[4] Average hydrodynamic diameters, D_h, were determined by DLS measurements, obtaining values ranging from 130 to 300 nm (Figure 4.15a). Critical aggregation concentration (CAC) for **75/25**, **50/50** and **25/75** relations were found to be 34, 21 and 14 μg mL^{-1} respectively (Figure 4.16), while the CAC for **PEG$_{45}$-*b*-PC(Azo)$_{18}$** was 32 μg mL^{-1}. The decrease of the CAC, associated to an increase of the thermodynamic stability of the resulting self-assemblies, can be correlated with an enhancement of the hydrophobic interactions on increasing the number of aliphatic chains at the polycarbonate block. Therefore, even if the calculated mass fraction of the hydrophobic block decreases, its hydrophobic character increases and leads to a lower CAC.[5]

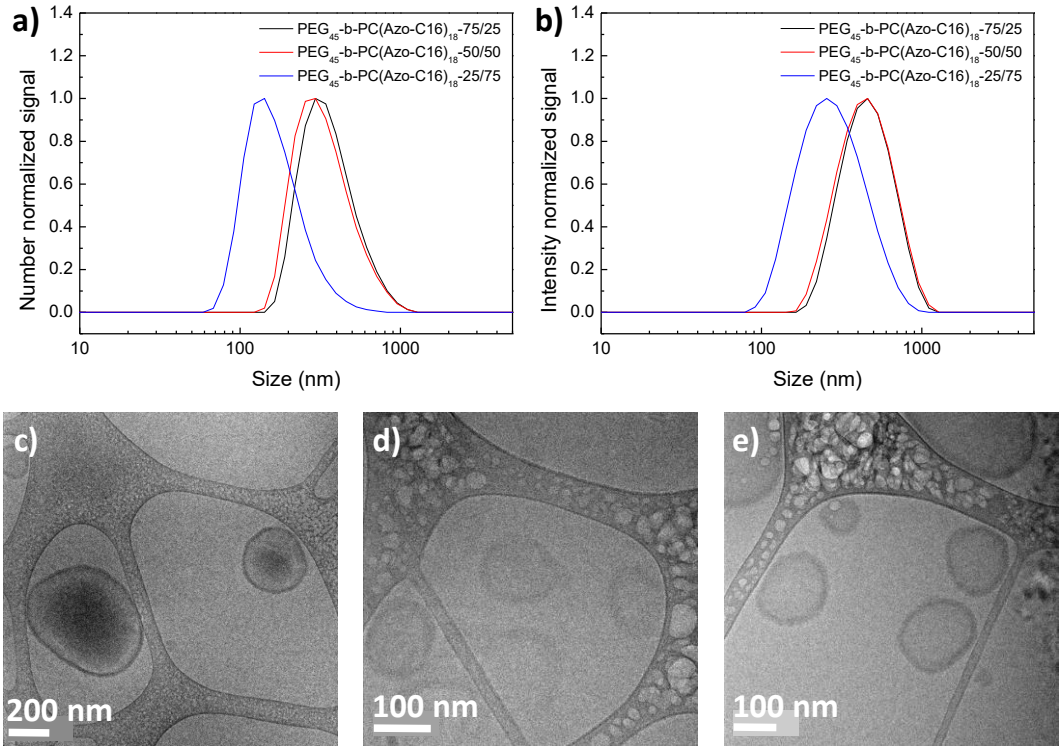

Figure 4.15: Analysis of the self-assembled structures from **PEG$_{45}$-*b*-PC(Azo-C16)$_{18}$** series. DLS distribution curves in number (a) and intensity (b). Cryo-TEM images of **PEG$_{45}$-*b*-PC(Azo-C16)$_{18}$ 75/25** (c), **PEG$_{45}$-*b*-PC(Azo-C16)$_{18}$ 50/50** (d) and **PEG$_{45}$-*b*-PC(Azo-C16)$_{18}$ 25/75** (e).

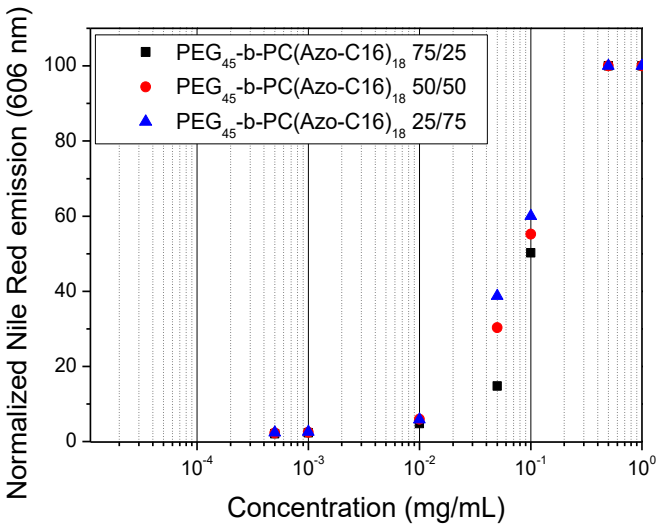

Figure 4.16: Normalised fluorescence emission of Nile Red at 606 nm (λexc = 550 nm) versus the copolymer concentration for **PEG$_{45}$-*b*-PC(Azo-C16)$_{18}$** series. CAC was determined from the intersection of the two extrapolated lines.

For **PEG$_{45}$-*b*-PC(AzoOMe-C16)$_{18}$** series, vesicles were observed on Cryo-TEM images with diameters ranging from 80 to 300 nm (Figure 4.17). For **PEG$_{45}$-*b*-PC(AzoOMe-C16)$_{18}$ 75/25**, the vesicles had smooth regular shapes with no imperfections having a wall thickness around 15 nm (Figure 4.17). For **PEG$_{45}$-*b*-PC(AzoOMe-C16)$_{18}$ 50/50** the size of the vesicles was rather heterogeneous. Besides, vesicles with smooth well-defined membranes coexisted with vesicles exhibiting diffuse, rough and irregular contours. For **PEG$_{45}$-*b*-PC(AzoOMe-C16)$_{18}$ 25/75** vesicles coexisted with worm like micelles (Figure 4.17). As a matter of fact, the morphology generated by self-assembly in water depends on the hydrophobic mass fraction, however, the existence of large transition regions where more than one type of morphology coexist is not uncommon for amphiphilic BCs.[6] In particular, coexistence of worm like and vesicles self-assemblies were described by Disher *et al*. for an amphiphilic diblock copolymer that consist of an intrinsically crystallisable hydrophobic block of PCL.[7] These studies on PEG-*b*-PCL demonstrated that crystallisation of the hydrophobic domains of the self-assemblies occurs, provoking the rigidity of vesicles. The relative roughening and irregular vesicles contour of **PEG$_{45}$-*b*-PC(AzoOMe-C16)$_{18}$ 50/50** and **PEG$_{45}$-*b*-PC(AzoOMe-C16)$_{18}$ 25/75** could be tentatively related to the tendency of the aliphatic chains towards crystallization observed in the bulk.[7,8] Sphere equivalent diameters were measured by DLS, D_h were in the range from 60 to 100 nm (Figure 4.17a).

CAC values of 30, 33 and 35 μg mL^{-1} for **75/25**, **50/50** and **25/75** relations were determined using Nile Red method (Figure 4.18), while the CAC value measured for **PEG$_{45}$-*b*-PC(AzoOMe)$_{18}$** was 33 μg mL^{-1}. In contrast to **PEG$_{45}$-*b*-PC(Azo-C16)$_{18}$** series, the increase of hydrophobicity due to the presence aliphatic side chains in **PEG$_{45}$-*b*-PC(AzoOMe-C16)$_{18}$** does not influence the CAC values.

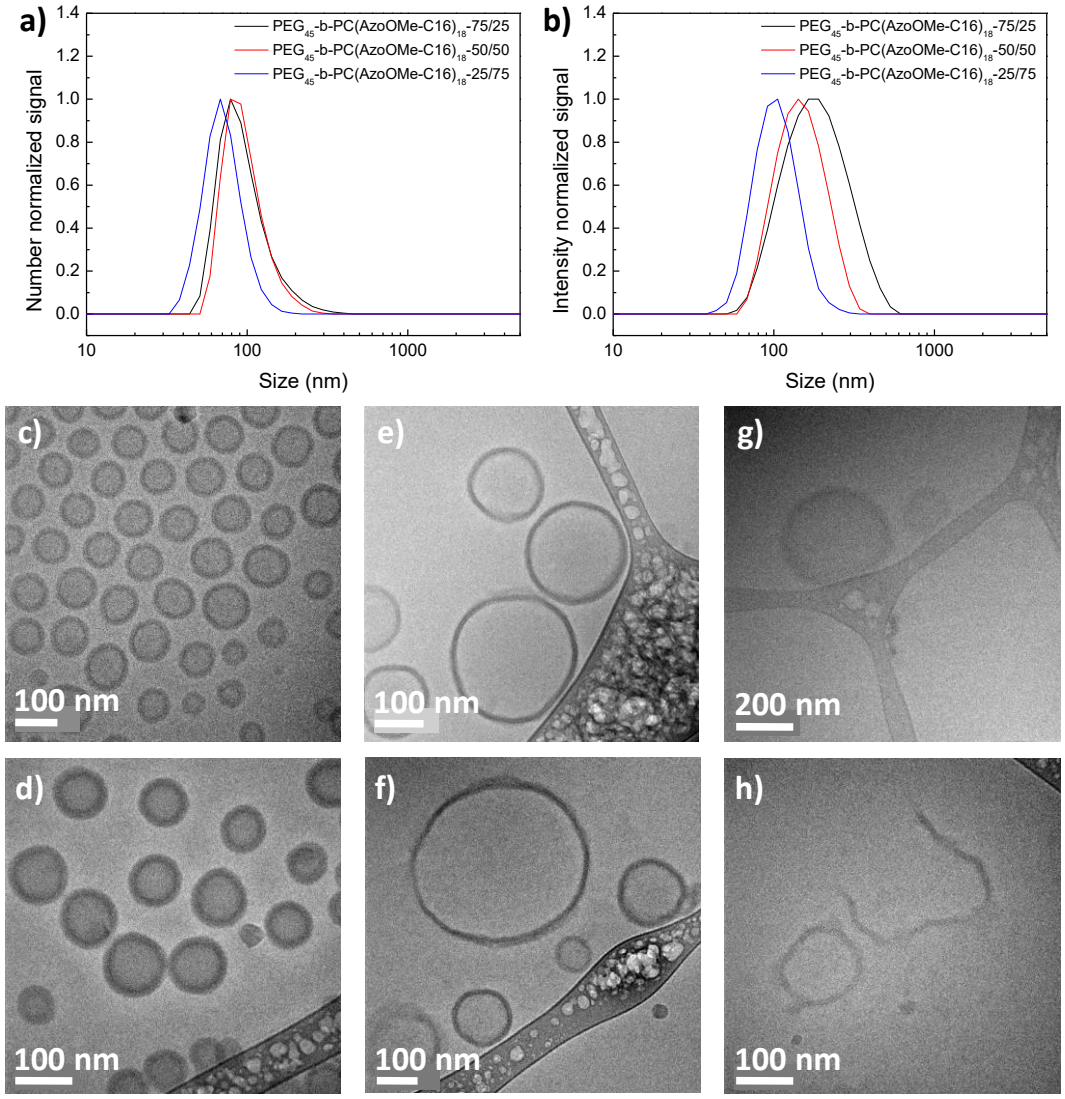

Figure 4.17: Analysis of the self-assembled structures from **PEG$_{45}$-*b*-PC(AzoOMe-C16)$_{18}$** series. DLS distribution curves in number (a) and intensity (b). Cryo-TEM images of **PEG$_{45}$-*b*-PC(AzoOMe-C16)$_{18}$ 75/25** (c and d), **PEG$_{45}$-*b*-PC(AzoOMe-C16)$_{18}$ 50/50** (e and f) and **PEG$_{45}$-*b*-PC(AzoOMe-C16)$_{18}$ 25/75** (g and h).

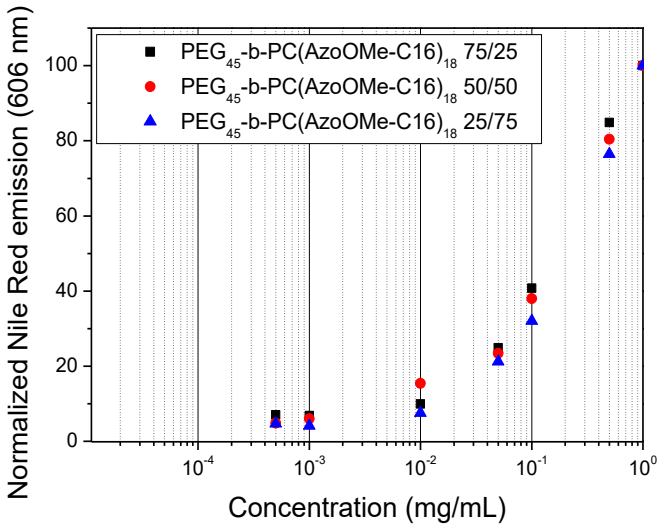

Figure 4.18: Normalised fluorescence emission of Nile Red at 606 nm (λ_{exc} = 550 nm) versus the copolymer concentration for **PEG$_{45}$-*b*-PC(AzoOMe-C16)$_{18}$** series. CAC was determined from the intersection of the two extrapolated lines.

4.5 Light responsiveness of PEG$_{45}$-*b*-PC(Azo-C16)$_{18}$ self-assemblies

UV-Vis spectra of **PEG$_{45}$-*b*-PC(Azo-C16)$_{18}$** series in THF solution showed the characteristics peaks associated to *trans*-4-isobutyloxy-4'-oxyazobenzenes moieties, one intense peak centred at 360 nm associated to π-π* transition and one much less intense centred at 450 nm associated to the forbidden n-π* transition (Figure 4.19). Indeed, the intensity of the bands decreased in parallel to the content of azobenzene in the hydrophobic block. Under irradiation with a low intensity UV lamp (emitting between 350 and 400 nm and with an irradiance of 3.5 μW cm^{-2} at 365 nm), *trans*-to-*cis* isomerization took place as deduced from the decrease of the π-π* band intensity and the increase in the n-π* band intensity. A photostationary state was reached at times less than 15 s for all polymers independently of the azobenzene content.

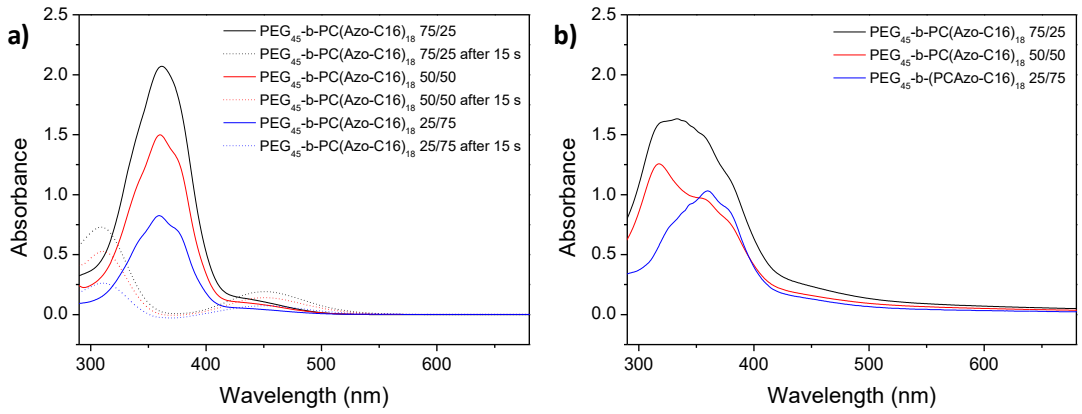

Figure 4.19: UV-Vis spectra of 10^{-4} M (referred to the hydrophobic block repetitive unit) THF solutions before (solid lines) and after 15 s UV illumination (dashed lines) (a) and of water suspensions at a concentration of 1 mg mL^{-1} (b) from **PEG$_{45}$-*b*-PC(Azo-C16)$_{18}$** series.

UV-VIS spectra of the vesicular suspensions from **PEG$_{45}$-*b*-PC(Azo-C16)$_{18}$** series were registered at a copolymer concentration of 1 mg mL^{-1}, observing a broadening of the signals in comparison to spectra from THF solutions (Figure 4.19). For **PEG$_{45}$-*b*-PC(Azo-C16)$_{18}$ 75/25** and **PEG$_{45}$-*b*-PC(Azo-C16)$_{18}$ 50/50**, the spectra presented similar characteristics than those observed for **PEG$_{45}$-*b*-PC(Azo)$_{18}$** (Figure 3.18), a strong blue-shift of the π-π* band from 360 to 320 nm was observed that

indicated the dominating presence of H-aggregates. Besides, two shoulders at 360 and 375 nm were observed corresponding to the non-aggregated and J-aggregated azobenzene units. For **PEG$_{45}$-*b*-PC(Azo-C16)$_{18}$ 25/75** the π-π* band was centred at 360 nm, with two shoulders at 325 and 375 nm, from H-aggregates and J-aggregates. This smaller shifting of the π-π* band accompanied by the narrowing of the band indicates that the formation of aggregates is hindered by the presence of an increasing number of alkyl chains in the hydrophobic block.

Upon UV illumination a decrease in the intensity of the π-π* band of the *trans*-azobenzene unit was observed, accompanied by an increase in the intensity of the n-π* band due to the *cis*-azobenzene isomer, evidencing the *trans-to-cis* isomerisation (Figure 4.20). For **PEG$_{45}$-*b*-PC(Azo-C16)$_{18}$ 75/25** a photostationary state was reached in times less than 120 s, which is less that the time required for **PEG$_{45}$-*b*-PC(Azo)$_{18}$**, while for **PEG$_{45}$-*b*-PC(Azo-C16)$_{18}$ 50/50** and **PEG$_{45}$-*b*-PC(Azo-C16)$_{18}$ 25/75** the photostationary state were reached at times less than 90 s and 60 s, respectively. Therefore, the results indicated that the aggregation of azobenzene units restricts photoisomerization. After 24 h in dark, the intensity of the π-π* band was partially recovered, evidencing the back *cis*-to-*trans* isomerization. For **PEG$_{45}$-*b*-PC(Azo-C16)$_{18}$ 75/25**, the initial shape of the π-π* band was almost recovered after 24 h in the dark. However, for **PEG$_{45}$-*b*-PC(Azo-C16)$_{18}$ 50/50**, the π-π* recovered band on the spectra was centred at 360 nm instead of 330 nm. For **PEG$_{45}$-*b*-PC(Azo-C16)$_{18}$ 25/75**, the initial spectrum was fully recovered with the π-π* band located again at 360 nm.

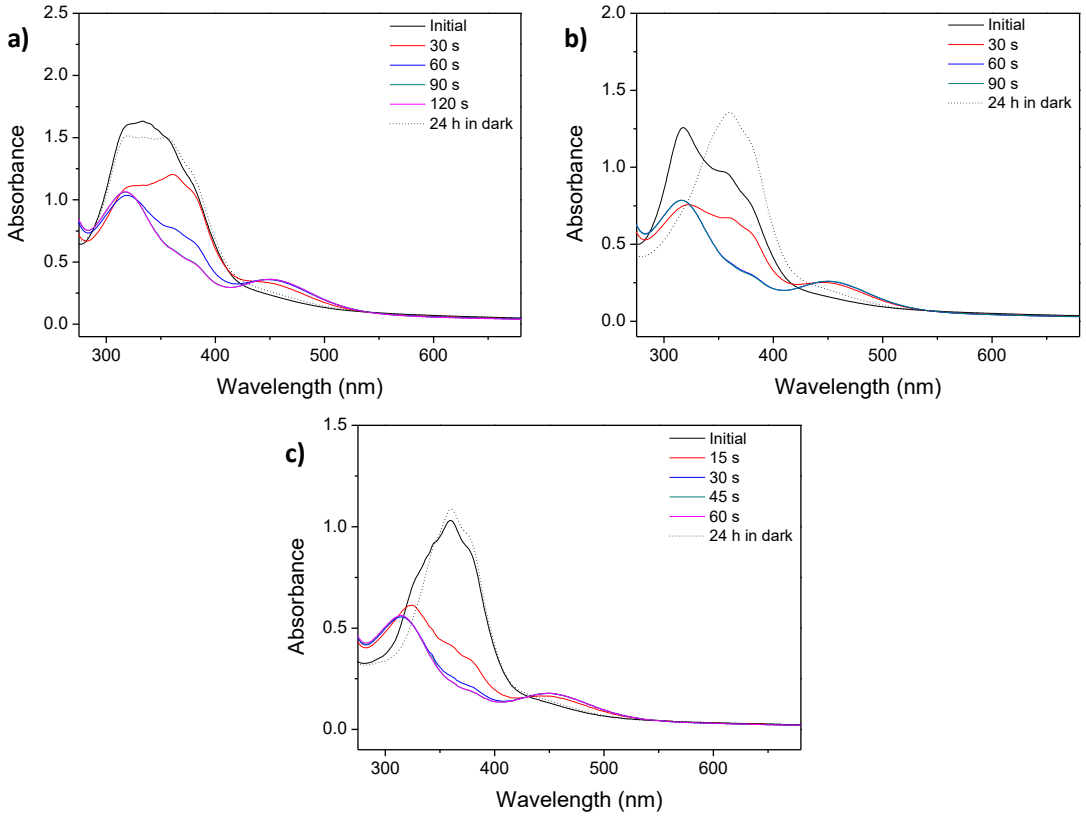

Figure 4.20: UV-Vis spectra of 1 mg mL^{-1} self-assemblies water suspensions upon UV light illumination for different times and subsequent storage for 24 h in the dark. **PEG$_{45}$-*b*-PC(Azo-C16)$_{18}$ 75/25** (a), **PEG$_{45}$-*b*-PC(Azo-C16)$_{18}$ 50/50** (b) and **PEG$_{45}$-*b*-PC(Azo-C16)$_{18}$ 25/75** (c).

Once proved the isomerization of azobenzene units, we investigated if the isomerization of azobenzene units located in the hydrophobic part of the vesicles membrane was able to induce appreciable morphological changes in the vesicular morphology. For **PEG$_{45}$-*b*-PC(Azo-C16)$_{18}$ 75/25**, the behaviour of the vesicles after UV illumination was similar to the reported previously in **Chapter 3** for **PEG$_{45}$-*b*-PCAzo$_{18}$** as the same folded vesicles with non-continuous contours were appreciated on the Cryo-TEM images (Figure 4.21). By DLS a slight increase in the size dispersity of the self-assemblies was observed (Figure 4.22). Under UV illumination, Cryo-TEM images taken from **PEG$_{45}$-*b*-PC(Azo-C16)$_{18}$ 50/50** showed a deformation of the vesicles with small spherical swellings emanating from the membrane, also the formation of smaller vesicles was observed (Figure 4.21). This is in concordance with DLS measurements where a tail at smaller sizes of the main size distribution peak was observed (Figure 4.22). Vesicles exhibiting such budding

division have been described for photosensitive liposomes.[9] On the contrary, vesicles from **PEG$_{45}$-*b*-PC(Azo-C16)$_{18}$ 25/75**, retained their initial features after being irradiated and DLS only registered a slight increase in the D_h (Figure 4.21 and Figure 4.22). Therefore, lowering the concentration of azobenzene at the inner membrane of the vesicles clearly influenced the morphological changes on the self-assemblies observed upon UV illumination, from clear disruption of the vesicular structure for higher azobenzene contents to a retention of the morphology for lower azobenzene contents. The tuning of the response to UV light irradiation on varying the concentration of azobenzene moieties of the hydrophobic block is in accordance with the tendency observed in the LDBCs functionalised with azobenzene units and aliphatic chains in different proportions reported by Blasco *et al.*[10]

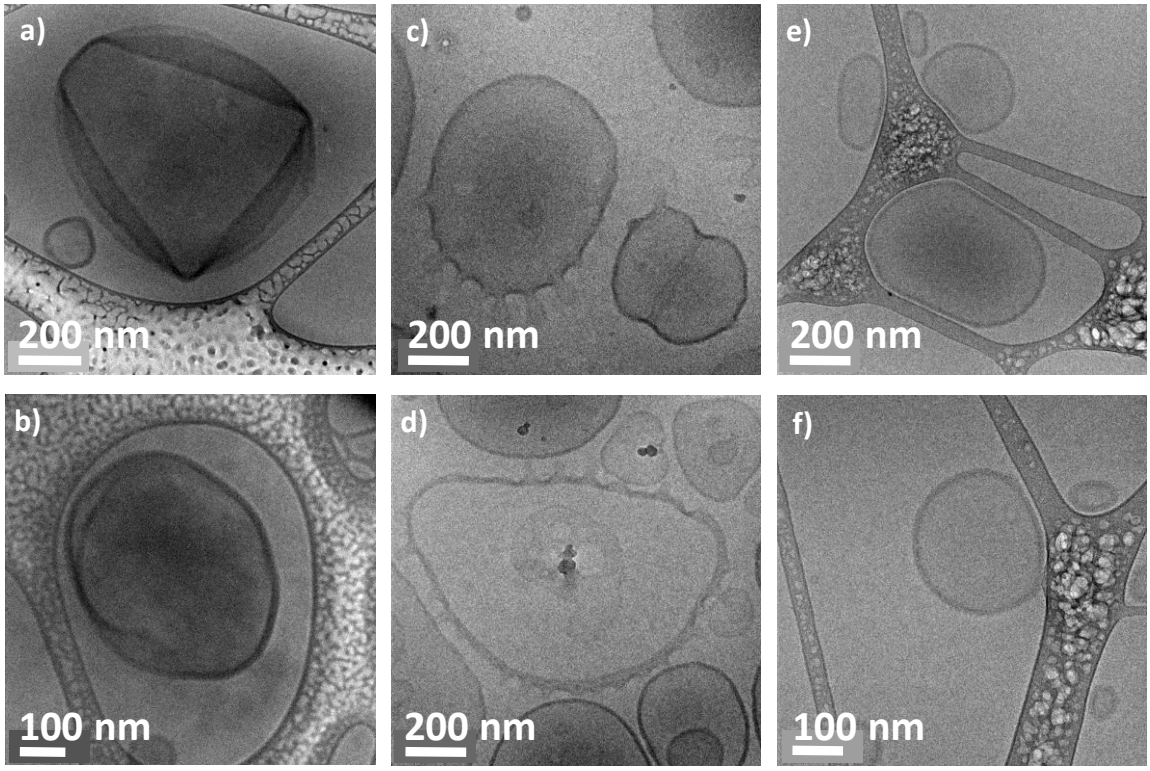

Figure 4.21: Cryo-TEM images after 10 min UV illumination from **PEG$_{45}$-*b*-PC(Azo-C16)$_{18}$ 75/25** (a and b), **PEG$_{45}$-*b*-PC(Azo-C16)$_{18}$ 50/50** (c and d) and **PEG$_{45}$-*b*-PC(Azo-C16)$_{18}$ 25/75** (e and f).

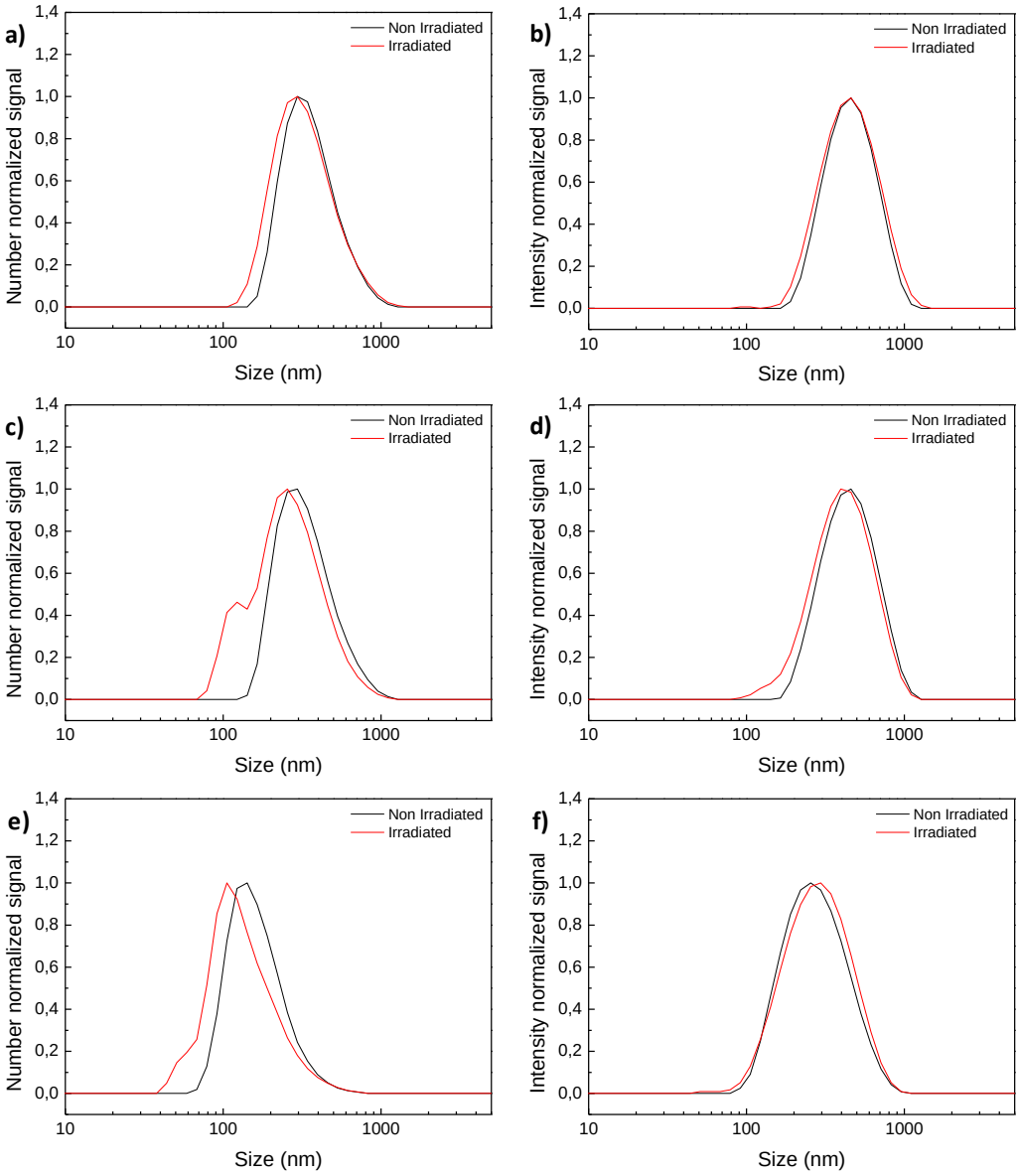

Figure 4.22: DLS traces before and after 10 min UV irradiation from **PEG_{45}-*b*-PC(Azo-C16)$_{18}$ 75/25** (a and b), **PEG_{45}-*b*-PC(Azo-C16)$_{18}$ 50/50** (c and d) and **PEG_{45}-*b*-PC(Azo-C16)$_{18}$ 25/75** (e and f).

4.6 Light responsiveness of PEG$_{45}$-*b*-PC(AzoOMe-C16)$_{18}$ self-assemblies

UV-Vis spectra of **PEG$_{45}$-*b*-PC(AzoOMe-C16)$_{18}$** series were registered in THF solution at a concentration of 10^{-4} M (referred to the hydrophobic block repetitive unit). Spectra showed the two bands characteristics from *trans-2*,2',5,5'-tetramethoxy-4-oxyazobenzene unit, one intense centred at 320 nm associated to π-π* transition and one of lower intensity, associated to n- π* transition and centred at 470 nm (Figure 4.23). The intensity of the bands decreased proportionally to the content of 2,2',5,5'-tetramethoxy-4-oxyazobenzene unit in the hydrophobic block. Although *trans*-to-*cis* isomerization could be induced both with 625 and 530 nm light, in basis to results reported in **Chapter 3**, only the response under 530 nm illumination was investigated as it is the only wavelength able to induce morphological changes in **PEG$_{45}$-*b*-PCAzoOMe$_{18}$**. After 530 nm light illumination (irradiance of 30 μW cm^{-2}) a photostationary state was reached in times less than 15 s, with a remarkable decrease in the intensity of the π-π* band and a strong blue-shift of the n-π* band from 470 to 435 nm, indicating the occurrence of *trans*-to-*cis* isomerization (Figure 4.23).

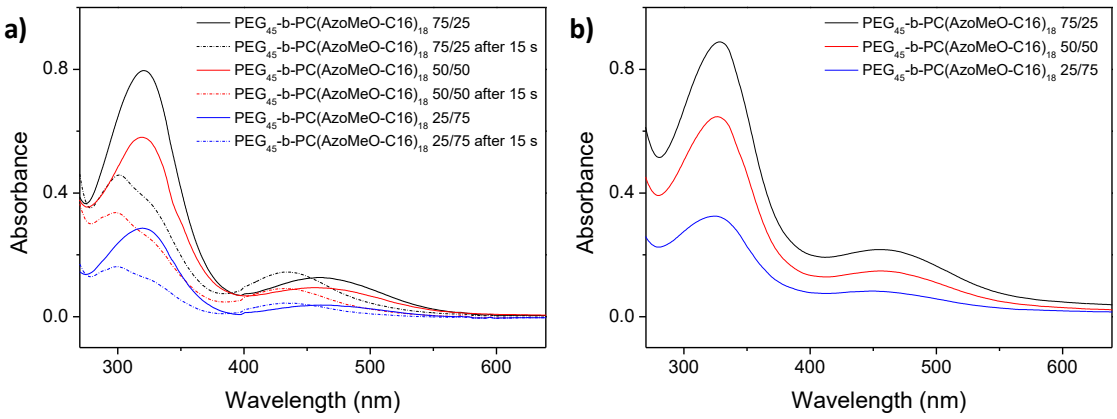

Figure 4.23: UV-Vis spectra of 10^{-4} M (referred to the hydrophobic block repetitive unit) THF solutions before (solid lines) and after 15 s 530 nm illumination (dashed lines) (a) and of water suspensions at a concentration of 1 mg mL^{-1} (b) from **PEG$_{45}$-*b*-PC(AzoOMe-C16)$_{18}$** series.

UV-Vis spectra from the vesicular suspensions of **PEG$_{45}$-*b*-PC(AzoOMe-C16)$_{18}$** series showed a slight blue-shift in the n-π* band from 470 to approximately 450 nm (Figure 4.23).

By irradiating the vesicular suspensions with 530 nm light, a decrease in the intensity of the π-π* band was observed, accompanied by a displacement in the n-π* band, from 470 to 435 nm, evidencing the *trans*-to-*cis* isomerization of 2,2',5,5'-tetramethoxy-4-oxyazobenzene units (Figure 4.24). For **PEG$_{45}$-*b*-PC(AzoOMe-C16)$_{18}$ 75/25** the photostationary state was reached in less than 30 s, for **PEG$_{45}$-*b*-PC(AzoOMe-C16)$_{18}$ 50/50** in less than 15 s, while for **PEG$_{45}$-*b*-PC(AzoOMe-C16)$_{18}$ 25/75** the photostationary state was reached in times below 10 s. Again, by reducing the number of azobenzene moieties in the side chain of the hydrophobic block, the photoisomerization was faster. After 24 h in the dark, the intensity of the π-π* band was partially recovered for **PEG$_{45}$-*b*-PC(AzoOMe-C16)$_{18}$ 75/25** and **50/50**, whereas for **PEG$_{45}$-*b*-PC(AzoOMe-C16)$_{18}$ 25/75** it was not recovered at all (Figure 4.24).

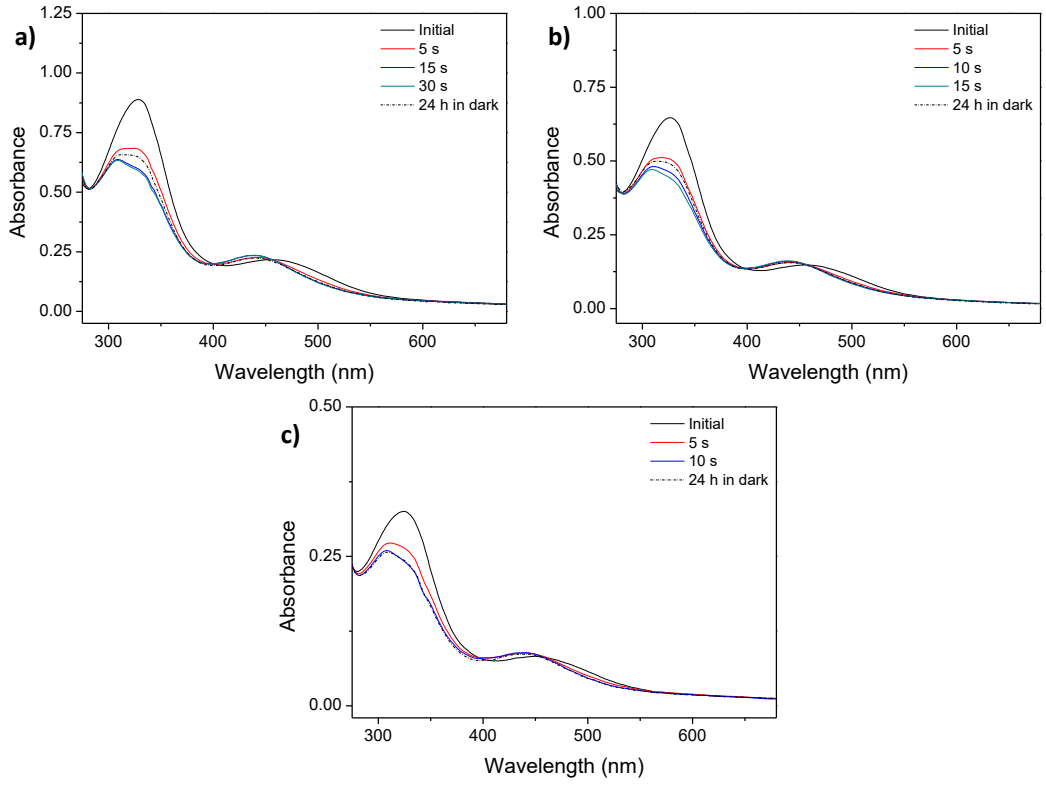

Figure 4.24: UV-Vis spectra of 1 mg mL^{-1} self-assemblies water suspensions upon 530 nm light illumination for different times and subsequent storage for 24 h in the dark for **PEG$_{45}$-*b*-PC(AzoOMe-C16)$_{18}$ 75/25** (a), **PEG$_{45}$-*b*-PC(AzoOMe-C16)$_{18}$ 50/50** (b) and **PEG$_{45}$-*b*-PC(AzoOMe-C16)$_{18}$ 25/75** (c).

Samples were analysed by Cryo-TEM after being exposed to 530 nm light to assess any possible change on the self-assembled morphologies. However, recorded images of irradiated samples (Figure 4.25) were very similar to those of non irradiated ones (Figure 4.17). For **PEG$_{45}$-*b*-PC(AzoOMe)$_{18}$**, the number of vesicles was noticeably inferior after 530 nm light irradiation (Figure 3.26), while for **PEG$_{45}$-*b*-PC(AzoOMe-C16)$_{18}$ 75/25** approximately the same number of well-defined unaltered vesicles were monitored (Figure 4.25). Cryo-TEM images taken for **PEG$_{45}$-*b*-PC(AzoOMe-C16)$_{18}$ 50/50** and **PEG$_{45}$-*b*-PC(AzoOMe-C16)$_{18}$ 25/75** showed vesicles with blurred contours and for **PEG$_{45}$-*b*-PC(AzoOMe-C16)$_{18}$ 25/75** also worm micelles were observed, as before irradiating with 530 nm (Figure 4.25). After 530 nm light irradiation for 5 min, DLS only registered appreciable changes for **PEG$_{45}$-*b*-PC(AzoOMe-C16)$_{18}$ 75/25**, whereas no appreciable changes in the apparent D_h or in the dispersity of the self-assemblies was detected for **PEG$_{45}$-*b*-PC(AzoOMe-C16)$_{18}$ 50/50** and **PEG$_{45}$-*b*-PC(AzoOMe-C16)$_{18}$ 25/75** (Figure 4.26).

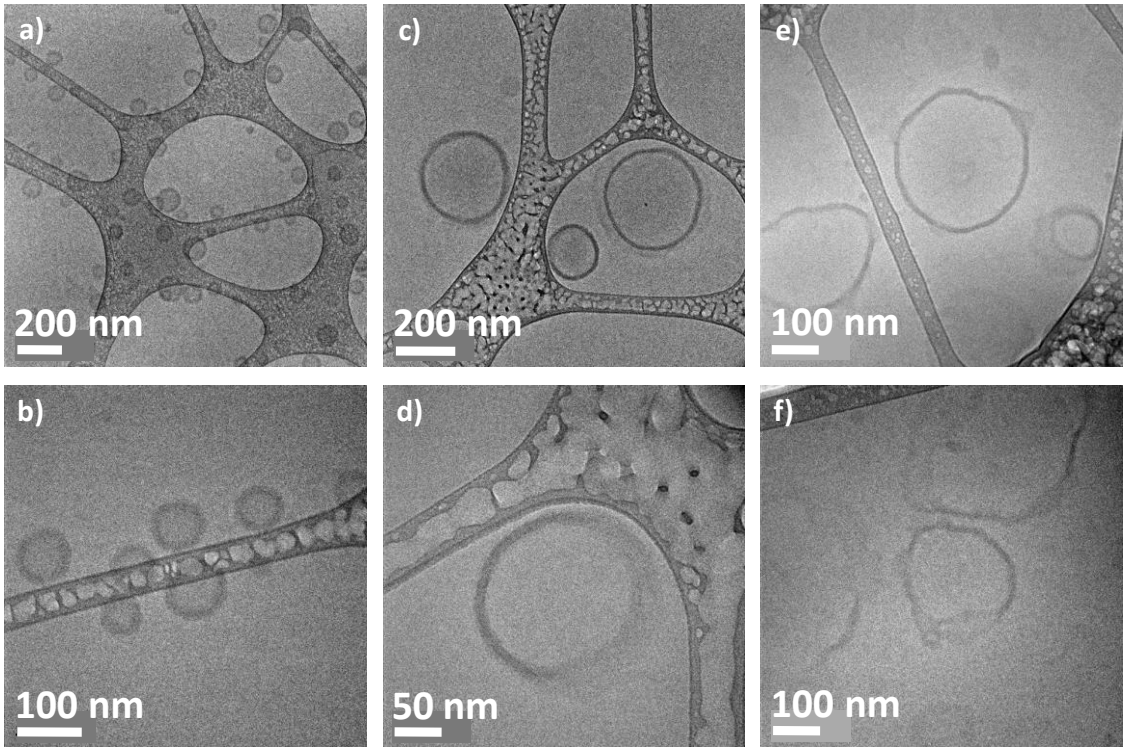

Figure 4.25: Cryo-TEM images after 5 min 530 nm irradiation from **PEG$_{45}$-*b*-PC(AzoOMe-C16)$_{18}$ 75/25** (a and b), **PEG$_{45}$-*b*-PC(AzoOMe-C16)$_{18}$ 50/50** (c and d) and **PEG$_{45}$-*b*-PC(AzoOMe-C16)$_{18}$ 25/75** (e and f).

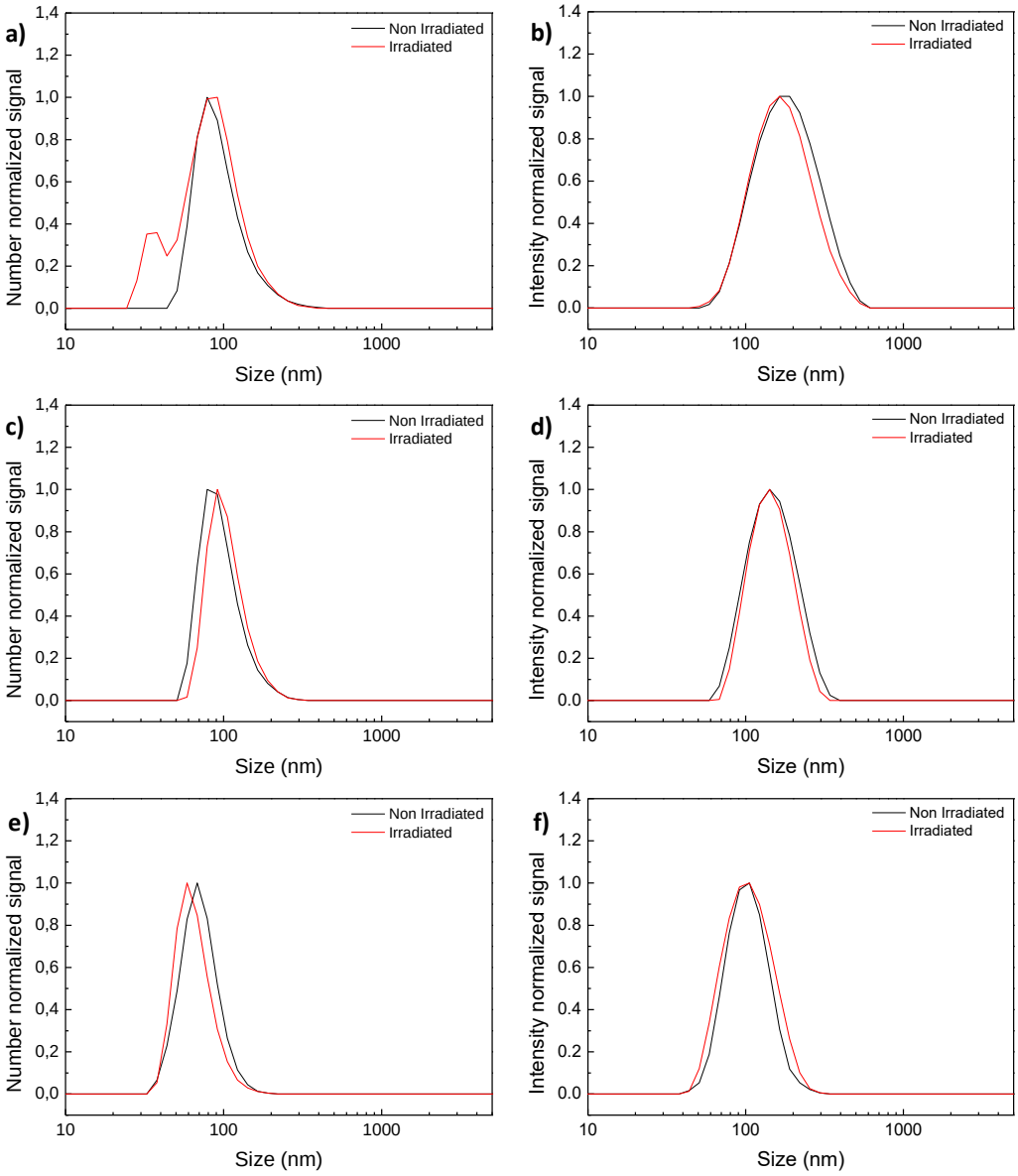

Figure 4.26: DLS traces before and after 5 min 530 nm irradiation from **PEG$_{45}$-*b*-PC(AzoOMe-C16)$_{18}$ 75/25** (a and b), **PEG$_{45}$-*b*-PC(AzoOMe-C16)$_{18}$ 50/50** (c and d) and **PEG$_{45}$-*b*-PC(AzoOMe-C16)$_{18}$ 25/75** (e and f).

4.7 Encapsulation and light-induced release of molecular probes

Encapsulation and light triggered release of encapsulated fluorescent molecular probes was investigated using Nile Red, which being hydrophobic would be inserted at the membrane, and Rhodamine B, which being hydrophilic would be loaded at the aqueous internal cavity of the vesicles.

Nile Red is strongly fluorescent upon excitation with 550 nm light in non-polar media but the fluorescence is severely quenched in water. Changes in the emission of Nile Red upon light irradiation, and after storing the samples in the dark 24 h were measured. Nile Red loaded vesicles from **PEG_{45}-*b*-PC(Azo-C16)$_{18}$** series showed a strong fluorescence evidencing that Nile Red was loaded into the hydrophobic vesicles membrane (Figure 4.27). Given that the BC concentration is the same in all cases, spectra compiled in Figure 4.27 also show that encapsulated Nile Red amount seems to be lowered on increasing the number of aliphatic chains at the membrane and decreasing the number of azobenzene units. The reduced Nile Red loading abilities on increasing the aliphatic chain content may be explained from a lower compatibility between Nile Red and aliphatic chains than between Nile Red and azobenzene units.[2]

Under UV light irradiation a sharp decrease in Nile Red emission was observed in all cases in about the same timescale (Figure 4.27). After storing in the dark for 24 h, the Nile Red emission was only partially recovered for **PEG_{45}-*b*-PC(Azo-C16)$_{18}$ 75/25** vesicles, which seems to evidence the partial release of Nile Red under light stimulation. However, for **PEG_{45}-*b*-PC(Azo-C16)$_{18}$ 50/50** and **PEG_{45}-*b*-PC(Azo-C16)$_{18}$ 25/75** vesicles Nile Red emission was recovered almost to the initial non-irradiated values which would indicate that the probe was not released to the medium. This was somehow unexpected for **PEG_{45}-*b*-PC(Azo-C16)$_{18}$ 50/50** given the morphological membrane alterations observed by Cryo-TEM but not for **PEG_{45}-*b*-PC(Azo-C16)$_{18}$ 25/75**.

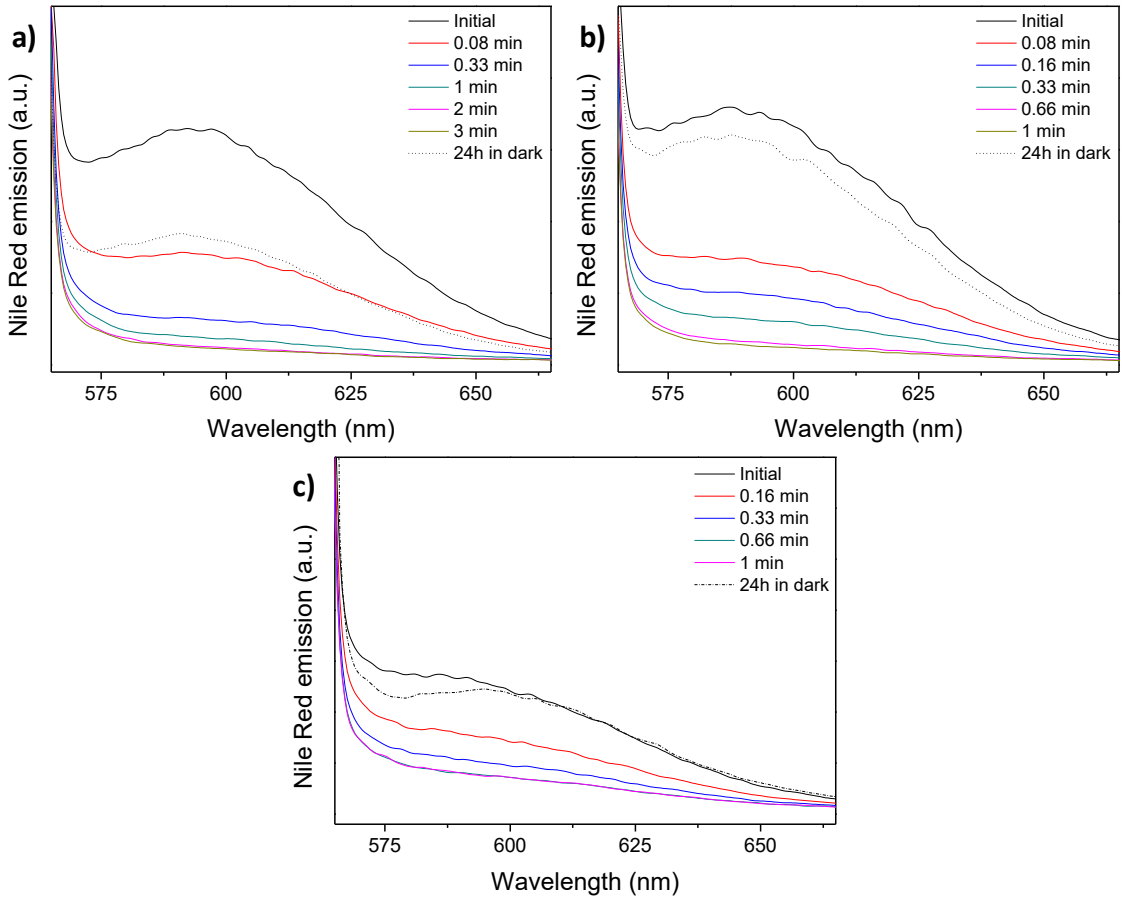

Figure 4.27: Emission spectra (excitation wavelength 550 nm) of the Nile Red loaded vesicles recorded after UV light illumination for different time intervals and subsequent storage for 24 h in the dark for **PEG$_{45}$-*b*-PC(Azo-C16)$_{18}$ 75/25** (a), **PEG$_{45}$-*b*-PC(Azo-C16)$_{18}$ 50/50** (b) and **PEG$_{45}$-*b*-PC(Azo-C16)$_{18}$ 25/75** (c).

Also vesicles from **PEG$_{45}$-*b*-PC(AzoOMe-C16)$_{18}$** series were loaded with Nile Red, but in this case Nile Red emission upon excitation at 550 nm was almost negligible when compared to **PEG$_{45}$-*b*-PC(AzoOMe)$_{18}$** or **PEG$_{45}$-*b*-PC(Azo-C16)$_{18}$** series (Figure 4.28). Upon 530 nm irradiation, subtle increases in the emission were observed for the first 30 s of irradiation were in the timescale in which the photostationary state is reached, as stablished in **Chapter 3** for **PEG$_{45}$-*b*-PC(AzoOMe)$_{18}$**. At longer irradiation times, and after 24 h in the dark, no changes were detected.

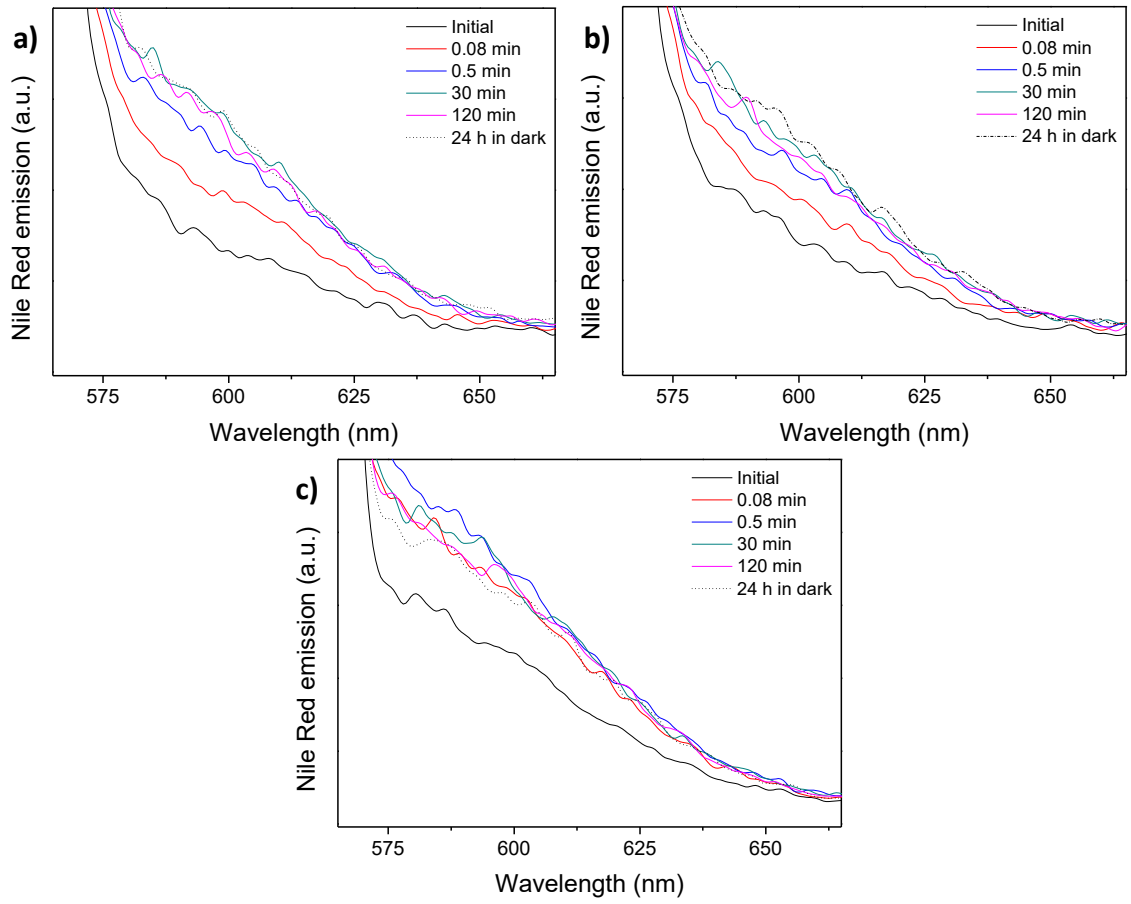

Figure 4.28: Emission spectra (excitation wavelength 550 nm) of the Nile Red loaded vesicles recorded after 530 nm light illumination for different time intervals and subsequent storage for 24 h in the dark for **PEG$_{45}$-*b*-PC(AzoOMe-C16)$_{18}$ 75/25** (a), **PEG$_{45}$-*b*-PC(AzoOMe-C16)$_{18}$ 50/50** (b) and **PEG$_{45}$-*b*-PC(AzoOMe-C16)$_{18}$ 25/75** (c).

Vesicles of **PEG$_{45}$-*b*-PC(Azo-C16)$_{18}$** and **PEG$_{45}$-*b*-PC(AzoOMe-C16)$_{18}$** series were also loaded with Rhodamine B. The amount of Rhodamine B entrapped in the vesicles was determined by HPLC. For **PEG$_{45}$-*b*-PC(Azo)$_{18}$** approximately 0.1 molecules of Rhodamine B per molecule of BC were detected. For **PEG$_{45}$-*b*-PC(Azo-C16)$_{18}$ 75/25** the value lowered to 0.02 molecules of Rhodamine B per molecule of BC, while Rhodamine B was not detected under the used experimental conditions for **PEG$_{45}$-*b*-PC(Azo-C16)$_{18}$ 50/50** and **PEG$_{45}$-*b*-PC(Azo-C16)$_{18}$ 25/75**. The same results were obtained for **PEG$_{45}$-*b*-PC(AzoOMe-C16)$_{18}$** series. Therefore, increasing the content of aliphatic chains in the side chain of the hydrophobic block led to a drastic decrease in the amount of Rhodamine B encapsulated in the vesicles. The membrane structure of the vesicles is crucial because it regulates their permeability. Disher *et al.* demonstrated that vesicles of BCs with a crystallisable hydrophobic block have

membranes that are rigid and leaky, which was attributed to defects formed between adjacent polymer crystalline domains.[7] Accordingly, the results can be tentatively explained on the basis of the leakiness of the cargoes. Even if vesicles should be loaded with Rhodamine B, premature release occurs during the dialysis step so the cargoes are removed.

The reduced loading ability of these vesicles on increasing the aliphatic chain content at the membrane could be tentatively rationalized in terms of crystallisation tendency of the aliphatic chains observed in bulk combined with the lower transition temperatures. It has been described in the literature that increasing crystallisability has a negative effect on the loading efficiency.[6,11]

According to this, only Rhodamine B loaded **PEG_{45}-*b*-PC(Azo-C16)$_{18}$ 75/25** and **PEG_{45}-*b*-PC(AzoOMe-C16)$_{18}$ 75/25** vesicles were further investigated. Samples were irradiated with either UV light for 10 min or 530 nm light for 5 min respectively, dialysed against Milli-Q water (Slide-A-Lyzer 2kDa, ThermoScientific), and the fluorescence of the dialysis water measured at different times. Up to 56 h after light irradiation, a continuous increase in Rhodamine B emission was measured (Figure 4.29). Some fluorescence was observed in the blank reference experiments without light irradiation, though it is much weaker than the emission detected for the irradiated samples. Thus, we conclude that in both cases release of Rhodamine B from the inner cavity of the vesicles to the surrounding water can be stimulated by light.

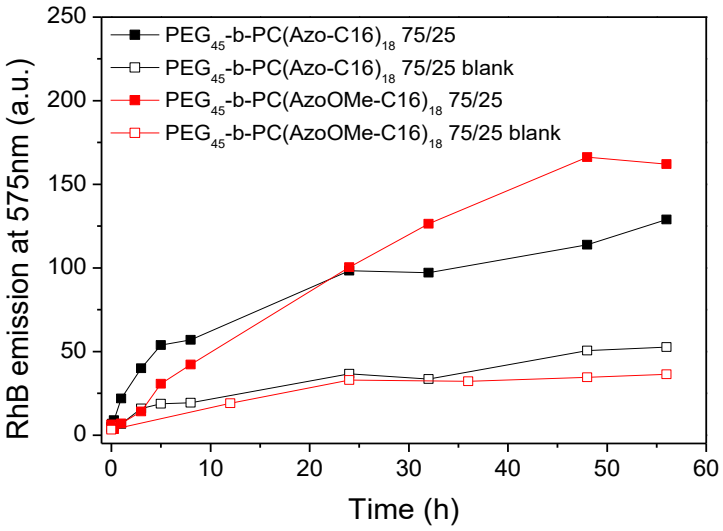

Figure 4.29: Evolution of Rhodamine B fluorescence of the dialysis water, measured for different time intervals after light irradiation and without light irradiation, for **PEG$_{45}$-*b*-PCAzoOMe$_{18}$** and **PEG$_{45}$-*b*-PC(AzoOMe-C16)$_{18}$ 75/25**.

4.8 Conclusions

Amphiphilic BCs functionalised at the hydrophobic block with either 4-isobutyloxy-4'-oxyazobenzene or 2,2',5,5'-tetramethoxy-4-oxyazobenzene and hexadecyloxy chains in several molar proportions have been synthesised by combination of ROP of **MPC** and **MCC** and CuAAC. The length of the hydrophilic and hydrophobic blocks in all the synthesized copolymers is the same than the reported for **PEG$_{45}$-*b*-PC(AzoOMe)$_{18}$** and **PEG$_{45}$-*b*-PC(AzoOMe)$_{18}$** in **Chapter 3**. For **PEG$_{45}$-*b*-PC(Azo-C16)$_{18}$** series, the assembly properties have been preserved and vesicles were formed in all cases, in accordance to the parent **PEG$_{45}$-*b*-PC(Azo)$_{18}$** described in Chapter 3.

The response to UV light of the vesicles has been maintained on reducing the number of azobenzene units up to a relation 50%. However, when azobenzene content has been reduced to 25%, vesicles do not suffer any apparent morphological changes upon UV illumination. For **PEG$_{45}$-*b*-PC(AzoOMe-C16)$_{18}$** series, the assembly properties in water are greatly altered on incorporating aliphatic chains. With 75% of azobenzene content, the BC self-assembles in regular vesicles. However, with 50 and 25% azobenzene contents heterogeneous self-assemblies are observed where vesicles of different sizes coexist with rough contoured vesicles or worm like micelles. No morphological changes upon 530 nm illumination are observed for the self-assemblies of these series.

Loading and release abilities of the vesicles have been significantly affected by the presence of aliphatic chains at the membrane, in particular **PEG$_{45}$-*b*-PC(AzoOMe-C16)$_{18}$** series. For vesicles with contents of aliphatic chains in the side chain of the hydrophobic block up of 50% and 75% have no interest for light controlled release as they seem to undergo a premature delivery of hydrophilic cargoes by physical diffusion. This has been tentatively related with the high crystallisability tendency of the aliphatic chains of the hydrophobic domains observed in bulk. With 75% of azobenzene, loading ability of the vesicles have been still maintained. For **PEG$_{45}$-*b*-PC(Azo-C16)$_{18}$ 75/25**, UV light stimulated release of Rhodamine B has been demonstrated. Also, for **PEG$_{45}$-*b*-PC(AzoOMe-C16)$_{18}$ 75/25**

release is induced by 530 nm light. Future work may be aimed at diluting the light-responsive units with non-crystallisable groups, such as ramified aliphatic chains.

4.9 Experimental section

4.9.1 Synthesis and characterisation of MCC

5-Methyl-5-hexadeciloxycarbonyl-1,3-dioxan-2-one (**MCC**) was synthesised following previous reported methods for **MPC**, from 2,2-bis(hydroxymethyl)propionic acid *via* esterification of the carboxyl group with 1-bromohexadecane in presence of KOH and closure of the carbonate ring with ethyl chloroformate (Figure 4.30).

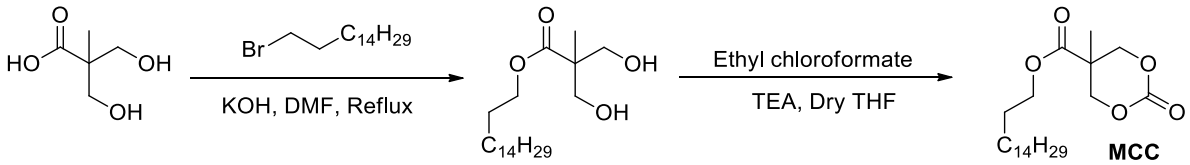

Figure 4.30 Synthesis of 5-methyl-5-hexadeciloxycarbonyl-1,3-dioxan-2-one (**MCC**).

Synthesis and characterisation of hexadeciloxy-2,2-Bis(hydroxymethyl)propionate. 2,2-bis(hydroxymethyl) propionate (13.17 g, 98.3 mmol) and potassium hydroxide (5.51 g, 98.3 mmol) were solved in dimethylformamide (30 mL) and heated to 80 °C. After 1 hour, the temperature is lowered to 40 °C and hexadecyl bromide (30.0 g, 98.3 mmol) added dropwise over 30 min. The mixture was allowed to stir for 48 h. Solvent was evaporated by distillation and the residue solved in dichloromethane, removing the precipitate by filtration. Evaporation of dichloromethane gave a yellowish oil that was purified by silica column chromatography, starting with dichloromethane as eluent and finishing with a mixture dichloromethane / methanol (95:5). Product was isolated as a colourless oil that after several hours crystallised to a white solid. Yield = 42%. FTIR (KBr, υ_{max}/cm^{-1}): 3410 (O-Hst), 2940 (Csp^3-Hst), 1740 (C=Ost). NMR ^{1}H [400 MHz, $CDCl_3$, δ (ppm)]: 4.18 - 4.11 (m, 2H), 3.93 - 3.85 (m, 2H), 3.73 -3.66 (m, 2H), 2.98 (s, broad, 2H), 1.75 - 1.55 (m, 2H), 1.47 - 1.15 (m, 26H), 1.06 (s, 3H), 0.95 -0.79 (m, 3H). NMR ^{13}C [100 MHz, $CDCl_3$, δ (ppm)]: 176.2, 68.1, 65.3, 49.3, 34.1, 33.0, 32.0, 29.8, 29.8, 29.8, 29.8, 29.7, 29.7, 29.6, 29.6, 29.5, 29.3, 28.9, 28.7, 28.3, 26.0, 22.8, 17.3, 14.2

Synthesis and characterisation of 5-methyl-5-hexadeciloxycarbonyl-1,3-dioxan-2-one (MCC). Hexadeciloxy-2,2-bis(hydroxymethyl)propionate (12.00 g, 68.9 mmol) and ethyl chloroformate (14.96 g, 137.9 mmol) were solved in anhydrous THF (50 mL) under argon atmosphere and cooled with an ice bath. After 30 minutes, triethylamine (TEA) (13.93 g, 137.9 mmol) was added dropwise over 30 minutes. After 15 minutes, the ice bath was removed and the reaction allowed to stir at room temperature for 24 hours. The crude reaction was filtered and the resulting solution evaporated to dryness. The solid was purified by silica column chromatography, using dichloromethane as eluent. The resulting solid was solved in the minimum amount of THF and precipitated in diethyleter/ethyl acetate. The solid was isolated by filtration, obtaining a white powder. Yield 35%. FTIR (KBr, υ_{max}/cm^{-1}): 2920 (Csp^3-H^{st}), 1760 (C=O^{st}), 1143 (C-O^{st}). NMR ^1H [400 MHz, $CDCl_3$, δ (ppm)]: 4.72 - 4.62 (m, 2H), 4.23 - 4.14 (m, 4H), 1.73 - 1.57 (m, 2H), 1.42 - 1.16 (m, 29H), 0.86 (t, J = 7.2 Hz, 3H). NMR ^{13}C [100 MHz, $CDCl_3$, δ (ppm)]: 171.2, 147.6, 73.1, 66.5, 40.3, 32.0, 29.8, 29.8, 29,8, 29.7, 29.7, 29.6, 29.5, 29.3, 28.5, 25.8, 22.9, 17.7, 14.2.

4.9.2 General procedure for the synthesis of PEG_{45}-*b*-PC(P-C16)$_{18}$ block copolymers

A solution of PEG_{45}-OH, DBU and TU in dry dichloromethane ($[MPC+MCC]_0$= 1.0 M) was previously dried for 12 h over activated 4Å molecular sieves under Ar atmosphere. This solution was added *via* cannula to a Schlenk flask charged with a mixture of monomers under Ar atmosphere. Equivalents of each reactive for 75/25, 50/50 and 25/75 relations are summarized in the table below. The reaction was stirred at 35 °C for 8 h, then concentrated under vacuum. Copolymers were isolated by silica column chromatography using dichloromethane/ethyl acetate (8/2) as eluent. e.g. PEG_{45}-*b*-(PC-C16)$_{18}$ 75/25: FTIR (KBr, υ_{max}/cm^{-1}): 3525 (O-H), 3292 (Csp-H), 2906 (Csp^3-H), 2123 (Csp-Csp), 1758 (C=O). ^1H NMR (400 MHz, $CDCl_3$, δ, ppm]: 4.75 – 4,67 (m), 4.37 – 4.21 (m), 3.79 – 3.40 (m), 3.37 (s), 2.53 (m), 1.68 – 1.53 (m), 1.40 – 1.15 (m), 0.86 (t, J = 7.1 Hz) (s).

Table 4.3: Equivalents of the reagents introduced in ring opening polymerisation reactions.

Copolymer	PEG45-OH	DBU	TU	MPC	MCC
PEG_{45}-*b*-$(PC\text{-}C16)_{18}$ 75/25	1	0.23	1.15	17.25	5.75
PEG_{45}-*b*-$(PC\text{-}C16)_{18}$ 50/50	1	0.23	1.15	11.50	11.50
PEG_{45}-*b*-$(PC\text{-}C16)_{18}$ 25/75	1	0.23	1.15	5.75	17.25

4.9.3 General procedure for the side chain functionalisation by CuAAC

A Schlenk flask charged with the azide **N_3-Azo** or **N_3-AzoOMe** (2 mol), the corresponding propargyl functionalised copolymer **PEG_{45}-b-$(PC\text{-}C16)_{18}$ 75/25**, **PEG_{45}-b-$(PC\text{-}C16)_{18}$ 50/50** or **PEG_{45}-b-$(PC\text{-}C16)_{18}$ 25/75** (1 mol of propargyl group), CuBr (0.3 mol) and PMDETA (0.3 mol) was flushed with Ar. Then, deoxygenated and distilled DMF (5 mL) was added. The reaction was maintained at 40 °C for 5 days. The crude reaction was diluted with dichloromethane and washed three times with distilled water. The organic fraction was dried over $MgSO_4$ and evaporated to dryness. Residual azide was removed by preparative SEC using Biobeds SX-1 and dichloromethane as eluent. Copolymer containing fractions were filtered through a 0.22 μm PTFE filter and evaporated to dryness. Isolated yield 75-80%.

Characterisation data of PEG_{45}-*b*-$PC(Azo\text{-}C16)_{18}$ series, e.g. 75/25: FTIR (KBr, υ_{max}/cm^{-1}): 3149 (Csp^2-H^{st}), 2906 (Csp^3-H^{st}), 1758 ($C{=}O^{st}$), 1605 (CAr-CAr^{st}), 1496, 1468 ($N{=}N^{st}$), 1154 ($C\text{-}O^{st}$). ^1H NMR [400 MHz, $CDCl_3$, δ, ppm]: 7.89 – 7.78 (m), 7.62 (s), 7.03 – 6.90 (m), 5.24 (s), 4.44 – 4.17 (m), 4.12 – 4.05 (m), 4.04 – 3.91 (m), 3.82 – 3.73 (m), 3.70 - 3.58 (s, broad), 3.38 (s), 2.17 – 2.04 (m), 2.01 – 1.85 (m), 1.84 – 1.64 (m), 1.63 – 1.55 (m), 1.55 – 1.45 (m), 1.44 – 1.33 (m), 1.31 – 1.14 (m), 1.04 – 0.97 (m), 0.91 – 0.80 (m). GPC data: PEG_{45}-*b*-$PC(Azo\text{-}C16)_{18}$ 75/25 M_n = 10600, $Đ$ = 1.06 PEG_{45}-*b*-$PC(Azo\text{-}C16)_{18}$ 50/50 M_n = 11600, $Đ$ = 1.06 PEG_{45}-*b*-$PC(Azo\text{-}C16)_{18}$ 25/75 M_n = 10400, $Đ$ = 1.06.

Characterisation data of PEG_{45}-*b*-$PC(AzoOMe\text{-}C16)_{18}$ series, e.g. 75/25: FTIR (KBr, υ_{max}/cm^{-1}): 3138 (Csp^2-H^{st}), 2926 (Csp^3-H^{st}), 2102, 1750 ($C{=}O^{st}$), 1600 (CAr-CAr^{st}),

1470 (N=Nst), 1253, 1123 (C-Ost). ^{1}H NMR [400 MHz, $CDCl_3$, δ, ppm]: 7.65 (s), 7.21 - 7.12 (m), 6.69 - 6.58 (m), 6.19 (s), 5.24 (s), 4.42 - 4.31 (m), 4.30 - 1.18 (m), 4.14 4.04 (m), 4.02 - 3.93 (m), 3.93 – 3.88 (m), 3.85 - 3.75 (m), 3.67 - 3.59 (s, broad), 3.37 (s), 2.00 - 1.88 (m), 1.85 -1.67 (m), 1.65 – 1.46 (m, two peaks), 1.45 – 1,34 (m), 1.32 – 1.15(m), 0.91 -0.81 (m). GPC data: PEG_{45}-*b*-PC(AzoOMe-C16)$_{18}$ 75/25 M_n = 8850, *Đ* = 1.11 PEG_{45}-*b*-PC(AzoOMe-C16)$_{18}$ 50/50 M_n = 9700, *Đ* = 1.10 PEG_{45}-*b*-PC(AzoOMe-C16)$_{18}$ 25/75 M_n = 9400, *Đ* = 1.09.

4.9.4 Thermal characterisation

Thermogravimetric analysis (TGA): TGA was performed at 10 °C min^{-1} under nitrogen atmosphere using a TGA Q5000IR from TA Instruments. TGA data were given as the onset of the decomposition curve.

Differential scanning calorimetry (DSC): DSC was performed using a DSC Q2000 from TA Instruments with samples (approx. 3 mg) sealed in aluminium pans at a scanning rate of 10 or 20 °C min^{-1} under a nitrogen atmosphere. Melting temperatures were read at the maximum of the transition peaks, and glass transition temperatures were read at the midpoint of the heat capacity increase.

4.9.5 Preparation and characterisation of self-assemblies

Self-assembly procedure. Milli-Q® water was gradually added to a solution of the copolymer (5 mg) in spectroscopic grade THF (1 mL) previously filtered through a 0.2 μm polytetrafluoroethylene (PTFE) filter. The self-assembly process was followed by measuring the loss of transmitted light intensity at 650 nm due to scattering as a function of water content. When a constant value of turbidity was reached, the resulting suspension was filtered through a 5 μm cellulose acetate filter and dialyzed against water using a Spectra/Por dialysis membrane (MWCO, 1 kDa) for 2 days to remove THF, changing water 3 times. Water suspensions of the polymeric self-assemblies were diluted with Milli-Q® water to a final concentration 1 mg mL^{-1}.

Determination of the Critical Aggregation Concentration and loading of Nile Red. Critical aggregation concentration (CAC) was determined by fluorescence

spectroscopy using Nile Red. 87 μL of a solution of Nile Red in dichloromethane (3.7×10^{-5} M) was added into a vial and the solvent evaporated. Then, 600 μL of the aqueous suspension of the polymeric aggregates with concentrations ranging from 1.0×10^{-4} to 1.0 mg mL^{-1} were added and stirred overnight in orbital shaker. The emission spectrum of Nile Red was registered from 560 to 700 nm while exciting at 550 nm.

Preparation of Cryo-TEM samples. 3 μL of a 1.0 mg mL^{-1} vesicular water dispersion was placed on a TEM Quantifoil carbon grid, excess of solvent was blotted away with filter paper and the grid freeze-plunged into liquid ethane using a FEI Vitrobot (FEI Company). Samples were maintained under liquid nitrogen with a Gatan TEM cryo-holder (FEI Company).

4.9.6 Irradiation Experiments

Irradiation experiments with UV light. Samples, either THF solutions at a concentration of 10^{-4} M (referred to the repetitive azobenzene unit) or aqueous suspensions of self-assemblies at a concentration of 1 mg BC mL^{-1}, were irradiated in a quartz UV cuvette, path length of 10 mm for THF solutions and 1 mm for aqueous suspensions, with a compact low-pressure fluorescent lamp Philips PL-S 9W emitting between 350 and 400 nm. Irradiance in the sample at 365 nm was 3.5 μW cm^{-2}.

Irradiation experiments with visible light. Samples, either THF solutions at a concentration of 10^{-4} M (referred to the repetitive azobenzene unit) or aqueous suspensions of self-assemblies at a concentration of 1 mg mL^{-1}, were irradiated in a quartz UV cuvette, path length of 10 mm for THF solutions and 1 mm for aqueous suspensions, with green (530 nm) or red light (625 nm) using a Mightex LCS-0530-15-22 or a Mightex LCS-0625-07-22 high power LED respectively. Irradiance in the sample at 530 or 625 nm was 30 μW cm^{-2}.

4.9.7 Encapsulation and light-stimulated release of Rhodamine B

Encapsulation of Rhodamine B. Rhodamine B loaded vesicles were prepared as described in **4.9.4 Self-assembly procedure** by adding a solution of Rhodamine B in water (the concentration was adjusted to have a final feed stock of 5 molecules of Rhodamine B per molecule of block copolymer) to a solution of the copolymer (5 mg) in spectroscopic grade THF (1 mL). Non-encapsulated Rhodamine B was removed during dialysis.

Rhodamine B concentration was determined by high performance liquid chromatography (HPLC) using a Waters 600 controller pump system with a mixture acetonitrile/100 mM ammonium acetate in water (8:2) as the mobile phase at a 1 mL min^{-1} flow rate, a column Waters Spherisorb 5µm C8 (4.6 × 250 mm, particle size 5 µm and pore size 80 Å) as stationary phase and a Waters 2998 PDA detector at 550 nm. Rhodamine B loaded self-assemblies water suspensions (250 µL) were diluted with acetonitrile (250 µL), sonicated for 10 min and injected into the HPLC system.

Light stimulated release of Rhodamine B. 0.6 mL aliquots of Rhodamine B loaded vesicular suspensions were placed in a glass vial and irradiated as described in **4.9.5 Irradiation Experiments**. Aliquots where then placed into a Slide-A-Lyzer™ 2K MWCO and 0.5 mL Dialysis Cassettes, dialysed against fresh Milli-Q water and the fluorescence of the dialysis water measured at different times.

4.10 References

(1) Kunze, L.; Wolfs, J.; Verkoyen, P.; Frey, H. Crystalline CO 2 -Based Aliphatic Polycarbonates with Long Alkyl Chains. *Macromol. Rapid Commun.* **2018**, *39*, 1800558. https://doi.org/10.1002/marc.201800558.

(2) Li, F.; Danquah, M.; Mahato, R. I. Synthesis and Characterization of Amphiphilic Lipopolymers for Micellar Drug Delivery. *Biomacromolecules* **2010**, *11*, 2610–2620. https://doi.org/10.1021/bm10056lv.

(3) Le Meins, J.-F.; Schatz, C.; Lecommandoux, S.; Sandre, O. Hybrid Polymer/Lipid Vesicles: State of the Art and Future Perspectives. *Mater. Today* **2013**, *16*, 397–402. https://doi.org/10.1016/j.mattod.2013.09.002.

(4) Rideau, E.; Dimova, R.; Schwille, P.; Wurm, F. R.; Landfester, K. Liposomes and Polymersomes: A Comparative Review towards Cell Mimicking. *Chem. Soc. Rev.* **2018**, *47*, 8572–8610. https://doi.org/10.1039/C8CS00162F.

(5) Owen, S. C.; Chan, D. P. Y.; Shoichet, M. S. Polymeric Micelle Stability. *Nano Today* **2012**, *7*, 53–65. https://doi.org/10.1016/j.nantod.2012.01.002.

(6) Won, Y.-Y.; Brannan, A. K.; Davis, H. T.; Bates, F. S. Cryogenic Transmission Electron Microscopy (Cryo-TEM) of Micelles and Vesicles Formed in Water by Poly(Ethylene Oxide)-Based Block Copolymers. *J. Phys. Chem. B* **2002**, *106*, 3354–3364. https://doi.org/10.1021/jp013639d.

(7) Rajagopal, K.; Mahmud, A.; Christian, D. A.; Pajerowski, J. D.; Brown, A. E. X.; Loverde, S. M.; Discher, D. E. Curvature-Coupled Hydration of Semicrystalline Polymer Amphiphiles Yields Flexible Worm Micelles but Favors Rigid Vesicles: Polycaprolactone-Based Block Copolymers. *Macromolecules* **2010**, *43*, 9736–9746. https://doi.org/10.1021/ma101316w.

(8) Qi, H.; Zhou, H.; Tang, Q.; Lee, J. Y.; Fan, Z.; Kim, S.; Staub, M. C.; Zhou, T.; Mei, S.; Han, L.; Pochan, D. J.; Cheng, H.; Hu, W.; Li, C. Y. Block Copolymer Crystalsomes with an Ultrathin Shell to Extend Blood Circulation Time. *Nat. Commun.* **2018**, *9*, 3005. https://doi.org/10.1038/s41467-018-05396-x.

(9) Ishii, K.; Hamada, T.; Hatakeyama, M.; Sugimoto, R.; Nagasaki, T.; Takagi, M. Reversible Control of *Exo* - and *Endo* -Budding Transitions in a Photosensitive Lipid Membrane. *ChemBioChem* **2009**, *10*, 251–256. https://doi.org/10.1002/cbic.200800482.

(10) Blasco, E.; Serrano, J. L.; Piñol, M.; Oriol, L. Light Responsive Vesicles Based on Linear–Dendritic Block Copolymers Using Azobenzene–Aliphatic Codendrons. *Macromolecules* **2013**, *46*, 5951–5960. https://doi.org/10.1021/ma4009725.

(11) Tyrrell, Z. L.; Shen, Y.; Radosz, M. Fabrication of Micellar Nanoparticles for Drug Delivery through the Self-Assembly of Block Copolymers. *Prog. Polym. Sci.* **2010**, *35*, 1128–1143. https://doi.org/10.1016/j.progpolymsci.2010.06.003.

CHAPTER 5

DRUG LOADED AMPHIPHILIC BC NANOCARRIERS CELL VIABILITY STUDIES

5.1 Introduction and aims

The use of polymeric self-assemblies as drug nanocarriers has been recognised as an attractive strategy to overcome the side effects of drugs and improve the therapeutic effects of traditional formulations. Amongst their benefits are the improved solubilisation of non-soluble drugs in physiological media, reduction of secondary effects, protection of the drug until it reaches the site of action or the possibility of controlled release at the specific targeting sites.[1,2,3] The objective of this chapter was to evaluate the cytotoxicity of some of the self-assembled structures reported in previous chapters and their potential for effective loading and delivering of drugs.

The selected drug was Paclitaxel, an hydrophobic chemotherapeutic agent with activity against different human cancers and a very low solubility in water (Figure 5.1).[4,5] The self-assemblies selection was based on their demonstrated capability to encapsulate small fluorescent molecular probes and release them upon visible or NIR light irradiation. Cell viability of two cell lines, Huh-5-2 and HeLa, was tested against the selected amphiphilic BCs. Then, Paclitaxel loaded self-assemblies were tested as drug delivery systems and their cytotoxicity compared with that of free Paclitaxel.

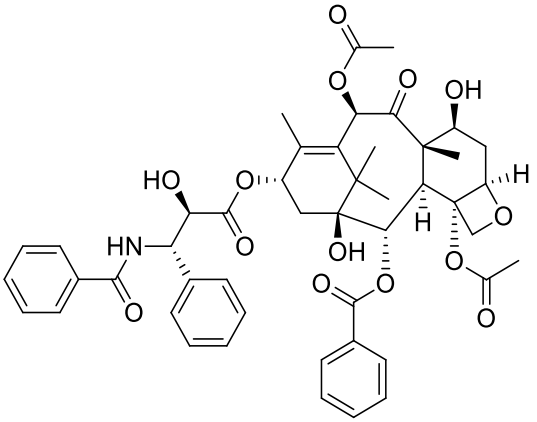

Figure 5.1: Paclitaxel.

According to the objective, the main tasks carried out in this chapter were:

- Encapsulation of Paclitaxel on amphiphilic BCs selected from the previous chapters.
- Determination of the concentration of encapsulated Paclitaxel and characterisation of the self-assembled structures with encapsulated Paclitaxel.
- Evaluation of the cytotoxicity of the unloaded polymeric nanocarriers against HeLa and Huh-5-2 cell lines.
- Study of the cytotoxicity of Paclitaxel loaded polymeric nanocarriers against HeLa and Huh-5-2 cell lines.
- Study of the photoinduced release of Paclitaxel and its influence on the cell viability.

5.2 Nanocarriers from coumarin ester based amphiphilic BCs

It was stated in **Chapter 2** that the self-assembled micelles from **PEG-*b*-PC(DAP/T$_1$Cou)** and **PEG-*b*-PC(Cou)** were able to encapsulate Nile Red, which is a fluorescent hydrophobic molecular probe, and release it under light stimulation. Encouraged by the findings, the drug loading abilities of the micelles was investigated using Paclitaxel, a hydrophobic anticancer drug.

Paclitaxel was loaded into the micelles by the co-solvent method during the self-assembly process, starting from a solution of the copolymer and the drug in THF and adding water slowly. The organic solvent was removed by dialysis while the residual unloaded Paclitaxel was eliminated by filtration through 0.22 μm filters. The amount of Paclitaxel loaded in the polymeric micelles was determined by high performance liquid chromatography (HPLC) after disrupting the micelles in an organic solvent. Then, Drug loading (DL) capacities and encapsulation efficiency (EE) were determined using Equation 5.1 and Equation 5.2.

Equation 5.1
$$\text{DL (\%)} = 100 \times \frac{\text{Encapsulated Paclitaxel mass}}{\text{Total micelles mass}}$$

Equation 5.2
$$\text{EE (\%)} = 100 \times \frac{\text{Encapsulated Paclitaxel mass}}{\text{Feed Paclitaxel mass}}$$

The results are summarized in Table 5.1. Indeed, the incorporation efficiency generally depends on the initial amount of drug added on the loading process. In this case rather high EE values, about 40-50%, were reached in all cases considering the moderate-to-low Paclitaxel/polymer mass ratios used, which ranged from 0.6:5.0 to 2.4:5.0. Analysis of the data showed that EE values were higher for **PEG-*b*-PC(Cou)** than for **PEG-*b*-PC(DAP/T$_1$Cou)**. Besides, the EE of **PEG-*b*-PC(DAP/T$_1$Cou)** micelles was just above 40% independently of the initial amount of drug used. Likewise, DL was also higher for **PEG-*b*-PC(Cou)** than for **PEG-*b*-PC(DAP/T$_1$Cou)** self-assemblies. DLs about 20% were reached for **PEG-*b*-PC(Cou)** and **PEG-*b*-PC(DAP/T$_1$Cou)**, but such highly loaded micelles ended up into a macroscopic precipitate within a few hours of their preparation. Nevertheless, stable micellar suspensions were obtained with DL of 11.2 and 10.0% (corresponding to 46.8 and 41.9% encapsulation efficiencies) for **PEG-*b*-PC(Cou)**

and **PEG-*b*-PC(DAP/T$_1$Cou)** respectively. Paclitaxel is poorly soluble in water with reported solubility values below 10 μg mL^{-1}.[4,5] Therefore, by using these polymeric self-assemblies Paclitaxel concentration values were increased up to 253 μg mL^{-1} with **PEG-*b*-PC(Cou)** and 186 μg mL^{-1} with **PEG-*b*-PC(DAP/T$_1$Cou)** (Table 5.1).

Table 5.1: Characterisation of Paclitaxel loaded micelles.

Polymer	Feed ratio Paclitaxel/copolymer (mg/mg)	EE (%)	DL (%)	Paclitaxel concentration		Stability
				μg mL^{-1}	μM	
PEG-*b*-PC(Cou)	0.6 / 5.0	50.8	6.1	87	0.102	Good
PEG-*b*-PC(Cou)	1.2 / 5.0	46.8	11.2	253	0.296	Good
PEG-*b*-PC(Cou)	2.4 / 5.0	44.0	21.1	453	0.531	Precipitate
PEG-*b*-PC(DAP/T$_1$Cou)	0.6 / 5.0	40.8	4.9	91	0.107	Good
PEG-*b*-PC(DAP/T$_1$Cou)	1.2 / 5.0	41.9	10.0	186	0.218	Good
PEG-*b*-PC(DAP/T$_1$Cou)	2.4/ 5.0	40.7	19.5	424	0.497	Precipitate

Paclitaxel loaded micelles were characterised by DLS measurements and no appreciable changes in the D_h were observed for loaded **PEG-*b*-PC(Cou)** micelles when compared to unloaded ones. Whereas, those from **PEG-*b*-PC(DAP/T$_1$Cou)** suffered a slight decrease in the D_h (Figure 5.2).

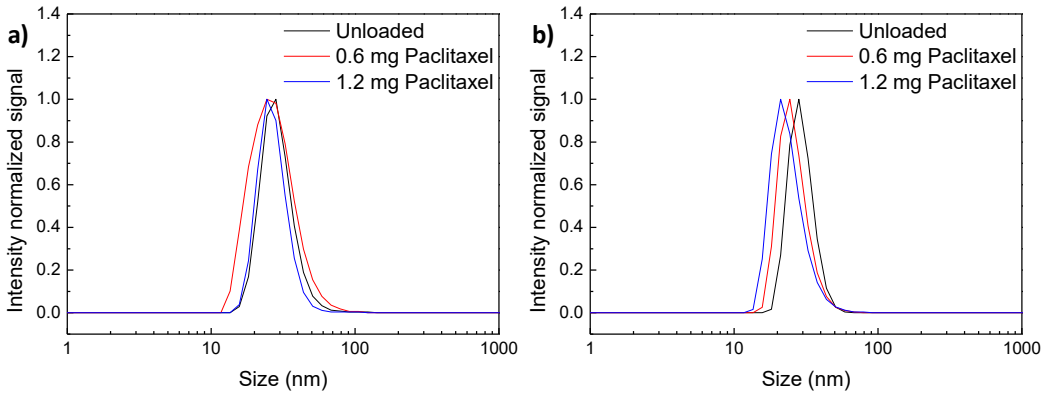

Figure 5.2: Paclitaxel loaded micelles DLS measurements for **PEG-*b*-PC(Cou)** (a) and **PEG-*b*-PC(DAP/T$_1$Cou)** (b).

Cell viability of HeLa and Huh-5-2 cell lines against unloaded micelles, Paclitaxel loaded micelles and free Paclitaxel was assayed using the 3-(4,5-dimethylthiazol-2-yl)-2,5-diphenyltetrazolium bromide (MTT) assay for

incubation times of 72 h (see Experimental Section for further details). In order to have comparable data, concentration of Paclitaxel was the same in experiments with Paclitaxel loaded micelles and free Paclitaxel. Also, the polymer concentration was the same for experiments with Paclitaxel loaded micelles and unloaded micelles. The results of cell viability studies are collected in Figure 5.3.

Unloaded micelles from **PEG-*b*-PC(Cou)** and **PEG-*b*-PC(DAP/T_1Cou)** showed no cytotoxicity below a 3 μg mL^{-1} copolymer concentration. At concentrations above 5 μg mL^{-1} cell viability decreased sharply, being the cytotoxicity of **PEG-*b*-PC(DAP/T_1Cou)** micelles appreciable higher than those from **PEG-*b*-PC(Cou)** (Figure 5.3 a and b).

Cell viability of HeLa cells against Paclitaxel loaded **PEG-*b*-PC(Cou)** and **PEG-*b*-PC(DAP/T_1Cou)** micelles was evaluated for Paclitaxel concentrations ranging from 1.38 to 0.02 nM. Paclitaxel loaded **PEG-*b*-PC(Cou)** and **PEG-*b*-PC(DAP/T_1Cou)** micelles showed a much higher cytotoxicity at concentrations below 0.4 nM than free Paclitaxel (Figure 5.3 b and d). Free Paclitaxel half maximal inhibitory concentration (IC50) was found to be 0.2 nM at 72 h incubation time, whereas the IC50 for encapsulated Paclitaxel was found to be below the lowest encapsulated Paclitaxel concentration, 0.02 nM, both for **PEG-*b*-PC(Cou)** and **PEG-*b*-PC(DAP/T_1Cou)** Paclitaxel loaded micelles, which is more than ten times lower.

In comparison to free Paclitaxel, when encapsulated Paclitaxel show enhanced cytotoxicity, the copolymer concentration was below 0.15 μg mL^{-1}. Because at this polymer concentration unloaded micelles showed no cytotoxicity, this suggests that the enhanced cytotoxicity of encapsulated Paclitaxel is due to a more effective delivery of Paclitaxel to the cells in comparison to free Paclitaxel, and not by effect of the copolymer by itself (Figure 5.3). In an attempt to gain information about the internalisation of loaded micelles into the cells, studies by confocal microscopy were carried out. Unfortunately, as stated in **Chapter 2**, coumarin fluorescence is self-quenched in the micelles core and it was not possible to track the internalisation processes.

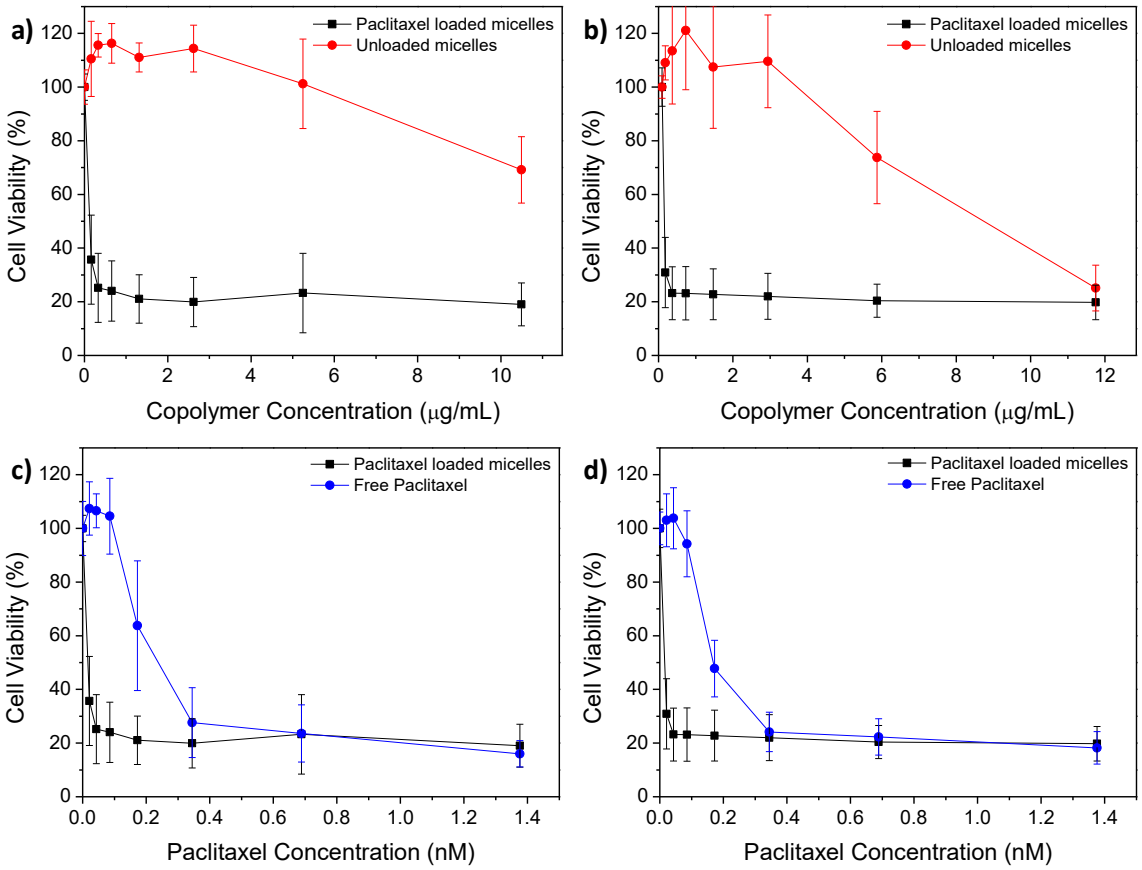

Figure 5.3: Paclitaxel loaded micelles (black), unloaded micelles (red) and free Paclitaxel cytotoxicity (blue) cell viability study against HeLa cell line for **PEG-*b*-PC(Cou)** (a and c) and **PEG-*b*-PC(DAP/T$_1$Cou)** (b and d).

Aimed by the great difference in the effectivity of encapsulated and free Paclitaxel at low concentrations, a time-lapse study in a bright-field microscope was carried out at a 0.02 nM Paclitaxel concentration and the same incubation conditions than those for the cell viability studies. Images are shown in Figure 5.4 for **PEG-*b*-PC(Cou)** and Figure 5.5 for **PEG-*b*-PC(DAP/T$_1$Cou)**. For encapsulated Paclitaxel, in either **PEG-*b*-PC(Cou)** or **PEG-*b*-PC(DAP/T$_1$Cou)** micelles, after 10 h of incubation the majority of the cells appear detached from the plate, whereas after 20 h most of them seem to be apoptotic. However, for free Paclitaxel, after 40 h, most of cells were still attached to the flask and in good shape evidencing the improved delivery of Paclitaxel to cells when using any of the described polymeric micelles as nanocarriers.

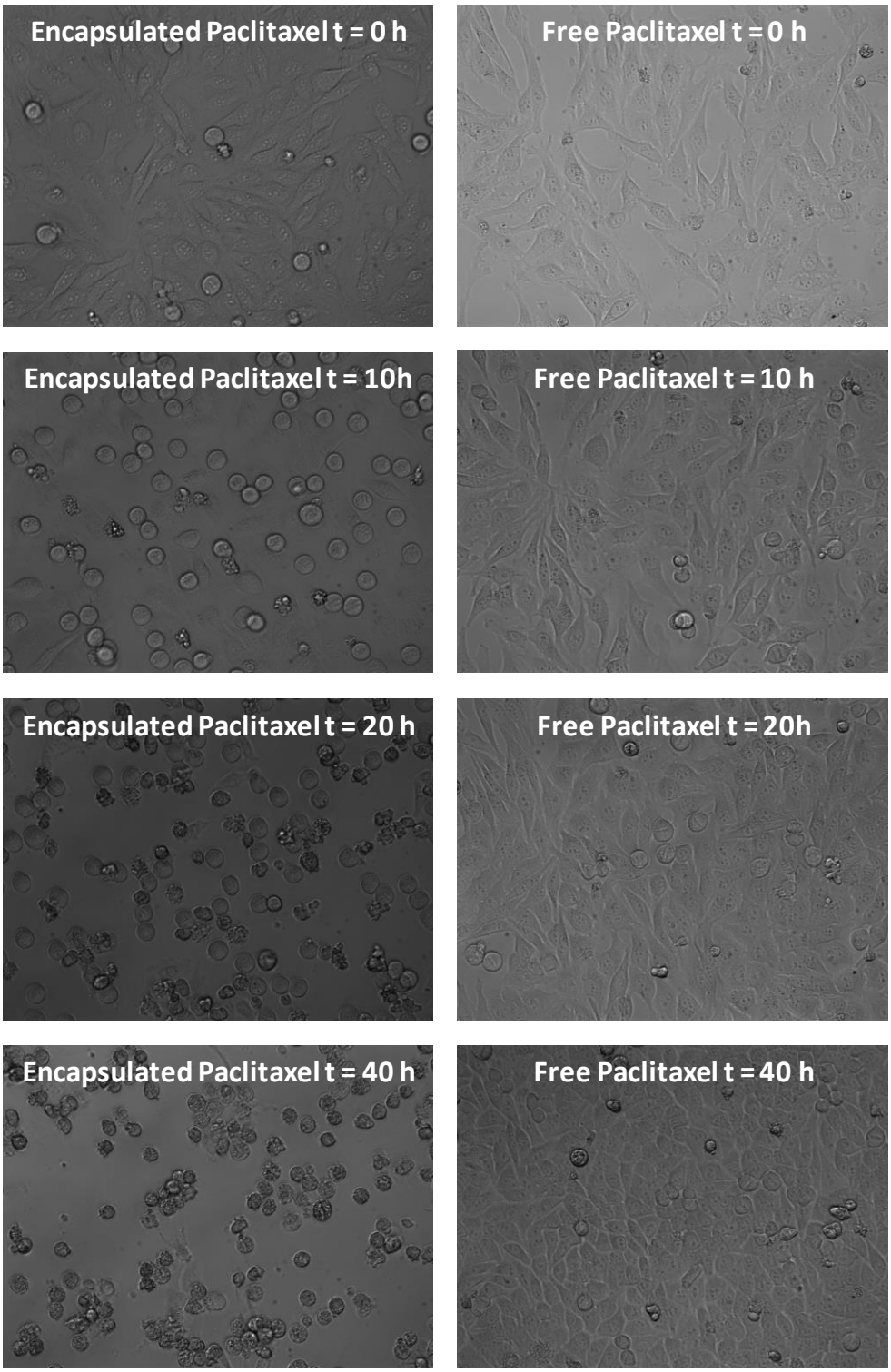

Figure 5.4: Time-lapse studies in a bright field microscope at a 0.02 nM Paclitaxel concentration and different incubation times for Paclitaxel loaded **PEG-*b*-PC(Cou)** micelles (0.16 μg mL^{-1}) and free Paclitaxel in HeLa cell line.

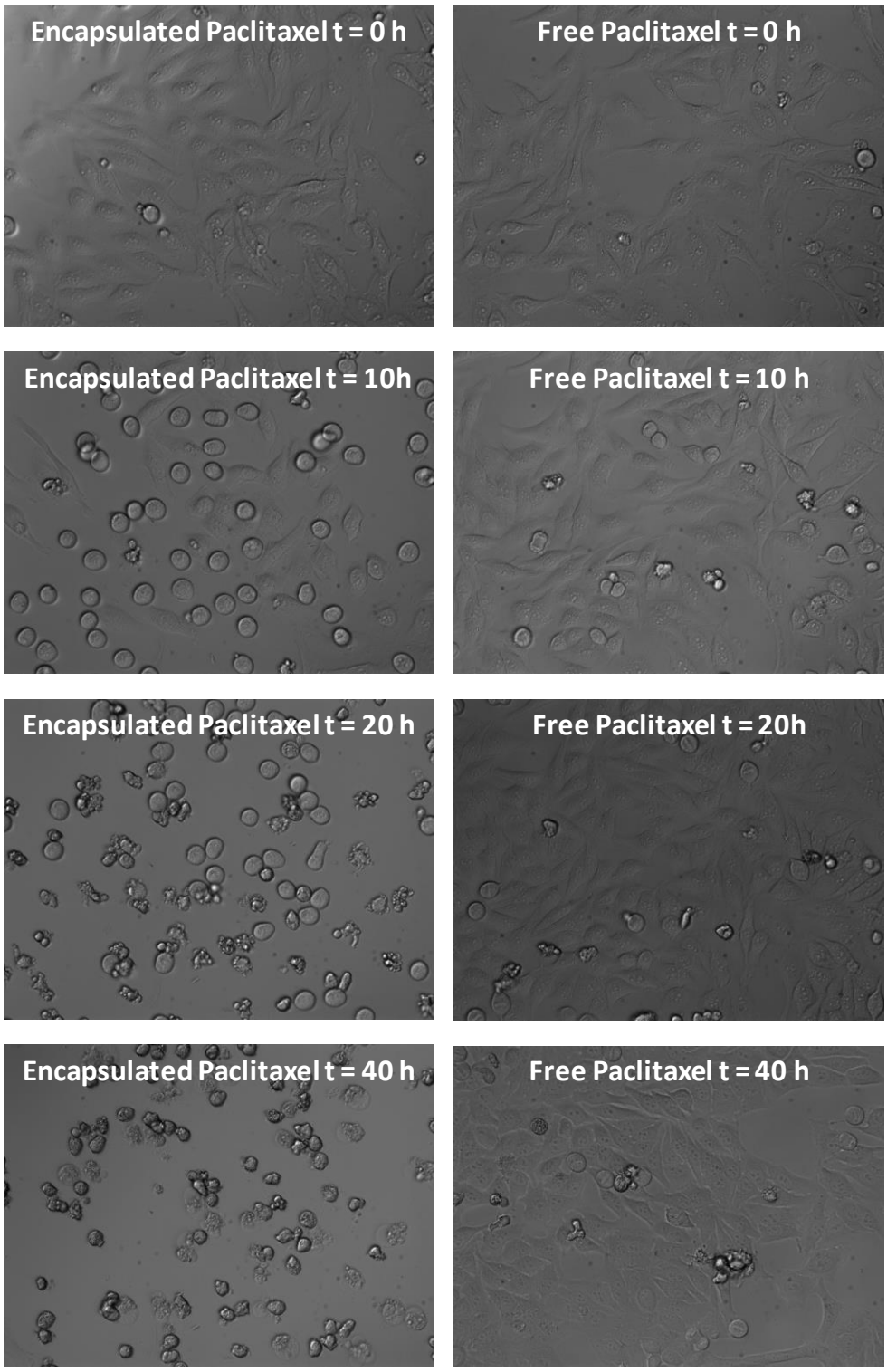

Figure 5.5: Time-lapse studies in a bright field microscope at a 0.02 nM Paclitaxel concentration and different incubation times for Paclitaxel loaded **PEG-*b*-PC(DAP/T$_1$Cou)** micelles (0.18 μg mL^{-1}) and free Paclitaxel in HeLa cell line.

For Huh-5-2 cell line, unloaded micelles from **PEG-*b*-PC(Cou)** and **PEG-*b*-PC(DAP/T$_1$Cou)** showed no cytotoxicity in the range of polymer concentration studied, from 10.5 to 0.16 μg mL^{-1} (Figure 5.6 a and b). Again, Paclitaxel loaded **PEG-*b*-PC(Cou)** and **PEG-*b*-PC(DAP/T$_1$Cou)** micelles showed higher cytotoxicity in comparison to free Paclitaxel in all the concentrations range studied, from 1.37 to 0.02 nM. Paclitaxel loaded **PEG-*b*-PC(Cou)** and **PEG-*b*-PC(DAP/T$_1$Cou)** micelles had an IC50 around 0.7 nM, while the IC50 of free Paclitaxel was not detected in the range of concentration studied, being the highest concentration 1.37 nM.

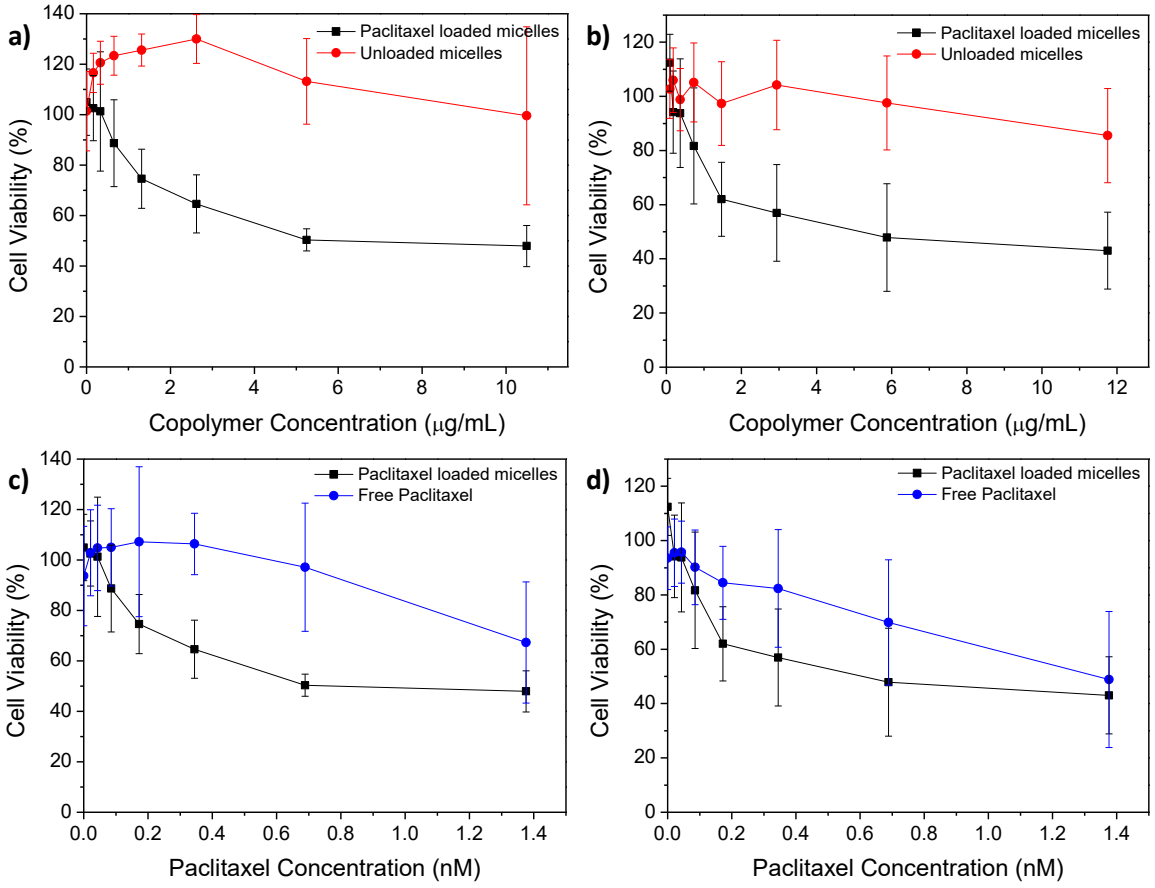

Figure 5.6: Paclitaxel loaded micelles (black), unloaded micelles (red) and free Paclitaxel cytotoxicity (blue) study against Huh-5-2 cell line for **PEG-*b*-PC(Cou)** (a and c) and **PEG-*b*-PC(DAP/T$_1$Cou)** (b and d).

Time-lapse studies were also performed to gain information about differences in the behaviour between encapsulated and free Paclitaxel within the incubation time, at a Paclitaxel concentration of 0.17 nM, which it is the concentration at which the difference in cell viability between encapsulated and free Paclitaxel is greater. Due

to different morphology of HeLa and Huh-5-2 cell lines, for Huh-5-2 differences were not as apparent, though differences were observed after 20 and 40 h incubation times between encapsulated and free Paclitaxel, as the number of detached cells is appreciable higher for the Paclitaxel loaded self-assemblies than for free Paclitaxel (Figure 5.7 and Figure 5.8)

Preliminary *in vitro* test to evaluate the light release of Paclitaxel from loaded micelles and its effect on cytotoxicity were carried using UV light. However, two decisive obstacles were found. Firstly, Paclitaxel was not stable under UV. Secondly, the death of cells was detected at shorter irradiation times than those required in **Chapter 2** for the liberation of Nile Red. Unfortunately, the use of NIR light source was not available for *in vitro* experiments. Thus, the irradiation with UV or NIR light was discarded and attention was focussed on the copolymers with azobenzene units responsive under visible light reported in **Chapter 3** and **Chapter 4.**

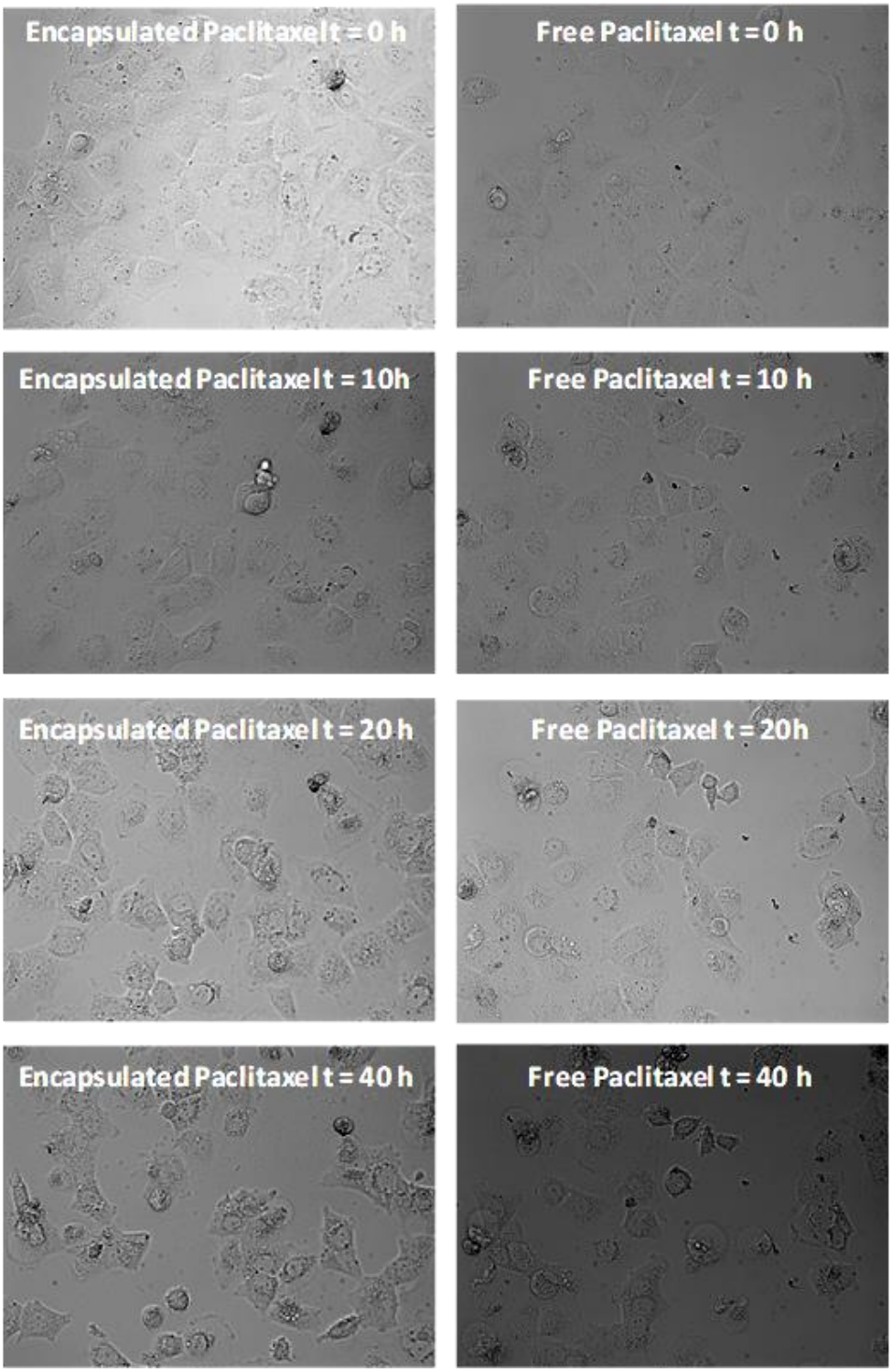

Figure 5.7: Time-lapse studies in a bright field microscope at a 0.17 nM Paclitaxel concentration and different incubation times for **PEG-b-PC(Cou)** Paclitaxel loaded micelles (1.31 μg mL^{-1}) and free Paclitaxel in Huh-5-2 cell line.

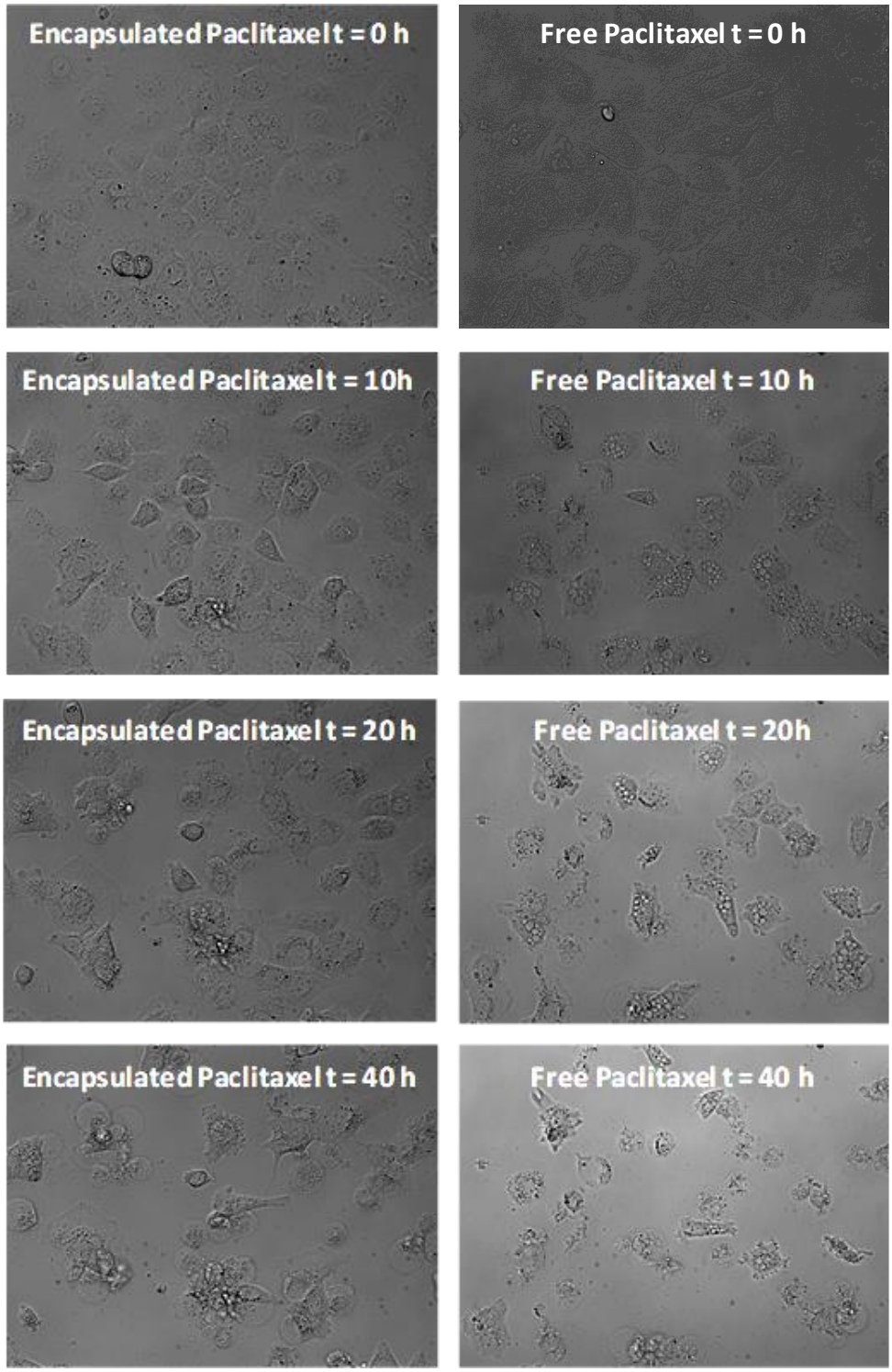

Figure 5.8: Time-lapse studies in a bright field microscope at a 0.17 nM Paclitaxel concentration and different incubation times for **PEG-b-PC(DAP/T$_1$Cou)** Paclitaxel loaded micelles (1.47 μg mL^{-1}) and free Paclitaxel in Huh-5-2 cell line.

5.3 Nanocarriers from azobenzene amphiphilic BCs

Based on results presented in **Chapter 3** and **Chapter 4**, vesicles from **PEG$_{45}$-*b*-PC(AzoOMe)$_{18}$** and **PEG$_{45}$-*b*-PC(AzoOMe-C16)$_{18}$ 75/25** for *in vitro* studies with Paclitaxel. The selection was made according their loading and releasing ability activated by visible light demonstrated with molecular fluorescent probes.

Paclitaxel loaded **PEG$_{45}$-*b*-PC(AzoOMe)$_{18}$** and **PEG$_{45}$-*b*-PC(AzoOMe-C16)$_{18}$ 75/25** vesicles were prepared as described for coumarin based micelles using a 1.2:5.0 Paclitaxel/copolymer mass ratio. Being poorly water soluble drug, Paclitaxel should be physically entrapped within the hydrophobic membrane of the vesicle upon self-assembly. Encapsulation efficiencies and total amount of encapsulated Paclitaxel were similar for both systems, with EE around 28% and DL around 6.8% and good stability over 1 week (Table 5.2). Paclitaxel concentration was found to be approximately 115 μg mL^{-1} (Table 5.2), lower than the concentration reached with the micelles from **PEG-*b*-PC(DAP/T$_1$Cou)** and **PEG-*b*-PC(Cou)** but still higher than Paclitaxel solubility in water.[6]

Table 5.2: Characterisation of Paclitaxel loaded vesicles.

Polymer	Feed ratio Paclitaxel/copolymer (mg/mg)	EE (%)	DL (%)	Paclitaxel concentration		Stability
				μg mL^{-1}	μM	
PEG$_{45}$-*b*-PC(AzoOMe)$_{18}$	1.2 / 5.0	28.8	6.9	115	0.135	Good
PEG$_{45}$-*b*-PC(AzoOMe-C16)$_{18}$ 75/25	1.2 / 5.0	27.9	6.7	112	0.131	Good

Encapsulation of Paclitaxel led to a notable increase in the D_h and dispersity of the self-assemblies from **PEG$_{45}$-*b*-PC(AzoOMe)$_{18}$** while the size and dispersity of Paclitaxel loaded **PEG$_{45}$-*b*-PC(AzoOMe-C16)$_{18}$ 75/25** vesicles remained almost constant (Figure 5.9).

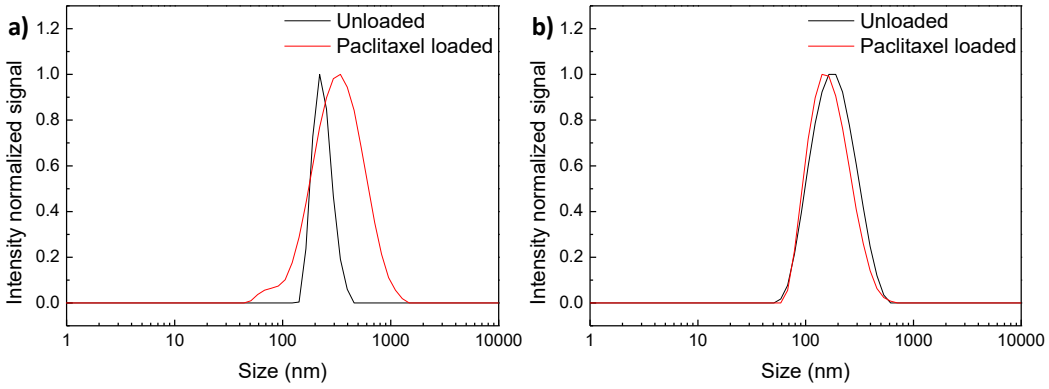

Figure 5.9: Paclitaxel loaded vesicles DLS measurements for **PEG45-*b*-PC(AzoOMe)$_{18}$** (a) and **PEG$_{45}$-*b*-PC(AzoOMe-C16)$_{18}$ 75/25** (b).

Even if loading capabilities were almost identical for **PEG$_{45}$-*b*-PC(AzoOMe)$_{18}$** and **PEG$_{45}$-*b*-PC(AzoOMe-C16)$_{18}$ 75/25** vesicles, visible light induced release using 530 nm light was investigated only for **PEG$_{45}$-*b*-PC(AzoOMe)$_{18}$** as it proved to have better response to light in **Chapter 3**. Initially, the effect of the illumination conditions was assessed. Cells were incubated for 24 h, then illuminated at 530 nm for 10 min and finally incubated by additional 48 h, proving the tolerance of the cells to these conditions.

Thus, cell viability studies were performed with Paclitaxel loaded **PEG$_{45}$-*b*-PC(AzoOMe)$_{18}$** vesicles, free Paclitaxel and unloaded vesicles. Cells were incubated for 24 h, then half of the plates were illuminated for 10 min with 530 nm light, and finally incubated for additional 48 h. Cell viability was not affected by unloaded **PEG$_{45}$-*b*-PC(AzoOMe)$_{18}$** vesicles if polymer concentration was kept below 4 μg mL^{-1}. At the same polymer concentration, Paclitaxel loaded vesicles showed an enhanced cytotoxicity in comparison to free Paclitaxel in all the range of concentrations studied (Figure 5.10). Paclitaxel loaded vesicles showed an IC50 of approximately 0.025 nM whereas the IC50 of free Paclitaxel is about 0.2 nM (Figure 5.10), eight times superior. Therefore, Paclitaxel cytotoxicity is enhanced by encapsulation into the self-assemblies

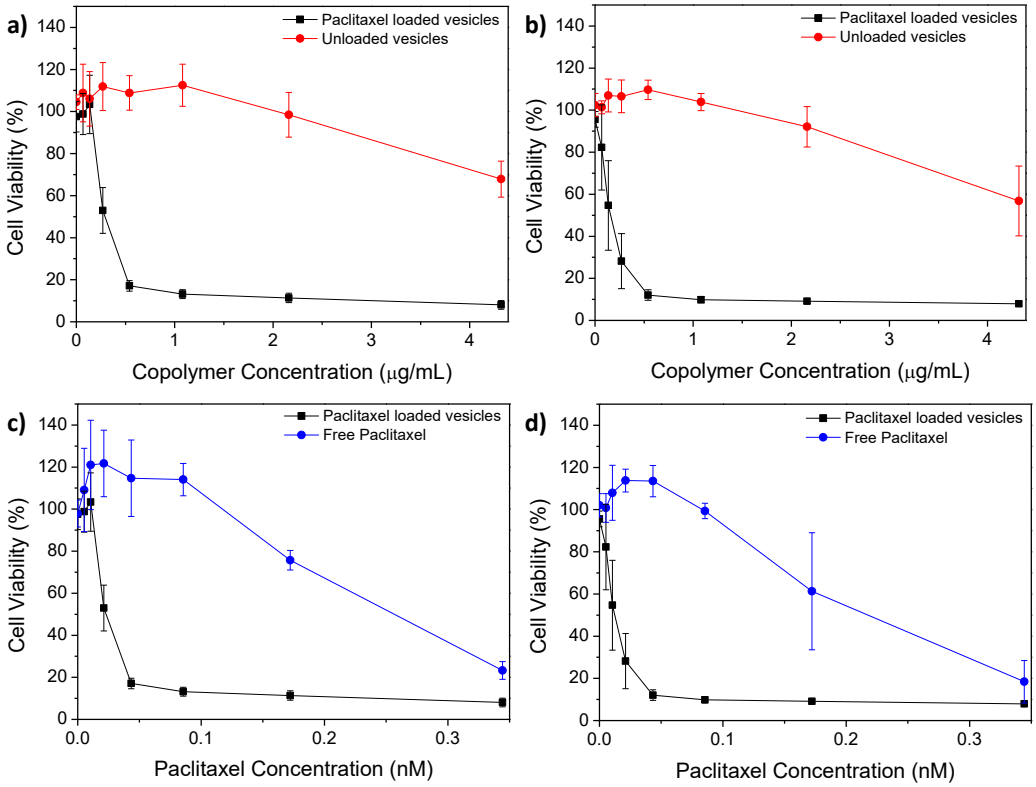

Figure 5.10: Paclitaxel loaded vesicles (black), unloaded vesicles (red) and free Paclitaxel cytotoxicity (blue) study against HeLa cell line for **PEG_{45}-*b*-PC(AzoOMe)$_{18}$** without (a and c) and with 10 min 530 nm illumination (b and d).

Similar general tendencies were observed upon illumination. However, the IC50 was approximately 0.013 nM for Paclitaxel loaded self-assemblies, which is half of the IC50 value determined for the non-illuminated conditions. Thus, at the same Paclitaxel concentration, toxicity was improved by 530 nm light irradiation (Figure 5.11). Because the effect of light and the copolymer concentration have been discarded, the conclusions is that visible light stimulates the release of Paclitaxel

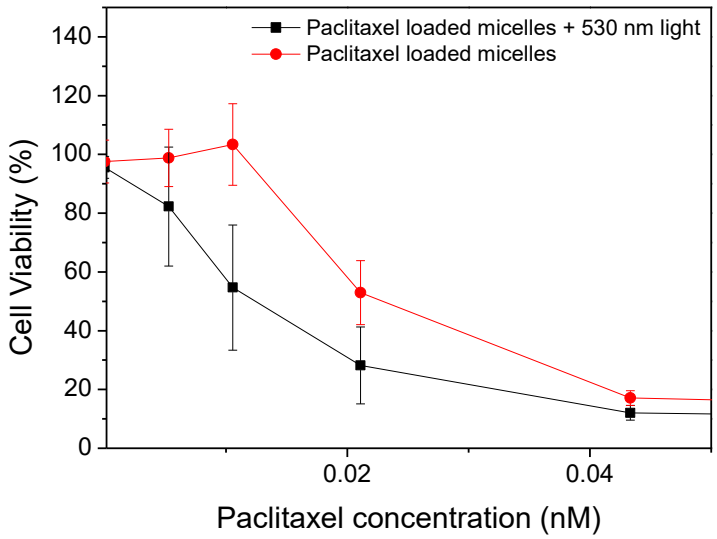

Figure 5.11: Paclitaxel loaded vesicles cytotoxicity study against HeLa cell line with and without 530 nm light irradiation at low Paclitaxel concentrations.

5.4 Conclusions

Micelles from **PEG-*b*-PC(Cou)** and **PEG-*b*-PC(DAP/T$_1$Cou)**, reported in **Chapter 2**, and vesicles from **PEG$_{45}$-*b*-PC(AzoOMe)$_{18}$** and **PEG$_{45}$-*b*-PC(AzoOMe-C16)$_{18}$ 75/25**, reported in **Chapter 3** and **Chapter 4**, have proved to be suitable polymeric nanocarriers for a stable encapsulation of Paclitaxel, enhancing greatly in all cases its solubility in water, specially the micelles.

The copolymers studied in this chapter have proved to be not cytotoxic against the studied cell lines, HeLa and Huh-5-2, except at high copolymer concentrations. However, these cytotoxic polymer concentrations are higher than the ones required to have Paclitaxel loaded micelles with effective therapeutic activity. Encapsulation of Paclitaxel into the self-assemblies has proved to increase Paclitaxel cytotoxicity against HeLa and Huh-5-2 cell lines, which accompanied by the low cytotoxicity of the self-assemblies by itself, seems to indicate an increased effectiveness in the delivery of Paclitaxel to cells.

Finally, it has been demonstrated that Paclitaxel release can be stimulated by irradiation with 530 nm light using **PEG$_{45}$-*b*-PC(AzoOMe)$_{18}$** vesicles.

5.5 Experimental Section

5.5.1 Preparation of Paclitaxel loaded self-assemblies

Milli-Q® water was gradually added to a solution of the copolymer (5 mg) and Paclitaxel (0.6, 1.2 or 2.4 mg) in spectroscopic grade THF (1 mL) previously filtered through a 0.2 μm polytetrafluoroethylene (PTFE) filter. The self-assembly process was followed by measuring the loss of transmitted light intensity at 650 nm due to scattering as a function of water content. When a constant value of turbidity was reached, the resulting suspension was filtered through a 5 μm cellulose acetate filter and dialyzed against water using a Spectra/Por dialysis membrane (MWCO, 1 kDa) for 2 days to remove THF, changing water 3 times. The dialyzed suspensions were then filtered with a 0.45 μm for **PEG-*b*-PC(DAP/T_1Cou)** and **PEG-*b*-PC(Cou)** or a 5.0 μm for **PEG_{45}-*b*-PC(AzoOMe)$_{18}$** and **PEG_{45}-*b*-PC(AzoOMe-C16)$_{18}$ 75/25** to remove non-encapsulated Paclitaxel.

5.5.2 Determination of Paclitaxel concentration

Paclitaxel concentration was determined by high performance liquid chromatography (HPLC). HPLC measurements were carried out using a Waters 600 controller pump system with a mixture acetonitrile/water (1:1) as the mobile phase at a 1 mL min^{-1} flow rate, a column Waters Spherisorb 5μm C8 (4.6 x 250 mm, particle size 5 μm and pore size 80 Å) as stationary phase and a Waters 2998 PDA detector at 227 nm.

Paclitaxel loaded self-assemblies water suspensions (250 μL) were diluted with acetonitrile (250 μL), sonicated for 10 min and injected into the HPLC system.

5.5.3 Cell culture

HeLa cells were grown in Dulbecco's modified Eagle's medium (DMEM; Gibco), supplemented with 1x non-essential amino acids (Gibco), 100 IU mL^{-1} penicillin (Gibco), 100 μg mL^{-1} streptomycin (Gibco).

Huh-5-2 cells were grown in Dulbecco's modified Eagle's medium (DMEM; Gibco), supplemented with 1x non-essential amino acids (Gibco), 100 IU mL^{-1} penicillin (Gibco), 100 μg mL^{-1} streptomycin (Gibco) and 250 μg mL^{-1} geneticin G418 (Gibco).

5.5.4 Cytotoxicity assays

HeLa or Huh 5-2 cell lines were seeded at a density of approximately $7x10^3$ cells per well in a 96-well plate with a volume of 100 μL of DMEM (supplemented as described in **Section 4.2.3**). After 24 h, DMEM was removed and 100 μL of DMEM with serial dilutions of the tested compounds (Paclitaxel loaded self-assemblies, free Paclitaxel and unloaded self-assemblies) were added. Cells were allowed to proliferate at 5% CO_2 concentration and 37 °C for 72 h. Cell number was determined by CellTiter 96 Aqueous One Solution Cell Proliferation Assay (Promega)

5.5.5 Determination of the phototoxicity of 530 nm light.

HeLa cells were seeded at a density of approximately $7x10^3$ cells per well in six 96-well plates with a volume of 100 μL of DMEM (supplemented as described in **Section 4.2.3**). After 24 h of incubation, half of the plates were illuminated with 530 nm light (Irradiance in the sample at 530 was 30 μW cm^{-2}). After a total of 72h of incubation, cell number was determined by CellTiter 96 Aqueous One Solution Cell Proliferation Assay (Promega).

5.5.6 Cytotoxicity assays including 530 nm light illumination

HeLa cell lines were seeded at a density of approximately $7x10^3$ cells per well in a 96-well plate with a volume of 100 μL of DMEM (supplemented as described in **Section 4.2.3**). After 24 h, DMEM was removed and 100 μL of DMEM with serial dilutions of the tested compounds (Paclitaxel loaded self-assemblies, free Paclitaxel and unloaded self-assemblies) were added. After 24 h of incubation, the plates were illuminated with 530 nm light (Irradiance in the sample at 530 was 30 μW cm^{-2}). Cells were allowed to proliferate at 5% CO_2 concentration and 37 °C for 48 h. Cell number was determined by CellTiter 96 Aqueous One Solution Cell Proliferation Assay (Promega)

5.6 References

(1) Cabral, H.; Miyata, K.; Osada, K.; Kataoka, K. Block Copolymer Micelles in Nanomedicine Applications. *Chem. Rev.* **2018**, *118*, 6844–6892. https://doi.org/10.1021/acs.chemrev.8b00199.

(2) Panyam, J.; Labhasetwar, V. Biodegradable Nanoparticles for Drug and Gene Delivery to Cells and Tissue. *Adv. Drug Deliv. Rev.* **2003**, *55*, 329–347. https://doi.org/10.1016/S0169-409X(02)00228-4.

(3) Chen, G.; Roy, I.; Yang, C.; Prasad, P. N. Nanochemistry and Nanomedicine for Nanoparticle-Based Diagnostics and Therapy. *Chem. Rev.* **2016**, *116*, 2826–2885. https://doi.org/10.1021/acs.chemrev.5b00148.

(4) Choi-Sledeski, Y. M.; Wermuth, C. G. Designing Prodrugs and Bioprecursors. In *The Practice of Medicinal Chemistry*; Elsevier, 2015; pp 657–696. https://doi.org/10.1016/B978-0-12-417205-0.00028-6.

(5) Surapaneni, M. S.; Das, S. K.; Das, N. G. Designing Paclitaxel Drug Delivery Systems Aimed at Improved Patient Outcomes: Current Status and Challenges. *ISRN Pharmacol.* **2012**, *2012*, 1–15. https://doi.org/10.5402/2012/623139.

(6). Chen, W.; Meng, F.; Cheng, R.; Zhong, Z. pH-Sensitive Degradable Polymersomes for Triggered Release of Anticancer Drugs: A Comparative Study with Micelles. *J. Control. Release* **2010**, *142*, 40–46. https://doi.org/10.1016/j.jconrel.2009.09.023.

Conclusiones

A continuación, se resumen el trabajo realizado y los resultados obtenidos en cada uno de los capítulos en los que se ha organizado esta tesis doctoral.

Capítulo 2: Se han sintetizado copolímeros dibloque anfífilos funcionalizados en la cadena lateral del bloque hidrófobo con unidades de éster de cumarina mediante una aproximación supramolecular o mediante una aproximación covalente. Sobre un polímero de policarbonato biodegradable obtenido por polimerización controlada por apertura de anillo se han insertado por medio de reacciones altamente eficaces, o bien un análogo de una nucleobase capaz de reconocer la unidad timina portadora del éster de cumarina por enlace de hidrogeno, o directamente el éster de cumarina por enlace covalente. Estos polímeros son capaces de autoensamblarse en micelas al ser dispersados en agua y encapsular moléculas pequeñas. Se ha comprobado que la presencia de estas unidades de éster de cumarina en la estructura del copolímero permite usar estos sistemas como nanotransportadores en los que la liberación es estimulada con luz NIR, más penetrante y menos perjudicial en tejidos biológicos que la luz UV, usada como prueba de concepto. Se ha demostrado que la inserción de la unidad de éster de cumarina mediante una aproximación supramolecular proporciona materiales con un comportamiento equiparable a los obtenidos mediante aproximación covalente.

Capítulo 3: Se han preparado una serie de copolímeros dibloque anfífilos funcionalizados en la cadena lateral del bloque hidrófobo de policarbonato alifático con unidades azobenceno tetra-*orto*-metoxi sustituidas sensibles a la luz visible. El comportamiento de estos sistemas se ha comparado con polímeros análogos que incluyen una unidad azobenceno sensible a la luz UV cuyo comportamiento está bien establecido. Estos copolímeros bloque se han obtenido por polimerización controlada por apertura de anillo organocatalizada. En función de la longitud del bloque hidrófilo se han obtenido micelas o vesículas. Se ha demostrado que es posible la encapsulación de Rojo de Nilo en micelas y vesículas, y de Rodamina B en vesículas, y su liberación al aplicar luz de 530 nm.

Capítulo 4: Tomando como punto de partida los polímeros que forman vesículas descritos en el Capítulo 3, se ha estudiado el efecto que provoca en la encapsulación y liberación estimulada con luz la disminución del número de unidades azobenceno en la cadena lateral del bloque hidrófobo incorporando en su lugar cadenas alquílicas. Se ha encontrado que la presencia de cadenas alquílicas en la cadena lateral del bloque hidrófobo disminuye notablemente su capacidad de encapsulación. Manteniendo en el polímero una proporción molar de azobenceno del 75% se han obtenido vesículas capaces de encapsular Rodamina B y liberarla mediante la actuación de luz.

Capítulo 5: Se ha comprobado la viabilidad celular de las micelas estudiadas en el Capítulo 2 y de las vesículas sensibles en el visible estudiadas en los Capítulos 3 y 4 en las líneas celulares HeLa y Huh-5-2, así como su capacidad de encapsular un fármaco hidrófobo, Paclitaxel. Se ha encontrado que para ello son más adecuadas las micelas por ser capaces de cargar más fármaco. La utilización de estos autoensamblados cargados con Paclitaxel ha permitido incrementar la efectividad del mismo frente a las líneas celulares estudiadas. Por último, se ha demostrado un incremento en la citotoxicidad del Paclitaxel tras inducir su liberación con 530 nm usando las vesículas sensibles en el visible.

Como conclusiones más relevantes de este trabajo podemos establecer que:

- Se ha diseñado una estrategia versátil para la obtención de copolímeros anfífilos biodegradables fotoestimulables formados por un segmento hidrófilo de polietilenglicol y un segmento hidrófobo de policarbonato alifático. La estrategia combina la polimerización por apertura de anillo organocatalizada de carbonatos cíclicos utilizando un macroiniciador de polietilenglicol, lo que permite evitar el uso de catalizadores metálicos durante la polimerización, y reacciones de química click, lo que permite una funcionalización post-polimerización del bloque hidrófobo completa y homogénea.
- La funcionalización supramolecular permite obtener nanotransportadores, no solamente basados en azobencenos fotoisomerizables, sino también con unidades en las que la luz induce cambios químicos más significativos como la

escisión de un enlace en los ésteres de cumarina. Se dispone así de una estrategia de funcionalización post-polimerización versátil que permite acceder a sistemas con respuesta al NIR, más interesante desde el punto de vista de las aplicaciones biomédicas que la luz UV.

- Es posible diseñar sistemas de liberación estimulada con luz visible de 530 nm utilizando la unidad 2,2',5,5'-tetrametoxi-4-oxiazobenceno. Los autoensamblados preparados no son citotóxicos en las líneas celulares investigadas y permiten incrementar la concentración de Paclitaxel en medio acuoso y su efectividad frente a las líneas celulares estudiadas.
- Aunque es necesario optimizar las condiciones, la dilución de las unidades azobenceno en estos sistemas es posible hasta cierto limites sin perder la capacidad de respuesta a la luz visible.
- Finalmente, como conclusión más relevante, se ha demostrado la liberación de Paclitaxel inducida por luz visible de 530 nm en cultivos celulares.